Study Of The Photodegradation And Photostability Of Anti-Cancer Drugs In Different Media Towards The Development Of Both New Actinometers And Liquid Formulations

Lok Yan Lee

A thesis submitted in partial fulfilment of the requirements for the degree of Doctor of Philosophy (PhD) to be awarded by De Montfort University

Leicester School of Pharmacy
De Montfort University
Leicester

May 2016
(Revised Version)

DECLARATIONS

This thesis contains original work undertaken by the author for the award of Doctor of Philosophy at De Montfort University (Leicester), except where due reference is made to other authors.

No part of the material presented in this thesis has been submitted for any other academic degree or qualification in this or any other higher education institution.

ABSTRACT

This study aims at tackling some of the problems often encountered in photostability testing and liquid formulation development. Three anti-cancer drugs will be employed as models; Dacarbazine (DBZ) has well established photostability issues, Axitinib (AXI) and Sunitinib (SUT) are two new drugs only commercially available in solid dosage forms.

In ethanol, the photokinetics of these drugs were well described by the newly proposed Φ-order kinetic mathematical model. This has confirmed the photoreversible character of AXI and SUT's and unimolecular photoreaction of DBZ's photodegradations. Also, the Φ-order kinetics is proven to describe them better than the usually used classic thermal reaction orders.

In aqueous solution, the drugs were found to undergo thermal and photochemical complex degradations, involving at least 3 photoproducts. A new photokinetic approach has been proposed in this work to solving and unravelling the attributes of such complex mechanisms.

For the first time, the quantum yields (QY) of the three drugs were determined and found to increase with irradiation wavelength. SUT's QY were comparable in ethanol and water (QY_{460} = 0.02), DBZ was found to be more photoefficient in water (QY_{330} = 0.04 and 0.1, respectively) and AXI in water (QY_{330} = 0.06 and 0.03).

Φ-order kinetics' potential for the development of reliable actinometers of the three drugs, without prior knowledge of unknown reaction parameters, has also been established.

A general equation to describe the isotherm of a (G_n:H_m) guest-host multicomponent complex was proposed in this work to palliate the lack of a strategy for characterising nanosponge-drug complexes. It provides information on both stiochiometry and association constant of the complex. The results indicate that hydrophobic AXI forms a 1:0.8 complex, indicating the possibility of multiple association sites and/or different types of binding.

The newly developed AXI/nanosponge liquid formulation has significantly increased solubility (5000-fold) and thermal stability. Furthermore, the photostability of DBZ and SUT were considerably improved by using a strategy based on light-absorption competitors. Their initial velocities reduced from 10 and 3 s^{-1} (respectively) to 1 and 0.13 s^{-1}.

The successful application of these methods to the model anti-cancer drugs has set out new approaches that might be found useful for future treatments of photodegradation data, development of drug-actinometers and liquid formulations of drugs.

ACKNOWLEDGEMENT

My deepest gratitude goes to my supervisor, Dr Mounir Maafi. Without his never-failing support and guidance throughout these years, this would not have been possible. Words cannot express how grateful I am to have been given the opportunity to do a PhD and to learn so much from him. His patience, genuine care, concern and faith in me kept me going. Honestly, I am just forever indebted to him for everything. Thank You, Dr Maafi!

Thank you to Dr Michael Goodman, my second supervisor, for his time and commitment.

I would also like to express my sincere thanks to my uni parentals: Unmesh Desai and Nasmin Juma, for always being available when I need them. Their academic support and personal cheering are greatly appreciated.

Last and not least: my beloved parents, brothers and friends, whose endless love, patience and encouragement have helped carried me through everything. Thank you all for being there through every excruciating step and mood change with me!

JOURNAL PUBLICATIONS

A list of publications from this PhD.

Maafi M. and **Lee L.Y.** (2015) Actinometric and Φ-order photodegradation properties of anti-cancer Sunitinib, *Journal of Pharmaceutical and Biomedical Analysis*, 110:34-41

Maafi M. and **Lee L.Y.** (2015) Determination of Dacarbazine Φ-Order Photokinetics, Quantum Yields, and Potential for Actinometry, *Journal of Pharmaceutical Sciences*, 104(10):3501–350

Maafi M. and **Lee L.Y.** (2016) Anti-cancer Axitinib Φ-Order photokinetics and Actinometry*, New Journal of Chemistry,* Manuscript under consideration.

Maafi M. and **Lee L.Y.** (2016) On The Fluorimeteric Characterization Of Nanosponge:Drug Complexes In Aqueous Solutions*, Photochemical & Photobiological Sciences*, In preparation.

GLOSSARY AND ABBREVIATIONS

A_{tot}	Total absorbance of the sample
$A_{tot}^{\lambda_{irr}/\lambda_{obs}}(y)$	the total absorbance of the reaction medium at reaction time ($y = 0, \infty$) when irradiated at certain wavelength and observed at another wavelength
$A_{tot}^{\lambda_{irr}/\lambda_{irr}}(z)$	the total absorbance of the reaction medium at reaction time (z= $0, \infty$) when irradiated at certain wavelength and at the same wavelength
$A_{tot}^{\lambda_{isos}/\lambda_{obs}}(w)$	the total absorbance of the reaction medium at reaction time ($w = 0, \infty$) when irradiated at the isosbestic point and observed at another wavelength
AXI	Axitinib
AB(1Φ)	a unimolecular photoreaction mechanism, where the initial species (A) photo-transforms into a product (B) with an efficiency ΦA→B
AB(2Φ)	a mechanism which involves two reversing photochemical reactions between the drug and its photoisomer
β-Ca	Beta-Carotene
$C_X(h)$	Concentration of species X at the reaction time (h = 0, pss, ∞)
CD	Cyclodextrin
DBZ	Dacarbazine
DMSO	Dimethysulfoxide
EMA	European Medicines Agency
E-S	*E*-isomer of species S
$F_{\lambda_{irr}}(t)$	the photokinetic factor including the absorbance recorded at the reaction time
$Fl_{tot,i,j}^{\lambda_{obs}}$	Total fluorescence intensity at a specific wavelength of observation, with nanosponge "*j*" concentration and "i" guest concentration
$Fl_{0,(G_n:(CD_p)_m)}^{\lambda_{obs}}$	the fluorescence intensity of the medium when every guest molecule is complexed
$Fl_{0,G,i}^{\lambda_{obs}}$	the native fluorescence of the guest at "*i*" concentration
$G_n:(CD_p)_m$	guest (G):cycldoextrin (CD) complex containing "*n*" number of guest species and a polymer "*m*" (one or more) cyclodextrin chain-molecules that may encompass each up to "*p*" cyclodextrin monomer–units
HP-β-CD	2-Hydroxypropyl- Beta-Cyclodextrin
$K_{A \leftrightharpoons B}^{\lambda_{isos}}$	the equilibrium constant which expresses the ratio of species' concentrations at pss for the isosbestic irradiation
k_X^m	the overall rate constant of the reaction of species X (e.g A→B or $A \leftrightharpoons B$), where m is photochemical (λ_{irr}) or thermal (Δ)

$l_{\lambda_{obs}}$	the optical path length of the monitoring light inside the sample
$l_{\lambda_{irr}}$	the optical path length of the irradiation beam inside the sample
PA	Peak Area
PP	Photoproduct, product formed through photoreaction
PSS	Photostationary State, where the reaction have reached equilibrium.
OHCl	Ondansetron Hydrochloride
$P_{\lambda_{irr}}$	the radiant power
RK	Runge-Kutta
RMM	Relative Molecular Mass
S_0	Switch off time
SSY	Sunset Yellow
SUT	Sunitinib Malate
S/x-CDP	Formulation containing species S and α- or β-CDP
TRZ	Tartrazine
VAN	Vanillin
x-CD	Cyclodextrin monomer, where x is α, β or γ
x-CDP	Cyclodextrin Polymer, where x is α, β or γ
Z-S	*Z*-isomer of species S
$\Phi_{i\rightarrow j}^{\lambda_{irr}}$	The quantum yield at the irradiation wavelength between species
$\varepsilon_X^{\lambda_{irr}}$	the extinction coefficients of species X
λ_{irr}	Wavelength of Irradiation, the wavelength used to irradiate the sample
λ_{obs}	Wavelength of Observation, the wavelength at which the sample was observed
λ_{isos}	Wavelength of Isosbestic point, wavelength where the total absorbance of the reactive medium does not change because the absorbance of the species are the same
$\lambda_{irr}/\lambda_{obs}$	Irradiated at a wavelength and observed at another
$\beta_{\lambda_{irr}}$	Proportionality factor between the overall rate-constant and the radiant power
$v_{0(n)}^{\lambda_{irr}/\lambda_{obs}}$	the reaction's initial velocity, where n is cld. (calculated from theoretical equation) or mod. (determined from differential equation of the Φ-order kinetic model equation).

LIST OF FIGURES

LIST OF TABLE

LIST OF SCHEMES

CONTENTS PAGE

CHAPTER ONE

AIMS AND INTRODUCTION

1.1. INTRODUCTION

The process of pharmaceutical formulation development involves many stages and testing that leads to a final product which is suitable for patient use. However, many limitations are encountered, such as the evaluation and quantification of drugs' photostability data, the suitability of the actinometers used for photostability studies and the development of liquid formulations that are soluble and stable. This study aims to address these issues through the use of three anti-cancer drugs: Dacarbazine, Axitinib and Sunitinib.

Photostability testing is an integral part of drug development as specified by the International Conference on Harmonisation (ICH) [1]. However, the lack of a standardised methodology or comparative measure for determining a drug's photokinetics means that the photoreactivity of different drugs, or the same drug measured at different irradiation conditions, cannot be directly compared.

Furthermore, it is often questioned whether the quinine hydrochloride chemical actinometer recommended by the ICH [1] for use with photostability studies meets the generally accepted requirements of a chemical actinometer [2-4]. Not only must it be calibrated for each type of light source that might be used for photostability testing, but also its response is temperature dependent [4].

In the pharmaceutical industry, the lack of commercially available oral liquid dosage forms is an on-going problem [5] – limiting their availability to paediatric and geriatric patients, and those with dysphagia who require medicines to be delivered via nasogastric or gastrostomy tubes [5]. However, challenges with the solubility and stability (including light stability) of active compounds of liquid drug preparations often means that new drugs are only available in solid dosage forms [6]. Consequently, drugs are often prepared extemporaneously as oral liquid formulations by crushing or opening marketed tablets and capsules. In many cases, the

stability of these extemporaneous preparations, which may affect their tolerability, are yet to be established [5].

These issues will be discussed and solutions to solve them proposed in the 10 chapters of this thesis.

Chapter 1 to 3 provides an overview of the work to be presented, current literature in the subject and the methods employed in this study.

An overview of the current literature on the three model drugs can be found in chapter 4. To the best of our knowledge, there are no published photokinetic studies on the three drugs. In addition, a stable liquid formulation does not currently exist for these drugs.

The following chapters (Chapter 5-10) can be divided into two main sections.

The first section seeks to quantify photokinetic data obtained from drug photodegradation reactions. For simple, thermally stable, unimolecular AB(1Φ) and photoreversible AB(2Φ) drug photodegradations, the recently developed Φ-order kinetics model can be applied (Chapter 5). Successful application of this approach strongly suggests that drug photodegradations are better described by Φ-order than the classic zero, first and second thermal reaction orders.

In aqueous solution, the degradation of these three drugs was found to obey much more complex mechanisms and thus required other means of evaluation. Chapter 6 presents a new, alternative method which circumvents the limitations of published chemometric approaches, to elucidate, quantify and evaluate complex drug photodegradation. This new approach enabled the determination of different aspects of the reaction, with a better performance compared to classic separation techniques (including the elucidation of all species' spectra).

New techniques for the development of drug actinometers are described in chapter 5 and 6. The methods presented here can easily be applied to many other photolabile drugs for

development of reliable actinometers, even without prior knowledge of other reaction parameters.

The second part of this study focuses on the quantification of the effect of both cyclodextrin monomer and polymers with the aim to developing stable liquid formulations of three very light-sensitive anti-cancer drugs – one of which is practically insoluble in water.

However, the means of evaluating the interaction/association between drug and cyclodextrin polymers does not currently exist in the literature and so a new mathematical framework proposed will be presented in Chapter 7. Not only does it does not require precise knowledge of the species' masses, it does not impose preselected stoichiometries, to provide reliable information on both stiochiometry and association constant of the complex.

For the first time, a comprehensive approach is presented to address these issues by considering both inclusion complexation with cyclodextrins (Chapter 8) and the use of light absorption competitors (Chapter 9). Until now, a systematic study of the effect of cyclodextrin monomers and polymers has never been presented for these drugs.

Chapter 10 proposes soluble aqueous formulations for the three drugs that present improved thermal and/or photochemical stabilities. It offers potential solutions to the problems that stand in the way of making these and other similar drugs more widely available.

The final chapter (Chapter 11) represents the main conclusions from the work presented and the results of this study.

1.2. REFERENCES

1. ICH Q1B. (1996) Photostability testing of new drug substances and products. Federal Register 62(95):27115–27122.

2. Baertschi S.W. (1197) Commentary on the quinine actinometry system described in the ICH draft guideline on photostability testing of new drug substances and products, *Drug Stability*, 1(4):193-195
3. Albini A. and Fasani E. (*Ed.*) (1998) Drugs: Photochemistry and Photostability, Cambridge, UK: The Royal Society of Chemistry.
4. Tønnesen H.H. (1996) Photostability of Drugs and Drug Formulations, 2nd Edition, London: Tylor & Francis
5. Haywood A. and Glass B.D. (2013) Liquid Dosage Forms Extemporaneously Prepared from Commercially Available Products – Considering New Evidence on Stability, *Journal of Pharmacy and Pharmaceutical Sciences*, 16(3):441-455
6. Allen L.V. Jr., Popovich N.G. and Ansel H.C. (2014) Dosage Form Design: Pharmaceutic and Formulation Considerations, In: Ansel's pharmaceutical dosage forms and drug delivery systems, USA: Wolters Kluwer Health/Lippincott Williams & Wilkins

CHAPTER TWO

DRUG PHOTODEGRADATION AND PHOTOSTABLIZATION OVERVIEW

2.1. DRUG PHOTODEGRADATION

Exposure of certain materials to light can cause various changes to their properties. This is often seen as a change in colour, such as the colour of products fading or glasses that darken when exposed to sunlight [1].

Light can also have an effect on pharmaceuticals. There are a large number of drugs that require protection from light as outlined by the European Pharmacopoeia [2]. The number of drugs identified as photochemically unstable (photoreactive or photolabile) is steadily increasing as new drugs are discovered and existing drugs re-examined [3]. However, drugs that are being labelled sensitive to light do not necessary all carry the same consequence; as some drugs, after weeks of exposure, only a small percentage is lost, while others degrade in just a few minutes [4].

The loss of therapeutic potency of the pharmaceutical is inevitable but the photodegradation of drugs should not be considered just as a decomposition process. It involves phenomena, such as generation of free radicals, transfers of energy and luminescence, which could result in the formation of photoproducts. Some of these could have toxic effect on the patient [5].

It is true that the stability of drugs can also be influenced by other factors such as temperature, moisture and oxidation; but photochemical processes can have severe pharmaceutical and medicinal consequences. Due to the fact that most drugs absorbed within the UV and Visible region of light, the matter should not be considered trifling as light can essentially change the properties of many therapeutic agents during production, storage, handling, administration and even in the patient after their administration (*in vivo*) [3].

In general, the drug substance would mainly experience exposure to visible light, from cool white fluorescent tubes. Many drug substances are white in colour, meaning little or no visible

light are absorbed by these compound. But it is important to note that all lamps emit some radiation in the UV region of the spectrum [6].

In modern hospital pharmacies, drugs are often stored in unit-dose containers on open shelves [6]. In many cases, the protective commercial pack is removed – leaving the drug product unprotected. They can then be exposed to fluorescence tubes and/or filtered daylight for several days or weeks [7]. Moreover, in accordance to the Food and Drug Administration's (FDA) Compliance Policy [8], repackaged drugs can utilize an expiration date up to 6 months from date of repackaging without conducting stability studies.

Therefore, knowledge about the photostability of the drug substance *in vitro* is essential to evaluate any precautions needed and ensure good quality over the entire life span of the drug.

2.2. PHOTOSTABILITY TESTING

In January 1998, the International Conference on Harmonisation of Technical Requirements for Registration of Pharmaceuticals for Human Use (ICH) made photostability testing of all new drug substances and products an "integral part of stress testing" [9]. Their Q1B guideline [9] on photostability testing provides guidance on the basic information required to characterise the drug's light sensitivity and stability, for submission in registration applications. It also gives instructions to help applicants identify the likelihood of degradation, which in turn helps establish the degradation pathways, products and the intrinsic stability of the molecule.

However, despite the regulation's insistence in generating photostability data in accordance to its instructions (or set in comparison to them), it contains issues that are unclear including the design of the testing protocol, which is left to the applicant's discretion. The applicant must establish how the product will be used, to devise appropriate photostability studies and so

allowing alternative approaches "to demonstrate that light exposure does not results in unacceptable change".

The lack of a standardised methodology or comparative measure for determining drugs' photokinetics means that the photoreactivity of different drugs, or the same drug measured at different irradiation conditions, cannot be directly compared.

2.3. KINETICS OF DRUG PHOTOREACTIONS

In the literature [6,10-29], photochemical reaction data are commonly treated with conventional thermal reaction kinetic zero-, first- and second-order models.

In many cases [10-29], only part of the kinetic data of photodegradation is used for such classical treatments. In some cases, it was found that no kinetic model can be accurately applied to the reaction kinetic data [26-29]. Piechocki and Thoma [10] showed that partial reaction data could equally be fitted with both zero and first order models (Fig 2.1).

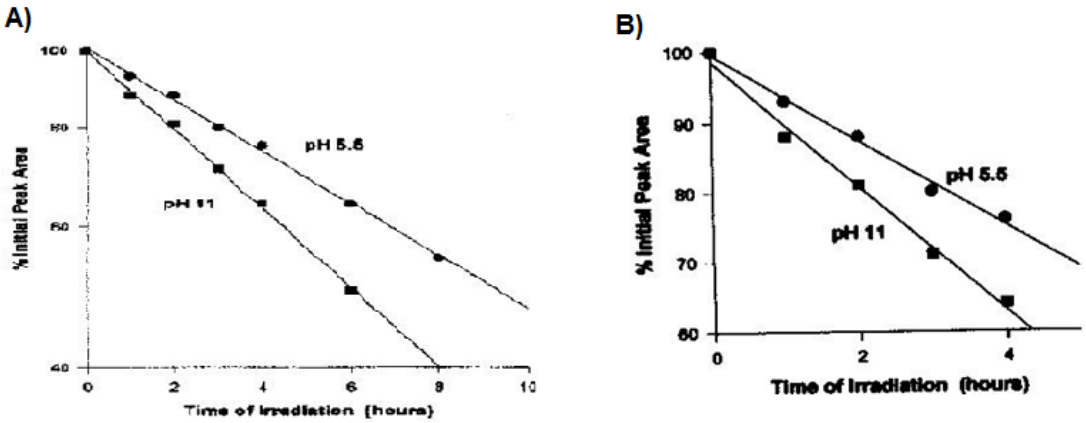

Fig 2.1: Partial photodegradation data of benzydamine hydrochloride (5 x 10^{-5} M) that was fitted with (A) first-order kinetics and later a good fit was also obtained for (B) a zero-order model [10]

However, only poor fitting is found when the full photodegradation data was fitted with the conventional (classical thermal) models [30]. This clearly shows that the kinetics models developed for thermal reactions may not be suitable for photochemical reactions.

In contrast to thermal reactions, the different equations depends on three parameters – the intensity of the irradiation (P), the extinction coefficient (ε) and quantum yield (Φ) of the drug at a specific wavelengths. The quantum yield for photoreaction can be defined as the number of drug molecules that undergo photoreaction divided by the number of photons absorbed [10]. Without first defining these parameters, the photoreactivity of different drugs, or the same drug measured at different irradiation conditions, cannot be directly compared.

The differential equation (Eq.1) for the photochemical reaction AB(1Φ), that is species A transforming into species B, can be expressed as [30]:

$$\frac{dC_A(t)}{dt} = -\Phi_{AB}^{\lambda_{irr}} \times \varepsilon_A^{\lambda_{irr}} \times C_A(t) \times P^{\lambda_{irr}} \times l_{\lambda_{irr}} \times F_{\lambda_{irr}}(t) \qquad \text{Eq.1}$$

Where $C_A(t)$ is the concentration of A at any time, $\varepsilon_A^{\lambda_{irr}}$ the extinction coefficient of A, $\Phi_{AB}^{\lambda_{irr}}$ the quantum yield of the reaction, $P^{\lambda_{irr}}$ the light intensity received and $l_{\lambda_{irr}}$ the path length of the excitation light. The photokinetic factor $F_{\lambda_{irr}}(t)$ is a time-dependent function expressed as:

$$F_{\lambda_{irr}}(t) = \frac{1-10^{-\left(A_{tot}^{\lambda_{irr}}(t)\right)}}{A_{tot}^{\lambda_{irr}}(t)} \qquad \text{Eq.2}$$

in which $A_{tot}^{\lambda_{irr}}$ is the total absorbance of the reaction medium.

In the general case, Eq.1 cannot be integrated due to the time-variation of the photokinetic factor, which is dependent on the total absorbance of the medium at the irradiation wavelength.

However, recently, it has been successfully integrated in closed-form and was shown that a drug following the AB(1Φ) photodegradation mechanism obeys well a Φ-order kinetic [30-32]. The Φ-order kinetic described well the whole set of AB(1Φ) photodegradation data and readily allowed the determination of the reaction photochemical quantum yield from the reaction overall rate-constant. Nevertheless, it has a limited application as they are specific to unimolecular AB(1Φ) drug photodegradations.

2.3.1. Computational Techniques

In some studies, data analysis of complex photodegradation mechanisms are overcome by the use of computational techniques, which involves the use of mathematical software procedures to analyse data obtained from dynamic and unstable systems [33]. Common chemometrics techniques used in combination with UV-Vis spectrophotometry are spectral curve deconvolution multivariate curve resolution (MCR) methods, Principal Component Regression (PCR) and non-linear iterative partial least squares (NIPALS) [33]. These models enable complex drug photodegradation pathways to be resolved, the number of species, their individual spectra, their concentration profiles and rate-constant to be extracted from mixed spectral photokinetic data [34-41]. The NIPALS method will also provide the equilibrium constant [40].

However, these methods do not provide a unique answer and is only applicable to systems where two correlated spectra can be recorded on each sample [40]. Otherwise, chromatographic data is required to determine the component spectral profiles and concentrations.

More importantly, these models are based on the thermal differential equations - which are completely different to that of photokinetic. Thus, the current methods of resolving

photokinetic data gives thermal rate constants for photochemical reaction and do not provide information of Φ.

2.4. EFFECT OF SOLVENT

When comparing photostability data, the choice of solvent is vital as this may significantly affect the results of photodegradation processes [10]. Systematic studies on the effect of solvents on a range of pharmaceutics have been carried out and many reviews available [41-53]. All of which were found to give different mechanisms, different number of photoproducts and different rate of photodegradation in different media [50-53].

Table 2.1: Apparent first-order rate constants (k_{obs}) for the photodegradation of various drugs in water and organic solvents using chromatographic assays

	k_{obs} x 10^3 (min^{-1}) ± SD			
Solvents	**Riboflavin [50]**	**Norfloxacin [51]**	**Moxifloxacin [52]**	**Levofloxacin [53]**
Water	4.61 ± 0.25	1.59 ± 0.13	32.6 ± 0.13	99.8 ± 0.35
Acetonitrile	3.81 ± 0.16	0.80 ± 0.12	20.4 ± 0.10	76.6 ± 0.31
Methanol	3.64 ± 0.17	0.61 ± 0.09	18.1 ± 0.11	71.4 ± 0.33
Ethanol	3.45 ± 0.15	0.45 ± 0.05	15.5 ± 0.09	68.0 ± 0.23
1-Propanol	3.34 ± 0.16	0.37 ± 0.11	13.5 ± 0.05	63.2 ± 0.27
1-Butanol	3.28 ± 0.13	0.34 ± 0.08	12.4 ± 0.08	61.6 ± 0.20

Even minor addition of one solvent to another can alter the photoreactivity of the drug [6]. Addition of 6.5 mM carbon tetrachloride to a sample of 6-methoxy-2-naphthylacetic acid prepared in acetonitrile caused the photodegradation rate to increase nearly 10 times [54]. Thus, these considerations are important in the formulation of drugs where organic solvents are used as cosolvents [55,56].

It should also be noted that 92 percent of blood plasma is water and that drugs are taken with water, some pharmaceutical excipients releases moisture or strongly absorbs water from the air [55].

Thus photochemical studies in both polar and apolar media provides useful information for predicting drug photoreactivity in lipophilic environment.

2.5. CYCLODEXTRINS

Cyclodextrins (CD) are cyclic oligosaccharides consisting of glucopyranose units linked by α-(1,4) bonds (Fig 2.2). They possess the unique ability to accommodate hydrophobic 'guests' within the cavity of their bucket-shaped structure. Since its discovery, cyclodextrin's ability to form inclusion complexes has been found to have profound effects on the properties of guest molecules [57].

There are different pharmaceutical products containing cyclodextrins that are now available on the market worldwide and numerous food products, cosmetics and other commercial products contain cyclodextrins [58,59] In the pharmaceutical industry, cyclodextrins are most commonly used to aid the dissolution of poorly soluble drugs [60-64].

There are three main types of cyclodextrins: α-, β- and γ-CD. They are referred to as the first generation cyclodextrins. They consist of six, seven and eight α-(1,4) linked glycosyl units (respectively). Of the three CDs, β-CD is the most predominance, the cheapest and most useful.

Table 2.2: Natural cyclodextrins and their properties.

Cyclodextrin	α-CD	β-CD	γ-CD
No. of Glucose Units	6	7	8
Molecular Mass (g mol^{-1})	972	1135	1297
Cavity Diameter (nm)	0.47 - 0.53	0.60 - 0.65	0.75 - 0.83
Solubility (25°C, %w/v)	14.5	1.85	23.2

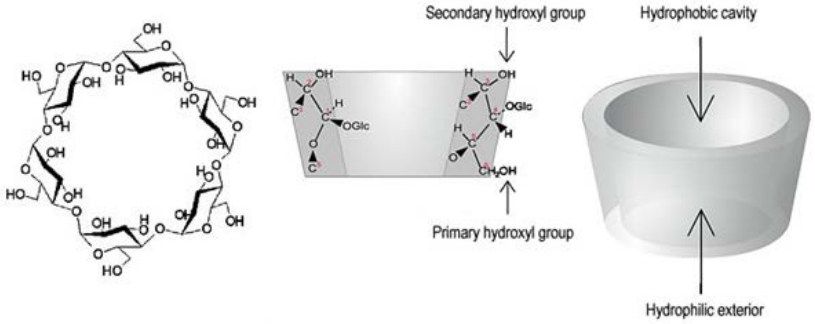

Fig 2.2: The Molecular structure of β-cyclodextrin, cross-section of a cyclodextrin molecule showing the arrangement of the glucose units and conical representation showing hydrophilic exterior and hydrophobic cavity [65].

Due to their unique property, the use of cyclodextrins as pharmaceutical excipients has grown rapidly over the last two decades [66]. They have also been used to improve the stability of drugs, including photostability. When highly photolabile pharmaceutics are entrapped within the cavity of cyclodextrins, their photodegradation rates could be reduced [67-71] - such as ibuprofen [68], shikon [69], nicardipine [70] and doxorubicin [71].

However, formation of an inclusion complex does not necessarily lead to a stabilization of the guest molecule. This was reported for the case of midazolam [72], molsidomine [73], naproxen [74], and flutamide [75]. A 20-fold increase in photodecomposition quantum yield of the latter was reported [75]. No kinetics were given for the others.

Nonetheless, the low water solubility and toxicity of parent CDs limit their further application in pharmaceutical formulations [76].

2.5.1. Cyclodextrin Polymers

Apart from the naturally occurring cyclodextrins, many cyclodextrin derivatives have been synthesised. Depending on the substituent, the properties (stability and solubility) of the cyclodextrin derivatives are usually slightly different from that of their parent cyclodextrins.

Of particular interest are products containing two or more covalently linked cyclodextrin-units called cyclodextrin polymers (CDP).

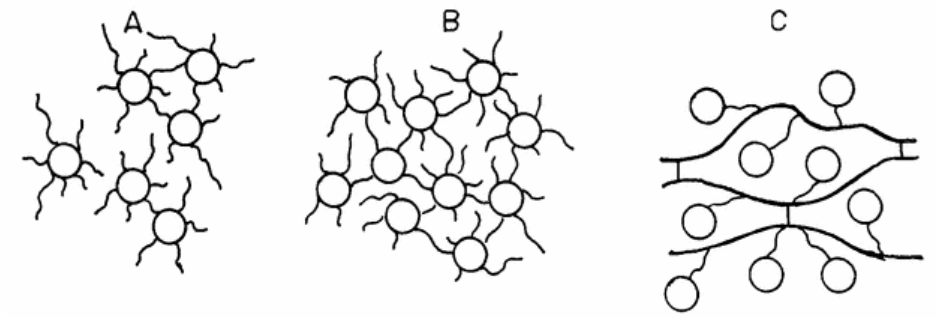

Fig. 2.3: Schematic representation of the three main types of cyclodextrin polymers. (A) soluble, (B) insoluble, (C) immobilised cyclodextrin polymer [77]

However, the slow development of CD polymers over the last 40 years has moderated their true potential. But, recent advances in nanotechnology has increased attention paid to cyclodextrin polymers for applications in the field of nanomedicines. Nanomedicine proposes the use of these systems to improve many current cancer treatments by increasing aqueous solubility of poorly water-soluble drugs, sustaining delivery of drugs and modifying pharmacokinetics, biodistribution and cellular trafficking of the active substances included within the nanostructure [78].

2.5.2. Characterisation of Cyclodextrin Polymers

Most guest/cyclodextrin complexes are thought to be inclusion complexes but cyclodextrins are also known to form non-inclusion complexes in which the guest molecule is linked at the

external part of the cyclodextrin [79]. Depending on the size of the guest and the host molecules, one guest molecule can interact with more than one host molecules (Fig. 2.4); or one CD interacting with one or two guest molecules.

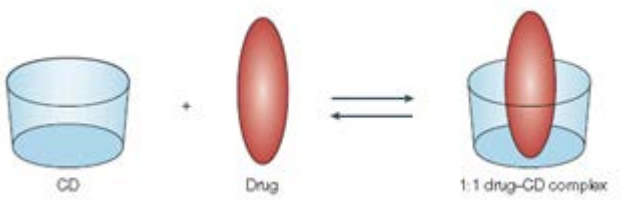

Fig 2.4: Diagrammatic representation of a 1:1 guest-CD inclusion complexes formed

In some instances, depending on the size of the CD size, only parts of the guest can be included. Thus, multiple inclusion equilibria can coexist in one solution [79].

Several methods can be used for characterisation of a CD inclusion complex: circular dichroism [80], fluorescence spectroscopy [81], ^{1}HNMR [82], IR and Raman spectroscopies [83]. Stoichiometry and association (or binding) constant of the complexes can be determined from all methods, but information on the structure can only be obtained from ^{1}HNMR [82].

Determination of complex parameters (stoichiometry and association constant) is often achieved by applying Benesi-Hildebrand or Job's method to experimental data [80, 82, 83]. However, Job's method only gives indication of the stoichiometry, not association constant. Benesi-Hildebrand assumes a 1:1 stiochiometry, lacks sensitivity for low concentrations and accuracy drops rapidly as K increases [84]. Furthermore, multiple types of inclusion complex (1:1, 1:2 or 2:1) can be found in one solution as stoichiometries are assume and experimental data are fitted to the corresponding model [85].

Thus, despite its growing popularity, method for characterising complexes with CD polymers are not yet as extensively examined as the monomers. Current methods of determining the stoichiometry and association constant of inclusion complexes are, as discussed, limited in itself and more so when applied to cyclodextrin polymers. So, often the stoichiometry for CD-P complexes are assumed or not stated [79,80].

2.6. PHOTOSTABILIZATION WITH CYCLODEXTRIN POLYMERS

In many cases, suitable light-resistant packaging can prevent or reduce photodecomposition of drugs [4]. However, very often drugs are removed from their original packaging and stored in unit-dose containers, leaving them unprotected. Furthermore, exposure to light during administration is unavoidable and so it might be necessary to photostabilize the drug itself.

Cyclodextrin polymer's ability of encapsulate molecules have been used to improve drug photostability. They protect the photolabile drug by physically quenching the electronic excited states of drug molecules, draining off the energy from absorption of light before the drug molecule has the opportunity to undergo photodegradation [10]. Therefore, when unstable molecules are entrapped within the cavity of cyclodextrins, their decomposition rates could be reduced [68-71] or increased [72-75].

Even with the growth of nanomedicine, there have been very few examples of where CDPs have been used to protect the encapsulated molecules from light [78, 86-90] or from chemical and enzyme-induced degradation [92]. Nanosponges are mainly used for increasing drug solubility.

5-fluoroucil (5-FU) is a chemotherapy drug known to be very light-sensitive. Encapsulation of the drug in β-CDP protected the drug for 6 months and maintained its cytoxicity [90].

β-CDP has been used in buccal formulations of Resveratrol - a polyphenolic compound endowed with multiple health benefits. However, its limited bioavailability and poor photostability in solution hinders its use in pharmaceutical applications. Complexation of the drug with β-CDP significantly improved its solubility, permeation of the active pharmaceutical ingredient (API) and photostability (Fig. 2.5) [86]. However, little detail were provided for the photodegradation study other than that complexation with CDP improved the drug's photostability. No kinetics were given.

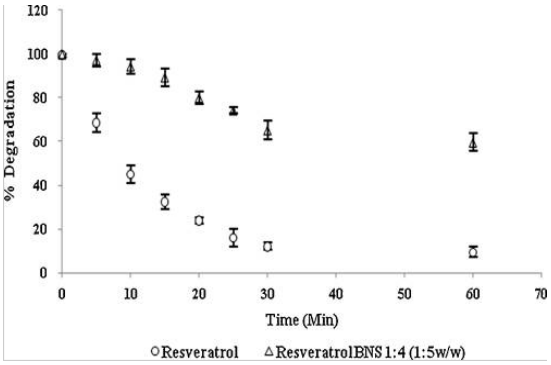

Fig. 2.5: Photodegradation of resveratrol and complex when exposed to UV lamp at 10 cm distance and quantitatively analysed by HPLC [86]

Gamma-oryzanol, a ferulic acid ester mixture used as sunscreen in the cosmetics industry, is another pharmaceutic whose use was limited by its photochemical instability [87]. Encapsulation of the compound in cyclodextrin-based nanosponges was found to provide good protection from UV-induced oxidation (Table 2.3).

Another example is when camptomethecin (CPT) was also encapsulated in β-CDP. CPT is a potent anti-tumour agent but has poor water-solubility and high chemical instability - limiting its therapeutic use. However, encapsulation in β-CD nanosponges enable large amounts of the drug to be solubilised and increased its thermal stability [88]. Thus, prolonging its shelf life.

Table 2.3: rate constant (k) values obtained using pseudo-first order kinetic model and correlation coefficient (R^2) of free gamma-oryzanol (GO) or complexed (GO/NS) photodegradation in different media under UVA irradiation (6.0×10^{-4} W cm^{-2}) for 60 min at 10 cm distance. [87]

	GO		GO/NS	
	$k \times 10^3$ (min^{-1})	R^2	$k \times 10^3$ (min^{-1})	R^2
Water/ethanol (20/80 v/v)	7.8 ± 0.4	0.995	-	-
Tween 20/water (40/60 v/v)	6.2 ± 0.1	0.819	-	-
HEC gel	11.8 ± 0.5	0.994	3.1 ± 0.1	0.971
O/W emulsion (E1)	5.3 ± 0.3	0.881	0.6 ± 0.1	0.843

2.7. LIGHT ABSORPTION COMPETITORS

Alternative to microencapsulation, inactive substances (pharmaceutical excipients) can be added to the drug to provide photoprotection [6,10,90-93]. However, for this the excipient must have an absorption spectrum that overlays the photolabile drug [90-93]. The idea is that the excipient will compete with the drug for the energies from the light source and as a result, reducing the amount of damage done to the drug by reducing the amount of light absorbed [90-93].

Excipients with similar absorption spectra to the drug can be incorporated into the formulation, film coating or capsule shell. This was shown to be effective when addition of curcumin and riboflavin 5-phosphate significantly enhanced the photostability of nifedipine [93] or when red iron oxide was added to the film coating of Axitinib tablets [94].

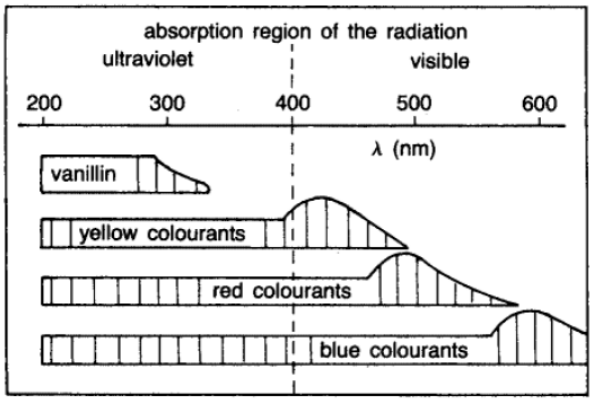

Fig. 2.6: Principle of photostabilzation through spectral overlay with absorbing excipients [6]

Obviously, not only does the excipient requires the appropriate absorption spectrum for overlay, but it must also be pharmaceutically inactive, non-toxic and be photostable itself. Hence, the potentially useful materials is limited [90].

2.8. FORMULATION

There are two main goals of pharmaceutical formulation [58,95,96]. First, to produce a drug that is stable to ensure that efficacy and safety characteristics of the active substance are maintained. Second, to make drug administration easier and more convenient to the patient who will use it.

As mentioned above, photochemical reaction are affected by the medium and so exposure of drug formulations to light can impact its stability. Thus, the excipient and preparation type (i.e. solid dosage, liquid and topical forms) can influence the photostability of the active ingredient. The effect of excipients on the stability of drug formulation is often difficult to predict [58]. They can initiate, propagate or participate in photochemical reactions.

Common excipients such as sugar, starches, polyvinylpyrrolidone (PVP), mannitol and lactose are all vulnerable to free radical attacks, which in many cases destabilizes the formulation [6,

56, 57]. Furthermore, non-ionic surfactants for emulsions of oral or topical preparations susceptible to oxidation could influence the photoreactivity of drugs.

Although in solid state, photodegradation takes place on the surface, the degree of degradation depends very much on the excipients, the colour, thickness, coating, source and intensity of the light.

Similarly, sample close to the surface of a solution will absorb most of the light.

2.9. CONCLUSION

Photodecomposition of unstable drug formulations could lead to undesirable side effects. A loss of potency of the drug and the development of adverse effects may be due to the formation of photoproducts during storage or administration. Therefore, photostability testing of drug substances is important for the evaluation of the overall photosensitivity of the material for development. Hence, the photostability of drug substances has developed into an important area of research, especially as more drugs are considered photolabile.

When enclosed in the packaging, the drug is normally well protected from light exposure. However, it is also important to note those periods of time when the dosage forms are not covered by packaging - i.e. both during the process of manufacturing itself and during handling by the patient on application at home or in hospital. In this respect, the kinetics of degradation are strongly dependent on light intensity and spectral distribution of the light source used. Thus, the need to know the photochemistry of the drugs used is essential to provide important information to evaluate precautions required for handling and packaging, potential adverse effects, therapeutic aspects and new drug delivery systems

The ICH made photostability testing of all new drug substances and products an "integral part of stress testing", but fails to provide clear protocols on the treatment and analysis of photokinetic data. Thus, very often the zero-, first- and second-order thermal kinetic model are implemented. These were used irrespective of the drug's photochemical mechanism or the influence of the irradiation wavelength and intensity of the light source.

Recent advances in nanotechnology increased interest in the use of cyclodextrin polymers for stable drug delivery systems. They have been shown to improve many current cancer treatments by increasing aqueous solubility of poorly water-soluble drugs, sustaining delivery of drugs and modifying pharmacokinetics, biodistribution and cellular trafficking of the active substances included within the nanostructure. Although it is not as extensively examined as the other areas, nanosponges have been shown to improve the thermal and photo-stability of drugs.

Overall, there are many aspects in photochemistry of pharmaceutics that are lacking and in this study they will be examined through the use of three very light-sensitive anti-cancer drugs: Dacarbazine, Axitinib and Sunitinib.

2.10. REFERENCES

1. Bamfield P. and Hutchings M.G. (2010) Chromic Phenomena: Technological Applications of Colour Chemistry, 2nd Edition, Cambridge: Royal Society of Chemistry Publishing
2. Tønnesen H.H. (2001) Formulation and Stability Testing of Photolabile Drugs, International Journal of Pharmaceutics, 225:1-14.
3. Tønnesen H.H. (2008) Photoreactivity of Drugs, Available at: www.dnva.no/geomed/solarpdf/Nr_8_Hjorth_Tonnesen.pdf [Acessed 05/02/2012]
4. Florence A.T. and Attwood D. (1998) Physicochemical Principles of Pharmancy, 3rd Edition, Wales: Creative Print & Design
5. Cosa G. (2004) Photodegradation and photosensitization in pharmaceutical products: Assessing drug phototoxicity, Pure and Applied Chemistry, 76(2):263–275
6. Tønnesen H.H. (ed.) (2004) Photostability of Drugs and Drug Formulations, 2nd Edition, USA:CRC Press LLC

7. Tønnesen H.H. and Karlsen J. (1995) Photochemical degradation of components in drug formulations. III. A discussion of experimental conditions, *PharmEuropa*, 7:137-141

8. Food and Drug Administration (2015) Compliance Policy Guidance Manual Section 480.200 Expiration Dating of Unit Dose Repackaged Drugs [Online] Available at: http://www.fda.gov/ICECI/ComplianceManuals/CompliancePolicyGuidanceManual/ucm074409.htm [Accessed 31/07/2015]

9. ICH Q1B. (1996) Photostability testing of new drug substances and products. Federal Register 62(95):27115–27122.

10. Piechocki J.T. and Thoma K. ed. (2010) Pharmaceutical photostability and stabilization technology, New York: Informa Healthcare

11. Al Omari M.M., Zoubi R.M., Hasan E.I., Khader T.Z. and Badwan A.A. (2007) Effect of light and heat on the stability of montelukast in solution and in its solid state, *Journal of Pharmaceutical and Biomedical Analysis*, 45(3):465-471

12. Malesuik M.D., Gonçalves H.M., Paim C.S., Schapoval E.E. and Steppe M. (2009) LC: analysis of photodegradation kinetics of nitazoxanide in pharmaceutical formulations, *Journal of Chromatographic Science*, 47(9):745-748

13. Alsarra A.L (2004) Develeopment of a stability-indicating HPLC method for the determination of montelukast in tablets and human plasma and its applications to pharmacokinetic and stability studes, *Saudi Pharmaceutical Journal,* 12(4):136-143

14. Wang J. and Moore D.E. (1992) A study of the photodegradation of benzydamine in pharmaceutical formulations using HPLC with diode array detection, *Journal of Pharmaceutical and Biomedical Analysis*, 10(7):535-540

15. Gu L. Chiang H.S. and Johnson D. (1988) Light Degradation of Ketorolac Tromethamine, *International Journal of Pharmaceutics*, 41(2):105-113

16. Pickett J.E. and Moore J.E. (1995) Photodegradation of UV absorbers: Kinetics and structural effects, *Die Angewandte Makromolekulare Chemie*, 232(1):229–238

17. Doll T.E. and Frimmel F.H. (2003) Fate of pharmaceuticals - photodegradation by simulated solar UV-light, *Chemosphere*, 52:1757-1769

18. Prabhakaran D., Sukul P. Lamshöft M. Maheswari M.A., Zühlke S. and Spiteller M. (2009) Photolysis of difloxacin and sarafloxacin in aqueous systems, *Chemosphere*, 77(6):739-746

19. Litvić M., Šmic K., Vinković V. and Filipan-Litvić M. (2012) A study of photodegradation of drug rosuvastatin calcium in solid state and solution under UV and visible light irradiation; the influence of certain dyes as efficient stabilizers, *Journal of Photochemistry and Photobiology A: Chemistry*, 252:84-92

20. Wood M.J., Irwin W.J. and Scott D.K. (1990) Photodegradation of doxorubicin, daunorubicin and epirubicin measured by high-performance liquid chromatography, *Journal of Clinical Pharmacy and Therapeutics*, 15(4):291-300

21. Moore D.E. and Zhou W. (1994) Photodegradation of sulfamethoxazole: a chemical system capable of monitoring seasonal changes in UVB intensity*, Photochemistry and Photobiology*, 59(5):497-502

22. Valero M. and Costa S.M.B. (2003) Photodegradation of Nabumetone in aqueous solutions, *Journal of Photochemistry and Photobiology*, 157(1):93-101

23. Maquille A. and Jiwan J.L.H. (2009) LC–MS characterization of metoclopramide photolysis products, *Journal of Photochemistry and Photobiology A: Chemistry*, 205:197-202

24. Malesuik M.D., Gonçalves H.M.L., Paim C.S., Schapoval E.E.S. and Steppe M. (2009) LC: Analysis of Photodegradation Kinetics of Nitazoxanide in Pharmaceutical Formulations, *Journal of Chromatographic Science*, 47:745-748

25. Mielcarek J., Stobiecki M. and Frański R. (2000) Identification of photodegradation products of nilvadipine using GC-MS, *Journal of Pharmaceutical and Biomedical Analysis*, 24(1):71-79

26. Roman J., Breier A.R. and Steppe M. (2011) Stability Indicating LC Method to Determination of Sodium Montelukast in Pharmaceutical Dosage Form and its Photodegradation Kinetics, *Journal of Chromatographic Science*, 49(7):540-546

27. Matsuura I., Imaizumi M. and Sugiyama M. (1990) Method of kinetic analysis of photodegradation: nifedipine in solutions, *Chemical and Pharmaceutical Bulletin*, 38(6):1692-1696

28. de Haro Moreno A. and Salgado H.R.N. (2012) Stability Study and Degradation Kinetics of Ceftazidime in Pharmaceutical Preparations, Adavances in Analytical Chemistry, 2(1):1-5

29. Ji Y., Zeng C., Ferronato C., Chovelon J.M. and Yang X. (2012) Nitrate-induced photodegradation of atenolol in aqueous solution: Kinetics, toxicity and degradation pathways, *Chemosphere*, 88(5):644-649

30. Maafi M and Brown R.G. (2007) The kinetic model for AB(1Φ) systems: A closed-form integration for the differential equations with a variable photokinetic factor, *Journal of Photochemistry and Photobiology A: Chemistry*, 187:319-324

31. Maafi M. (2010) The potential of AB(1Φ) systems for direct Actinometry. Diarylethenes as successful actinometers for the visible range, *Phys. Chem. Chem. Phys.* 12:13248-13254

32. Maafi M and Maafi W (2013) Modelling nifedipine photodegradation, photostability and actinometric properties, *International Journal of Pharmaceutics*, 456:153-164

33. El-Gindy A. and Hadad G.M. (2012) Chemometrics in Pharmaceutical Analysis: An Introduction, Review, and Future Perspectives, *Journal of AOAC International*, 95(3):609-623

34. Shamsipur M., Hemmateenejad B., Akhond M., Javidnia K. and Miri R. (2003) A study of the photo-degradation kinetics of nifedipine by multivariate curve resolution analysis, *Journal of Pharmaceutical and Biomedical Analysis*, 31(5):1013-1019

35. Borgen O.S. and Kowalski B.R. (1985) An extension of the multivariate component-resolution method to three components, Analytica Chimica Acta, 174:1–26

36. De Lucas M., Mas S., Ioele G., Oliverio F., Ragno G. and Tauler R. (2010) Kinetic studies of nitrofurazone photodegradation by multivariate curve resolution applied to UV-spectral data, International Journal of Pharmaceutics, 386(1–2):99-107

37. Shahjahan M. and Enever R.P. (1996) Photolability of nitrofurazone in aqueous solution II. Kinetic studies, International Journal of Pharmaceutics, 143:83-92

38. Javidnia K., Hemmateenejada B., Miri R. and Saeidi-Boroujeni M. (2008) Application of a self-modeling curve resolution method for studying the photodegradation kinetics of nitrendipine and felodipin, Journal of Pharmaceutical and Biomedical Analysis, 46: 597–602

39. De Luca M., Tauler R., Ioele G. and Ragno G. (2013) Study of photodegradation kinetics of melatonin by multivariate curve resolution (MCR) with estimation of feasible band boundaries, Drug Testing and Analysis, 5(2):96-102

40. Kubista M., Sjöback R. and Albinsson B. (1993) Determination of Equilibrium Constants by Chemometric Analyisis of Spectroscopic Data, *Analytical Chemistry*, 65:994-996

41. Bahrpeyma S., Hemmateenejad B. and Javidnia K. (2016) Photo-degradation study of dacarbazine by spectrophotometric-chemometrics and HPLC methods, *Journal of the Iranian Chemical Society*, 13(2):221-229

42. Amis E.S. and Hinton J.F. (1973) Solvent Effect on Chemical Phenomena, New York: Academic Press

43. Laidler K.J. (1987) Chemical Kinetics, Third Ed., New York: Harper & Row

44. Amis E. S. (1966) Solvent Effects on Reaction Rates and Mechanisms, New York: Academic Press.

45. Kosower E. M. (1968) An Introduction to Physical Organic Chemistry, New York: Wiley.

46. Entelis S.G. and Tiger R.P. (1976) Reaction Kinetics in the Liquid Phase, New York: Wiley.

47. Reichardt C. (1988) Solvents and Solvent Effects in Organic Chemistry, second ed., New York: VHC Publishers.

48. Connors K. A. (1990) Chemical Kinetics: the Study of Reaction Rates in Solution; New York: VHC Publishers.

49. Pross A. (1995) Theorectical and Physical Principles of Organic Reactivity, New York: Wiley

50. Buncel E., Stairs R.A. and Wilson H. (2003) The Role of the Solvent in Chemical Reactions, New York: Oxford University Press.

51. Ahmad I., Fasihullah Q., Noor A., Ansari I.A. and Ali Q.N. (2004) Photolysis of riboflavin in aqueous solution: a kinetic study, *International Journal of Pharmaceutics*, 28: 199–208

52. Ahmad I., Bano R, Musharraf S.G., Sheraz M.A., Ahmed S., Tahir H., ul Arfeen Q., Bhatti M.S., Shad Z. and Hussain S.F. (2015) Photodegradation of norfloxacin in aqueous and organic solvents: A kinetic study, *Journal of Photochemistry and Photobiology A: Chemistry*, 302:1-10

53. Ahmad I., Bano R., Musharraf S.G., Ahmed S., Sheraz M.A., ul Arfeen Q., Bhatti M.S. and Shad Z. (2014) Photodegradation of moxifloxacin in aqueous and organic solvents: a kinetic study, AAPS PharmSciTech, 15(6):1588-1597

54. Ahmad I., Bano R., Sheraz M.A., Ahmed S., Mirza T. and Ansari S.A. (2013) Photodegradation of levofloxacin in aqueous and organic solvents: a kinetic study, *Acta Pharmaceutica*, 63(2):223-229

55. Boscá F., Canudas N., Marín M.L. and Miranda M.A. (2000) A Photophysical and Photochemical Study of 6-Methoxy-2-naphthylacetic Acid, the Major Metabolite of the Phototoxic Nonsteroidal Antiinflammatory Drug Nabumetone, *Photochemistry and Photobiology*, 71(2): 173 – 177

56. Connors K.A., Amidon G.L. and Stella V.J. (1986) Chemical Stability of Pharmaceuticals: A Handbook for Pharmacists, 2nd Edition, New York: Wiley & Sons

57. Tønnesen H.H. (2001) Review - Formulation and stability testing of photolabile drugs, *International Journal of Pharmaceutics*, 225(1):1–14

58. Del Valle E.M.M. (2004) Cyclodextrins and their uses: a review, *Process Biochemistry*, 39(9): 1033–1046

59. Davis M.E. and Brewster M.E., 2004, Cyclodextrin-Based Pharmaceutics: Past, Present and Future, *Nature Reviews: Drug Discovery*, 3:1024-1035

60. Loftsson, T. and Brewster M.E. 2010, Pharmaceutical Applications of Cyclodextrins: Basic Science and Product Development, *Journal of Pharmacy and Pharmacology*, 62:1607-1621

61. Arima H., Miyaji T., Irie T., Hirayama F. and Uekama K. (1998) Enhancing effect of hydroxypropyl-β-cyclodextrin on cutaneous penetration and activation of ethyl 4-biphenylyl acetate in hairless mouse skin, *European Journal of Pharmaceutical Sciences*, 6:53-59

62. Cappello B., De Rosa G., Giannini L., La Rotonda M.I., Mensitieri G., Miro A., Quaglia F. and Russo R. (2006) Cyclodextrin-containing poly(ethyleneoxide) tablets for the delivery of poorly soluble drugs - Potential as buccal delivery system, *International Journal of Pharmaceutics*, 319:63-70.

63. Jansook P., Stefánsson E., Thorstiendóttir M., Sigurdsson B.B., Krisjánsdóttir S., Bas J.S., Sigurdsson H.H. and Loftsson T. (2010) Cyclodextrin solubilization of carbonic anhydrase inhibitor drugs- Formulation of dorzolamide eye drop microparticle suspension, European *Journal of Pharmaceutics and Biopharmaceutics*, 76:208-214.

64. Loftsson T. and Stefánsson E. (1997) Effect of cyclodextrins on topical drug delivery to The Eye, *Drug Development Industry of Pharmaceuticals*, 23:473-481.

65. [The Molecular structure of β-cyclodextrin, cross-section of a cyclodextrin molecule showing the arrangement of a glucose unit and conical representation showing hydrophilic exterior and hydrophobic cavity] n.d. [Online Image] Available from http://www.chemiedidaktik.uni-wuppertal.de/disido_cy/cyen/info/03_physical_cy.htm [Accessed 21/07/2012]

66. Fenyvesi E. (1988) Cyclodextrin Polymers in the Pharmaceutical Industry*, Journal of Inclusion Phenomena*, 6:537-545

67. Loftsson T. and Brewster M.E. (2010) Pharmaceutical Applications of Cyclodextrins: Basic Science and Product Development, Journal of Pharmacy and Pharmacology, 62:1607–1621.

68. Wang Q., Li S., Che X., Fan X. and Li C. (2010) Dissolution improvement and stabilization of ibuprofen by co-grinding in a β-cyclodextrin ground complex, *Asian Journal of Pharmceutical Sciences*, 5(5):185-190.

69. Chen C.Y., Chen F.A., Wu A.B., Hsu H.C., Kang J.J. and Cheng H.W. (1996) Effect of hydropropyl-β-cyclodextrin on the solubility, photostability and in-vitro permeability of alkannin shikonin enantiomers, *International Journal of Pharmaceutics*, 141:171-178.

70. Pomponio R., Gotti R., Fiori J., Cavrini V., Mura P., Cirri M. and Maestrelli F. (2004) Photostability studies on nicardipine–cyclodextrin complexes by capillary electrophoresis, *Journal of Pharmaceutical and Biomedical Analysis*, 35:267-275.

71. Peng M., Liu Y., Zhang H., Cui Y., Zhai G. and Chen C. (2010) Photostability Study of Doxorubicin Aqueous Solution Enhanced by Inclusion Interaction between Doxorubicin and Hydroxypropyl-β-cyclodextrin, *Chinese Journal of Chemistry*, 28:1291-1295.

72. Lebete M.L. (2001) The influence of a methylated-β-Cyclodextrin on the solubility and photostability of midazolam in aqueous solution, MSc Thesis, Rhodes University

73. Piel G., Pochet L., Delattre L. and Delarge J. (1996) Study of the influence of g-cyclodextrin on the molsidomine photostability In: Szejtli J. and Szente L., ed. (2012) *Proceedings of the Eighth International Symposium on Cyclodextrins*, Netherlands: Springer Science & Business Media

74. Jiménez M.C., Miranda M.A. and Tormos R. (1997) Photochemistry of naproxen in the presence of β-cyclodextrin, *Journal of Photochemistry and Photobiology A: Chemistry*, 104:119-121.

75. Sortino S., Giuffrida S., De Guldi G., Chillemi R., Petralia S., Marconi G., Condorelli G. and Sciuto S. (2001) The photochemistry of flutamide and its inclusion complex with beta-

cyclodextrin. Dramatic effect of the microenvironment on the nature and on the efficiency of the photodegradation pathways, *Photochemistry and Photobiology*, 73(1):6-13

76. Irie T. and Uekama K. (1997) Pharmaceutical applications of cyclodextrins. III. Toxicological issues and safety evaluation, *Journal of Pharmaceutical Sciences*¸ 86(2):147-162
77. Qian L., Guan Y. and Xiao H. (2008) Preparation and characterisation of inlcuion complexes of a cationic-β-cyclodextrin polymer with butylparaben or triclosan, *International Journal of Pharmacy*, 357:244-251
78. Trotta F., Dianzani C., Caldera F., Mognetti B. and Cavalli R. (2014) The application of nanosponges to cancer drug delivery, *Expert Opinion*, 11(6):931-941
79. Bilensoy E. (Ed.) (2011) Cyclodextrins in Pharmaceutics, Cosmetics, and Biomedicine: Current and Future Industrial Applications, New Jersey: John Wiley & Sons Inc.
80. Liang W., Yang C., Nishijima M., Fukuhara G., Mori T., Mele A., Castiglione F., Caldera F., Trotta F. and Inoue Y. (2012) Cyclodextrin nanosponge-sensitized enantiodifferentiating photoisomerization of cyclooctene and 1,3-cyclooctadiene, Beilstein Journal of Organic Chemistry, 8:1305–1311
81. Sainz-Rozas P.R., Isasi J.R. and González-Gaitano G. (2005) Binding of dibenzofuran and its derivatives to water-soluble β-cyclodextrin polymers, *Journal of Photochemistry and Photobiology A: Chemistry*, 173(3):248–257
82. Zhang W., Gong X., Cai Y., Zhang C., Yu X., Fan J., Diao G. (2013) Investigation of water-soluble inclusion complex of hypericin with β-cyclodextrin polymer, *Carbohydrate Polymers*, 95(1):366-370
83. Liu C., Zhang W., Yang H., Sun W., Gong X., Zhao J., Sun Y. and Diao G. (2014) A Water-Soluble Inclusion Complex of Pedunculoside with the Polymer β-Cyclodextrin: A Novel Anti-Inflammation Agent with Low Toxicity, *PLoS ONE*, 9(7):e101761
84. Duchêne D. (2011) Cyclodextrins and Their Inclusion Complexes, In: Cyclodextrins in Pharmaceutics, Cosmetics, and Biomedicine: Current and Future Industrial Applications, Bilensoy E. *e.d*. USA: John Wiley & Sons, Inc.
85. Tablet C., Matei I. and Hillebrand M. (2012) The Determination of the Stoichiometry of Cyclodextrin Inclusion Complexes by Spectral Methods: Possibilities and Limitations, In: Stoichiometry and Research - The Importance of Quantity in Biomedicine, Innocenti A. *e.d*. InTech
86. Ansari, K., Vavia, P., Trotta, F. and Cavalli, R. (2011). Cyclodextrin-Based Nanosponges for Delivery of Resveratrol: In Vitro Characterisation, Stability, Cytotoxicity and Permeation Study, *AAPS PharmSciTech*, 12(1):279-286.
87. Sapino S., Carlotti M.E., Cavalli R., Ugazio E., Berlier G., Gastaldi L. and Morel S. (2013) Photochemical and antioxidant properties of gammaoryzanol in beta-cyclodextrin-based nanosponges, *Journal of Inclusion Phenomena and Macrocyclic Chemistry*, 75(1): 69-76.
88. Trotta F., Zanetti M. and Cavalli R. (2012) Cyclodextrin-based nanosponges as drug carriers, Beilstein Journal of Organic Chemistry, 8:2091-2099
89. Swaminathan S., Pastero L., Serpe L., Trotta F., Vavia P., Aquilano D., Zara G. and Cavalli R. (2010) Cyclodextrin-based nanosponges encapsulating camptothecin: physicochemical characterization, stability and cytotoxicity, *European Journal of Pharmaceutics and Biopharmaceutics*, 74(2):193-201
90. Crowley P.J. (1999) Excipients as Stabilizer, *Pharmaceutical Science & Technology Today*, 2(6):237-243

91. Rowe R.C., Sheskey P.J. and Weller P.J. (2003) Handbook of Pharmaceutical Excipients, Pharmaceutical Press and American Pharmaceutical Association

92. Albini A. and Fasani E. (1998) Drugs Photochemistry and Photostability, Cambridge: The Royal Society of Chemistry

93. Thoma K. and Klimek R. (1991) Photostabilization of drugs in dosage forms without protection from packaging materials, *International Journal of Pharmaceutics*, 67(2):169–175

94. Gierer D.S., Morgado J.E., Murphy B.J. and Simmons D.M., Pfizer Inc. (2013) Pharmaceutical compositions of n-methyl-2-[3-((e)-2-pyridin-2-yl-vinyl)-1h-indazol-6-ylsulfanyl]-benzamide, U.S., Pat. WO 2013046133 A1

95. Sousa e Silva J.P. (2013) Pharmaceutical Formulation, *Pharmaceutica Analytica Acta*, 4(1):145

96. World Health Organisation (2001) Guidelines for the formulation, implementation, monitoring and evaluation of national drug policies [Online] Available at: http://apps.who.int/medicinedocs/en/m/abstract/Js16220e/ [Acessed 30/01/2016]

CHAPTER THREE

MATERIALS AND METHODS

3.1. MATERIALS AND EQUIPMENTS

3.1.1. CHEMICAL, SOLVENTS AND DRUGS

3.1.1.1. Drugs

Dacarbazine (DBZ, ≥98%), 5-(3,3-dimethyltriazen-1-yl)imidazole-4-carboamide, was purchased from Sigma-Aldrich (Dorset, UK).

Axitinib (AXI, >99%), N-Methyl-2-((3-((1E)-2-(pyridin-2-yl)ethenyl)-1H-indazol-6-yl)sulfanyl)benzamide, was purchased from Selleck Chemicals (Suffolk, UK).

Sunitinib Malate (SUT, >99%), N-[2-(diethylamino)ethyl]-5-[(Z)-(5-fluoro-2-oxo-1H-indol-3-ylidene)methyl]-2,4-dimethyl-1H-pyrrole-3-carboxamide; (2S)-2-hydroxybutanedioic acid, was purchased from Selleck Chemicals (Suffolk, UK).

8-Anilino-1-naphthalenesulfonic acid ammonium salt (ANS, ≥90%) was purchased from Sigma-Aldrich (Dorset, UK).

3.1.1.2. Solvents

Ethanol (99.8%), methanol (99.8%), acetonitrile (99.9%) and formic acid (99.8%) were from Fisher Scientific (Loughborough, UK). Distilled water was also used as solvent.

3.1.1.3. Chemicals

Tartrazine (TRZ, ≥85%), Sunset Yellow (SSY, ≥90%), Quinoline Yellow (QY, ≥95%), β-Carotene (β-Ca, 95%), Ondansetron Hydrochloride (OHCl, ≥98%) and Vanillin (VAN, ≥98%) were purchased from Sigma-Aldrich (Dorset, UK) as powders.

Cyclodextrin monomers (α-CD, 2-Hydroxypropyl-β-CD and γ-CD) and β-cyclodextrin polymer (β-CDP) were purchased from Sigma-Aldrich (Dorset, UK) in powder form.

α-Cyclodextrin polymer (α-CDP) and γ-Cyclodextrin polymer (γ-CDP) were purchased from CycloLab (Hungry) in powder form.

All solvents and chemicals were of analytical grade or higher.

Table 3.1: Molecular weight of cyclodextrin monomers and polymers

	CYCLODEXTRIN					
	α-CD	**HP-β-CD**	**γ-CD**	**α-CDP**	**β-CDP**	**γ-CDP**
Mw (g/mol)	972.84	1460	1297.12	-[a]	15000	-

[a] not available

3.1.2. INSTRUMENTS

3.1.2.1. Spectrophotometers

For monochromatic irradiation studies, absorption spectra were recorded with an Agilent 8453 Diode Array Spectrophotometer, using the Agilent ChemStation kinetics software provided by Agilent Technologies. Measurements were done with a thermostatically controlled Peltier cuvette holder designed for a 1 cm cuvette.

For polychromatic studies, a ThermoScientific™ Helios Omega Spectrophotometer was used. It operated on remote setting for reading the absorbance, the absorbance data was collated using VISIONlite™ software. The scan speed was 600 nm/min at 0.5 nm interval.

3.1.2.2. Monochromatic Irradiation set-up

The irradiation light for monochromatic irradiation was an Ushio 1000 W xenon arc-lamp housed within a shell (model A6000) and was powered by a power supply (model LPS-1200). The whole equipment was manufactured by Photon Technology International Corporation.

The lamp was connected to a monochromator (model 101), a f/2.5 monochromator with a 1200 groove/300 nm blaze grating, which enables selection of the irradiation wavelength.

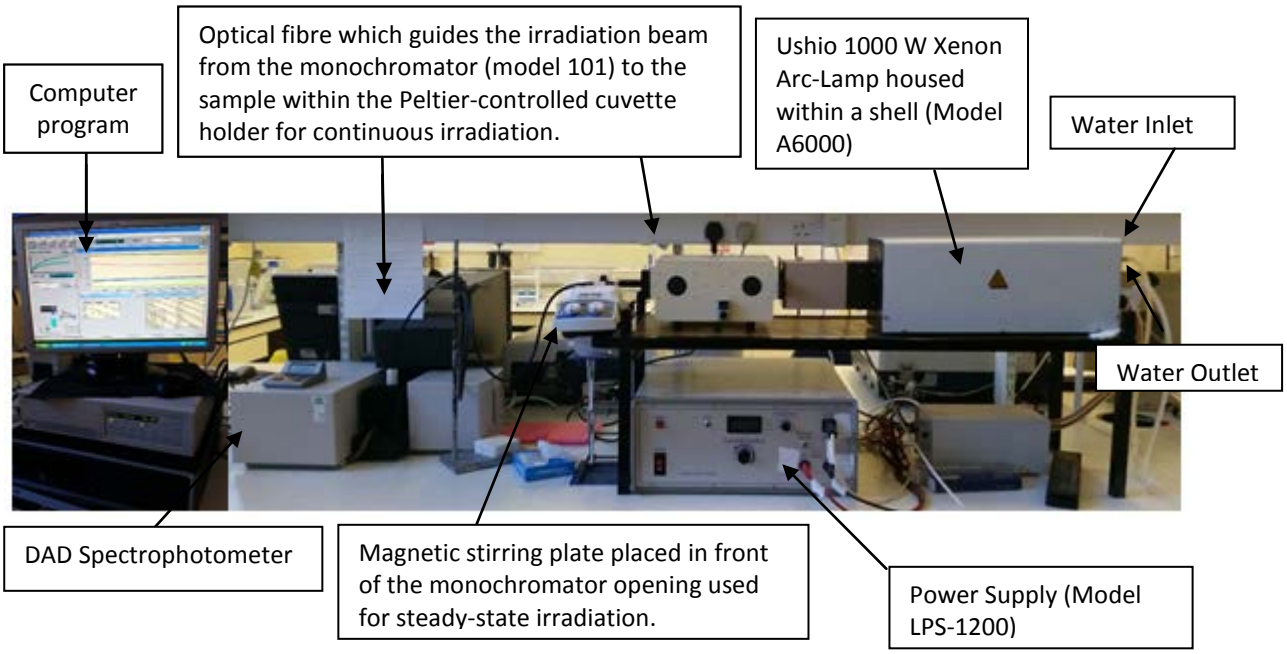

Fig 3.1: Monochromatic photolysis set-up for continuous and steady-state irradiations

3.1.2.3. Radiant Power Meter

The radiant power was measured using a Radiant Power/Energy meter (Oriel Model 70260).

Light intensity is expressed as milliwatts per centimetre square (mW/cm^2) by the radiant power meter.

3.1.2.4. Fluorescence Spectrometer

Fluorescence spectra were measured using a PerkinElmer LS 55 Fluorometer controlled via the FL Win Lab program as provided by PerkinElmer (USA).

Light from an excitation source passes through a filter or monochromator and hits the sample. A proportion of the excitation light is absorbed by the sample, and molecules in the sample fluoresce. The fluorescent light is emitted in all directions. Some of this fluorescent light passes through a second filter or monochromator and reaches a detector, which is usually placed at 90° to the incident light beam to avoid the risk of interference of the transmitted or reflected excitation light reaching the detector.

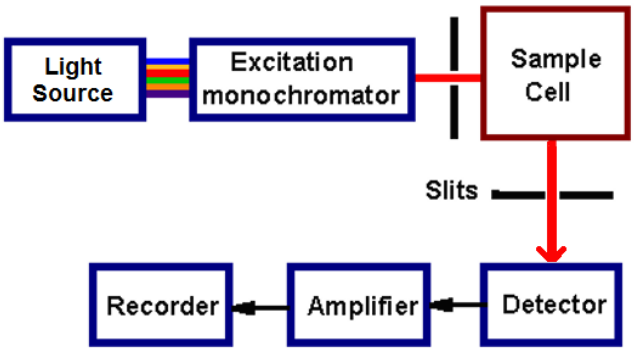

Fig 3.2: Illustration of the key components of a fluorometer.

3.1.2.5. High Performance Liquid Chromatography

Separation was achieved on a Gemini C_{18} reverse phase column 5 µm, 2.1 x 50 mm (Phenomenex, UK) fitted to a PerkinElmer Series 200 Pump and UV/Vis Detector, and a 600 Series Link interface; all of which were controlled remotely using TotalChrom software (PerkinElmer, USA).

3.1.2.6. Rotary Evaporator

Evaporation of solvents for Drug/CDP formulation were achieved on the Büchi Rotavapor R-210 (Büchi, Switzerland) fitted with a Büchi Rotavapor R-114 Vacuum. The rotary evaporation setup consists of a motor unit, which is attached to the evaporation flask containing the sample to be dried.

3.1.2.7. ATR-FTIR Spectroscopy

Infrared spectra were recorded with Bruker's ALPHA Attenuated Total Reflection (ATR) Fourier Transform Infrared (FTIR) Spectrometer using the OPUS software.

3.1.2.8. Scanning Electron Microscope

An Evo 15 Scanning Electron Microscope (SEM, Zeiss, Cambridge) analysis was used for visualising the surface texture of the samples. The instrument was controlled through the program SmartSEM V05.07 provided by Zeiss.

3.2. METHODS

3.2.1. Preparation of Solutions

Stock solutions of each compound were prepared by weighing accurately an amount of powder in a volumetric flask using an analytical balance. The powder was then dissolved using either ethanol or distilled water. This was immediately wrapped in aluminium foil to prevent light exposure and placed in an ultrasonic bath (FB11024, Fisherbrand, UK) to ensure complete dissolution. Stock solutions were kept refrigerated at T<5°C.

The concentration of the solutions was calculated using the following:

$$Concentration\ (M) = \frac{mass\ of\ solute\ (g)}{RMM\left(\frac{g}{mol}\right) \times Final\ Volume\ (L)} \qquad \textbf{Eq. 1}$$

Dilutions of the solutions were prepared by transferring a specific volume of the stock solution into another volumetric flask using a Gilson® pipette. The diluted solutions were stored and protected from light in the same conditions as above until used.

3.2.2. Calibration Graph

For spectrophotomeric calibrations, the blank experiment consisted of 2 mL of the solvent. Then specific volumes (µL) of the stock solution was added to 2 mL of solvent using a 50 µL microsyringe (Phenomenex, UK). The spectrum of the diluted solutions were measured and recorded. The calibration graph were built by plotting absorbance readings at a specific wavelength of observation against increasing concentrations.

For calibration on HPLC, increasing concentrations of the drug was injected. The chromatogram of this solution was measured and the peak area recorded. Calibration graph of the analyte was obtained by plotting peak area (PA) against increasing concentrations.

The blank experiment for fluorimeter was 2 mL of water. Specific volumes (µL) of AXI was spiked into the 2 mL solvent and the excitation and emission spectra of each solution was measured and recorded. Calibration graph of the analyte was obtained by plotting relative fluorescence intensity at a specific wavelength of observation ($Fl_{\lambda_{obs}}$) against increasing concentrations.

For each, a line of best fit was drawn, correlation co-efficient (r^2) calculated and the linear range determined (Table 3.2).

Table 3.2: The linear range of DBZ, AXI and SUT in ethanol and water, the equation of the line and correlation co-efficient (r^2)

Drug	Solution	Linearity Range /M	Equation of the line	correlation co-efficient /r^2
Spectrophotometer				
Dacarbazine	Ethanol	x 10^{-6} – x 10^{-5}	A_{330} =	
	Water	5.37 x 10^{-6} – 9.27 x 10^{-5}	A_{330} = 19749 x C_0 + 0.0062	0.9988
Axitinib	Ethanol	1.03 x 10^{-6} – 6.32 x 10^{-5}	A_{332} = 35712 x C_0 – 0.0008	0.9995
	Water	1.03 x 10^{-6} – 3.98 x 10^{-5}	A_{330} = 29995 x C_0 + 0.0007	0.9991
Sunitinib	Ethanol	4.68 x 10^{-7} – 6.26 x 10^{-5}	A_{430} = 26279 x C_0 + 0.0064	0.9999
	Water	2.34 x 10^{-6} – 7.22 x 10^{-5}	A_{430} = 24948 x C_0 + 0.0136	0.9986
HPLC				
Dacarbazine	Ethanol	4.82 x 10^{-5} – 5.49 x 10^{-4}	PA = 1x10^{10} x C_0 - 497703	0.995
Axitinib	Ethanol	2.76 x 10^{-6} – 2.33 x 10^{-5}	PA = 1x10^{11} x C_0 + 15215	0.9971
Sunitinib	Ethanol	4.99 x 10^{-6} – 2.15 x 10^{-4}	PA = 5x10^{9} x C_0 + 15376	0.9973
Fluorimeter (λ_{ex} = 332 nm ; λ_{em} = 418 nm)				
Axitinib	Water	2.58 x 10^{-6} – 3.62 x 10^{-6}	Fl_{419} = 2x10^{6} x C_0 + 0.0793	0.9895

3.2.3. Monochromatic Photolysis Procedure

3.2.3.1. Continuous Irradiation

The monochromator was set to a specific wavelength for irradiation (λ_{irr}) and the excitation beam was guided through an optical fibre impinging upon the top of the sample cuvette. Accordingly, the direction of the irradiation and analysis light were perpendicular (Fig. 3.1).

2 mL of solvent was placed in the 1 cm quartz cuvette and a blank (zero concentration) is taken on the spectrophotometer. Pure ethanol was used for studies in organic solvent and distilled water was used for studies in aqueous media. For studies in ethanol/water solutions, specific

volumes (µL) of ethanol were spiked into 2 mL of water as the blank for these studies – the percentage of ethanol not exceeding 2.5% v/v. Studies in the presence of CDs, TRZ, SSY, QY, β-Ca, OHCl and VAN, 2 mL solutions containing the excipient (no drug) were the blank; so that only the drug's absorbance is observed.

The intensity of light at the end of the optical fibre was measured by placing the end of the optical fibre perpendicularly onto the radiometer probe. The reading was recorded before and after each photolysis.

Specific volumes (µL) of the drug solution - taken with a 50 µL Hamilton Microsyringe - were added to 2 mL of solvent.

UV-Visible spectra were recorded set intervals throughout the set time of photolysis, using the Agilent 8453 ChemStation kinetics computer program.

The sample was stirred continuously with a magnetic flea during all experiments to ensure homogenisation of solution and maximum exposure, a temperature of 22°c was maintained (unless stated otherwise) and the sample was shielded from ambient light.

Due to limit of the temperature controller and the sensitivity of SUT to temperature in water, an ice bath was employed for photolysis. The sample was placed in a small beaker containing ice and placed on top of a Fisher Scientific™ magnetic stirrer (FB65312). The solution shielded from ambient light by a covering with a much larger beaker that has been completely wrapped in foil.

SUT sample was removed from the ice bath and placed into the UV spectrometer (with thermostat set at the lowest possible, 6°C) at 5 minutes intervals and irradiated monochromatically using the optical fibre for 1 minute. This was repeated until a plateau was achieved – i.e. the end of the reaction was reached.

3.2.3.2. Steady-State Photolysis Procedure

General analysis was carried out as described above. However, instead of irradiating using the optical fibre, the sample was placed directly in front of the monochromator opening, clamped into place by a lab stand (Fig. 3.1).

The intensity of light behind and in front of the cell were measured and recorded before and after each photolysis. Thus, the amount of light absorbed by the sample is known.

A magnetic stirring plate was placed under the sample cell to ensure the sample was stirred continuously with a magnetic flea.

At regular intervals the sample would be removed from the clamp and its absorption spectrum measured using the spectrophotometer until the end of the reaction.

3.2.4. Polychromatic Ambient Photolysis Procedure

The blank experiment was carried out as described above.

During preparation of the analytical sample, the cuvette was covered in aluminium foil to avoid light exposure. The sample was stirred to ensure homogeneity and then the initial absorbance spectrum was taken. The cuvette was then placed on a magnetic stirrer on a laboratory worktop without any light protection (foil removed), positioned to allow adequate ambient light exposure. A plastic lid was placed on top of the cuvette to prevent evaporation of the sample.

The sample was stirred continuously with a magnetic flea, on a magnet stirrer, during all experiments to ensure homogenisation of solution and maximum exposure, ambient room temperature in the range 20°C-25°C were recorded.

Absorbance spectra were recorded at regular intervals until the end of the photoreaction, which was indicated by no/little change in absorbance.

For HPLC analysis, injections were made at regular intervals until the end of the reaction. The peak areas plotted against time.

3.2.5. Stability Of The Drugs In The Absence Of Light

Instrumental set-up and sample preparation were carried out as above, except the contents of the cuvette were protected by a cap which completely covered the top of the cuvette. The analytical sample was continuously stirred and thermalstatically maintained at a set temperature.

Under ambient conditions, the cuvette was covered with aluminium foil. This was only removed when the sample was analysed at intervals. The sample was continuously stirred on a stirring plate.

UV-Visible spectra were recorded using a computer program as described above.

3.2.6. Chromatographic Conditions

Separation of the drugs and their products were achieved with mobile phase of water and acetonitrile or methanol (Table 3.3). An injection loop of 20 µl was used and the detector was set at specific wavelengths.

Table 3.3: Chromatographic conditions for the separation of the drugs and their photoproducts.

Drug	Mobile Phase		A %	B %	Flow Rate ml/min	Detector Wavelength / nm	Overall Run Time / min
	A	B					
DBZ	water (adjusted to pH 3 with glacial acetic acid)	acetonitrile	70	30	0.5	236	10
AXI	water (0.1 % v/v formic acid)	methanol	40	60	2.0	332	4
SUT	water (adjusted to pH 3 with glacial acetic acid)	acetonitrile	67	33	1.0	350	6

3.2.7. Kinetic Data Treatment Using MathCad

Differential equations obtained based on the proposed photodegradation mechanism are entered into the computer program (MathCad 2000) which uses the numerical method of Runge-Kutta 5th order (RK-5) to generate values of the integral at specific times. Therefore, the values obtained describe the behaviour of the reaction through variation of concentration of all reaction species over time.

These values were converted into absorbance and fitted with experimental data in excel. The input data corresponding to unknown reaction parameters are optimised until a unique fit between theoretical RK-5 traces and experimental data is achieved.

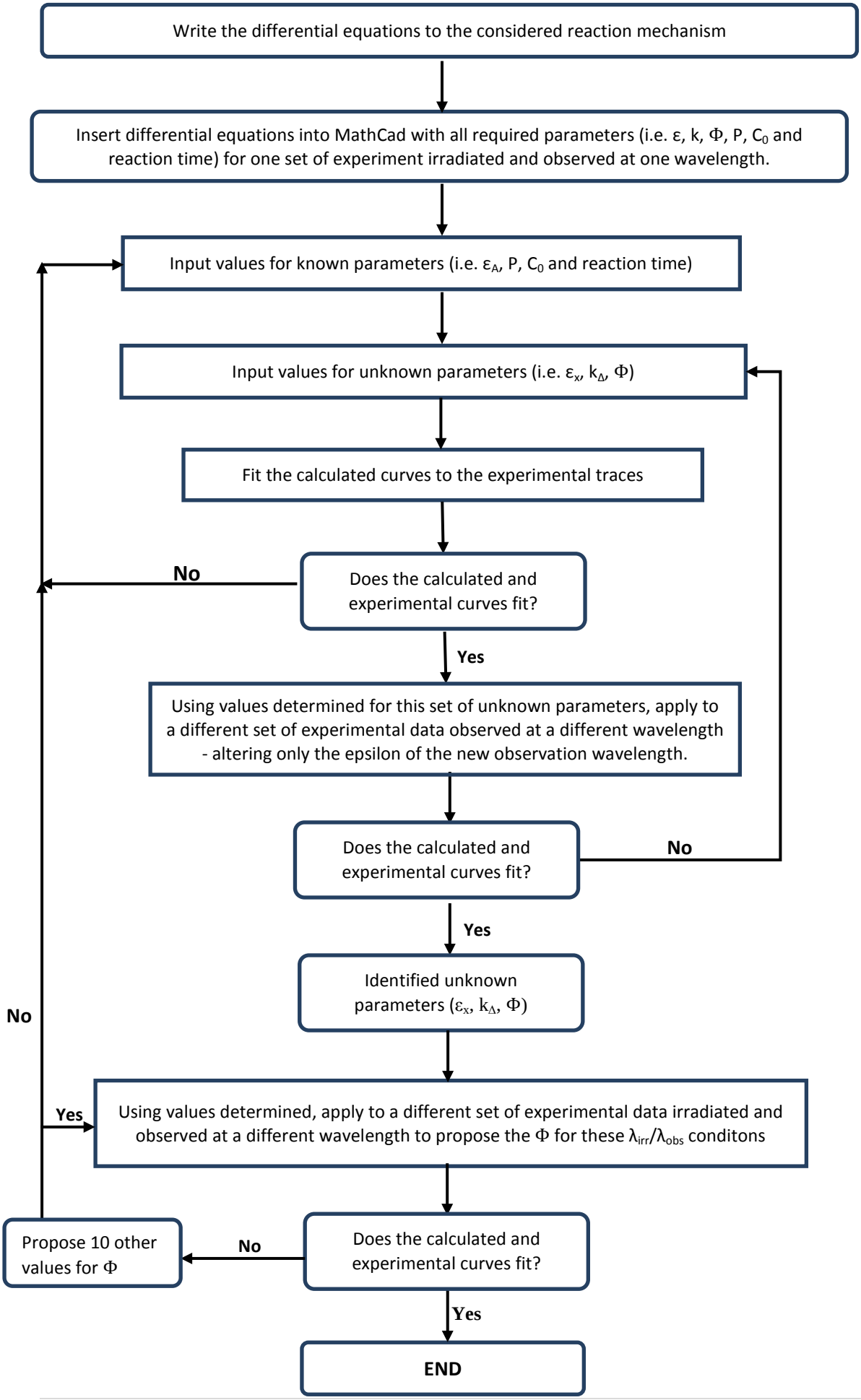
Write the differential equations to the considered reaction mechanism
Insert differential equations into MathCad with all required parameters (i.e. ε, k, Φ, P, C_0 and reaction time) for one set of experiment irradiated and observed at one wavelength.
Input values for known parameters (i.e. ε_A, P, C_0 and reaction time)
Input values for unknown parameters (i.e. ε_x, k_Δ, Φ)
Fit the calculated curves to the experimental traces
Does the calculated and experimental curves fit?
No
Yes
Using values determined for this set of unknown parameters, apply to a different set of experimental data observed at a different wavelength - altering only the epsilon of the new observation wavelength.
Does the calculated and experimental curves fit?
No
Yes
Identified unknown parameters (ε_x, k_Δ, Φ)
No
Yes
Using values determined, apply to a different set of experimental data irradiated and observed at a different wavelength to propose the Φ for these $\lambda_{irr}/\lambda_{obs}$ conditons
Propose 10 other values for Φ
No
Does the calculated and experimental curves fit?
Yes
END

3.2.8. Fluorescence Analysis

Solution of α-CD, HP-β-CD, α-CDP, β-CDP and γ-CDP were made in various concentrations.

The fluorescence spectrum of a cuvette containing 2 mL of water (no sample) was measured. This is then spiked with a known volume of sample stock solution and its excitation and emission spectra was determined.

The cuvette is then washed and replaced with 2 mL of CD at increasing concentrations (0 - 25 mg/mL). For each CD concentration, the initial excitation and emission spectra of the CD were measured before adding the analytical sample and the spectra recorded again.

The fluorescence emission intensities for each were then plotted against CD concentrations in excel to give one isotherm. This is then repeated for different AXI concentrations and then different CDs.

3.2.9. Formulation of AXI/CDP Complex

Ensuring that all solutions are protected from light at all-time using foil, 5 mg of AXI was dissolved in 0.5 mL ethanol in a small vial. In a 25 mL round-bottomed flask, 50 mg α-CDP or 200 mg β-CDP were dissolved in 1 mL. The AXI solution was then added to the flask containing the CDP solution.

If the solution becomes cloudy, either β-CDP or AXI had precipitated back into solution; one of the two solvents was not of sufficient quantity. Cautious additions of both solvents brought both solutes back into solution – i.e. a clear solution has achieved.

The complex solution was then evaporated, ensuring that exposure to light and heat is limited at all-time by covering with foil and storing and evaporating at low temperature.

Once the AXI/CDP complex had dried, 1 mL of double distilled water was added, ensuring complete dissolution by using an ultrasonic bath. If complete complexation (a clear solution) was not achieved, then 20 mg of CDP was added into the solution, dissolved with water and ethanol and evaporated. This was again tested with 1 mL of water. The process was repeated until a clear solution was achieved when 1 mL of double distilled water was added to the dried AXI/CDP complex.

3.2.10. Solubility limit Testing of Formulations

Double distilled water in aliquots of 0.1 mL were added to the dried AXI/CDP complex until a clear solution was achieved. An ultrasonic bath was used in-between each addition for water to ensure complete dissolution.

As AXI is not water soluble, a clear solution would be a strong indication that a water soluble complex was achieved. However, if the solution was cloudy and ethanol is required to achieve a clear solution, then a water soluble complex was not formed and more cyclodextrin was needed to be added.

Small aliquots were used to determine the minimum volume of water required to completely solubilize the formulation.

3.2.11. Photostability Testing of Formulations

Instrumental set-up were as described in 3.2.3.

The blank experiment for this was carried out with a specific amount of CDP (Table 3.4) dissolved in 2 mL water.

Specific amount of the AXI/CDP formulation was then dissolved in a certain amount of double distilled water (Table 3.4) (Cell 1). AXI/α-CDP samples were dissolved in 0.8 mL and AXI/β-CDP

samples were dissolved in 1 mL of water. An initial absorption spectrum of the sample was taken, by spiking 40 µL of sample from Cell 1 into 2 mL of water (cell 2) to get a measurable concentration.

Table 3.4: Amount of sample required for analysis

Sample	CDP (mg)	AXI (mg)	Total Mass (mg)	Volume of Sample (mL)	Volume of Water (mL)	Concentration (mg/mL)	AXI Concentration (mg/mL)
	AXI/α-CDP Formulation						
Dry sample	300	5	305	-	-	-	-
Cell 1	24	0.4	24.4	-	0.8	30.5	0.2
Cell 2	0.96	0.016	0.976	0.04	2	0.488	0.008
	AXI/β-CDP Formulation						
Dry Sample	770	5	775	-	-	-	-
Cell 1	59.6	0.4	60	-	1	77.5	0.2
Cell 2	0.92	0.0154	0.9354	0.04	2	0.4677	0.0077

Specific amount of the AXI/CDP formulation was then dissolved in a certain amount of double distilled water (Table 3.3) (Cell 1). AXI/α-CDP samples were dissolved in 0.8 mL and AXI/β-CDP samples were dissolved in 1 mL of water. An initial absorption spectrum of the sample was taken, by spiking 40 µL of sample from Cell 1 into 2 mL of water (cell 2) to get a measurable concentration.

Cell 1 was then placed into the spectrophotometer's sample holder with a magnetic flea and irradiated monochromatically at 360 nm using the optical fibre, whilst stirred and thermostatically maintained at 22°C.

At timed intervals sample analysis was carried out by stopping the irradiation of Cell 1, removed the cell from the sample holder of the spectrophotometer and placed on the bench shielded from light with a large beaker covered in aluminium foil. Than 40 µL of Cell 1 was

spike into 2 mL of water (cell 2) for analysis. This continued until a plateau was reached – i.e. the reaction has stopped.

Changes in absorbance at two specific wavelengths (330 nm and 380 nm) were recorded and plotted against time.

Ambient photostability tests were carried out in the same way, except the sample was exposed to polychromatic ambient fluorescent light and temperature. Experiments where the sample was stirred and not stirred were also carried out under ambient conditions.

3.2.12. Thermal Stability Testing Of Formulations

Instrumental set-up and sample preparation were carried out as above (Section 3.2.11), except the sample was not irradiated. The analytical sample was continuously stirred and thermalstatically maintained at a set temperature.

UV-Visible spectra were recorded using a computer program as described above.

3.2.13. Samples for FTIR and SEM Characterisation

Analysis were carried out directly on the powder samples of AXI, αCD-P, AXI/αCD-P formulation, AXI/αCD-P physical mixture, β-CDP, AXI/ β-CDP formulation and AXI/β-CDP physical mixture were used. Physical mixtures were prepared by mixing AXI and α-CDP or β-CDP in the ratio as found for the formulations.

CHAPTER FOUR

DRUG LITERATURE SURVEY

4.1. INTRODUCTION

Cancer is one of the most serious health problems in the Western Hemisphere [1]. Overall, the last 65 years have seen a significant progress in the discovery and development of anti-cancer drugs. Even though the treatments devised for some forms of cancer have a high success rate, patients often tolerate unpleasant side effects. In the last decade, however, there has there been more success in developing targeted drugs and therapies [1].

Amongst the large variety of cancer treatments, some involve the use of photodynamic therapy (PDT) and photochemical internalisation (PCI) to activate light-sensitive drugs and to facilitate intracellular delivery [2].

Despites these advances, the delivery of anti-cancer drugs is still a challenging problem [3]. Recent advances in nanotechnology have opened new venues for anti-cancer nanomedicine and stable delivery systems [4].

Overall, there are very few published studies on the photostability of anti-cancer drugs both in formulation and in solution [5], despite this kind of information is a requirement by the ICH recommendations [6].

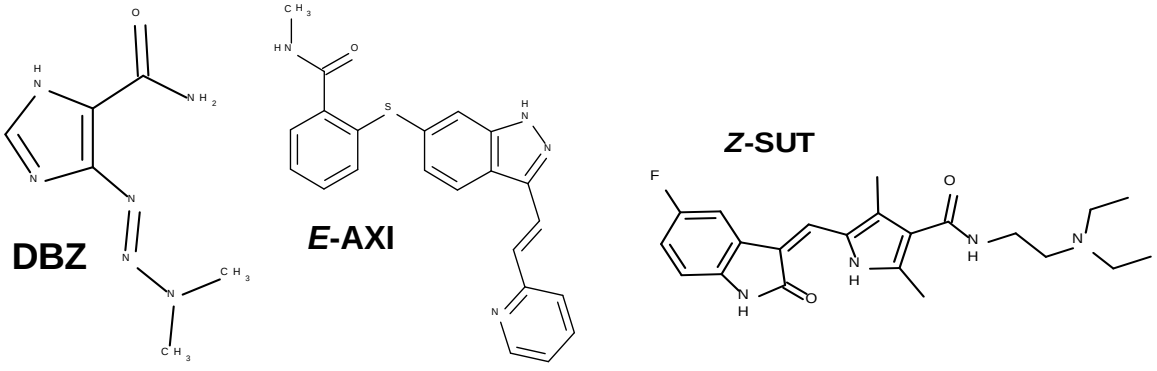

Scheme 4.1: Molecular structures of Dacarbazine, Axitinib and Sunitinb

In this study, photostability aspects of three different drugs: Dacarazbine (DBZ), Axitinib (AXI) and Sunitinib (SUT) (Fig. 4.1 and Table 4.1), will be investigated as examples of recent and old anti-cancer medication.

DBZ was proposed in the late 1970's as the most effective single agent in the treatment of metastatic malignant melanoma and Hodgkin's disease [7] and is sometimes used in combination with other drugs for soft tissue sarcomas [8]. Dacarbazine is supplied as a sterile, lyophilized powder for injection, which is reconstituted with water before use [9]. Due to its hydrophilicity, DBZ is incompletely absorbed when dispensed orally [10].

However, its usefulness is limited by adverse side effects such local venous pain, nausea, haematotoxicity and influenza-like syndrome and more importantly its sensitivity to light [11]. The majority of the side effects, in particular local venous pains, were found to be caused by its photodegradation products and not dacarbazine itself [9,12-19].

Table 4.1: Manufacturer and brand names of dacarbazine, axitinib and suntinib and the year they were approved by three major agencies

Drug (Commercial Name)	**Manufacturer**	**Year Approved for Use**		
		U.S. Food and Drug Administration	**European Medicines Agency**	**National Institute for Health and Care Excellence**
Dacarbazine (DTIC-Dome)	Bayer	1975	2002	2001
Axitinib (Inlyta)	Pfizer	2012	2012	2015
Sunitinib (Sutent)	Pfizer	2006	2006	2009

AXI and SUT are oral multi-targeted tyrosine kinase inhibitors part of a new emerging cancer targeted therapies [20]. SUT is the first-line treatment of advanced and/or metastatic renal cell carcinoma as appraised by NICE in 2009 [21]. In the case where the treatment with SUT is unsuccessful, AXI is given [22]. Some results suggested that *Z*-SUT might be active against

breast cancer and its efficacy and toxicity do not appear to be affected by patient age, including children and elderly [23]. AXI is currently on clinical trial for treatment of thyroid cancer [24].

Suntinib and Axtinib are commercially available only as a capsule and red tablet (respectively). No liquid formulations of the drugs were available for clinical use. However, pharmacist and nurses frequently encounter patients with nasogastric tube or those unable to swallow oral medications for other reasons [25]. Even though it is advised against, current practice is to crush the tablet and administering it as a suspension [25].

During early clinical development, the powder-in-bottle (PIB) approach was tested. It consists of using apple juice to constitute SUT extemporaneously in the clinic as a solution or a suspension [26]. However, after exposure to ambient light and room temperature, degradation was observed but not quantified.

There have been some attempts to address the issue of liquid formulations through the use of commercially available vehicle Ora-Plus® and Ora-Sweet® [27]. Suspensions were prepared in amber plastic bottles, three were stored at room temperatures and three were refrigerated. All suspensions were found to be chemically and physically stable over the experimental period of 60 days.

However, SUT is still limited to oral administration and the needs of patients requiring alternative routes of administration (such as parenteral or nasogastric intubation) is not met. Yet, crushing/disintegrating tablets in water to prepare AXI suspensions can hugely impact on the drug's stability, especially when exposed to light, and the safety of pharmacists and nurses who would require protection from inadvertent exposure.

4.2. THERMAL STABILITY

DBZ was reported to be stable for in many conditions as when stored in the dark in aqueous solutions (prepared from DBZ's commercial formulation which also contains a pH 3.5 citrate buffer and 37.5 mg of mannitol, at least 24 hours at room temperature and at least 96 hours at 2-6°C) [28], following cycles of freeze-thawing in human plasma and urine [29,30] or when prepared in 50 % (v/v) methanol/water, even when subjected to dry heat degradation at 105°C for 60 min, only 4.05 % degradation was observed.

Many authors [31-34] reported AXI and SUT to be thermally stable at room temperature either after 24 hours of storage in human plasma or when stored in a solution of acetonitrile/water/formic acid (20:80:0.1, v/v/v), sweat, human plasma and methanol. However, AXI has been reported to give an oxidative thermal degradant in solid tablet form [35].

4.3. PHOTOSTABILITY

Photodecomposition of DBZ in aqueous solutions by both natural and fluorescence light has been confirmed and proven by a number of studies. Most of which reported 10% loss after 24 hours of exposure to fluorescent light at room temperature and a higher loss if exposed to direct sunlight [12,19,36-44]. When photodecomposition was forced (i.e. exposing the drug to intensive light), 0.1 mg/mL DBZ rapidly deteriorated, the reaction completing in just 1 hour [12, 42, 43].

Exposure of AXI and SUT (Fig. 4.1) to light has been reported to induce photoisomerization of the compounds, *E*- to *Z*- [31,34,45-47] and *Z*- to *E*- [26,32,33,48-51], respectively. One study has reported a dimer in addition to the Z-AXI isomer [35], Fig 4.2.

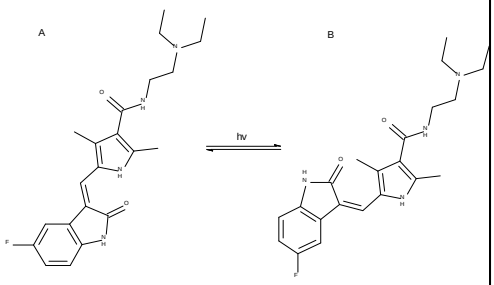

Fig 4.1: Reversible photoisomerisation of Z-SUT and E-SUT

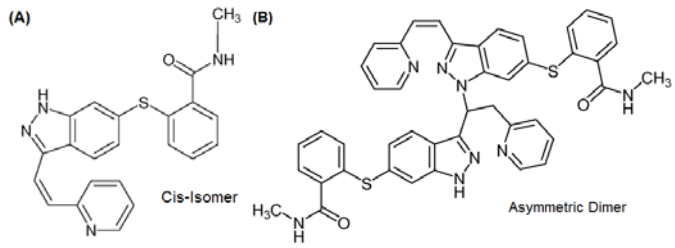

Fig 4.2: Axitinib's photoproducts identified by Pfizer in solid dosage form: (A) cis-isomer, (B) asymmetric dimer

To the best of our knowledge, there are no published kinetic studies on the photodegradation of *E*-AXI and *Z*-SUT [5,52,53]. Despite the fact that skin reactions are recognised side effects of sunitinib therapy with an adverse impact on quality of life. Its presence in patients' skin and sweat was evidenced [54], and its effects in skin photoirritation and phototoxicity have also been reported [55].

Noticeably, despite a large number of studies reported, so far, on the photodegradation and photostabilization of DBZ, only a few included kinetic studies. Nevertheless, the photodegradation reaction order of DBZ is still controversial as it was reported to obey both pseudo-first-order [39] and zero-order [42] kinetics in solution.

For the three drugs, the quantum yields of the photoreaction steps have not yet been reported in the literature.

4.4. PHOTOSTABILIZATION

Protection methods of using opaque [11,12,14] and light filtering [13] infusion sets showed to be effective in protecting DBZ from photodegradation. Yet, this does not protect the drug from degradation during preparation.

Thus far, only one study [42] attempted to photoprotect DBZ solutions with the use of excipients, glutathione (GSH). GSH is a natural antioxidant produced in the human liver. Unfortunately, it inhibits DBZ-induced cell apoptosis [56]. Therefore, although GSH has been shown to increase DBZ's photostability [42], it is not commercially used. Therefore, there is still a need for studies in that area.

During formulation development of AXI, the conventional hypromellose white coating system was found to provide the drug with no protection against light [34]. This was then adjusted to include red iron oxide and was found to give better protection against light [34,45]. There are no other examples to protect AXI from light, especially in solution.

In the case of SUT, there are no reports on any attempts to photostabilize it in any form.

4.5. CONCLUSION

Cancer is one of the most serious health problems that generally require heavy medical treatments. It is important to ensure that no additional burden is put on patients by administration modes and/or low quality of drugs. In this respect, understanding, quantifying and improving photostability of drugs is one important element that may enhance the quality of life of the patients. At least, such information can provide precautions for handling, packaging and administering drugs. It also fulfils one of the ICH Q1b recommendations for these drugs.

As discussed in the previous and this chapter, there are many aspects of drugs' photodegradation that are lacking in the specialized literature. This study will be looking at some of them through the use of new photokinetic approaches using the three anti-cancer drugs DBZ, AXI and SUT, as template examples.

4.6. REFERENCES

1. Thurston D.E. (2006) Chemistry and Pharmacology of Anticancer Drugs, CRC Press
2. Norum O.J., Selbo P.K., Weyergang A., Giercksky K.E. and Berg K. (2009) Photochemical internalization (PCI) in cancer therapy: from bench towards bedside medicine, *Journal of Photochemistry and Photobiology B: Biology*, 96(2):83-92
3. Trotta F., Dianzani C., Caldera F., Mognetti B. and Cavalli R. (2014) The application of nanosponges to cancer drug delivery, *Expert Opinion*, 11(6):931-941
4. Jain V., Jain S. and Mahajan S.C. (2015) Nanomedicines based drug delivery systems for anti-cancer targeting and treatment, Current Drug Delivery, 12(2):177-91.
5. Piechocki J.T. and Thoma K. ed. (2010) Pharmaceutical photostability and stabilization technology, New York: Informa Healthcare
6. ICH Q1B. (1996) Photostability testing of new drug substances and products. Federal Register 62(95):27115–27122.
7. Bonifazi E., Angelini G. and Meneghini C.L. (1981) Adverse Photo Reaction to Dacarbazine (DTIC) *Contact Dermatitis*, 7(3):161
8. Nussbaumer S., Bonnabry P., Veuthey J. and Fleury-Souverain S. (2011) Analysis of anticancer drugs: A review, *Talanta*, 85:2265-2289.
9. Asahi M., Matsushita R., Kawahara M., Ishida T., Emoto C., Suzuki N., Kataoka O., Mukai C., Hanaoka M., Ishizaki J., Yokogawa K. and Miyamoto K. (2002) Causative agent of vascular pain among photodegradation products of dacarbazine, *Journal of Pharmacy and Pharmacololgy*, 54(8):1117-22.
10. Avendaño C. and Menéndez J.C. (2008) Medicinal Chemistry of Anticancer Drugs, Elsevier, pp. 165
11. Koriech O.M. and Shükla V.S. (1981) Dacarbazine (DTIC) in Malignant Melanoma: Reduced Toxicity with Protection From Light, *Clinical Radiology*, 32:53-55.
12. Baird G.M. and Willoughby M.L.N. (1978) Photodegradation of Dacarbazine, The Lancet, 2:681.
13. Kirk B. (1987) The Evaluation of a Light-Protective Giving Set: The Photosensitivity of Intravenous Dacarbazine Solutions, *Intensive Therapy and Clinical Monitoring*, 8:78-86.
14. Iwamoto T., Hiraku Y., Okuda M. and Kawanishi S. (2008) Mechanism of UVA-dependent DNA damage induced by an antitumor drug dacarbazine in relation to its photogenotoxicity, *Pharmaceutical Research*, 25(3)598-604
15. Treudler R., Geogieca J., Geilen C.C. and Orfanos C.E. (2004) Dacarbazine but not Temozolomide Induces Phototoxic Dermatitis in Patients with Malignant Melanoma*, Journal of the American Academy of Dermatology*, 50(5):783-785
16. Shükla V.S. (1980) A Device to Prevent Photodegradation of Dacarbazine (DTIC), *Clinical Radiology*, 31:239-240.
17. Shükla V.S. and Koriech O.M. (1981) Dacarbazine (DTIC) in Malignant Melanoma: Reduced Toxicity with Protection From Light, *Clinical Radiology*, 32:53-55
18. Yung C.W., Winston E.M and Lorincz A.L. (1981) Dacarbazine-induced photosensitivity reaction, *Journal of the American Academy of Dermatology*, 49(5):541-543

19. Bolling R., Meyer-Hamme S. and Schauder S. (1980) Photosensitization with DTIC therapy in metastatic malignant melanoma, *Der Hautarzt*, 31(11):602-5

20. Haouala A., Zanolari B., Rochat B., Montemurro M., Zaman K., Duchosal M.A., Ris H.B., Leyvraz S., Widmer N. and Decosterd L.A. (2009) Therapeutic Drug Monitoring of the new targeted anticancer agents imatinib,nilotinib, dasatinib, sunitinib, sorafenib and lapatinib by LC tandem mass spectrometry. *Journal of Chromatography B*, 877:1982-1996

21. National Institute for Health and Care Excellence (2009) Sunitinib for the first-line treatment of advanced and/or metastatic renal cell carcinoma [online] Available at https://www.nice.org.uk/guidance/ta169 [Accessed 01/08/2015]

22. National Institute for Health and Care Excellence (2015) Axitinib for treating advanced renal cell carcinoma after failure of prior systemic treatment [online] Available at https://www.nice.org.uk/guidance/ta333 [Accessed 01/08/2015]

23. Adams V.R. and Leggas M. (2007) Sunitinib malate for the treatment of metastatic renal cell carcinoma and gastrointestinal stromal tumors, *Clinical Therapeutics*, 29(7):1338-1353.

24. Locati L.D., Licitra L., Agate L., Ou S.H., Boucher A., Jarzab B., Qin S., Kane M.A., Wirth L.J., Chen C., Kim S., Ingrosso A., Pithavala Y.K., Bycott P. and Cohen E.E. (2014) Treatment of advanced thyroid cancer with axitinib: Phase 2 study with pharmacokinetic/pharmacodynamic and quality-of-life assessments, *Cancer*, 120(17):2694-703

25. Borst D.L., Arruda L.S., MacLean E., Pithavala Y.K. and Morgado J.E. (2014) Common questions regarding clinical use of axitinib in advanced renal cell carcinoma, *American Journal of Health-System Pharmacy*, 71:1092-1096

26. Sistla A., Sunga A., Phung K., Koparkar A. and Shenoy N. (2004) Powder-in-bottle formulation of SU011248. Enabling rapid progression into human clinical trials, *Drug Development and Industrial Pharmacy*, 30(1):19-25

27. Navid F., Christensen R., Minkin P., Stewart C.F., Furman W.L. and Baker S. (2008) Stability of Sunitinib in Oral Suspension, *The Annals of Pharmacotherapy*, 42(7):962-966

28. Aatmani M.E., Poujol S., Astre C., Malosse F. and Pinguet F. (2002) Stability of Dacarbazine in Amber Glass Vials and Polyvinyl Chloride Bags, *American Society of Health-System Pharmacists*, 59:1351-1356.

29. Malik M.Z, Ahmad M. and Muahammad S. (2013) Rapid and simultaneous determination of adriamycin, bleomycin, vinblastine and dacarbazine in plasma of hodgkin's lymphoma patients by a reversed phase HPLC method, *Journal of the Chilean Chemical Society*, 58(2): 1674-1677

30. Fiore D., Jackson A.J., Didolkar M.S. and Dandu V.R. (1985) Simultaneous determination of dacarbazine, its photolytic degradation product, 2-azahypoxanthine, and the metabolite 5-aminoimidazole-4-carboxamide in plasma and urine by high-pressure liquid chromatography, *Antimicrobial Agents and Chemotherapy*, 27(6): 977–979

31. Bouchet S., Chauzit E., Ducint D., Castaing N., Canal-Raffin M., Moore N., Titier K. and Molimard M. (2011) Simultaneous determination of nine tyrosine kinase inhibitors by 96-well solid-phase extraction and ultra-performance LC/MS-MS, *Clinica Chimica Acta*, 412(11–12):1060-1067

32. Sistla A., Yang W.L. and Shenoy N. (2006) High-performance liquid chromatography method for determination of reversible isomers of SU5416, *Journal of Chromatography A*, 1110:73-80

33. De Brujin P., Sleijfer S., Lam M., Mathijssen R.H.J., Wiemer E.A.C. and Loos W. (2010) Bioanalytical method for the quantification of sunitinib and its n -desethyl metabolite SU12662 in human plasma by ultra performance liquid chromatography/ tandem triple-quadrupole mass spectrometry, *Journal of Pharmaceutical and Biomedical Analysis*, 51:934-941.

34. Minkin P., Zhao M., Chen Z., Ouwerkerk J., Gelderblom H. and Baker S.D. (2008) Quantification of sunitinib in human plasma by high-performance liquid chromatography-tandem mass spectrometry, *Journal of Chromatography B*, 874:84-88

35. Gierer D.S., Morgado J.E., Murphy B.J. and Simmons D.M., Pfizer Inc. (2013) Pharmaceutical compositions of n-methyl-2-[3-((e)-2-pyridin-2-yl-vinyl)-1h-indazol-6-ylsulfanyl]-benzamide, U.S., Pat. WO 2013046133 A1

36. Aatmani M.E., Poujol S., Astre C., Malosse F. and Pinguet F. (2002) Stability of Dacarbazine in Amber Glass Vials and Polyvinyl Chloride Bags, *American Society of Health-System Pharmacists*, 59:1351-1356.

37. Stewart J.T., Warren F.W., King D.T. and Fox J.L. (1996) Stability of Odansetron Hydrochloride and Five Antineoplastic Medications, *American Society Health-System Pharmacists*, 53:1297-300.

38. Stewart J.T., Warren F.W., King D.T., Venkateshwaran T.G., Ponder G.W. and Fox J.L. (1997) Stability of Ondansetron Hydrochloride, Doxorubicin Hydrochloride, and Dacarbazine or Vincristine Sulfate in Elastomeric Portable Infusion Devices and Polyvinyl Chloride Bags, *American Society of Health-System Pharmacists*, 54:915-20.

39. Shetty B.V., Schowen R.L., Slavik M. and Riley C.M. (1992) Degradation of Dacarbazine in Aqueous Solution, *Journal of Pharmaceutical & Biomedical Analysis*, 10(9):675-683.

40. Shealy Y.F., Krauth C.A. and Montgomery J.A. (1962) Imidiazoles. I. Coupling reactions of 5-diazoimidazole-4-carboxamide, *Journal of Organic Chemistry*, 27:2150-2154.

41. Horton J.K. and Stevens M.F.G. (1981) Triazines and Related Products. Part 23. New Photo-products from 5-Diazoimidazole-4-carboxamide (Diazo-IC), *Journal of the Chemical Society Perkin Transaction 1*, 1433-1436.

42. Islam M.S. and Asker A.F. (1994) Photostabilization of Dacarabzine with Reduced Glutathione, *Parenteral Drug Association Journal of Pharmaceutical Science and Technology*, 48:38-40.

43. Lunn G., Rhodes S.W., Sansone E.B. and Schmuff N.R. (1994) Photolytic Destruction and Polymeric Resin Decontamination of Aqueous Solutions of Pharmaceuticals, *Journal of Pharmaceuti+cal Sciences,* 83(9):1289-1293

44. Horton J.K. and Stevens M.F.G. (1981) A New Light on the Photo-decomposition of the Antitumour Drug DTIC, *Journal of Pharmacy and Pharmacology*, 33(1):808-811

45. European Medicines Agency (2012) Committee for Medicinal Products for Human Use assessment report EMA/CHMP/453325/2012 Inlyta. [ONLINE] Available at: http://www.ema.europa.eu/docs/en_GB/document_library/EPAR_-_Public_assessment_report/human/002406/WC500132190.pdf [Accessed 09/12/12].

46. Likar M.D., Cheng G., Mahajan N. and Zhang Z. (2011) Rapid identification and absence of drug tests for AG-013736 in 1 mg Axitinib tablets by ion mobility spectrometry and DART™ mass spectrometry*, Journal of Pharmaceutical and Biomedical Analysis*, 55(3):569-573

47. Sparidans R.W., Iusuf D., Schinkel A.H., Schellens J.H.M. and Beijnen J.H. (2009) Liquid chromatography-tandem mass spectrometric assay for the light sensitive tyrosine kinase inhibitor Axitinib in human plasma, *Journal of Chromatography B*, 877(32):4090-4096

48. Zhao Y., Sukbuntherng J. and Antonian L. (2004) Simultaneous determination of Z-SU5416 and its interconvertible geometric E-isomer in rat plasma by LC/MS/MS, *Journal of Pharmaceutical and Biomedical Analysis*, 25:513-522

49. Etienne-Grimaldi, M. (2009) A routine feasible HPLC analysis for anti-angiogenic tyrosine inhibitor, sunitinib and its main metabolite SU12662, in plasma. *Journal of Chromatography B*, 877:3757-3761.

50. Zhou Q. and Gallo J.M. (2010) Quantification of Sunitinib in mouse plasma, brain tumor and normal brain using liquid chromatography-electrospray ionization-tandem mass spectrometry and pharmacokinetic application. *Journal of Pharmaceutical and Biomedical Analysis*, 51:958-964.

51. Rodamer, M. (2011) Development and validation of a liquid chromatography/tandem mass spectrometry procedure for the quantification of sunitinib (SU12662) and its active metabolite N-desethyl sunitinib (SU12662), in human plasma: Application to an explorative study. *Journal of Chromatography B*, 879:695-706.

52. Tønnesen H.H. (2004) Photostability of Drugs and Drug Formulations, 2nd ed., London:CRCPress

53. Ming L. (2012) Organic Chemistry of drug degradation, RSC Drug Discovery Series No.29, Cambridge: The Royal Society of Chemistry.

54. Lankheet N.A., Blank C.U., Mallo H., Adriaansz S., Rosing H., Schellens J.H., Huitema A.D. and Beijnen J.H. (2011) Determination of sunitinib and its active metabolite N-desethylsunitinib in sweat of a patient, Journal of Analytical Toxicology, 35(8):558-565.

55. European Medicines Agency. (2015) European Public Assessment Reports [Online] Available at: http://www.ema.europa.eu/docs/en_GB/document_library/EPAR_-_Summary_for_the_public/human/000687/WC500057689.pdf [Accessed 01/08/2015]

56. Abdalla M.Y. (2011) Glutathione as Potential Target for Cancer Therapy; More or Less is Good?, *Jordan Journal of Biological Sciences*, 4(3):119-124

CHAPTER FIVE

PHOTOKINETIC STUDIES OF THREE ANTI-CANCER DRUGS IN ETHANOLIC MEDIUM

5.1. INTRODUCTION

Dacarbazine (DBZ), Axitinib (AXI) and Sunitinib Malate (SUT) are anti-cancer drugs known to be photolabile in solution (Scheme 5.1). In the literature, there are no studies on the stability of DBZ in organic media and those reporting the observation of photodegradation of AXI and SUT studied the drugs in either dimethysulfoxide (DMSO) or plasma. However, no data on kinetics or quantum yields were given by the studies.

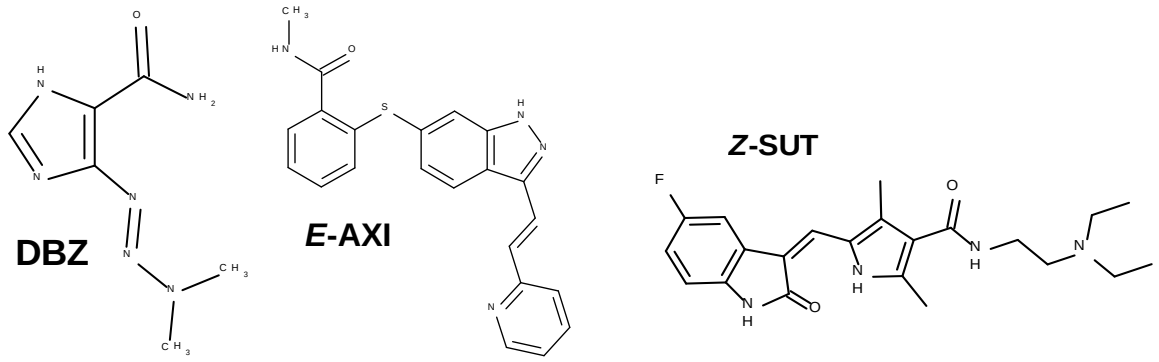

Scheme 5.1: Molecular structures of Dacarbazine (DBZ), Axitinib (E-AXI) and Sunitinb (Z-SUT)

This study aims to shed light on the photokinetic behaviour of DBZ, AXI and SUT in organic media through the application of the new Φ-order kinetic mathematical strategy for unimolecular (AB(1Φ), $A \rightarrow B$) and photoreversible reactions (AB(2Φ), $A \leftrightharpoons B$) [1,2], where A is the initial compound and B the photoproduct.

5.2. Φ-ORDER KINETIC MODEL

In the literature, photochemical reaction data are commonly treated with conventional thermal reaction kinetic models [3-13]. These models are used regardless of the presence of light in the reaction and the photodegradation pathway of the drug. In some cases, it was found that more than one kinetic order can be accurately applied to the reaction kinetic data [8,9,11,13].

In contrast to thermal kinetics, the rate constant of a photoreaction is dependent on three important factors – the intensity of the irradiation (P), the extinction coefficient (ε) and quantum yield (Φ) of the drug at specific wavelengths. Therefore, without first quantitatively defining the reaction kinetics, as well as the reaction parameters, the photoreactivity of different drugs, or the same drug measured at different irradiation conditions, cannot be directly compared.

Recently, a newly developed approach based on Φ-order kinetics has been proven to successfully describe the time evolution of the species concentrations when the reactive medium is subjected to non-isosbestic and monochromatic irradiation at constant temperature [14-18].

The Φ-order approach allows a unique characterisation of the kinetic data, provides an analytical equation for the overall reaction rate-constant and enables the quantification of the extinction coefficient and quantum yields. Thus, in great contrast to the thermal kinetic models, there is no possibility of multiple interpretations (more than one reaction order) of the same set of data. It also aids the determination a drug's suitability to act as actinometers.

5.2.1. Φ-order kinetic model for non-isosbestic irradiations

The model equation describing Φ-order kinetics for the photoreversible degradation of initial compound (A) to photoproduct (B) species is given by the general equation [15]:

$$A_{tot}^{\lambda_{irr}/\lambda_{obs}}(t) = A_{tot}^{\lambda_{irr}/\lambda_{obs}}(\infty) + \frac{A_{tot}^{\lambda_{irr}/\lambda_{obs}}(0) - A_{tot}^{\lambda_{irr}/\lambda_{obs}}(\infty)}{A_{tot}^{\lambda_{irr}/\lambda_{irr}}(0) - A_{tot}^{\lambda_{irr}/\lambda_{irr}}(\infty)} \times \frac{l_{\lambda_{obs}}}{l_{\lambda_{irr}}} \times Log\left[1 + \left(10^{\left[\left(A_{tot}^{\lambda_{irr}/\lambda_{irr}}(0) - A_{tot}^{\lambda_{irr}/\lambda_{irr}}(\infty)\right) \times \frac{l_{\lambda_{irr}}}{l_{\lambda_{obs}}}\right]} - 1\right) \times e^{-k_{A \leftrightharpoons B}^{\lambda_{irr}} \times t}\right] \quad \text{Eq.1}$$

where $A_{tot}^{\lambda_{irr}/\lambda_{obs}}(t)$, $A_{tot}^{\lambda_{irr}/\lambda_{obs}}(0)$, $A_{tot}^{\lambda_{irr}/\lambda_{obs}}(\infty)$, $A_{tot}^{\lambda_{irr}/\lambda_{irr}}(0)$ and $A_{tot}^{\lambda_{irr}/\lambda_{irr}}(\infty)$ are the total absorbance of the reaction medium at reaction time (t), at the start of the reaction (*t* = 0) and at infinity (∞), when irradiated at a certain wavelength and observed at the same wavelength ($\lambda_{irr}/\lambda_{irr}$) or irradiated and observed at different wavelengths ($\lambda_{irr}/\lambda_{obs}$).

The rate constant $k_{A\leftrightharpoons B}^{\lambda_{irr}}$ of the photoreaction is given by:

$$k_{A\leftrightharpoons B}^{\lambda_{irr}} = \left(\Phi_{A\to B}^{\lambda_{irr}} \times \varepsilon_A^{\lambda_{irr}} + \Phi_{B\to A}^{\lambda_{irr}} \times \varepsilon_B^{\lambda_{irr}}\right) \times l_{\lambda_{irr}} \times P_{\lambda_{irr}} \times F_{\lambda_{irr}}(\infty) = \beta_{\lambda_{irr}} \times P_{\lambda_{irr}} \qquad \text{Eq.2}$$

where $\Phi_{A\to B}^{\lambda_{irr}}$ and $\Phi_{B\to A}^{\lambda_{irr}}$ are the forward and reverse quantum yields at the irradiation wavelength (λ_{irr}), $\varepsilon_A^{\lambda_{irr}}$and $\varepsilon_B^{\lambda_{irr}}$ the extinction coefficients of A and B, $P_{\lambda_{irr}}$ the light intensity received, $l_{\lambda_{irr}}$ the path length of the irradiation light and $F_{\lambda_{irr}}(\infty)$ the photokinetic factor expressed as:

$$F_{\lambda_{irr}}(\infty) = \frac{1-10^{-\left(A_{tot}^{\lambda_{irr}/\lambda_{irr}}(\infty)\times\frac{l_{\lambda_{irr}}}{l_{\lambda_{obs}}}\right)}}{A_{tot}^{\lambda_{irr}/\lambda_{irr}}(\infty)\times\frac{l_{\lambda_{irr}}}{l_{\lambda_{obs}}}} \qquad \text{Eq.3}$$

Eq.1 can be used to describe the kinetic behaviour of any AB photoreaction at any observation/irradiation conditions. Thus, for an AB(2Φ) system where both species absorb at the irradiation wavelength , the absorbance at infinity will be represented by the photostationary state (pss). As a result, $A_{tot}^{\lambda_{irr}/\lambda_{obs}}(\infty)$ and $F_{\lambda_{irr}}(\infty)$ becomes $A_{tot}^{\lambda_{irr}/\lambda_{obs}}(pss)$ and $F_{\lambda_{irr}}(pss)$. For an unimolecular AB(1Φ) system where only the A absorbs at the irradiation wavelength, $A_{tot}^{\lambda_{irr}/\lambda_{obs}}(\infty)$, $\Phi_{B\to A}^{\lambda_{irr}}$ and $\varepsilon_B^{\lambda_{irr}}$ = 0 and $F_{\lambda_{irr}}(\infty)$ = ln(10) = 2.3. This returns Eq.1 to the model equations obtained through closed-form integration for this AB(1Φ) system [1].

The $\beta_{\lambda_{irr}}$ in Eq.2 is a proportionality factor between the overall rate-constant and the radiant power.

The details of the kinetic elucidation method [15] that allows the complete set of system unknowns to be worked out from the kinetic traces are presented in Annex A5.1.

5.3. STABILITY OF DBZ, AXI AND SUT IN ETHANOLIC SOLUTION

5.3.1 Electronic Spectral Characteristics of the Drugs

The UV-Vis spectra indicating the absorption characteristics of DBZ (1.37 x 10^{-5} M), *E*-AXI (1.77 x 10^{-5} M) and *Z*-SUT (8.94 x 10^{-6}) in Fig 5.1.

The electronic absorption spectrum of DBZ (1.37 x 10^{-5} M) in ethanol is characterised by two peaks situated at 235 nm and 325 nm attributing to the S_0 -> S_2 and S_0 -> S_1 (π -> π^*) transitions [19]. The electronic absorption spectra of AXI and SUT are characterised by four peaks. While, SUT's has a shoulder at 395 nm. As can be seen in Fig. 5.1, only SUT absorbs beyond the UV region (380 nm) into the visible region, which causes its powder and solutions to be yellow in colour.

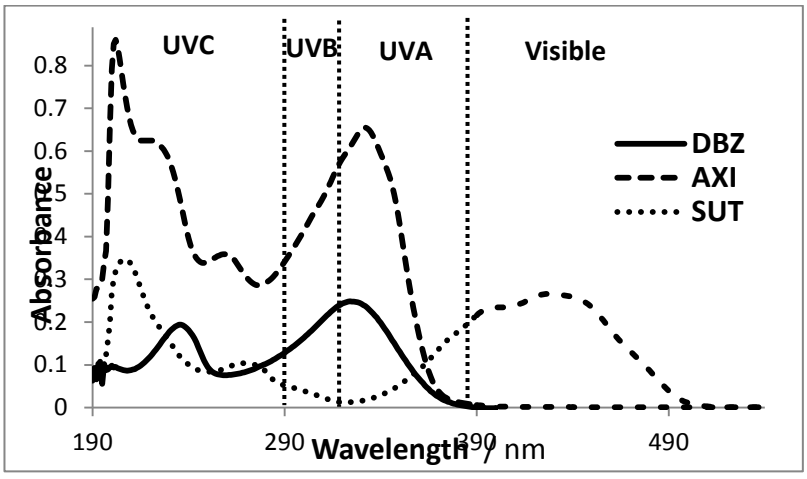

Fig. 5.1: UV/Vis Spectrum of 1.37 x 10^{-5} M DBZ, 1.77 x 10^{-5} M AXI and 8.94 x 10^{-6} M SUT in pure ethanolic solution before degradation. The UV/Vis regions as indicated [20]

5.3.2 Thermal Stability of the Drugs in Ethanol

In the literature, thermal stability of the three drugs in pure organic solution has never been reported, however our results correlate well with the few literature reports that mentions thermal stability for the three drugs. DBZ was reported to be stable for at least 24 hours at room temperature and at least 96 hours at 2-6°C when stored in the dark in aqueous solutions (prepared from DBZ's commercial formulation which also contains a pH 3.5 citrate buffer and 37.5 mg of mannitol) [21]. DBZ were also reported to be stable following cycles of freeze-thawing in human plasma and urine [22, 23]. These were confirmed by Lal Prasanth et al. [24] who prepared solutions of DBZ in 50 % (v/v) methanol/water, subjected it to dry heat degradation at 105°C for 60 min and found only 4.05 % degradation.

Many authors [25-28] reported AXI and SUT to be thermally stable at room temperature either after 24 hours of storage in human plasma or when stored in sweat, human plasma, methanol and a solution of acetonitrile/water/formic acid (20:80:0.1, v/v/v) mix.

In this study, no changes in absorbance were recorded for any of the drugs. Therefore, they can all be considered thermally stable in the given experimental conditions used in this study.

5.3.3 Photostability of the Drugs in Ethanol

There are currently no photostability studies on DBZ in pure organic solution in the literature. Although AXI and SUT have been studied in DMSO and plasma, full photochemical studies have never been carried out. Therefore, the kinetics and quantum yields for all three drugs are still unknown.

The continuous irradiation of the three drugs induced a decrease of a section of the spectrum and an increase of absorbance is in another section.

For all three drugs, a decrease of the main peak and formation of a new peak were observed. However, unlike the peaks for SUT and AXI, the DBZ peak at 325 nm depletes completely. No peaks and/or changes in absorbance were observed beyond 400 nm. SUT and its photoproduct share the same overall shape of the absorption spectra, as they totally overlap and no new features appears. For all solutions, no change in colour or formation of any precipitation was observed.

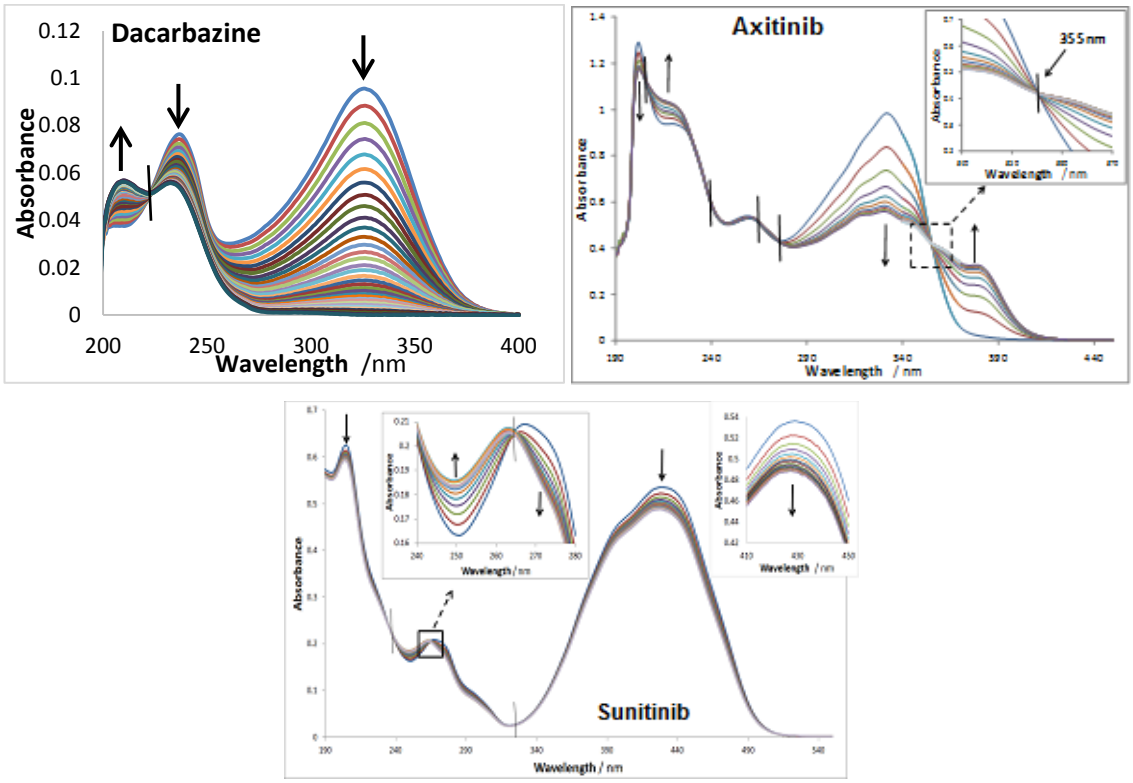

Fig 5.2: Evolution of the electronic absorption spectra of 5.47 x 10^{-6} M DBZ, 2.65 x 10^{-5} M *E*-AXI and .94 x 10^{-6} M *Z*-SUT in ethanol, when irradiated continuously with a monochromatic beam at 325 nm (1.84 x 10^{-6} einstein s^{-1} dm^{-3}), 355 nm (3.12 x 10^{-6} einstein s^{-1} dm^{-3}) and 430 nm (4.10 x 10^{-6} einstein s^{-1} dm^{-3}), repectively. Isosbestic points indicated by vertical lines.

The spectral evolution of DBZ produced only one identifiable isosbestic point, unlike AXI and SUT, where five and three isosbestic points can be seen, respectively (Table 5.1). The presence of isosbestic points indicates that no secondary reaction occurs during the reaction.

HPLC analysis showed only two peaks (the mother compound and its product) for all drugs (Fig. 5.3). This indicated an AB mechanism for all three drugs. The HPLC peaks representing AXI and SUT do not completely deplete, indicating the occurrence of an equilibrium between the drug and its photoproduct (PP). These features correspond to an AB(2Φ) photoreversible reaction mechanism. DBZ's peak, however, completely depletes suggesting a unimolecular AB(1Φ) reaction mechanism.

Table 5.1: Spectral changes observed when the drugs were monochromatically irradiated in ethanolic solution

Drug	Features of the Drug		Features of the Photoproduct		Isosbestic Points / nm
	Wavelength of interest λ_{obs} /nm	Log ε ($A_{tot}^{\lambda_{obs}}$)	Wavelength of interest λ_{obs} /nm	$A_{tot}^{\lambda_{obs}}$	
DBZ	235 <u>325</u>[a]	4.16 (0.079) 4.27 (0.103)	<u>208</u> 235	0.056 0.055	223
AXI	202 216 <u>332</u>	4.69 (1.291) 4.55 (0.936) 4.57 (0.982)	202 216 (318) <u>332</u> (347) 380	1.178 1.044 0.536 0.548 0.489 0.326	206 240 263 275 355
SUT	207 251 275 (400)[b] <u>430</u>	4.63 (0.382) 3.95 (0.079) 4.02 (0.093) 4.38 (0.216) 4.44 (0.248)	207 251 275 400 <u>430</u>	0.372 0.098 0.083 0.206 0.229	230 266 345

[a] underlined wavelengths represent the maximum
[b] values in brackets corresponds to shoulders
[C] to the end of the reaction

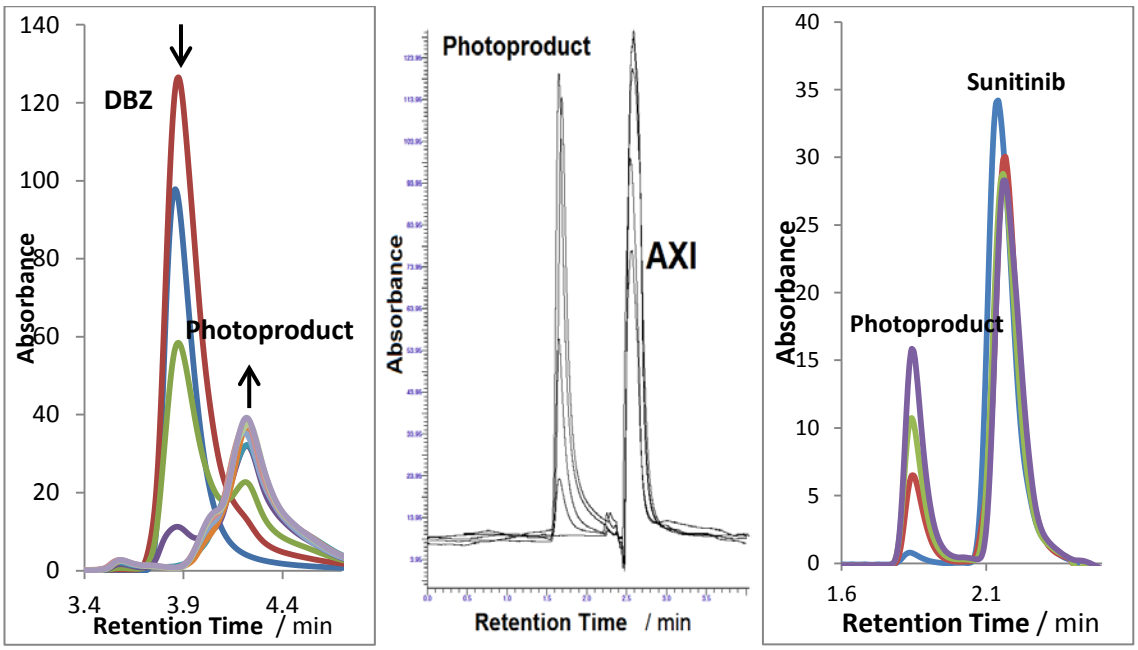

Fig 5.3: Chromatographic evolution of DBZ and its photoproduct (Left chromatogram), AXI and its photoproduct (middle chromatogram) and SUT and its photoproduct (right chromatogram)

The initial AXI and SUT were "*E*" and "*Z*" in conformations, respectively. The results obtained and the structure of the two drugs strongly suggests that upon irradiation, they transform into their *E*- and *Z*-isomers, respectively.

This conclusion matches well that reported in the literature where the *E/Z* photoisomerisation of AXI in the solid state [29] and in solution [25, 30, 31]; and SUT in solution [32]

HPLC analysis of the irradiated 5.49 x 10^{-4} M DBZ in 50% methanol/water solution [24] showed two peaks when kept in a UV chamber for 7 days (200 Watt hours/m^2) achieving a 52.3 % degradation.

Table 5.2: Retention time of the three drugs (A) and their photoproducts (B), calibration equation for the drugs, correlation coefficients (r^2) and linearity range of the drug.

Drug	Retention Times / min		Calibration Equation	Correlation Coefficient (r^2)	Linearity Range of A / M
	A	B			
DBZ	3.89	4.24	$y = 1 \times 10^{10} - 497703$	0.995	4.82×10^{-5} – 5.49×10^{-4}
AXI	2.52	1.70	$y = 1 \times 10^{11} + 15215$	0.997	2.76×10^{-6} – 2.33×10^{-5}
SUT	2.17	1.84	$y = 5 \times 10^{9} + 15376$	0.997	1.25×10^{-6} – 2.15×10^{-4}

5.3.4 Effect of irradiation wavelength on photodegradation traces

Photodegradation of drug substances strongly depends on the spectral properties of the drug substance and the spectral distribution of the light source [33, 34]. Knowledge of the drug's absorption spectra does not suffice to predict the causative wavelength range, since not all light absorbed induces photodegradation [35]. In the case of vitamin A, maximum rates of photolysis were observed over the range 330–350 nm [36]; and irradiation wavelength of 254 nm (UVC) was found to be most effective for vitamin E, whilst it remained stable under UVA (366 nm) irradiation [37].

In addition, it has been reported that irradiation of different wavelengths trigger different photochemical pathways leading to the formation of different photoproducts [38, 39].

Thus, it is important to consider the variation of drugs' reactivity with the irradiation wavelength range of the source.

In this context we studied the effect of the wavelength of the irradiation beam on the drugs' photodegradation reaction. For each drug, the kinetic traces of the degradation when irradiated at different irradiation wavelength were recorded at a specific observation

wavelength. The same kinetic behaviour was observed, indicating that the reaction is governed by the same mechanism.

At the longest wavelengths, the kinetic traces follows a smooth descend of the absorbance (at the λ_{max} of the longest wavelength peak) reaching zero or a photostationary state (pss) in the cases for AXI and SUT (Fig. 5.4). The behaviour of the traces agrees well with the Φ-order AB(1Φ) mechanism for DBZ and AB(2Φ) mechanism for AXI and SUT.

For the photodegradation of all three drugs, the experimental traces were all well fitted by Eq. 1, indicating that DBZ, AXI and SUT all obey Φ-order kinetics (Fig. 5.4).

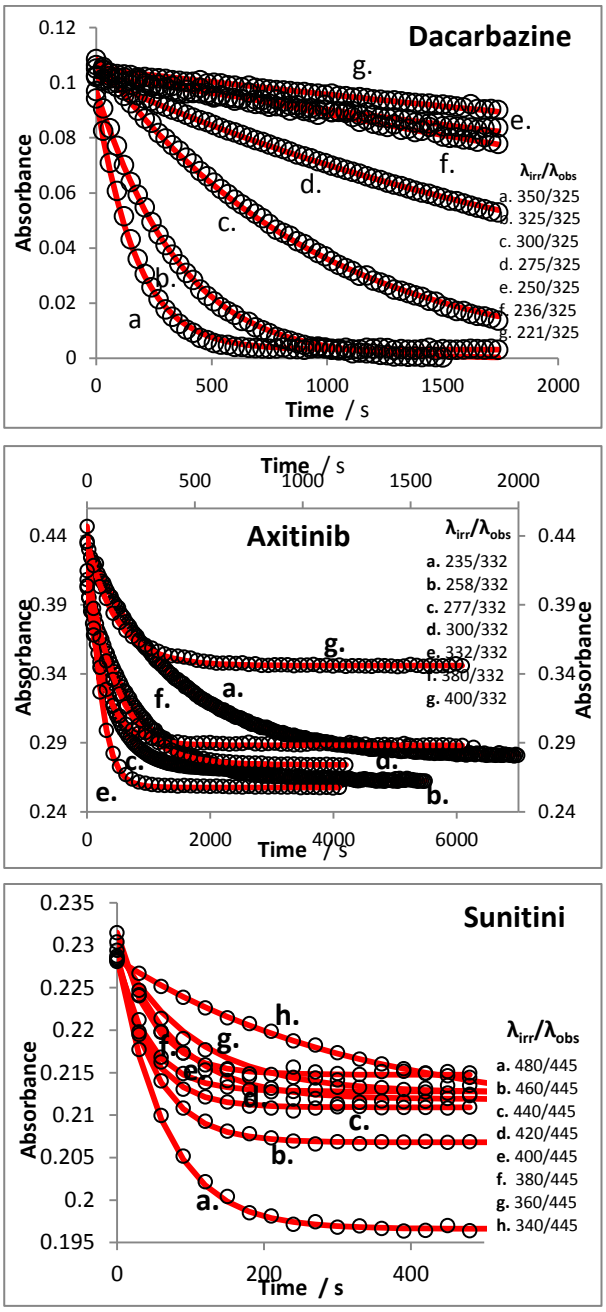

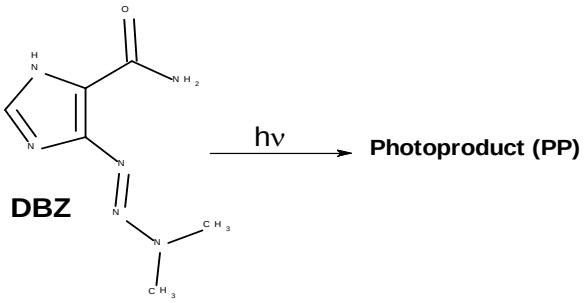

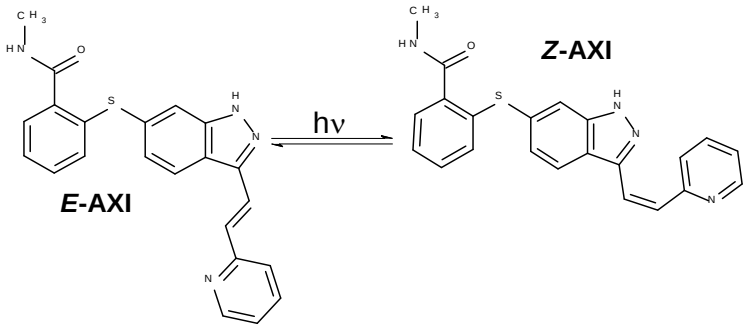

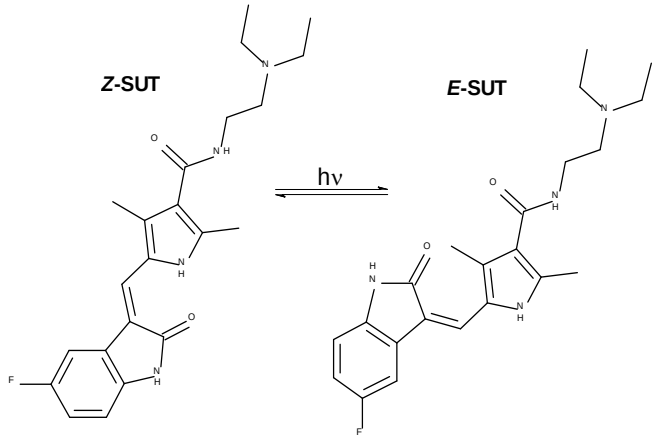

Fig. 5.4: (Left) Photokinetic traces of DBZ (5.47 x 10^{-6} M), AXI (2.65 x 10^{-5} M) and SUT (8.94 x 10^{-6} M) in ethanol at different irradiation wavelengths. Circles represent experimental data and the solid lines are the fitting of the traces to the Φ-order model. (Right) The unimolecular AB(1Φ) degradation mechanism of DBZ and AB(2Φ) photoreversible reaction of *Z*-AXI to *E*-AXI and *E*-SUT to *Z*-SUT. (A the mother compound and B the photoproduct)

Table 5.3: Overall Photoreaction rate-constants, spectroscopic and kinetic parameter values of DBZ, AXI and SUT for a set of monochromatic irradiations performed in ethanol at 22°C

λ_{irr} / nm	$A_{tot}^{\lambda_{irr}/\lambda_{obs}}(0)$	$P_{\lambda_{irr}}$ x 10^6 /einstein s^{-1} dm^{-3}	$A_{tot}^{\lambda_{irr}/\lambda_{irr}}(\infty)$	$k_{A \leftrightharpoons B}^{\lambda_{irr}}$ / s^{-1}
DBZ ($\lambda_{obs} = 325\ nm$)				
350	0.094	2.80	0.002	0.006200
345	0.093	2.17	0.000	0.005550
325	0.097	1.79	0.000	0.003300
300	0.109	1.30	0.010	0.001200
275	0.102	1.49	0.004	0.000455
250	0.106	1.55	0.007	0.000233
236	0.103	1.65	0.023	0.000195
221	0.105	1.28	0.013	0.000130
AXI ($\lambda_{obs} = 332\ nm$)				
400	0.437	3.56	0.020	0.00700
380	0.404	3.04	0.124	0.01000
332	0.447	1.80	0.258	0.02100
300	0.415	1.15	0.216	0.00710
277	0.408	1.18	0.192	0.00260
258	0.403	1.20	0.234	0.00125
235	0.435	1.31	0.343	0.00070
SUT ($\lambda_{obs} = 332\ nm$)				
480	0.229	4.85	0.058	0.0155
460	0.229	4.30	0.145	0.0195
440	0.228	4.07	0.221	0.0225
420	0.233	3.93	0.237	0.0230
400	0.239	3.48	0.219	0.0210
380	0.243	2.97	0.167	0.0130
360	0.247	2.67	0.085	0.0094
340	0.240	1.98	0.028	0.0030

The overall rate-constants obtained ($k_{A\rightarrow B}^{\lambda_{irr}}$) for DBZ and $k_{A\leftrightarrows B}^{\lambda_{irr}}$ for AXI and SUT), appeared to increase with wavelength (Table 5.3). However, as discussed earlier (Section 5.1), these values must be considered with care because they all depend on the intensity of the irradiation (*P*), optical path length of the irradiation beam inside the sample (l_{irr}), the extinction coefficients of both species (ε_A and ε_B) and quantum yields (Φ) of the drug at specific wavelengths, as shown by the equation of the rate constant (Eq. 2). Hence, it is necessary to determine all the parameters – in particular, the quantum yields – to allow comparison. Some literature reports that quantum yield is wavelength-dependent as it is the measure of the extent of a reaction relative to the number of radiation quanta absorbed [40]. In one study, the quantum yield of domoic acid photodegradation in seawater decreased with increasing wavelength and decreasing energy of incoming radiation, with the average value ranging from 0.03 to 0.20 in the wavelength range 280–400 nm. [41].

The rate constant of its photoreaction is given by Eq.2. Unlike AXI and SUT, DBZ follows an unimolecular AB(1Φ) reaction. Accordingly, Eq.1 (with $\Phi_{B\rightarrow A}^{\lambda_{irr}} = 0$) can be used to calculate the $\Phi_{A\rightarrow B}^{\lambda_{irr}}$ values for DBZ at different irradiation wavelengths (Table 5.6).

However, for AXI and SUT, obeying an AB(2Φ) reaction, there are three unknown parameters ($\Phi_{A\rightarrow B}^{\lambda_{irr}}$, $\Phi_{B\rightarrow A}^{\lambda_{irr}}$ and $\varepsilon_B^{\lambda_{irr}}$) that need to be determined through a stepwise method as described in Annex A5.2.

5.3.5 Determination of the Reaction Quantum Yields for an Isosbestic Irradiation

Firstly, the photodegradation reaction is subjected to a monochromatic irradiation at the isosbestic point (where $\varepsilon_B^{\lambda_{isos}} = \varepsilon_A^{\lambda_{isos}}$). Hence, reducing the number of unknowns to just $\Phi_{A\to B}^{\lambda_{irr}}$ and $\Phi_{B\to A}^{\lambda_{irr}}$.

This reaction is monitored by HPLC and the change in concentration of the species over time obtained (Table A5.1 in Annex A5.3).

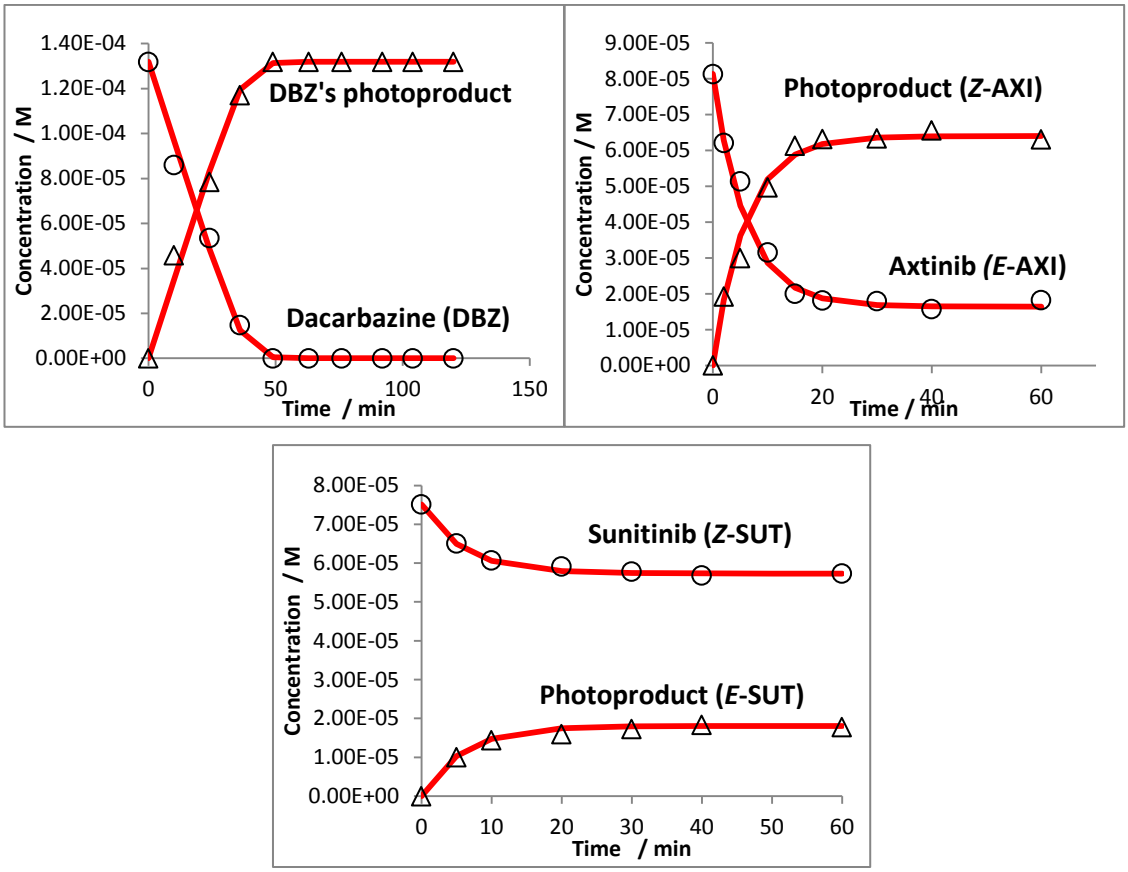

Fig. 5.5: Kinetic trace of the three drugs over photodegradation time and formation of the photoproduct monitored by HPLC when irradiated continuously with a monochromatic beam: DBZ (C_0 = 1.32 x 10^{-4} M) and its photoproduct (λ_{irr} = 325 nm, 1.02 x 10^{-6} einstein s^{-1} dm^{-3}, 22°C); *E*-AXI (C_0 = 8.13 x 10^{-5} M, C_∞ = 1.82 x 10^{-5} M) and its photoproduct (*Z*-AXI, C_∞ = 6.31 x 10^{-5} M)(λ_{irr} = 355 nm, 1.38 x 10^{-6} einstein s^{-1} dm^{-3}, 22°C). *E*-SUT (C_0 = 7.53 x 10^{-5} M, C_∞ = 5.73 x 10^{-5} M) and (*Z*-SUT, C_∞ = 1.78 x 10^{-5} M) (λ_{irr} = 345 nm, 2.19 x 10^{-6} einstein s^{-1} dm^{-3}, 22°C).

The concentration profiles (Fig. 5.5) were well fitted with the first-order equations (Table A5.2 in Annex A5.4). The values of their overall photodegration rate-constant ($k_{A\leftrightarrows B}^{\lambda_{isos}}$) was obtained as a fitting parameter, allowing the determination of the absolute quantum yields values for forward ($\Phi_{A\to B}^{\lambda_{isos}}$) and reverse ($\Phi_{B\to A}^{\lambda_{isos}}$) reaction steps and therefore, the equilibrium constant ($K_{A\leftrightarrows B}^{\lambda_{isos}}$).

The results found that, for both AXI and SUT, the *E*-isomers were much more photoreactive than the *Z*-isomer (Table 5.4). This is possibly due to steric effect, because in the *Z*-isomer form, the two large groups are closer to each other so they interfere more with each other than in the *E*-form.

Table 5.4: AXI's and SUT's quantum yield values at the isosbestic wavelength and their equilibrium constant ($K_{A\leftrightarrows B}^{\lambda_{isos}}$)

	λ_{isos} / nm	$\Phi_{A\to B}^{\lambda_{isos}}$	$\Phi_{B\to A}^{\lambda_{isos}}$	$K_{A\leftrightarrows B}^{\lambda_{isos}}$ / s^{-1}
AXI	355	0.068 ± 4.61 x 10^{-3}	0.020 ± 1.53 x 10^{-3}	3.46
SUT	345	0.020 ± 6.47 x 10^{-4}	0.064 ± 2.05 x 10^{-3}	0.315

5.3.6 Reconstruction of the whole spectrum of the photoproduct

The whole spectrum of the photoproduct could therefore be reconstructed using the value of $K_{A\leftrightarrows B}^{\lambda_{isos}}$ and eq.9 (Fig. 5.6).

The spectrum of DBZ's photoproduct is obtained at the end of DBZ photodegradation. It is characterised by two peaks at 210 nm and 232 nm and does not absorbed at all beyond 290 nm.

AXI, SUT and their respective photoproducts have overlapping electronic spectra, with the mother compound being characterised by higher values of absorption coefficient values everywhere, except where new absorption bands corresponding to the photoproduct appear.

For all three drugs, the formation of these new peaks belonging to the photoproduct are observed irrespective of the irradiation wavelength. Such features clearly point to the occurrence of a photochemical change and further confirms the reaction is governed by the same mechanism - as the same evolution is observed irrespective of the irradiation wavelength.

Unlike *E*-AXI, whose main absorption band tails off by 390 nm, its photoproduct (*Z*-AXI) absorbs in the visible region (400 – 800 nm).

5.3.7 Determination of the reaction quantum yields at different wavelengths

Once the absorption coefficients of the photoproducts are known for all wavelengths, the photochemical quantum yields at any irradiation wavelength can be determined.

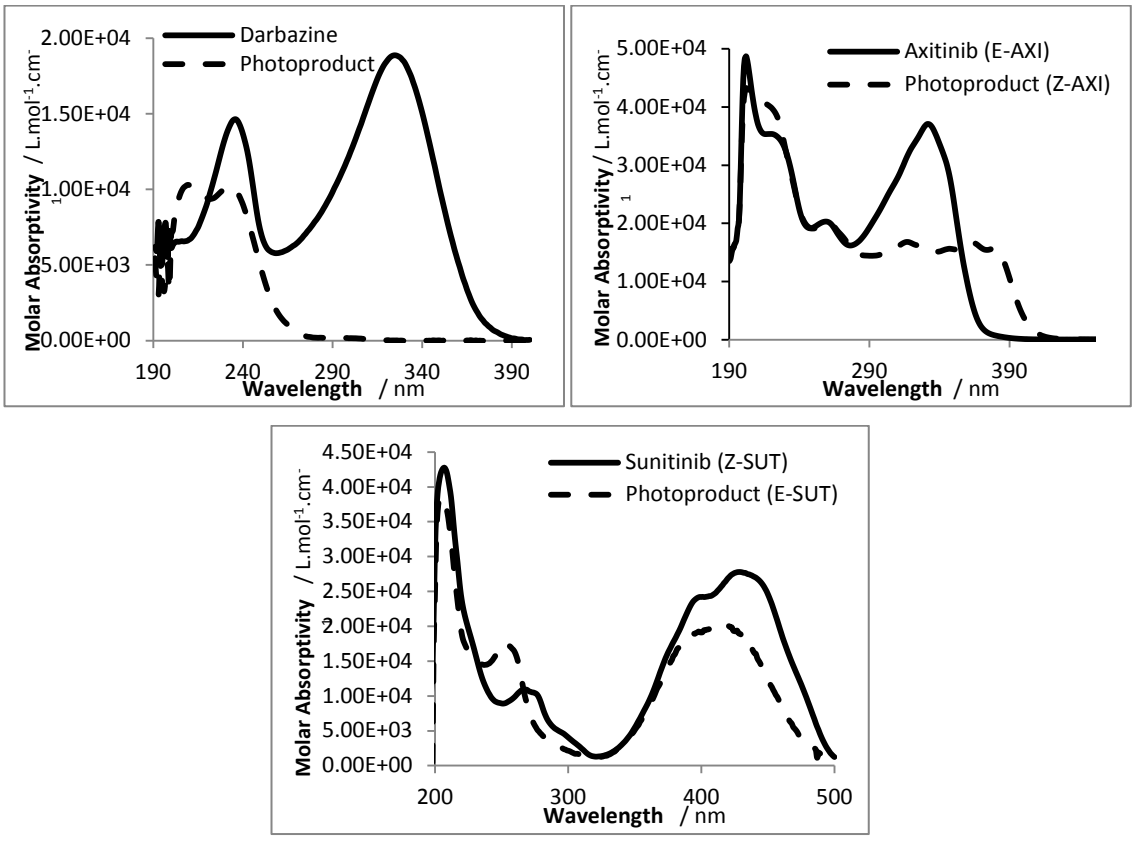

Fig. 5.6: Native and reconstructed electronic absorption spectra (absorption coefficient units) of DBZ and its photoproduct, *E*-AXI and its photoproduct (*Z*-AXI), *Z*–SUT and its photoproduct (*E*-SUT)

The forward quantum yields for DBZ and AXI (*E* → *Z*) have been found to be wavelength dependent. Their quantum yields increased with irradiation wavelength (Fig. 5.7) with a similar sigmoidal pattern. For DBZ, a 24.5-fold increase was recorded for $\Phi_{A\rightarrow B}^{\lambda_{irr}}$ values between 221 nm and 350 nm, and in the case of *Z*-AXI, a 226-fold increase between 235 nm and 400 nm (Table 5.5). This confirms that the photodegradation of DBZ and AXI is mainly driven by UVA–Visible light. However, the variation of AXI's $\Phi_{B\rightarrow A}^{\lambda_{irr}}$ values was just 17.5-fold – suggesting that the reverse reaction is less affected by the variation of the irradiation wavelength.

In contrast, the forward (*Z* → *E*) reaction of *Z*-SUT is less affected by the variation of the irradiation wavelength – having fairly similar $\Phi_{A\rightarrow B}^{\lambda_{irr}}$ values between 340 nm and 480 nm – than its reverse reaction (*E* → *Z*), in which a 2.69-fold increase in its $\Phi_{B\rightarrow A}^{\lambda_{irr}}$ values within the same wavelength range was recorded.

In the case of AXI and SUT, the fact that phototransformation of *E*-AXI and *E*-SUT is more efficient than that of *Z*-AXI and *Z*-SUT (Table 5.5) is probably due to geometric strain of the species. In the *Z*-isomer form, the two large groups are closer to each other. They potentially interfere more with each other than in the *E*-form, where the larger groups are farther apart and have a higher degree of freedom [42].

Excellent sigmoid correlation of the calculated quantum yield values ($\Phi_{cld.}$) against experimental values ($\Phi_{exp.}$) for these irradiation wavelengths (Fig. 5.7) was found. The sigmoid equation can be used to determine the quantum yield values at any wavelength in which the drug is photochemically reactive (Table 5.6).

It is evident from the quantum yield values of DBZ and AXI that these drugs are most photochemically reactive in the UVA-Visible range and that Z-SUT is equally reactive across the spectrum (Fig. 5.7). This poses great cause for concern as, of UV radiation reaching the Earth's surface, 95 % of it is UVA [43].

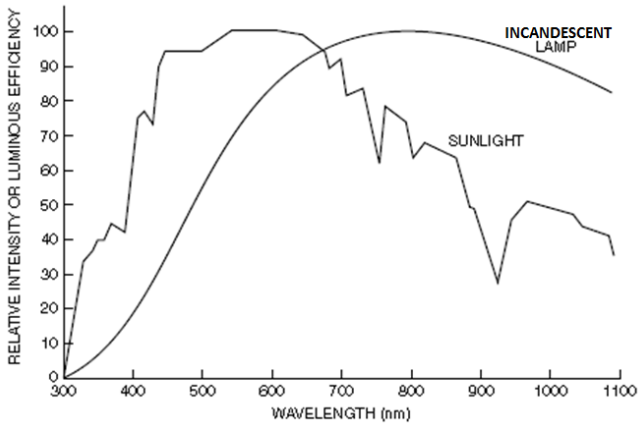

Fig. 5.8: Spectral distribution of sunlight compared with an incandescent lamp [3].

DBZ and AXI's maxima (325 nm and 330 nm, respectively) are located in the middle of the UVA region and SUT's main absorption band (340-500 nm, maximum at 430 nm) spans all the way from UVA to Visible light. UVA penetrate deep into the lower skin layers [3], increasing the possibility of photosensitivity and phototoxicity caused by the photodegradation of these drugs at skin surface level [3].

SUT was reported to be "probably phototoxic" in the European Medicines Agency's (EMA) European Public Assessment Reports (EPAR) [44]. Unfortunately, no further details were provided.

In another EMA report, the Committee for Medicinal Products for Human Use (CHMP), recognised AXI's potential to cause phototoxicity in eye and skin tissue [31]. However, negative phototoxicity and lack of photosensitive reaction was reported.

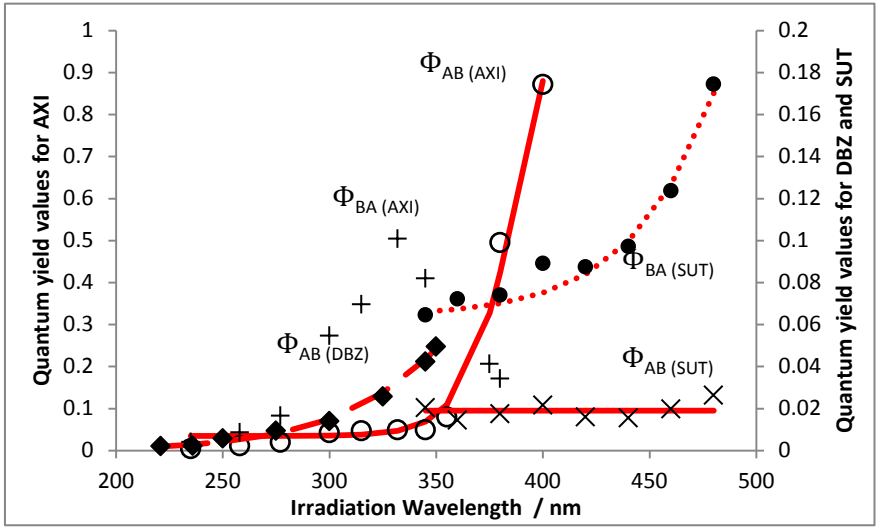

Fig 5.7: Sigmoid relationship obtained for the photochemical quantum yield of DBZ, *Z*-AXI and *Z*-SUT.

Table 5.6: Proposed sigmoid equation for the calculation of DBZ's, AXI's and SUT's quantum yield values at each irradiation wavelength (λ_{irr}) and the correlation coefficient (r^2) of the calculated quantum yield values ($\Phi_{cld.}$) against the experimental values ($\Phi_{exp.}$)

Drug	λ_{irr} Range / nm	Correlation of $\Phi_{cld.}$ against $\Phi_{exp.}$	Proposed Sigmoid Equation
DBZ	221 - 350	0.9952	$\Phi_{A\rightarrow B}^{\lambda_{irr}} = \frac{0.263}{1+399e^{-0.0265\times(\lambda_{irr}-180)}}$
AXI	235 – 400	0.9954	$\Phi_{A\rightarrow B}^{\lambda_{irr}} = \frac{1.80}{1+4\times10^{5}e^{-0.042\times(\lambda_{irr}-150)}}$
SUT	340 - 480	0.9778	$\Phi_{B\rightarrow A}^{\lambda_{irr}} = \left(\frac{0.73}{1+1300e^{-0.03\times(\lambda_{irr}-300)}}\right)+0.064$

Table 5.5: Quantum yield values for DBZ, AXI and SUT at different wavelengths of irradiation

λ_{irr} / nm	$P_{\lambda_{irr}}$ x 10^6 / einsteins^{-1} dm^{-3}	$A_{tot}^{\lambda_{irr}/\lambda_{obs}}(pss)$	$k_{A\leftrightharpoons B}^{\lambda_{irr}}$ / s^{-1}	$\nu_0^{\lambda_{irr}/\lambda_{obs}}$ / s^{-1}	$\varepsilon_A^{\lambda_{irr}}$ / M^{-1}cm^{-1}	$\varepsilon_B^{\lambda_{irr}}$ / M^{-1}cm^{-1}	$F_{\lambda_{irr}}(0)$	$\Phi_{A\rightarrow B}^{\lambda_{irr}}$	$\Phi_{B\rightarrow A}^{\lambda_{irr}}$
DBZ (λ_{obs} = 325)									
350	2.993	1.50 x 10^{-3}	0.00663	-*	9896	-*	2.295	0.049 ± 1.11 x 10^{-3}	-*
345	2.168	6.99 x 10^{-5}	0.00555	-	12580	-	2.303	0.042 ± 1.85 x 10^{-3}	-
325	2.156	8.04 x 10^{-5}	0.00417	-	18864	-	2.303	0.026 ± 5.51 x 10^{-3}	-
300	1.446	6.11 x 10^{-3}	0.00137	-	12469	-	2.271	0.014 ± 1.98 x 10^{-3}	-
275	1.440	3.51 x 10^{-3}	0.00045	-	7068	-	2.284	0.009 ± 2.20 x 10^{-3}	-
250	1.265	6.97 x 10^{-3}	0.00023	-	7157	-	2.266	0.006 ± 1.04 x 10^{-3}	-
236	1.493	2.23 x 10^{-2}	0.00020	-	14639	-	2.188	0.002 ± 2.43 x 10^{-4}	-
221	1.529	1.29 x 10^{23}	0.00013	-	9476	-	2.236	0.002 ± 3.72 x 10^{-4}	-

AXI (λ_{obs} = 332)								$\Phi_{Z\rightarrow E}^{\lambda_{irr}}$	$\Phi_{E\rightarrow Z}^{\lambda_{irr}}$
400	3.60	0.350	0.0063	-5.85×10^{-4}	154	3822	2.294	$0.871 \pm 2.04 \times 10^{-1}$	$0.070 \pm 9.68 \times 10^{-3}$
380	3.08	0.288	0.0097	-1.35×10^{-3}	753	15244	2.209	$0.495 \pm 7.97 \times 10^{-2}$	$0.034 \pm 2.14 \times 10^{-4}$
355	2.88	0.307	0.0192	-2.28×10^{-3}	16059	37064	1.326	$0.068 \pm 4.61 \times 10^{-3}$	$0.020 \pm 1.53 \times 10^{-3}$
332	1.78	0.265	0.0197	-2.28×10^{-3}	37064	16455	1.053	$0.062 \pm 9.88 \times 10^{-3}$	$0.110 \pm 2.83 \times 10^{-2}$
300	1.13	0.267	0.0074	-9.3×10^{-4}	23434	15116	1.324	$0.051 \pm 4.64 \times 10^{-3}$	$0.0699 \pm 2.14 \times 10^{-3}$
277	1.22	0.273	0.0026	-3.8×10^{-4}	16215	15683	1.525	$0.029 \pm 5.65 \times 10^{-3}$	$0.0195 \pm 1.87 \times 10^{-3}$
258	1.16	0.269	0.00124	-1.8×10^{-4}	20299	19939	1.404	$0.010 \pm 6.91 \times 10^{-4}$	$0.009 \pm 1.45 \times 10^{-4}$
235	1.44	0.297	0.00073	-9.8×10^{-5}	28113	27607	1.170	$0.004 \pm 3.63 \times 10^{-4}$	$0.004 \pm 7.17 \times 10^{-4}$
SUT (λ_{obs} = 445)								$\Phi_{E\rightarrow Z}^{\lambda_{irr}}$	$\Phi_{Z\rightarrow E}^{\lambda_{irr}}$
480	4.85	0.198	0.0155	-4.74×10^{-4}	9234	2911	1.93	$0.026 \pm 7.39 \times 10^{-4}$	$0.175 \pm 1.26 \times 10^{-2}$
460	4.30	0.208	0.0195	-4.09×10^{-4}	19048	8657	1.60	$0.020 \pm 3.63 \times 10^{-3}$	$0.124 \pm 1.26 \times 10^{-2}$
440	4.07	0.211	0.0225	-3.76×10^{-4}	27078	16133	1.39	$0.015 \pm 2.44 \times 10^{-3}$	$0.097 \pm 2.56 \times 10^{-3}$
420	3.93	0.233	0.023	-3.52×10^{-4}	26882	19993	1.37	$0.016 \pm 2.68 \times 10^{-3}$	$0.087 \pm 2.60 \times 10^{-3}$
400	3.48	0.239	0.021	-3.56×10^{-4}	24202	19116	1.43	$0.022 \pm 7.87 \times 10^{-3}$	$0.089 \pm 2.79 \times 10^{-3}$
380	2.97	0.243	0.013	-2.51×10^{-4}	18084	15922	1.59	$0.017 \pm 2.77 \times 10^{-3}$	$0.074 \pm 4.94 \times 10^{-3}$
360	2.67	0.226	0.0094	-1.92×10^{-4}	8993	8276	1.90	$0.014 \pm 4.06 \times 10^{-3}$	$0.067 \pm 1.78 \times 10^{-2}$
345	2.04	0.209	0.0035	-7.49×10^{-5}	4021	3863	2.12	$0.020 \pm 6.47 \times 10^{-4}$	$0.064 \pm 2.05 \times 10^{-3}$
340	1.98	0.221	0.003	-5.89×10^{-5}	2950	2817	2.17	$0.020 \pm 8.79 \times 10^{-4}$	$0.065 \pm 2.79 \times 10^{-3}$
320	1.33	0.211	0.0018	-4.46×10^{-5}	1307	1208	2.24	$0.046 \pm 3.79 \times 10^{-3}$	$0.145 \pm 1.20 \times 10^{-2}$
300	0.94	0.211	0.0013	-3.53×10^{-5}	4070	2151	2.15	$0.020 \pm 1.75 \times 10^{-3}$	$0.098 \pm 6.60 \times 10^{-3}$
260	1.16	0.214	0.00064	-1.74×10^{-5}	9894	16266	1.93	$0.004 \pm 1.24 \times 10^{-4}$	$0.007 \pm 2.57 \times 10^{-4}$
240	1.22	0.215	0.00057	-1.06×10^{-5}	10529	14604	1.92	$0.003 \pm 2.62 \times 10^{-4}$	$0.006 \pm 7.17 \times 10^{-4}$

* Not Applicable

Nonetheless, the effectiveness and tolerability of the drugs are essentially diminished by the development of activities such as photosensitive reactions [45-48], potentially causing severe impacts on the physical, psychological, and social well-being of patients.

Thus, understanding the photoreactivity of these drugs aids the development of stabilization/protection techniques for improved drug delivery and bioavailability.

The Φ-order kinetics, in this context, seem to be a good tool to harvest reliable data on drugs' photostability.

5.4. DEVELOPMENT OF ACTINOMETERS USING ANTI-CANCER DRUGS

The Φ-order kinetic models can also be used in the development of new actinometers.

In order to develop an actinometric method, solutions of DBZ, AXI and SUT were subjected to irradiation of varying radiant power at various wavelengths, spanning over regions mainly responsible for their photoreactivities. The experimental traces obtained were fitted with the Φ-order model and a good fitting was observed (Fig. 5.9), further confirming that the three drugs obey the Φ-order kinetics.

In accordance to Eq. 2, the higher the $P_{\lambda_{irr}}$ value, the faster the photodegration.

Therefore, plots of $k_{A \leftrightharpoons B}^{\lambda_{irr}}$ against $P_{\lambda_{irr}}$ for each set of experiments yielded linear correlations with r values over 0.95 and intercepts of practically zero value (Table 5.7). The factor $\beta_{\lambda_{irr}}$ is constant for a given irradiation wavelength and thus can be obtained from the equation of the line as the gradient.

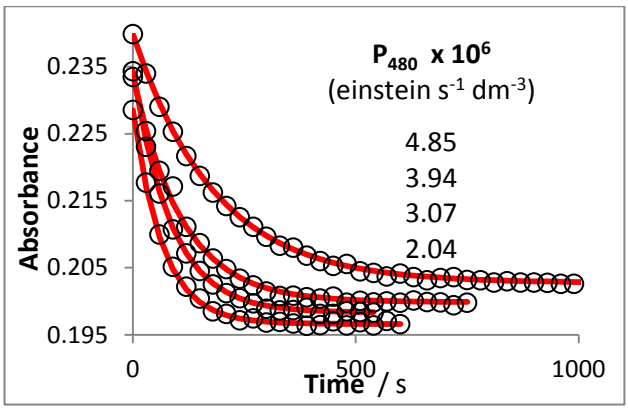

Fig 5.9: **Effect of increasing the radiant power of the monochromatic irradiation beam on the kinetic traces of SUT (8.94 x 10^{-6} M) when irradiated and observed at 480 nm. Circles represent experimental data and the solid lines are the fitting of the traces to the AB(2Φ) kinetic model.**

For all three drugs, the factor $\beta_{\lambda_{irr}}$ was plotted against irradiation wavelength and they were readily represented by a linear relationship (Fig. 5.10). The linear relationship easily enables the determination of the factor $\beta_{\lambda_{irr}}$ at any wavelength within their respective reactivity range (situated between 275-480 nm).

More importantly, this $\beta_{\lambda_{irr}}$ factor enables the development of a new actinometric method. Rearrangement of Eq.2 will allow the determination of the radiant power of an unknown, monochromatic light source within 275-480 nm.

The chemical actinometer recommended by the ICH (quinine hydrochloride) [49] presents various drawbacks that seriously hamper its application to photostability testing purposes [50-53]. The reproducibility and reliability of results obtain using quinine varies depending on the spectral power distribution of the light source, its location in the chamber and the timing which the measurement of the absorbance is taken [50]. Supposedly, these can be overcome by calibrating the system for the type of light source used. However, the calibration of quinine depends on its concentration [51]. Yet, quinine has been found to be sensitive to dissolved oxygen content and temperature [52].

Table 5.7: Correlation equations for the variation of the three drug's photodegradation overall rate-constants ($k_{A \leftrightharpoons B}^{\lambda_{irr}}$) with radiant power ($P_{\lambda_{irr}}$), the corresponding $\beta_{\lambda_{irr}}$ factor values, and the span of radiant power employed for various monochromatic irradiations.

Irradiation wavelength λ_{irr} /nm	Equation of the line $k_{A \leftrightharpoons B}^{\lambda_{irr}} = \beta_{\lambda_{irr}} \times P_{\lambda_{irr}} + \text{intercept}$	Correlation coefficient, r^2	$P_{\lambda_{irr}}$ x 10^6 / einsteins^{-1} dm^{-3}
DBZ			
350	2120.6 x P_{350} + 0.0002	0.9969	1.01 – 2.51
345	2589.8 x P_{345} - 0.0003	0.9830	0.95 – 2.20
325	4013.2 x P_{300} - 0.0024	0.9499	0.93 – 1.90
300	2499.3 x P_{300} - 0.0017	0.9987	1.05 – 1.31
275	326.26 x P_{275} - 0.0001	0.9991	0.78 – 1.64
AXI			
400	2193 x P_{400} - 0.0006	0.9599	1.59 – 3.51
380	3126.2 x P_{380} + 0.0003	0.9875	1.36 – 3.04
355	7691.6 x P_{355} - 0.0005	0.9894	1.25 – 2.62
332	14552 x P_{332} - 0.0071	0.9583	1.17 – 1.77
SUT			
480	3437.7 x P_{480} - 0.0013	0.9980	2.04 – 4.85
460	4301.4 x P_{460} + 0.001	0.9887	1.80 – 4.30
440	5521.9 x P_{440} + 0.0006	0.9882	1.77 – 4.07
420	5846.6 x P_{420} + 0.006	0.9851	1.66 – 3.93
400	5432.6 x P_{400} + 0.0023	0.9718	1.45 – 3.48
380	3740.9 x P_{380} + 0.0019	0.9959	1.19 – 2.97
360	5866.2 x P_{360} - 0.0064	0.9915	1.58 – 2.67
345	1938.1 x P_{345} - 0.0004	0.9941	1.42 – 2.04
340	1560.1 x P_{340} - 0.00007	0.9881	0.85 – 1.98
320	1096.2 x P_{320} + 0.00001	0.9954	0.61 – 1.33

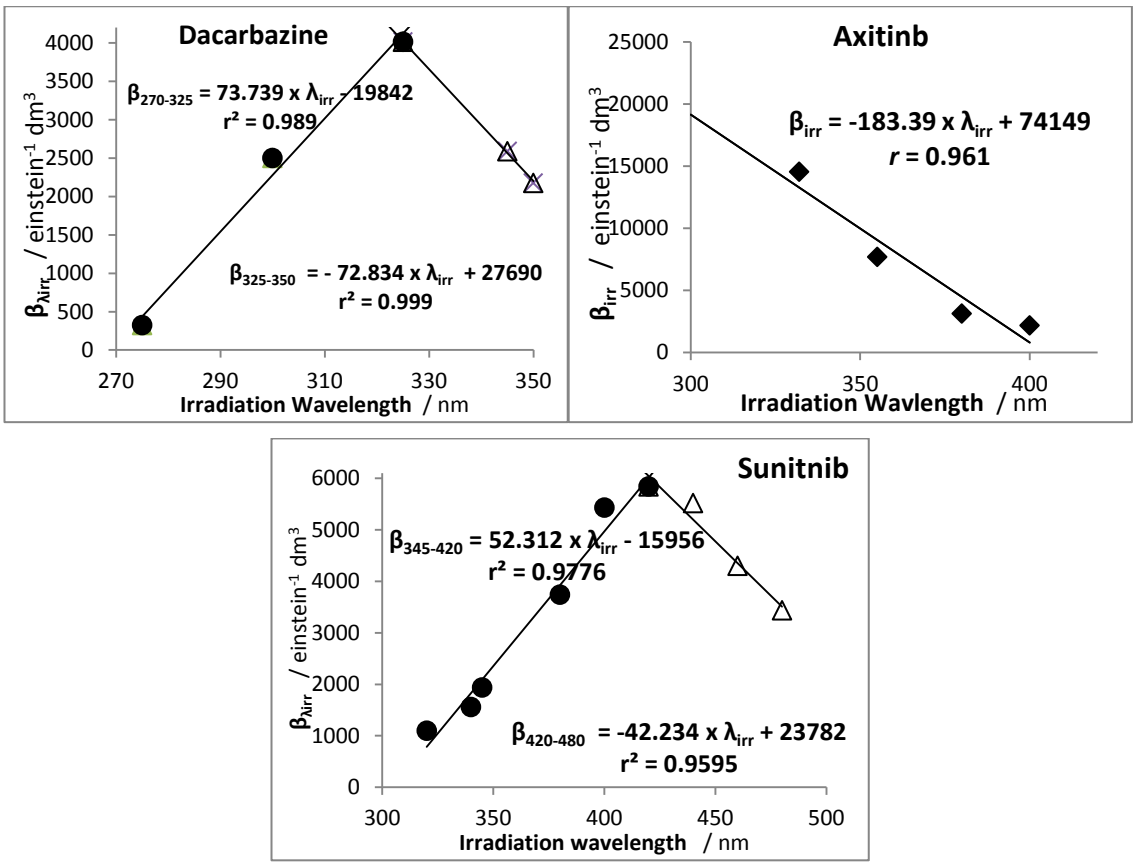

Fig 5.10: Linear correlation of $\beta_{\lambda_{irr}}$ with irradiation wavelength. $\beta_{\lambda_{irr}}$ is expressed in einstein^{-1} dm^3

In order to measure the radiant power of an unknown light source, a monochromatic irradiation of DBZ, AXI or SUT needs to be carried out in ethanol at the specified concentrations and at an irradiation wavelength within the specified range. The experimental trace obtained is then to be fitted with the Φ-order model (Eq. 1) to determine the overall rate-constant of the reaction. $\beta_{\lambda_{irr}}$ at any irradiation wavelength situated between 275-480 nm can readily be determined using Fig. 5.10. Subsequently, the radiant power can easily be worked out through the simple equations for $P_{\lambda_{irr}}$ presented in Table 5.8.

As long as the photochemical reaction obeys an AB mechanism, the present method will enable the development of reliable actinometers without prior knowledge of any of the

unknown reaction parameters. Thus, allowing more thermally-stable, simple AB(1Φ) and AB(2Φ) chemical actinometers to be developed.

DBZ, AXI and SUT make ideal chemical actinometers, which covers a wide range of the absorption spectrum (270 – 480 nm), spanning from UVB to visible. They are commercially available and relatively cheap. In contrast to some existing chemical actinometers, the three presented here are simple to prepare, thermally-stable and have a known reaction mechanism.

Table 5.8: Equations for calculation of the radiant power $P_{\lambda_{irr}}$ using the three drugs in ethanol

Irradiation wavelength range λ_{irr} / nm	Equation for $\beta_{\lambda_{irr}}$	Correlation coefficient, r^2	Equation for $P_{\lambda_{irr}}$
DBZ (5.47 x 10^{-6} M)			
270-235	$\beta_{270\text{-}325}$ = 73.739 x λ_{irr} - 19842	0.989	$\frac{k_{A\rightarrow B}^{\lambda_{irr}}}{73.739 \times \lambda_{\mathrm{irr}} - 19842}$
325-350	$\beta_{325\text{-}350}$ = -72.834 x λ_{irr} - 27690	0.999	$\frac{k_{A\rightarrow B}^{\lambda_{irr}}}{-72.834 \times \lambda_{\mathrm{irr}} - 27690}$
AXI (1.29 x 10^{-5} M)			
330-400	$\beta_{300\text{-}400}$ = -183.39 x λ_{irr} - 74149	0.961	$\frac{k_{A\leftrightarrows B}^{\lambda_{irr}}}{-183.39 \times \lambda_{\mathrm{irr}} + 74149}$
SUT (8.94 x 10^{-6} M)			
345-420	$\beta_{345\text{-}420}$ = 52.312 x λ_{irr} - 159256	0.978	$\frac{k_{A\leftrightarrows B}^{\lambda_{irr}}}{52.312 \times \lambda_{\mathrm{irr}} - 159256}$
420-480	$\beta_{420\text{-}480}$ = -42.234 x λ_{irr} + 23782	0.960	$\frac{k_{A\leftrightarrows B}^{\lambda_{irr}}}{-42.234 \times \lambda_{\mathrm{irr}} + 23782}$

These alternative actinometers eliminates the post-irradiation analytical procedures required with the standard ferrioxalate actinometry [54] - which needs phenanthroline (a complexation reagent) for colour development to enable in-situ quantification of the light intensity. The reproducibility and reliability of the results obtain has been reported to be sensitive to procedural variations [55-57].

The method adopted here can easily be applied to many other photolabile drugs following the same AB mechanism, regardless of a unimolecular or photoreversible system, as prior knowledge of other reaction parameters are (ε and Φ) not required – unlike the current requirements for chemical actinometric systems [58].

5.5. CONCLUSION

The photokinetic data of drugs are often treated using thermal zero-, first- and/or second-order thermal kinetic models, which gives poor fittings. This clearly shows that photokinetic data treatment is an area which requires crucial development to provide valid and reliable integration rate-law equations to describe and elucidate the kinetic behaviour of photodegradation reactions.

This study further confirms the usefulness of the new Φ-order approach to elucidate the kinetics of unimolecular and photoreversible reactions obeying an AB mechanism - filling a gap in photokinetic studies of drug photodegradation.

The photokinetic traces of DBZ, AXI and SUT were all well described by the newly proposed Φ-order model. These and previous results presented by our team [14-18] strongly suggests that photodegradation of drugs are better described by Φ-order than the classic thermal reaction orders.

The semi-empirical model elucidation method used is easy-to-implement, simple-to-achieve, reliable and effective. More importantly, it allows the determination of the quantum yield values - the only physical parameters capable of indicating the photoreactivity of a drug.

For the first time, the quantum yields of DBZ, *Z*-AXI and *Z*-SUT were found and determined to increase with irradiation wavelength. Between 2.7 and 266-fold increase was recorded for

DBZ, *Z*-AXI and *E*-SUT $\Phi_{A\rightarrow B}^{\lambda_{irr}}$ values. In contrast, the quantum yields of *E*-AXI and *E*-SUT were less affected by the variation of the irradiation wavelength of the same ranges.

These findings strongly suggest that the quantum yield of drugs' photodegradation should *a priori* be considered wavelength dependent, as also indicated by the results obtained for Nifedipine [14] and Montelukast [16]. Therefore, the average quantum yield values obtained using polychromatic irradiations, as reported on by many studies in the pharmaceutical literature [59-64], may be deemed unreliable and must be considered with caution.

The actinometric techniques presented here cover a wide spectral range (270 – 480 nm), spanning from UVB to visible - in addition to that covered by Nifedipine [14], Montelukast [16] and Diarylethene derivatives [65], which are developed the same way using the Φ-order model. The spectral range covers most BNF drugs' photodegradation causative ranges.

It is important to note that the approach adopted here can easily be applied to many other photolabile drugs following the same AB mechanism, regardless of a unimolecular or photoreversible system.

5.6. REFERENCES

1. Maafi M and Brown R.G. (2007) The kinetic model for AB(1Φ) systems: A closed-form integration for the differential equations with a variable photokinetic factor, *Journal of Photochemistry and Photobiology A: Chemistry*, 187:319-324
2. Maafi M and Maafi W (2014) Φ-order kinetics of photoreversible-drug reactions, *International Journal of Pharmaceutics*, 471:536-543.
3. Tønnesen H.H. (Ed.) (2004) Photostability of Drugs and Drug Formulations, Second Edition, US:CRC Press LLC
4. Piechocki J.T. and Thoma K. ed. (2010) Pharmaceutical photostability and stabilization technology, New York: Informa Healthcare
5. Al Omari M.M., Zoubi R.M., Hasan E.I., Khader T.Z. and Badwan A.A. (2007) Effect of light and heat on the stability of montelukast in solution and in its solid state, *Journal of Pharmaceutical and Biomedical Analysis*, 45(3):465-471

6. Malesuik M.D., Gonçalves H.M., Paim C.S., Schapoval E.E. and Steppe M. (2009) LC: analysis of photodegradation kinetics of nitazoxanide in pharmaceutical formulations, *Journal of Chromatographic Science*, 47(9):745-748

7. Alsarra A.L (2004) Develeopment of a stability-indicating HPLC method for the determination of montelukast in tablets and human plasma and its applications to pharmacokinetic and stability studes, *Saudi Pharmaceutical Journal,* 12(4):136-143

8. Roman J., Breier A.R. and Steppe M. (2011) Stability Indicating LC Method to Determination of Sodium Montelukast in Pharmaceutical Dosage Form and its Photodegradation Kinetics, *Journal of Chromatographic Science*, 49(7):540-546

9. Matsuura I., Imaizumi M. and Sugiyama M. (1990) Method of kinetic analysis of photodegradation: nifedipine in solutions, *Chemical and Pharmaceutical Bulletin*, 38(6):1692-1696

10. Wang J. and Moore D.E. (1992) A study of the photodegradation of benzydamine in pharmaceutical formulations using HPLC with diode array detection, *Journal of Pharmaceutical and Biomedical Analysis*, 10(7):535-540

11. Gu L. Chiang H.S. and Johnson D. (1988) Light Degradation of Ketorolac Tromethamine, *International Journal of Pharmaceutics*, 41(2):105-113

12. Zhou Z., Zhang Y., Wang H., Chen T. and Lu W. (2014) The Comparative Photodegradation Activities of Pentachlorophenol (PCP) and Polychlorinated Biphenyls (PCBs) Using UV Alone and TiO2-Derived Photocatalysts in Methanol Soil Washing Solution, *PLoS ONE*, 9(9):1-8

13. Pickett J.E. and Moore J.E. (1995) Photodegradation of UV absorbers: Kinetics and structural effects, *Die Angewandte Makromolekulare Chemie*, 232(1):229–238

14. Maafi M and Maafi W (2013) Modelling nifedipine photodegradation, photostability and actinometric properties, *International Journal of Pharmaceutics*, 456:153-164

15. Maafi M and Maafi W (2014) Φ-order kinetics of photoreversible-drug reactions, *International Journal of Pharmaceutics*, 471:536-543.

16. Maafi M and Maafi W (2014) Montelukast Photodegradation: Elucidation of Φ-Order Kinetics, Determination of Quantum Yields and Application to Actinometry, *International Journal of Pharmaceutics*, 471:544-552

17. Maafi M. and Lee L.Y. (2015) Actinometric and Φ-Order Photodegradation Properties of Anti-Cancer Sunitinib, *Journal of Pharmaceutical and Biomedical Analysis*, 110:34-41

18. Maafi M. and Lee L.Y. (2015) Determination of Dacarbazine Φ-Order Photokinetics, Quantum Yields, and Potential for Actinometry, *Journal of Pharmaceutical Sciences*, 104(10):3501-3509

19. Chiş M., Căinap C., Găbudean A., Focşan M., Leopold N. and Chiş V (n.d.) Density Function Theory, Babes Bolyai University: Romania [Online] http://www.phys.ubbcluj.ro/~vchis/cursuri/cspm/course8.pdf [Accessed 22/05/2015]

20. Hall A., Sims L.M. and Ballantyne J. (2014) Assessment of DNA damage induced by terrestrial UV irradiation of dried bloodstains: Forensic implications, *Forensic Science International: Genetics*, 8(1):24-32

21. Aatmani M.E., Poujol S., Astre C., Malosse F. and Pinguet F. (2002) Stability of Dacarbazine in Amber Glass Vials and Polyvinyl Chloride Bags, *American Society of Health-System Pharmacists*, 59:1351-1356.

22. Malik M.Z, Ahmad M. and Muahammad S. (2013) Rapid and simultaneous determination of adriamycin, bleomycin, vinblastine and dacarbazine in plasma of hodgkin's lymphoma patients by a reversed phase HPLC method, *Journal of the Chilean Chemical Society*, 58(2): 1674-1677

23. Fiore D., Jackson A.J., Didolkar M.S. and Dandu V.R. (1985) Simultaneous determination of dacarbazine, its photolytic degradation product, 2-azahypoxanthine, and the metabolite 5-aminoimidazole-4-carboxamide in plasma and urine by high-pressure liquid chromatography, *Antimicrobial Agents and Chemotherapy*, 27(6): 977–979

24. Lal Prasanth M.L. and Siddiraju S. (2014) Stability indicating HPLC method for the determination of Dacarbazine in pharmaceutical dosage form, *International Journal of Pharmacy*, 4(3):5-12

25. Bouchet S., Chauzit E., Ducint D., Castaing N., Canal-Raffin M., Moore N., Titier K. and Molimard M. (2011) Simultaneous determination of nine tyrosine kinase inhibitors by 96-well solid-phase extraction and ultra-performance LC/MS-MS, *Clinica Chimica Acta*, 412(11–12):1060-1067

26. Sistla A., Yang W.L. and Shenoy N. (2006) High-performance liquid chromatography method for determination of reversible isomers of SU5416, Journal of Chromatography A, 1110:73-80

27. De Brujin P., Sleijfer S., Lam M., Mathijssen R.H.J., Wiemer E.A.C. and Loos W. (2010) Bioanalytical method for the quantification of sunitinib and its n -desethyl metabolite SU12662 in human plasma by ultra performance liquid chromatography/ tandem triple-quadrupole mass spectrometry. Journal of Pharmaceutical and Biomedical Analysis, 51:934-941.

28. Minkin P., Zhao M., Chen Z., Ouwerkerk J., Gelderblom H. and Baker S.D. (2008) Quantification of sunitinib in human plasma by high-performance liquid chromatography-tandem mass spectrometry, Journal of Chromatography B, 874:84-88

29. Sparidans R.W., Iusuf D., Schinkel A.H., Schellens J.H.M. and Beijnen J.H. (2009) Liquid chromatography-tandem mass spectrometric assay for the light sensitive tyrosine kinase inhibitor Axitinib in human plasma, *Journal of Chromatography B*, 877(32):4090-4096

30. Likar M.D., Cheng G., Mahajan N. and Zhang Z. (2011) Rapid identification and absence of drug tests for AG-013736 in 1 mg Axitinib tablets by ion mobility spectrometry and DART™ mass spectrometry, *Journal of pharmaceutical and biomedical analysis*, 55(3):569-573

31. European Medicines Agency (2012) Committee for Medicinal Products for Human Use assessment report EMA/CHMP/453325/2012 Inlyta. [ONLINE] Available at: http://www.ema.europa.eu/docs/en_GB/document_library/EPAR_-_Public_assessment_report/human/002406/WC500132190.pdf [Accessed 09/12/12].

32. Rodamer, M. (2011) Development and validation of a liquid chromatography/tandem mass spectrometry procedure for the quantification of sunitinib (SU12662) and its active metabolite N-desethyl sunitinib (SU12662), in human plasma: Application to an explorative study. Journal of Chromatography B, 879:695-706.

33. Yoshioka S. and Stella V.J. (2001) Stability of Drugs and Dosage Forms, US: Springer

34. Thoma K. and Kubler N. (1996) Wavelength dependency of photodegradation processes of drug substances, *Pharmazie*, 51(9):660 - 664

35. Aman W. and Thoma K. (2003) Particular features of photolabile substances in tablets, *Pharmazie*, 58(9):645-650

36. Allwood M.C. and Plane J.H. (1986) The wavelength-dependent degradation of vitamin A exposed to ultraviolet radiation, *International Journal of Pharmaceutics*, 31(1):1-7

37. Tiburcio-Moreno J.A., Marcelín-Jiménez G., Leanos-Castaneda O.L., Yanez-Limon J.M. and Alvarado-Gil J.J. (2012) Study of the Photodegradation Process of Vitamin E Acetate by Optical Absorption, Fluorescence, and Thermal Lens Spectroscopy, *International Journal of Thermophysics*, 33(10): 2062-2068

38. Murata S., Kobayashi J., Kongou C., Miyata M., Matsushita T. and Tomioka H. (2000) Remarkable wavelength-dependent photoreactions of the bis(diazo) ketone having inequivalent diazo groups: studies in fluid solutions and in low-temperature matrixes, Journal of Organic Chemistry , 65(19):6082-6092

39. Horspool W.M. and Lenci F. (Ed.) (2003) CRC Handbook of Organic Photochemistry and Photobiology, Volumes 1 & 2, US: Taylor & Francis Inc

40. Rabek J.F. (1996) Photodegradation of Polymers: Physical Characteristics and Applications, US:Springer

41. Bouillon R.C., Knierim T.L., Kieber R.J., Skrabal S.A. and Wright J.L.C (2006) Photodegradation of the algal toxin domoic acid in natural water matrices, *Limnology and Oceanography*, 51(1):321-330

42. Bassotti E., Carbone P., Credi A., Di Stefano M., Masiero S., Negri F., Orlandi G. and Spada GP. (2006) Effect of strain on the photoisomerization and stability of a congested azobenzenophane: a combined experimental and computational study, *Journal of Physical Chemistry A*, 110(45):12385-94.

43. Moan J. (2001) Visible light and UV radiation. In Radiation at Home, Outdoors and in the Workplace edited by Brune D., Helborg R., Persson B.R.R. and Paakkonen R., Scandinavian Science Publishers., Oslo, Norway.

44. European Medicines Agency (2007) Sutent: European Public Assessment Report - Scientific Discussion. [ONLINE] Available at: http://www.ema.europa.eu/docs/en_GB/document_library/EPAR_-_Scientific_Discussion/human/000687/WC500057733.pdf [Accessed 20/10/13].

45. Boussemart L., Routier E., Mateus C., Opletalova K., Sebille G., Kamsu-Kom N., Thomas M., Vagner S., Favre M., Tomasic G., Wechsler J., Lacroix L. and Robert C. (2013) Prospective study of cutaneous side-effects associated with the BRAF inhibitor vemurafenib: a study of 42 patients, *Annals of Oncology: Official Journal for the European Society for Medical Oncology*, 24(6):1691-1697.

46. Lacouture M.E., Duvic M., Hauschild A., Prieto V.G., Robert C., Schadendorf D., Kim C.C., McCormack C.J., Myskowski P.L., Spleiss O., Trunzer K., Su F., Nelson B., Nolop K.B., Grippo J.F., Lee R.J., Klimek M.J., Troy J.L. and Joe A.K. (2013) Analysis of dermatologic events in vemurafenib-treated patients with melanoma, *The Oncologist*, 18(3):314-22.

47. Drummer R., Rinderknecht J. and Goldinger S.M. (2012) Ultraviolet A and Photosensitivity during Vemurafenib Therapy, *The New England Journal of Medicine,* 366(5):480-481

48. Gelot P., Dutartre H., Khammari A., Boisrobert A., Nguyen J.M., Schmitt C., Deybach J.C., Seite S. and Dréno B. (2012) Le vemurafenib: une photosensibilité UVA induite particulière, *Annales de Dermatologie et de Vénéréologie*, 139(12):B86

49. International Conference on Harmonisation of technical requirements for registration of pharmaceuticals for human use (1996) Stability testing: Photostability testing of new drug

substances and products – ICH Q1B. [Online] Available at: http://www.ich.org/fileadmin/Public_Web_Site/ICH_Products/Guidelines/Quality/Q1B/Step4/Q1B_Guideline.pdf [Accessed 21/05/2015]

50. Baertschi S.W., Alsante K.M. and Tønnesen H.H. (2010) A critical assessment of the ICH guideline on photostability testing of new drug substances and products (Q1B): Recommendation for revision, *Journal of Pharmaceutical Science*, 99(7):2934-2940

51. de Azevedo Filho C.A., de Filgueiras Gomes D., de Mélo Guedes J.P., Batista R.M. and Santos B.S. (2011) Considerations on the quinine actinometry calibration method used in photostability testing of pharmaceuticals, *Journal of Pharmaceutical and Biomedical Analysis*, 54(4):886–888

52. Baertschi S.W. (1997) Commentary on the quinine Actinometry system described in the ICH draft guideline on photostability testing of new drug substances and products, *Drug Stability*, 1:193–195

53. Allen J.M., Allen S.K. and Baertschi S.W. (2000) 2-Nitrobenzaldehyde: a convenient UV-A and UV-B chemical actinometer for drug photostability testing, *Journal of Pharmaceutical and Biomedical Analysis*, 24(2):167-178

54. Khun H.J., Braslavsky S.E. and Schmidt R. (2004) Chemical Actinometry (International Union Of Pure and Applied Chemistry's Technical Report), *Pure and Applied Chemistry,* 76(12):2105-2146

55. Bowman W.D. and Demas J.N. (1976) Ferrioxalate actinometry. A warning on its correct use, *Journal of Physical Chemistry*, 80(21):2434–2435

56. Kirk A.D. and Namasivayam C. (1983) Errors in ferrioxalate Actinometry, *Analytical Chemistry*, 55(14):2428–2429

57. Harris G., Dean Adams V., Moore W. and Sorensen D. (1987) Potassium Ferrioxalate as Chemical Actinometer in Ultraviolet Reactors, *Journal of Environmental Engineering*, 3(612):612-627

58. Favaro G. (1998) Actinometry: Concepts and Experiments, in Drugs: Photochemistry and Photostability (Edited By Albini A. and Fasani E.), Cambridge, UK: The Royal Society of Chemistry.

59. Fasani E., Dondi D., Ricci A. and Albini A. (2006) Photochemistry of 4-(2-Nitrophenyl)-1,4-dihydropyridines. Evidence for electron transfer and formation of an intermediate, *Photochemistry and Photobiology*, 82(1):225–230

60. Goldstein S., Aschengrau D., Diamant Y. and Rabani J. (2007) Photolysis of Aqueous H_2O_2: Quantum Yield and Applications for Polychromatic UV Actinometry in Photoreactors, *Environmental Science & Technology*, 41(21):7486-7490

61. Palm W.U. and Zetzsch C. (1995) Investigation of the Photochemistry and Quantum Yields of Triazines Using Polychromatic Irradiation and UV-Spectros Copy as Analytical Tool, *International Journal of Environmental Analytical Chemistry*, 65: 313-329

62. Vione D., Maddigapu P.R., De Laurentiis E., Minella M., Pazzi M, Maurino V., Minero C., Kouras S. and Richard C. (2011) Modelling the photochemical fate of ibuprofen in surface waters, *Water Research*, 45(20):6725-6736

63. Borowska E., Felis E. and Korneliusz M. (2015) Degradation of Sulfamethoxazole Using UV and UV/H_2O_2 Processes, *Journal of Advanced Oxidation Technologies*, 18(1):69-77

64. Passananti M. (2013) *Xenobiotics In The Environment: An Investigation On The Transformation Kinetics, The Environmental Metabolites And Their Formation Mechanisms*, Ph.D. University of Naples Federico II. Available at: http://www.fedoa.unina.it/9310/1/Passananti_Monica_25.pdf [Accessed 28/01/2016]

65. Maafi M. (2010) The potential of AB(1Φ) systems for direct Actinometry. Diarylethenes as successful actinometers for the visible range, *Phys. Chem. Chem. Phys.* 12:13248-13254

CHAPTER SIX

PHOTOKINETICS OF DBZ, AXI AND SUT IN AQUEOUS MEDIA

6.1. INTRODUCTION

The presence of even the smallest of impurity can influence a drug's efficacy and safety [1,2]. Thus, it is required by the International Conference on Harmonisation of Technical Requirements for Registration of Pharmaceuticals for Human Use (ICH) that a report on all new drugs' stability be prepared for submission in registration applications and photostability testing of all new drug substances and products was made an "integral part of stress testing" [3,4]. The ICH Q1b guideline [4] on photostability testing provides guidance on the basic information required to characterise the drug's light sensitivity and stability. If the Q1b document describes with some details test 1 and 2 it should also make provision for drugs' photostability tests in solution. For solution tests there are however no stipulated (i) experimental details, (ii) methods for the treatments of photodegradation data, and/or (iii) standardized quantification/evaluation methods, in the Q1b document. This aspect does not follow the general pattern adopted in ICH documents were generally detailed procedures are provided. The choice of methods for testing, quantification and evaluation of photostability in solution was essentially left to the discretion of the experimentalist.

The situation is even more acute when the photodegradation of drugs obeys complex (multistep) mechanisms that may involve both thermal and photochemical reactions yielding several products. Such complexity can be seen in the case of the ICH (Q1b) recommended actinometer, the quinine hydrochloride (QH) [4]. It has been clearly shown by many authors [5-8] that the application of QH is not reliable and far from being standardised. One of the main problems of QH is its unknown mechanism that was evidenced to involve concurrent photochemical and thermal processes [7]. In a larger view, this is not a rare situation in drugs' photodegradation. The lack of standardized methods is also related to the absence of kinetic methods able to handle photodegradation mechanisms. As it has been shown in chapter 3,

when integrated rate-laws are available, mostly for simple mechanisms, a considerable knowledge on the photodegradation reaction can be easily reached. Unfortunately for complex reactions, there is still no mathematical frameworks that would be useful.

In the literature, a few attempts used computational techniques to overcome such a problem [9-17]. Such kinetic treatments enabled the spectra of each species, the concentration profiles, and equilibrium constant to be extracted from mixed spectral data. However, these methods presented two serious limitations: (i) they employed differential equations suitable for thermal reactions (which are inapplicable for photochemical reactions, as discussed in chapter 3); and (ii) they generally assumed a "minimum" mechanism to the drugs' photodegradations studied.

This state of the matter has prompted us to propose, in this chapter, a new alternative method aiming at circumventing the limitations of the published approaches and which is able to elucidate, quantify and evaluate complex photodegradation of drugs. It has been developed here for the photokinetic analyses of DBZ, AXI and SUT.

6.2. ABSORPTION SPECTRA OF DRUGS IN WATER

The electronic absorption spectra of the three drugs in water show similar transitions and spectral characteristics to those observed in ethanol, with only some maxima/intensity differences, Fig. 6.1.

It is interesting to notice that, at low concentration, the hydrophobic AXI seem well solubilized in the predominantly aqueous mixture, water/ethanol (v/v, 97.5/2.5). This may provide evidence that small quantities of AXI may interact with water (especially in vivo) and hence may undergo degradation in this medium.

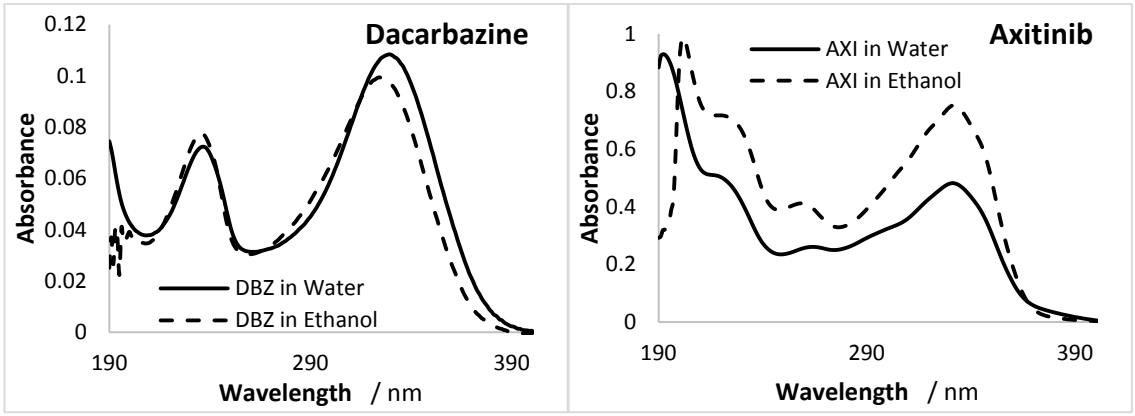

Fig. 6.1: Native absorption spectra of the drugs in water and ethanol: (left) Dacarbazine (DBZ, 5.38 x 10^{-6} M and 5.47 x 10^{-6} M respectively), (right) Axitinib (AXI, 2.29 x 10^{-5} M and 2.29 x 10^{-5} M respectively) (see SUT spectra in Annex A6.1).

6.3. THERMAL STABILITY IN AQUEOUS MEDIA

In Chapter 3, it had been established that all three drug (DBZ, AXI and SUT) were thermally stable in organic solutions. However, apart from DBZ which is known to be stable [18-23], AXI and SUT's thermal stability in aqueous media has not been reported in the literature. Hence, we studied the thermal behaviour of the three drugs kept in the dark at 22°C, stirred and regularly monitored by DAD analysis.

In water, AXI's and SUT's undergo a thermal degradation evidenced by a decrease of their respective absorption spectra. The more pronounced variation of absorbance recorded for AXI (Fig 6.2) was found to decrease at the same rate as a constant ratio of various peaks' absorbances was measured.

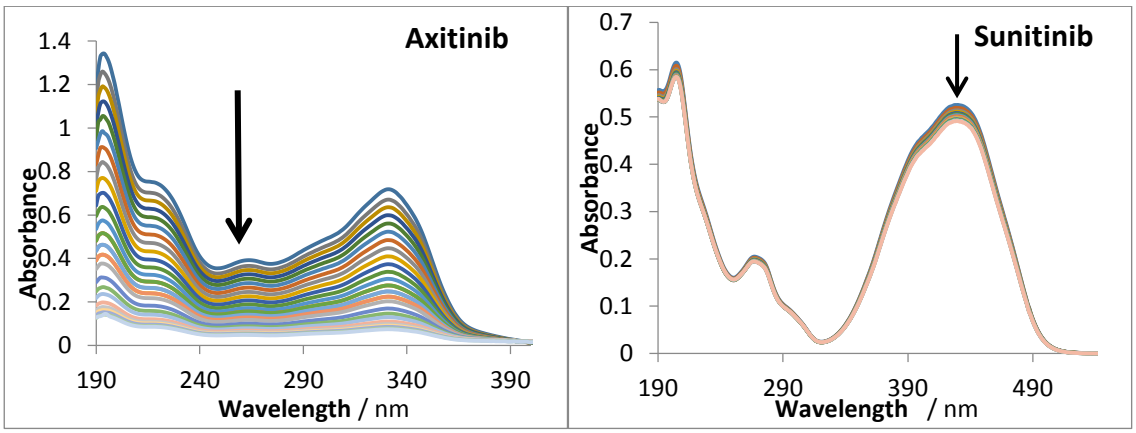

Fig 6.2: Changes in the spectrum of (left) 1.97 x10^{-4} M AXI 2.5% v/v ethanol/water solution and (right) 1.92 x 10^{-5} M SUT in water kept in the dark, stirred and thermalstatically maintained at 22°C

The kinetic traces of AXI and SUT (Fig. 6.3) mainly show two reaction regimes. In the case of AXI the first regime (~ 60 s) is slower than the second while the reverse situation is observed for SUT. For both drugs (labelled $A_{2,3}$ in Fig. 6.3), the two reaction stages suggest the presence of at least two products ($C_{2,3}$ and $D_{2,3}$).

The S1 section of SUT's trace is similar to the one observed in ethanol which tends to a plateau in S2. This might indicate that *Z*-SUT (A_3, in scheme 6.1) undergoes a thermal isomerisation to its *E*-isomer (in S1) as well as a degradation to another product (B_3 in S1 and C_3 in S2, respectively). The slow rate of formation of C_3 allow to suggest that this reaction step ($A_3 \rightarrow C_3$) is concurrent to the isomerisation but is only noticeable after the equilibrium is reached. Since, at this stage it wouldn't be possible to rule out the preservation of the double bond, we can postulate that a similar degradation could take place from B_3 (to D_3). *E*-AXI (A_2) however undergoes a priori a consecutive reaction involving C_2 and D_2. More evidence of this proposal will be provided from the analysis of the full thermal/photochemical reactions.

$$D_2 \xleftarrow{\Delta} C_{2,3} \xleftarrow{\Delta} A_{2,3} \underset{\Delta}{\rightleftharpoons} B_3 \xrightarrow{\Delta} D_3$$

Scheme 6.1: Proposed thermal degradation reaction mechanism for AXI and SUT

Fitting the traces (Fig. 6.3) on the bases of the mechanisms proposed in Scheme 1 (see corresponding differential equations of each drugs in annex A6.2), yielded the respective sets of kinetic parameters (Table 1).

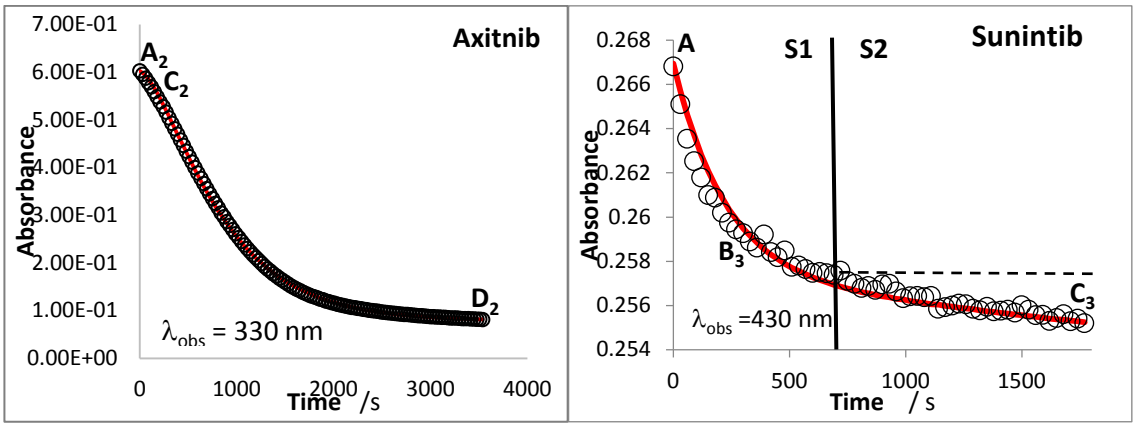

Fig 6.3: Thermaldegradation kinetic of 2.03 x 10^{-5} M AXI in 2.5 % (v/v) ethanol/water solution (right) and 1.12 x 10^{-5} M SUT (Left) when kept in the dark at 22°c, stirred, λ_{obs} = 330 nm, circles represent experimental data and the solid lines are the fitting of the trace based on scheme 6.1. Expected plateau indicated by the dotted lines and change in rate indicated by the solid line at 900 s, separating section 1 (S1) and section 2 (S2).

The reaction rates for AXI's thermal transformations indicate that the latter step of AXI's reaction ($C_2 \rightarrow D_2$) is more than two times faster than the former ($A_2 \rightarrow C_2$). The results of SUT's thermal degradation show that the formation of D_3 from B_3 is the slowest reaction, being 13 times slower than $A_3 \rightarrow C_3$. The reversible isomers rate constants are much faster than their side reactions with the forward reaction ($A_3 \rightarrow B_3$) is almost 4-fold slower than the reverse ($B_3 \rightarrow A_3$).

Table 6.1: Overall rate-constants for AXI and SUT thermal degradation reactions in aqueous solution

Drug (Concentration /M)	Epsilon of the Species at λ_{obs}		Process	k_x^{Δ} / s
AXI 1.93×10^{-5}	$A_{2\,(330)}$	31162	$A_2 \rightarrow C_2$	1.55×10^{-3}
	$C_{2\,(330)}$	27500		
	$D_{2\,(330)}$	4028	$C_2 \rightarrow D_2$	3.50×10^{-3}
SUT 1.12×10^{-5}	$A_{3\,(430)}$	26750	$A_3 \rightarrow B_3$	6.90×10^{-4}
	$B_{3\,(430)}$	19400	$B_3 \rightarrow A_3$	2.70×10^{-3}
	$C_{3\,(430)}$	19580	$A_3 \rightarrow C_3$	2.00×10^{-5}
	$D_{3\,(430)}$	15010	$B_3 \rightarrow D_3$	1.55×10^{-6}

6.4. KINETIC ANALYSIS OF THE DRUGS' PHOTODEGRADATION REACTIONS.

Monochromatic and continuous irradiation of the drugs in aqueous solution induces the decrease of the original peaks and the formation of new peaks (Fig. 6.4). One isosbestic point can be observed in the cases of SUT (at 266 nm) and AXI (at 360 nm), but no isosbestic points were recorded for DBZ.

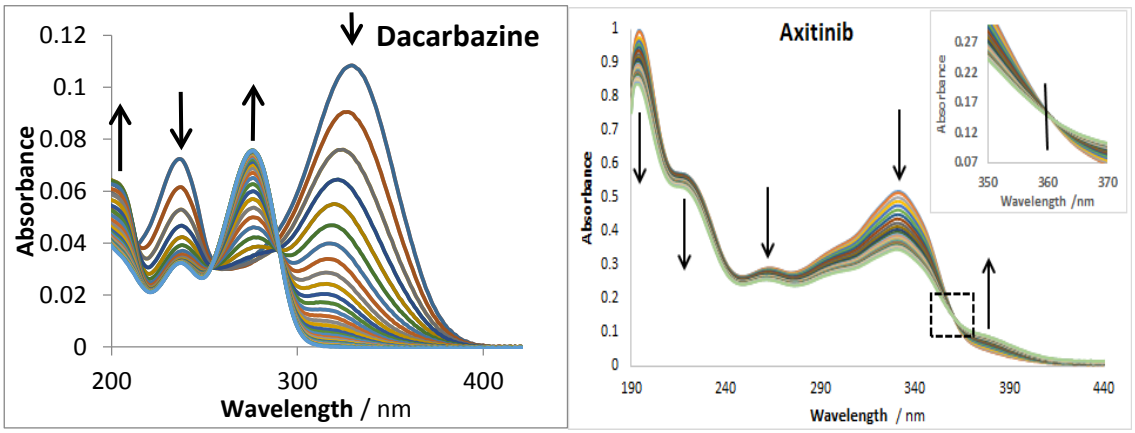

Fig 6.4: Evolution of the electronic absorption spectra under monochromatic irradiation of (Left) 5.38 x 10^{-6} M DBZ in water at λ_{irr} = 254 nm (7.06 x 10^{-7} einstein s^{-1} dm^{-3}, 22°C) and (Right) 2.03 x 10^{-5} M AXI in 2.5 % (v/v) ethanol/water solution, λ_{irr} = 360 nm (1.15 x 10^{-6} einstein s^{-1} dm^{-3}, 22°C). See Annex A6.3 for SUT

In contrast to the behaviour observed for AXI's thermal reaction, the successive spectra do not regularly decrease but are somewhat behaving similarly to what has been observed in ethanol. This would a priori suggest that the photochemical reaction (probably a photoisomerization) overtakes the thermal reactions which only becomes evident after the equilibrium (Fig. 6.5). At this stage a mechanism is proposed for AXI photodegradation (Scheme 6.2).

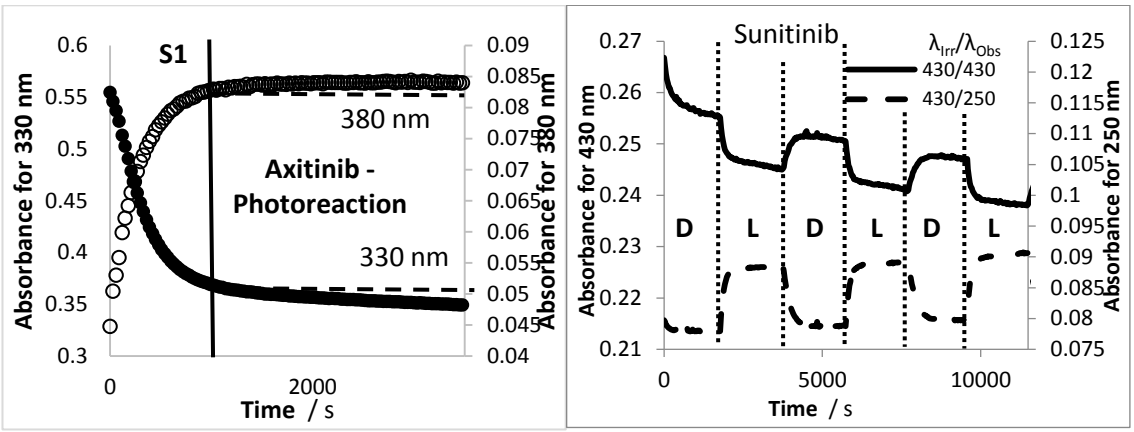

Fig. 6.5: Photokinetic trace obtained when 2.03 x 10^{-5} M AXI in 2.5 % (v/v) ethanol/water solution (left, λ_{irr} = 360 nm, 1.15 x 10^{-6} einstein s^{-1} dm^{-3}, 22°C) was irradiated continuously with a monochromatic beam. Change in rate indicated by the solid line, separating section 1 (S1) and section 2 (S2). Expected end of reaction (plateau) indicated by dotted line. (Right) 1.92 x 10^{-5} M SUT in water (λ_{irr} = 430 nm, 2.64 x 10^{-6} einstein s^{-1} dm^{-3}, 22°C). Interruptions as shown by the dotted lines (D=Dark, L=Light).

SUT's kinetic traces show an interesting reversibility between irradiated and non-irradiated intervals (Fig. 6.5), with a good reproducibility. A behaviour that strongly suggest that a photoequilibrium (probably a Z/E photoisomerisation as the one observed in ethanol) is concurrent to a thermal one. The regular decrease of the maximum absorbance during the cycles attests to an extra degradation process which might well be the thermal degradations shown in Scheme 6.1. Accordingly, a minimum mechanism for SUT overall degradation was proposed (Scheme 6.2).

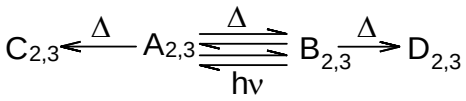

Scheme 6.2: Proposed photodegradation reaction mechanism for AXI and SUT

Most of DBZ's traces showed a monotonical increase or decrease followed by a plateau (λ_{obs} >300 nm) suggesting a rather unimolecular reaction. However, the trace obtained at 276/276 (Fig. 6.6) shows curves that successively decease, increase and decrease again; each characterised by a different length of time and slope. This indicates that there are at least three kinetic regimes (yielding three products: C_1, D_1 and E_1) involved in the overall reaction.

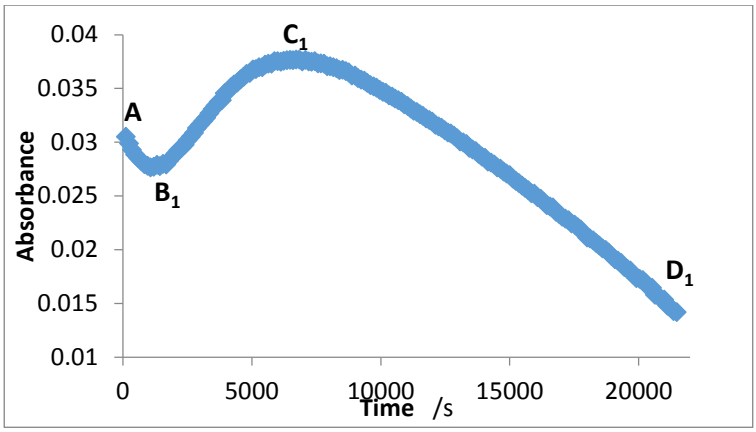

Fig 6.6: Changes in absorbance observed at 276nm when 5.38 x 10^{-6} M DBZ in water irradiated monochromatically at 276 nm (6.66 x 10^{-7} einstein s^{-1} dm^{-3}, 22°C)

The literature reports have proposed that the first step in the reaction is the breakage of the terminal N-N bond moiety separating the dimethylamine $N(CH_3)_2$ group from the rest of DBZ molecule [18-21]. However, this molecule is likely to absorb in the short wavelengths of the UV region and so might not be detected at 276 nm. Therefore, the proposed mechanism includes this species (E_1), Scheme 6.3)

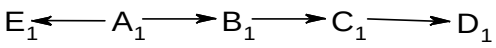

Scheme 6.3: Proposed degradation reaction mechanism for DBZ

Our proposed mechanism (scheme 6.3) is found to be in agreement with that proposed by the literature (scheme 6.4) [21,22]. It is worth noting that no colour change or absorbance band beyond 400 nm were observed in all our experiments regardless of the irradiation wavelength. This therefore means that the dimer reported as the last product by Saunders *et al.* [23] at λ_{max} = 550 nm was not produced in the experimental conditions used for the present work. This may be due to the fact that the maroon precipitate only forms at relatively high initial concentrations of DBZ.

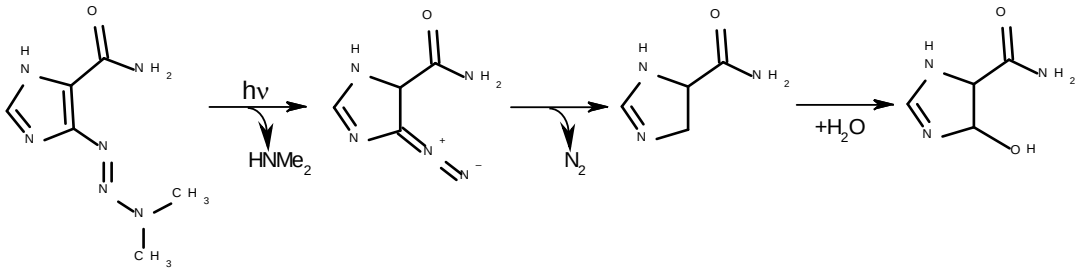

***Scheme 6.4*: Photodegradation pathways of dacarbazine proposed by Horton and Stevens [**21,22**]**

To shed more light on the reaction steps involved, solution of DBZ was subjected to irradiation for an interval of time then the irradiation was stopped and the solution monitored.

As can be seen in Fig. 6.7, when the light is off, the reaction does not stop but carries on apparently at a much slower rate than when the sample was being irradiated. This clearly indicates that either or both B_1 and C_1 are thermally active where their cumulative rate of thermal reactions seems to be considerably slower compared to the photodegradation rate of DBZ, i.e. $k^{\Delta}_{B_1 \to C_1} + k^{\Delta}_{C_1 \to D_1} \ll k^{h\nu}_{A \to B_1}$. From these observations, it is possible to deduce that if B_1 and C_1 were not photochemically active then the trace obtained under continuous irradiation would show a fast regime corresponding to the depletion of A_1, where B_1 and C_1 mostly

accumulate, which would be followed by a slower regime where B_1 and C_1 should thermally transform into D_1. This type of trace was not observed experimentally irrespective of the $\lambda_{irr}/\lambda_{obs}$ selected. Furthermore, when irradiation was resumed the rate of the reaction increased to a comparable level to that recorded at the light-off interval. Therefore, B_1 and C_1 must be photoactive.

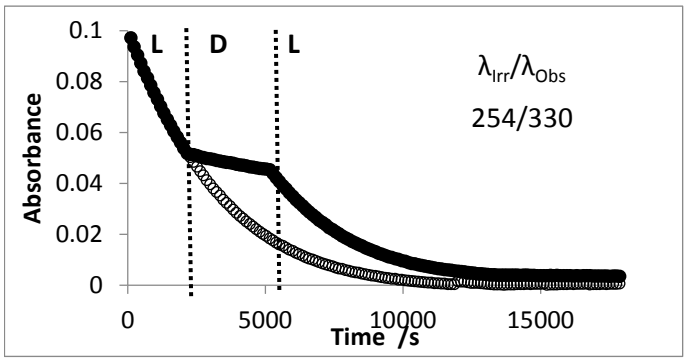

Fig. 6.7: Photokinetic of 5.38 x 10^{-6} M DBZ reaction with interrupted reaction (●) and uninterrupted reaction data (○). Interruption of irradiation as shown by the dotted lines (D=Dark, L=Light). (λ_{irr} = 254 nm, 7.06 x 10^{-7} einstein s^{-1} dm^{-3}, 22°C)

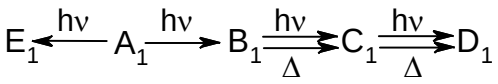

Scheme 6.5: Proposed degradation reaction mechanism for DBZ in water

It is however difficult to obtain evidence to whether any reversible reactions steps are involved in the overall mechanism. Accordingly, the proposed mechanism Scheme 6.3 must be amended so that species B_1 and C_1 are photochemically and thermally active (scheme 6.5).

The phototransformations of B_1 and C_1 has never been reported in the literature thus far. Generally, only DBZ (A_1) has been assumed to be photoactive and the rest of the intermediate species postulated in the mechanism assumed to be undergoing exclusively thermal reactions [17-24].

It is worth noting that photo and thermal mechanisms seem to produce the same species. There were no noticeable spectral features to indicate the occurrence of such differently absorbing products. This is corroborated by the literature reports which indicated only a few

products without any variation being observed when different experimental conditions were used.

The quick disappearance of all the products when the solution was subjected to irradiations at 330 and 360 nm strongly indicated that besides DBZ some photoproducts also absorb at these wavelengths or that the sum of thermal and photochemical rate constants of some of these products is relatively high. Species D_1 however is unlikely to absorb at this long wavelength range because the kinetic trace of the medium reaches a zero value at the end of the photoreaction.

The study of the thermal reactions is realised by performing an irradiation for some time (S_0) to produce the thermally instable photoproducts (B_1 and C_1), and then switch off this irradiation (similar to Fig. 6.7) and monitor the behaviour of the system for a sufficient time to be able to do kinetic measurements.

In this situation we will assume that all the five reaction species are present in solution. Their respective reaction initial concentrations at the switch off time (t = 0 at the end of S_O) will be labelled $[X]_{S_0}$.

According to the above proposed mechanism (Scheme 6.5) species A_1, E_1 and D_1 are thermally stable. Their cumulative absorbances will represent the background absorbance of the kinetic trace. The kinetics will involve the degradation of both species B_1 ($[B_1]_{S_0}$) via a consecutive reaction into C_1 and D_1, and species C_1 ($[[C_1]_{S_0}$) as a unimolecular transformation into D_1 (Scheme 6.6).

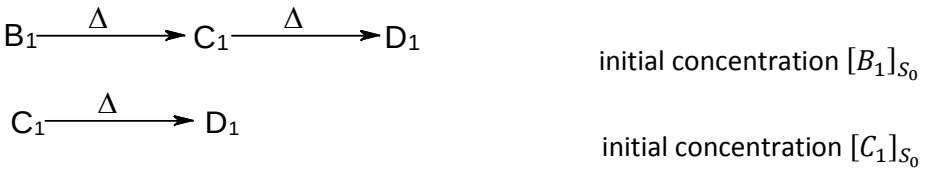

Scheme 6.6: consecutive reaction of B_1 and unimolecular reaction of C_1

Hence, the system of differential equations for these reactions is:

for the consecutive reaction:

$$\frac{dC_{B_1}}{dt}(t) = -k^{\Delta}_{B_1 \to C_1} \times C_{B_1} \quad \text{and} \quad \frac{dC_{C_1}(t)}{dt} = -k^{\Delta}_{C_1 \to D_1} \times C_{C_1} + k^{\Delta}_{B_1 \to C_1} \times C_{B_1} \quad \text{Eqs.1,2}$$

and for the unimolecular reaction of C_1

$$\frac{dC_{C_1}}{dt}(t) = -k^{\Delta}_{C_1 \to D_1} \times C_{C_1} \quad \text{Eq.3}$$

These equations can be solved in a closed form [25]. For the consecutive reaction, the integrated rate-laws are:

$$C_{B_1} = [B_1]_{S_0} \times e^{-k^{\Delta}_{B_1 \to C_1} \times (t - t_{S_0})} \quad \text{Eq.4.1}$$

$$C_{C_1} = [B_1]_{S_0} \times \frac{k^{\Delta}_{B_1 \to C_1}}{k^{\Delta}_{C_1 \to D_1} - k^{\Delta}_{B_1 \to C_1}} \times \left[e^{-k^{\Delta}_{B_1 \to C_1} \times (t - t_{S_0})} - e^{-k^{\Delta}_{C_1 \to D_1} \times (t - t_{S_0})} \right] \quad \text{Eq.4.2}$$

$$C_{D_1} = [B_1]_{S_0} \times \left[1 - \frac{k^{\Delta}_{C_1 \to D_1}}{k^{t}_{D} - k^{\Delta}_{B_1 \to C_1}} \times e^{-k^{\Delta}_{B_1 \to C_1} \times (t - t_{S_0})} + \frac{k^{\Delta}_{B_1 \to C_1}}{k^{\Delta}_{C_1 \to D_1} - k^{\Delta}_{B_1 \to C_1}} \times e^{-k^{t}_{D} \times (t - t_{S_0})} \right] \quad \text{Eq.4.3}$$

and for the unimolecular reaction of C_1, they are

$$C_{C_1} = [C_1]_{S_0} \times e^{-k^{\Delta}_{C_1 \to D_1} \times (t - t_{S_0})} \quad \text{Eq.4.4}$$

$$C_{D_1} = [C_1]_{S_0} \times \left[1 - e^{-k^{\Delta}_{C_1 \to D_1} \times (t - t_{S_0})} \right] \quad \text{Eq.4.5}$$

The total absorbances of the medium at the time of light switch off (t_{SO}) is the sum of the species individual absorbances at that time.

$$A^{\lambda_{irr}/\lambda_{obs}}_{tot}(t_{SO}) = \varepsilon^{\lambda_{irr}}_{A_1} \times [A_1]_{S_0} + \varepsilon^{\lambda_{irr}}_{B_1} \times [D_1]_{S_0} + \varepsilon^{\lambda_{irr}}_{C_1} \times [C_1]_{S_0} + \varepsilon^{\lambda_{irr}}_{D_1} \times [D_1]_{S_0} + \varepsilon^{\lambda_{irr}}_{E_1} \times [E_1]_{S_0} \quad \text{Eq.5}$$

The variation of the total absorbance after t_{SO} is given by the following expression that takes into account Eqs.4.

$$A_{tot}^{\lambda_{irr}/\lambda_{obs}}\left(t-t_{S_0}\right)=\left[\varepsilon_A^{\lambda}\times[A]_{SO}+\varepsilon_{D_1}^{\lambda_{irr}}\times[D_1]_{S_0}+\varepsilon_{E_1}^{\lambda_{irr}}\times[E_1]_{S_0}\right]+\varepsilon_{B_1}^{\lambda_{irr}}\times[B_1]_{S_0}\times e^{-k_{B_1\to C_1}^{\Delta}\times\left(t-t_{S_0}\right)}+\varepsilon_{C_1}^{\lambda_{irr}}\times\left([B_1]_{S_0}\times\frac{k_{B_1\to C_1}^{\Delta}}{k_{C_1\to D_1}^{\Delta}-k_{B_1\to C_1}^{\Delta}}\times\left[e^{-k_{B_1\to C_1}^{\Delta}\times\left(t-t_{S_0}\right)}-e^{-k_{C_1\to D_1}^{\Delta}\times\left(t-t_{S_0}\right)}\right]+[C_1]_{S_0}\times e^{-k_{C_1\to D_1}^{\Delta}\times\left(t-t_{S_0}\right)}\right)+\varepsilon_{D_1}^{\lambda_{irr}}\times\left([B_1]_{S_0}\times\left[1-\frac{k_{C_1\to D_1}^{\Delta}}{k_{C_1\to D_1}^{\Delta}-k_{B_1\to C_1}^{\Delta}}\times e^{-k_{B_1\to C_1}^{\Delta}\times\left(t-t_{S_0}\right)}+\frac{k_{B_1\to C_1}^{\Delta}}{k_{C_1\to D_1}^{\Delta}-k_{B_1\to C_1}^{\Delta}}\times e^{-k_{C_1\to D_1}^{\Delta}\times\left(t-t_{S_0}\right)}\right]+\varepsilon_E^{\lambda}\times[C_1]_{S_0}\times\left[1-e^{-k_{C_1\to D_1}^{\Delta}\times\left(t-t_{S_0}\right)}\right]\right)$$

Eq.6

Finally, the total absorbance of the medium can be expressed as a biexponential formula (Eqs.7):

$$A_{tot}^{\lambda_{irr}/\lambda_{obs}}\left(t-t_{S_0}\right)=\alpha+\beta\times e^{-k_{B_1\to C_1}^{\Delta}\times\left(t-t_{S_0}\right)}+\gamma\times e^{-k_{C_1\to D_1}^{\Delta}\times\left(t-t_{S_0}\right)}\quad\text{Eq.7.1}$$

$$\alpha=\left[\varepsilon_{A_1}^{\lambda_{irr}}\times[A_1]_{S_0}+\varepsilon_{B_1}^{\lambda_{irr}}\times[B_1]_{S_0}+\varepsilon_{C_1}^{\lambda_{irr}}\times[C_1]_{S_0}+\varepsilon_{D_1}^{\lambda_{irr}}\times[D_1]_{S_0}+\varepsilon_{E_1}^{\lambda_{irr}}\times[E_1]_{S_0}\right]\quad\text{Eq.7.2}$$

$$\beta=\varepsilon_{B_1}^{\lambda_{irr}}\times[B_1]_{S_0}+\varepsilon_{C_1}^{\lambda_{irr}}\times[B_1]_{S_0}\times\frac{k_{B_1\to C_1}^{\Delta}}{k_{C_1\to D_1}^{\Delta}-k_{B_1\to C_1}^{\Delta}}-\varepsilon_{D_1}^{\lambda_{irr}}\times[B_1]_{S_0}\times\frac{k_{C_1\to D_1}^{\Delta}}{k_{C_1\to D_1}^{\Delta}-k_{B_1\to C_1}^{\Delta}}\quad\text{Eq.7.3}$$

$$\gamma=\varepsilon_{C_1}^{\lambda_{irr}}\times[C_1]_{S_0}-\varepsilon_{C_1}^{\lambda_{irr}}\times[B_1]_{S_0}\times\frac{k_{B_1\to C_1}^{\Delta}}{k_{C_1\to D_1}^{\Delta}-k_{B_1\to C_1}^{\Delta}}+\varepsilon_{D_1}^{\lambda_{irr}}\times[B_1]_{S_0}\times\frac{k_{B_1\to C_1}^{\Delta}}{k_{C_1\to D_1}^{\Delta}-k_{B_1\to C_1}^{\Delta}}-\varepsilon_{D_1}^{\lambda_{irr}}\times[C_1]_{S_0}\quad\text{Eq.7.4}$$

Eq. 7.1 tends to α (as given in Eq.7.2) when t $\rightarrow \infty$ and tends to $A_{tot}^{\lambda_{irr}/\lambda_{obs}}(t_{S_0})$ (as given in Eq.6) when t $\rightarrow$ 0.

It is important to notice that the fitting of Eq.7.1 to experimental data makes it possible to determine the individual rate-constants of the reaction steps $B_1 \rightarrow C_1$ ($k_{B_1\to C_1}^{\Delta}$) and $C_1 \rightarrow D_1$ ($k_{C_1\to D_1}^{\Delta}$) without the need to know, beforehand, the absolute values of the remaining reactions parameters.

As shown in Fig. 6.8, the data corresponding to two observation wavelengths (216 and 330 nm) obey well the biexponential model given by Eq.7.1. This indicates that the thermal behaviour of the reaction involves at least two species, hence confirming the likelihood of the proposed thermal steps of the proposed mechanism in Scheme 5.

The fitting of the thermal kinetic data to Eq.7.1 yields also the values of the equation parameters (Table 6.2). The reaction rates for the thermal transformations $k^{\Delta}_{B_1 \rightarrow C_1}$ and $k^{\Delta}_{C_1 \rightarrow D_1}$, are of the same order of magnitude and overall indicate that the reactions involved in the thermal process are slow, with step $B_1 \rightarrow C_1$ being 40% faster than $C_1 \rightarrow D_1$.

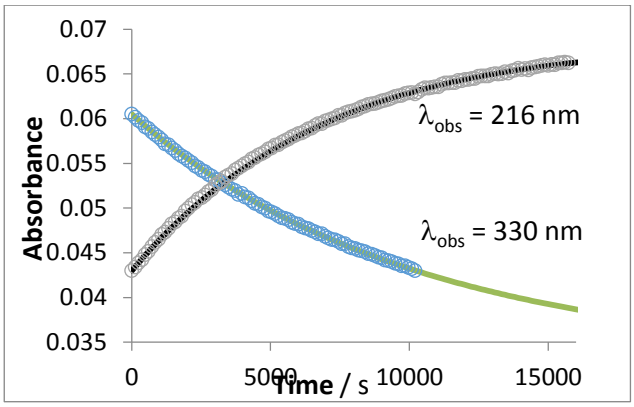

Fig. 6.8: Fitting of Eq. 7.1 to DBZ experiemental data for two wavelengths, 216nm and 330 nm.

Table 6.2: Equation parameters yielded from the fitting of Eq.7.1 to the thermal kinetic data.

Parameter of Eq.7.1	Values
$\boldsymbol{\alpha}$	0.0324
$\boldsymbol{\beta}$	0.015
$\boldsymbol{k^{\Delta}_{B_1 \rightarrow C_1}}$ [a]	1.2 x 10^{-4}
$\boldsymbol{\gamma}$	0.01311
$\boldsymbol{k^{\Delta}_{C_1 \rightarrow D_1}}$	7.3 x 10^{-5}

[a]: The rate-constants are expressed in s^{-1}.

6.5. RUNGE-KUTTA ANALYSIS OF THE PHOTODEGRADATION REACTION

One way to solve this kind of complex kinetic situations, where the integrated rate-law is not known, is to apply numerical integration methods [25]. Current methods used in the literature are all based in the thermal differential equations which, as discussed, are unsuitable for characterising photokinetic data.

For this purpose, we propose a new approach to solving such complex kinetics that has not been reported elsewhere in the literature. Firstly, define the system of differential equations

for the proposed mechanism of the considered overall photochemical reactions. Secondly, the unknown parameters of the reactive system ($\Phi_{i\to j}^{\lambda_{irr}}$, $\varepsilon_X^{\lambda_{irr}}$, and $k_{i\to j}^{\Delta}$ if not possible to determine it through experiments) are optimised until the data generated by the fifth-order Runge-Kutta (RK) fit well the experimental trace obtained at one $\lambda_{irr}/\lambda_{irr}$ (e.g. $\lambda_{254}/\lambda_{254}$). Thirdly, the newly defined $\varepsilon_X^{\lambda_{irr}}$, and $k_{i\to j}^{\Delta}$ parameters are then validated against a series of traces obtained for the same irradiation wavelength but at different observations (varying λ_{irr} in: $\lambda_{irr}/\lambda_{obs}$, e.g. $\lambda_{254/}$ λ_{obs}) spanning the whole spectrum of the drug. Fourthly, the quantum yields as supposed to be wavelength-dependent i.e. for the new fittings of $\lambda_{irr}/\lambda_{obs}$ traces, the values of $\Phi_{i\to j}^{\lambda_{irr}}$is changed and optimised until a good fit is obtained. The validation of the parameters and mechanism is performed on the experimental traces obtained at different irradiation conditions (varying λ_{obs} in: $\lambda_{irr}/\lambda_{obs}$, e.g. $\lambda_{irr/}$ λ_{330}).

If the newly defined parameter fails to fit any set of traces, the parameters are then considered incorrect and must be redefined until all sets of different traces can be fitted with just one set of parameter values that are unique to this drugs' kinetic data. If it turns out that it is impossible to fit the experimental data with any single set of parameters, then the conclusion should be that mechanism is not correct and hence a new improved mechanism should be proposed and the whole procedure repeated. Such an inclusive approach, which has never been developed in earlier studies, allows to define a reliable set of parameters and validate the likelihood of the mechanism proposed. We applied this approach to AXI, DBZ and SUT kinetics in water.

6.6. RATE LAWS OF THE SYSTEMS

The mathematical description of the photochemical/thermal mechanisms present for each drug is well provided by a system of differential equations (see Annex A6.4). For instance, and in accordance to scheme 6.5, DBZ's system of equations is written as:

$$\frac{dC_{A_1}}{dt}(t) = -\left(k_{A_1\to B_1}^{\lambda_{irr}} + k_{A_1\to E_1}^{\lambda_{irr}}\right) \times F_{\lambda_{\mathrm{irr}}}(t) \times C_{A_1} \quad \text{Eq.8}$$

$$\frac{dC_{B_1}}{dt}(t) = k_{A_1\to B_1}^{\lambda_{irr}} \times F_{\lambda_{\mathrm{irr}}}(t) \times C_{A_1} - k_{B_1\to C_1}^{\lambda_{irr}} \times F_{\lambda_{\mathrm{irr}}}(t) \times C_{B_1} - k_{B_1\to C_1}^{\Delta} \times C_{B_1} \quad \text{Eq.9}$$

$$\frac{dC_{C_1}}{dt}(t) = -k_{C_1\to D_1}^{\lambda_{irr}} \times F_{\lambda_{\mathrm{irr}}}(t) \times C_{C_1} - k_{C_1\to D_1}^{\Delta} \times C_{C_1} + k_{B_1\to C_1}^{\lambda_{irr}} \times F_{\lambda_{\mathrm{irr}}}(t) \times C_{B_1} + k_{B_1\to C_1}^{\Delta} \times C_{B_1} \quad \text{Eq.10}$$

$$\frac{dC_{D_1}}{dt}(t) = k_{C_1\to D_1}^{\lambda_{irr}} \times F_{\lambda_{\mathrm{irr}}}(t) \times C_{C_1} + k_{C_1\to D_1}^{\Delta} \times C_{C_1} \quad \text{Eq.11}$$

$$\frac{dC_{E_1}}{dt}(t) = k_{A_1\to E_1}^{\lambda_{irr}} \times F_{\lambda_{\mathrm{irr}}}(t) \times C_{A_1} \quad \text{Eq.12}$$

where t is the time, C_X is the concentration of species X, $k_{i\to j}^{\lambda_{irr}}$is the rate-constant of the photochemical reaction of species X, $k_{i\to j}^{\Delta}$ is the rate-constant of the thermal reaction of species X and $F_{\lambda_{\mathrm{irr}}}(t)$ the photokinetic factor.

The rate-constant of the photochemical reaction of species X ($k_{i\to j}^{\lambda_{irr}}$) is express by the following general formula:

$$k_{i\to j}^{\lambda_{irr}} = \Phi_{i\to j}^{\lambda_{irr}} \times \varepsilon_X^{\lambda_{irr}} \times l_{\lambda_{irr}} \times P_{\lambda_{irr}} \quad \text{Eq.13}$$

Where $\Phi_{i\to j}^{\lambda_{irr}}$ is the quantum yield of the photoreaction of species X at λ_{irr}, $\varepsilon_X^{\lambda_{irr}}$ is its absorption coeffient, $\mathrm{l_{irr}}$ the optical path length of the irradiation beam in the sample and $P_{\lambda_{irr}}$the radiant power at λ_{irr}.

The expression of $k_{i\to j}^{\lambda_{irr}}$ shows that the photochemical rate-constant directly depends on four quantities ($\Phi_{i\to j}^{\lambda_{irr}}$, $\varepsilon_X^{\lambda_{irr}}$, $l_{\lambda_{irr}}$ and $P_{\lambda_{irr}}$) that all depend on the wavelength of the irradiation beam. This means that the comparison of photoreaction rate-constants must be considered with care since only experiments where only one quantity is varied can be readily compared. For instance, if the experimental results show that a given trace 1 is faster that a trace 2, this might not automatically mean that the efficiency of the photoreaction is higher for experiment 1 (it can simply be explained by a higher quantity of the remaining three as expressed in $k_{i\to j}^{\lambda_{irr}}$ formula). This is an important difference with rate-constants measured for thermal reactions (where the temperature is the main factor).

The photokinetic factor involved in the system of differential equations is expressed as

$$F_{\lambda_{irr}}(t) = \frac{1-10^{A_{tot}^{\lambda_{irr}/\lambda_{obs}}}}{A_{tot}^{\lambda_{irr}/\lambda_{obs}}} \qquad \text{Eq.14}$$

with $A_{tot}^{\lambda_{irr}/\lambda_{obs}}$ is the total absorbance of the reaction medium measured at λ_{irr}.

$F_{\lambda_{irr}}(t)$ is time-dependent due to the variation of $A_{tot}^{\lambda_{irr}/\lambda_{obs}}$ with reaction time. Owing to that, the integration of photochemical reaction is made very difficult if at all possible. Only one example of closed-form integration of the unimolecular photoreaction has thus far been published [26].

Accordingly, the closed-form integration of the system of differential equations, such as that describing DBZ (Eqs. 8-12), AXI (Eqs. 13-19, Annex A6.4) and SUT (Eqs. 20-23, Annex A6.4) phototransformation, has remained impossible until now - despite some intensive attempts in our team.

DBZ's system of equations (Eqs. 8-12) involves nine unknown parameters, namely, three $k_{i\to j}^{\lambda_{irr}}$, two $k_{i\to j}^{\Delta}$, and four absorption coefficients $\varepsilon_X^{\lambda_{irr}}$, to be optimised (there are eighteen unknowns for AXI and nine for SUT, see Annex A6.4).

Due to the flexibility of a system depending on so many parameters, the optimisations were very difficult to achieve. Nonetheless, we have successfully proposed a mechanism for each drug of this study (Fig. 6.9, tables 6.3 and 6.4). It is important to mention that total solutions for the drugs kinetics not thus far been proposed in the literature. Also, the present study represents the first of its kind in the field of drugs' photodegradation based on a review of the main textbooks in photodegradation of drugs [7,8,24] and a wide number of papers and reviews in the field.

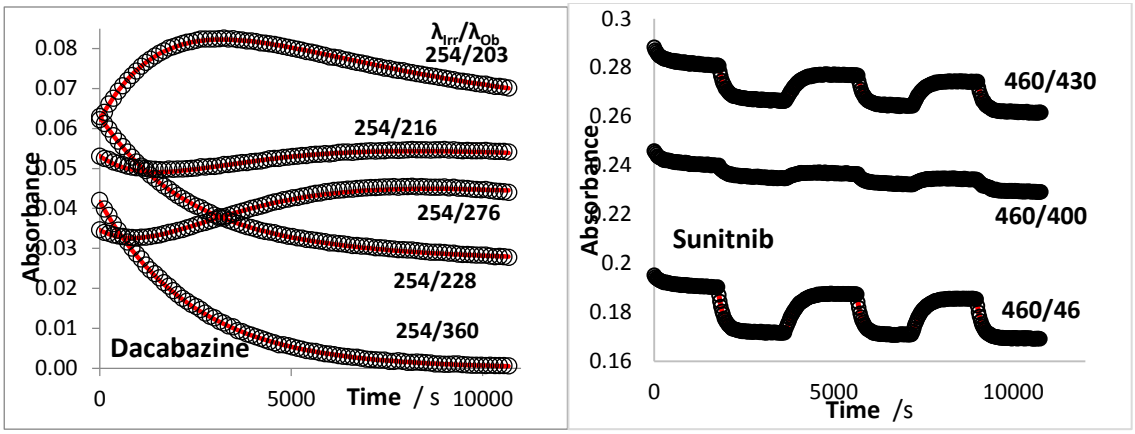

Fig 6.9: Fitting of experimental kinetics traces (open circles) recorded at a number of observation wavelengths (λ_{obs}) with RK data (lines). (left) 5.37 x 10^{-6} M DBZ (λ_{irr} = 254 nm, 7.06 x 10^{-7} einstein s^{-1} dm^{-3}, 22°C). (right) 1.12 x 10^{-5} M SUT (λ_{irr} = 460 nm, 2.66 x 10^{-6} einstein s^{-1} dm^{-3}, 22°C). See Annex A6.5 for AXI.

The kinetic treatments of DBZ and SUT have shown that the proposed mechanisms (schemes 6.5 and 6.2, respectively) were sufficient to fit the traces obtained at various irradiation and observation wavelengths. This in fact validates these mechanisms and confirms the thermal/photochemical reversibility of E/Z SUT in addition to side thermal degradations of

both isomers. There is also a confirmation of the involvement of thermal and photochemical reaction steps for the photodegradation of DBZ. This contrasts with the mechanisms proposed for these drugs in ethanol. It also stresses the need to acknowledge of SUT's thermal degradation in water for any patient use.

The case of AXI was special. The treatment based on the mechanism of scheme 6.2 was clearly unsatisfactory as it wasn't possible to fit all the photodegradation traces of this molecule. A number of other mechanisms were applied with little success (Annex A6.6). This led us into a more thorough analysis that *Z*- (A_2) and *E*- (B_2) isomers undergo a photoisomerisation through the double bond and both hold another moiety in their chemical structures (different from the double bond) that degrades thermally to C_2 and F_2 but it is reversed to the original isomers (A_2 and B_2) photochemically. This property could be attributed to the amide group that has been shown to react through this mechanism (Scheme 6.7, [27-30]).

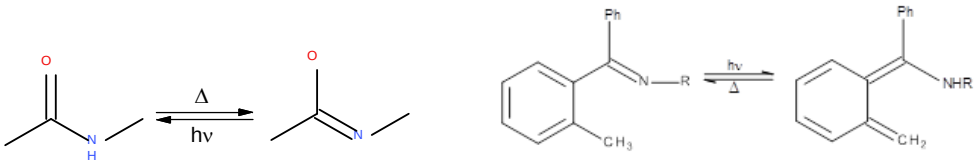

Scheme 6.7: Thermal and photo-induced tautomerisms

This "square" mechanism (A_2, B_2, C_2 and F_2) was insufficient to render account of the full kinetics. Therefore, degradation steps were added successively to B_2, C_2 and F_2 (as shown in Scheme 6.8) until a good correlation was finally find between the experimental traces and RK-5 data. This mechanism explains well the significantly different kinetic behaviours of AXI in the dark and under irradiation, where the pure thermal degradation of AXI (Fig. 6.2, right) is largely tamed when the solution is irradiated (Fig. 6.4, left).

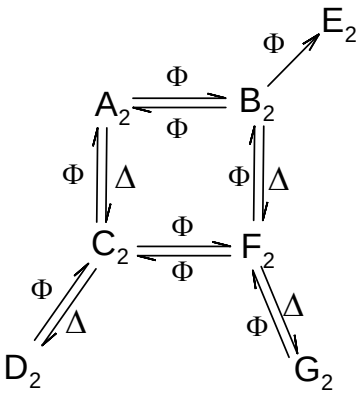

Scheme 6.8: Proposed degradation mechanism of AXI in aqueous solution

6.7. QUANTITATIVE PROPERTIES OF THE PHOTODEGRADATION REACTIONS

The RK treatment has also the advantage to provide a number of reaction parameters and species attributes without physical separation of the mixtures. The time-variation of the individual concentrations of all the species involved in the reaction is one of the properties that can supply information on the composition of the medium at any reaction time (Fig. 6.10). At a relatively low concentration (0.5 - 2 x 10^{-5} M, ~0.05-0.4 % w/v) and a radiant power of ca. 7 x 10^{-7} einstein s^{-1} dm^{-3} (~ 0.330 mW/cm^2), more than 85 % of DBZ (A_1) is depleted in less than 1.5 Hours, only up to 74 % of AXI (A_2) is missing in solution after 10^4 s (2.78 Hours), while just ~46 % of SUT (1.12 x 10^{-5} M, 0.3 % w/v) depletes in 3 Hours (2.66 x 10^{-6} einstein s^{-1} dm^{-3}, 0.692 mW/cm^2).

The maximum concentration (C_{max}) of species B_1 is reached at a much earlier time (~2400s) compared to species C_1 (~6000s) suggesting that the reactivity of C_1 is significantly slower than B_1. For DBZ, the ratio of the times corresponding to the maximum concentrations of C_1 and B_1 (6000/2400 ~ 2.5) is higher than that the ratio recorded for the thermal rate-constants of species B_1 and C_1 (1.64). This strongly indicates that the reactivity of species B_1 and C_1 must involve photochemical routes. Therefore, the supposition that these species react exclusively through thermal reactions is not sustainable. These results further support our proposed

mechanism combining both thermal and photochemical reactions of species B_1 and C_1, contrary to the literature, where only thermal reactions were proposed for these species [18-23].

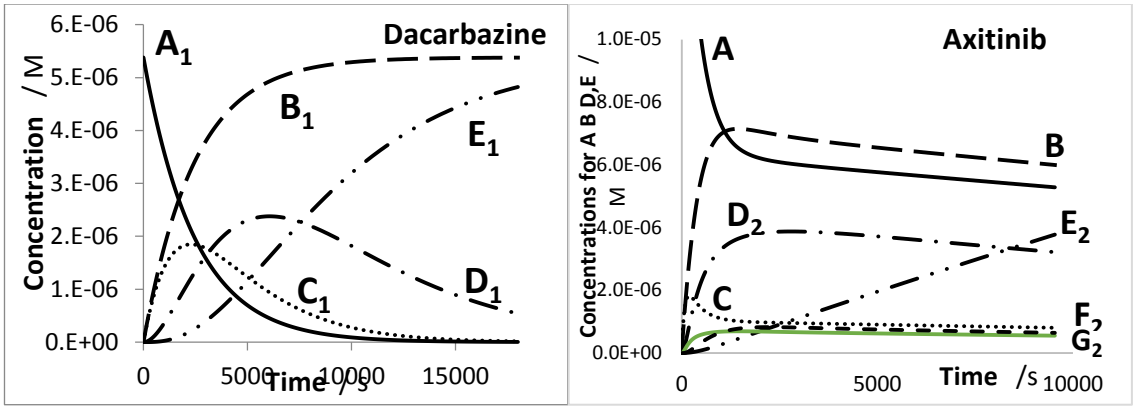

Fig 6.10: Concentration profiles obtained for (left) 5.38 x 10^{-6} M DBZ and its products when monochromatic irradiation at 254 nm (7.06 x 10^{-7} einstein s^{-1} dm^{-3}, 22°C).(right) 2.03 x 10^{-5} M AXI in 2.5 % (v/v) ethanol/water solution when monochromatically irradiated at 330 nm (6.99 x 10^{-7} einstein s^{-1} dm^{-3}, 22°C). Annex A6.7 for SUT

In both cases of AXI and SUT, almost all the photo/thermal products are present in solution after less than 2000 s (~35 min) which may raise the point to carefully consider, in future studies, the biological effects of these species.

The RK treatments provide also the quantum yield values of all the photochemical reaction steps at any irradiation wavelength (Table 6.3). This represent a significant advantage since even if the physical separation was performed it would still be almost impossible to determine the quantum yields of most of the species, using the classical methods, due to their thermal instability.

As it has been observed in ethanol, all species quantum yields were found to be wavelength dependent in water (table 6.3). This corroborates a number of results from our team [31-35], which do not agree with the literature's long standing concept that the quantum yields should

be wavelength independent [8]. In addition, for AXI, DBZ and SUT the quantum yields generally increase with the increase of the irradiation wavelength, most of them in a sigmoid pattern (Figs. 6.11, annex A6.9 for AXI) – indicating that they are most photochemically active in the UVA-Visible regions.

Table 6.3: Determined quantum yield values and estimated absorption coefficients of all species at various wavelengths

Dacarbazine (A_1)	**λ_{irr} /nm**	**203**	**216**	**228**	**237**	**254**	**276**	**330**	**360**
	$\Phi^{\lambda_{irr}}_{A_1 \rightarrow B_1}$	-[a]	-	-	0.0386	0.0362	0.0811	0.104	0.114
	$\Phi^{\lambda_{irr}}_{B_1 \rightarrow C_1}$	-	-	-	0.0762	0.0436	0.112	-	-
	$\Phi^{\lambda_{irr}}_{C_1 \rightarrow D_1}$	-	-	-	0.0223	0.0106	0.0136	-	0
	$\varepsilon^{\lambda_{irr}}_{A_1}$	11560	9868	11706	-	7363	6435	19672	7744
	$\varepsilon^{\lambda_{irr}}_{B_1}$	12490	4380	5050	-	5200	3970	6150	0
	$\varepsilon^{\lambda_{irr}}_{C_1}$	7890	9150	5550	-	6860	10550	0	0
	$\varepsilon^{\lambda_{irr}}_{D_1}$	4500	6960	4900	-	4190	7460	0	0
	$\varepsilon^{\lambda_{irr}}_{E_1}$	7150	2480	0	-	0	0	0	0

Axitinib (A_2)	**λ_{irr} /nm**	**230**	**264**	**280**	**300**	**320**	**330**	**340**	**360**	**380**
	$\Phi^{\lambda_{irr}}_{A_2 \rightarrow B_2}$	-	-	-	-	0.026	0.030	0.030	0.052	0.054
	$\Phi^{\lambda_{irr}}_{B_2 \rightarrow A_2}$	-	-	-	-	0.018	0.034	0.0235	0.0225	0.040
	$\Phi^{\lambda_{irr}}_{C_2 \rightarrow F_2}$	-	-	-	-	0.072	0.050	0.030	0.070	0.095
	$\Phi^{\lambda_{irr}}_{F_2 \rightarrow C_2}$	-	-	-	-	0.0015	0.120	0.030	0.020	0.200
	$\Phi^{\lambda_{irr}}_{C_2 \rightarrow A_2}$	-	-	-	-	0.210	0.250	0.140	0.005	0.550
	$\Phi^{\lambda_{irr}}_{F_2 \rightarrow B_2}$	-	-	-	-	0.088	0.330	0.230	0.530	0.480
	$\Phi^{\lambda_{irr}}_{D_2 \rightarrow C_2}$	-	-	-	-	0.049	0.150	0.155	0.650	0.135
	$\Phi^{\lambda_{irr}}_{G_2 \rightarrow F_2}$	-	-	-	-	0.125	0.150	0.350	0.100	0.450
	$\Phi^{\lambda_{irr}}_{B_2 \rightarrow E_2}$	-	-	-	-	0.00038	0.0019	0.0012	0.00063	0.0028
	$\varepsilon^{\lambda_{irr}}_{A_2}$	27681	17503	17176	21607	28333	31162	28377	9008	2474
	$\varepsilon^{\lambda_{irr}}_{B_2}$	-	20516	18269	21221	22921	22680	20174	12192	8500
	$\varepsilon^{\lambda_{irr}}_{C_2}$	-	16243	17510	21576	24576	27500	26280	8523	2250
	$\varepsilon^{\lambda_{irr}}_{D_2}$	2899	1976	1929	2296	2788	4028	2804	1297	796
	$\varepsilon^{\lambda_{irr}}_{E_2}$	-	8207	6975	9153	8833	8500	7745	1850	650
	$\varepsilon^{\lambda_{irr}}_{F_2}$	-	16434	17207	20514	19514	21500	19546	6263	1800
	$\varepsilon^{\lambda_{irr}}_{G_2}$	-	14376	16070	6504	7204	8050	6215	1011	500

S --	**λ_{irr} /nm**	**215**	**250**	**273**	**360**	**400**	**430**	**460**	**480**

	$\Phi_{A_3\rightarrow B_3}^{\lambda_{irr}}$	-	-	-	0.0134	0.019	-	0.019	0.0245
	$\Phi_{B_3\rightarrow A_3}^{\lambda_{irr}}$	-	-	-	0.028	0.029	-	0.040	0.060
	$\varepsilon_{A_3}^{\lambda_{\mathrm{irr}}}$	21380	7626	10259	8543	22120	26750	19281	9034
	$\varepsilon_{B_3}^{\lambda_{\mathrm{irr}}}$	18750	15322	5652	7655	19700	19400	8898	2511
	$\varepsilon_{C_3}^{\lambda_{\mathrm{irr}}}$	20100	8900	8500	5600	16550	19580	12550	6050
	$\varepsilon_{D_3}^{\lambda_{\mathrm{irr}}}$	17252	10252	5252	5252	5900	15010	10902	1500

The photochemical reactions of species A_1 and B_1 are comparable in magnitude and they are always slightly higher than the efficiency of species C_1 ($\Phi_{C_1\rightarrow D_1}^{\lambda_{irr}}$). These findings corroborate the difference recorded above on the times of maximum concentrations for B_1 and C_1 in the medium. It should be noted that this is the first time quantum yields have been determined and reported for DBZ and its degradation products (A_1, B_1 and C_1).

Changes in SUT's $\Phi_{A_3\rightarrow B_3}^{\lambda_{irr}}$ and $\Phi_{B_3\rightarrow A_3}^{\lambda_{irr}}$ values between the irradiation range (360-480 nm) in aqueous solution are comparable to that in ethanol of the same range (2-fold and 1.8-fold increase), where a 2.4-fold increase and 1.8-fold increases were observed for $\Phi_{A_3\rightarrow B_3}^{\lambda_{irr}}$ and $\Phi_{B_3\rightarrow A_3}^{\lambda_{irr}}$ respectively.

While AXI's Φ values for the similar λ_{irr} (320 – 380 nm) in water were found rather different to those in ethanol. $\Phi_{A_2\rightarrow B_2}^{\lambda_{irr}}$ in water was found to be 5-times smaller than that in ethanol and $\Phi_{B_2\rightarrow A_2}^{\lambda_{irr}}$ was 4.5-times greater in water.

Although, species B_2 is also photochemically produced from A_2 in water, the quantum yield values (Table 6.3) shows that B_2 is mainly formed from F_2, which is formed from C_2. This suggests that thermal degradation of A_2 to C_2 actually has a greater role to play in AXI's photochemical reaction in aqueous solution as well. Thus, a greater $\Phi_{B_2\rightarrow A_2}^{\lambda_{irr}}$ value, than in ethanol, to compensate for A_1 lost thermally.

Yet, for both AXI and SUT, the *Z*- to *E*- conversion was found to be more efficient - possibly due to steric effect in the *E*-isomers. While DBZ's Φ values were respectively almost 2 times higher than those recorded in ethanol.

Since carrying out a systematic study on the effect of the whole spectral range of the species absorption will be time consuming, it is better to find a mathematical model that can give the trend of the variation observed and estimate $\Phi_{i\rightarrow j}^{\lambda_{\mathrm{irr}}}$ value.

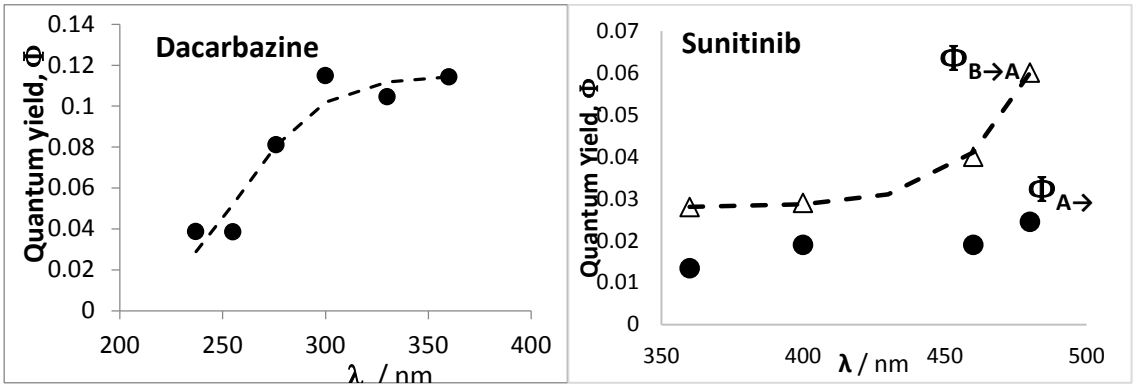

Fig 6.11: Sigmoid relationship obtained for the photochemical quantum yield of DBZ and SUT.

A sigmoid relationship fits the data obtained on $\Phi_{i\rightarrow j}^{\lambda_{\mathrm{irr}}}$. The following expressions are proposed for DBZ and SUT (respectively):

$$\Phi_{A_1\rightarrow B_1}^{\lambda_{irr}} = \frac{0.115}{1+630\times e^{-0.05\times(\lambda_{irr}-130)}} \text{ and } \Phi_{B_3\rightarrow A_3}^{\lambda_{irr}} = \frac{0.2}{1+42550\times e^{-0.05\times(\lambda_{irr}-300)}} + 0.028 \quad \text{Eq.16,17}$$

It should be noted that this is the first time quantum yields and concentration profiles have been determined and reported for DBZ, AXI, SUT and their degradation products.

Although many drugs are reported to be photolabile, quantum yields are less frequently determined. Therefore, many pharmaceuticals have no quantum yield data. Furthermore,

report quantum yields for a given drug are variable, predominantly due to the way the property is determined [36].

As discussed above, some of the system parameters optimised by the RK analysis are the absorption coefficients (ε_X^{λ}) of the reactive species (Fig. 6.12).

The spectrum of DBZ's species E_1 seems to mainly occur below the 200 nm limit with its cut off absorption limit situated at around 220 nm. This fits well with the structure of compound E ($HNMe_2$) as indicated in Scheme 6.4.

Remarkably enough, species C_1 and D_1 share very similar spectral shapes throughout the UV region 200 – 320 nm suggesting that they should have close chemical structures.

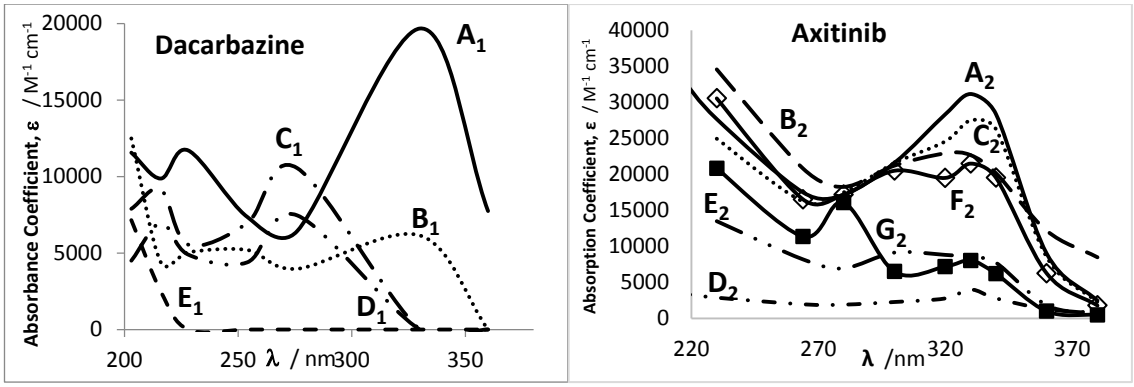

Fig 6.12: Estimated electronic absorption spectra of (left) DBZ, (right) AXI and their products

Beside DBZ (A_1), only species B_1 shows absorption in the visible region. Its maximum is found at approximately at 330 nm though its absorption coefficient is about the third of that of A_1. Here as well, we can postulate some similarity between the electronic distributions in the chemical structures for these two species.

The shapes of species B_1 and D_1 spectra are very similar to those recorded by Kawahara *et al.* [37], with maxima situated at 310 nm for B_1 and 220 nm for D_1. Therefore, the spectra

obtained by our RK treatment of DBZ kinetics show a good overall agreement with the literature.

The spectrum of all of SUT's species (Annex A6.8) are all very similar in shape, which suggests that they have close chemical structures. This correlates well with the small change in absorbance recorded across the absorption spectrum (200 – 450 nm).

Their maxima were all found to be situated around 430 nm (i.e. absorbing in the visible range). This agrees with the fact that the solution remained coloured after degradation. Although, the absorption coefficient of species D_3 is about half of A_3's (SUT), this is not as visible in the evolution spectra (Fig. 6.2 and 6.4), due to the slow thermal reactivity of the species (Table 6.1).

AXI and its products (except species G_2) all have their main absorbance coefficient maxima situated within 300-360 nm, as shown in Fig. 6.12, suggesting a rather similar chemical structure. Species C_2 and F_2 share very similar spectral shapes from 200 nm to 400 nm. These features would suggest that C_2 and F_2 should have close chemical structures, as is A_2 and B_2.

Here, only species B_2 have high absorbance beyond 360 nm – the same as in ethanol. Also, the electronic spectra of B_2 obtained here in water is extremely similar to that obtained in ethanol, strongly suggests that species B_2 is *Z*-AXI.

Species D_2's low absorbance coefficient throughout the spectrum corroborates well with the significant decrease seen in AXI's thermal evolution spectra (Fig. 6.2). Likewise, the high absorption coefficient of species E_2 explains well why AXI's photochemical spectral evolution does not decrease as it does under thermal conditions.

There are however no available data in the literature to compare our results with for AXI and SUT.

6.8. POTENTIAL DEVELOPMENT OF ACTINOMETERS

Solutions of DBZ in water were subjected to irradiation of varying radiant power at various wavelengths, spanning over its photoactive regions. The initial velocities (v_0) were then determined from a theoretical initial velocity equation ($v_{0(cld.)}^{\lambda_{irr}}$), Eq.18) [32] and values obtained from the RK treatment (section 6.7).

$$v_{0(cld.)}^{\lambda_{irr}} = \left(\varepsilon_{B_1}^{\lambda_{obs}} - \varepsilon_{A_1}^{\lambda_{obs}}\right) \times l_{\lambda_{obs}} \times \Phi_{A_1 \rightarrow B_1}^{\lambda_{irr}} \times \varepsilon_{A_1}^{\lambda_{irr}} \times l_{\lambda_{irr}} \times P_{\lambda_{irr}} \times F_{\lambda_{irr}}(0) \times C_0 \qquad \text{Eq.18}$$

Where $F_{\lambda_{irr}}(0)$ is calculated using the initial absorbance, $A_{tot}^{\lambda_{irr}/\lambda_{obs}}(0)$.

Alternatively, the initial velocity ($v_{0(mod.)}^{\lambda_{irr}/\lambda_{obs}}$) can also be determined by differential equation of the model equation describing unimolecular Φ-order kinetics at t=0 (eq. 12, Annex A6.3). Where $k_{\lambda_{irr}}$ can be determined through fitting with Φ-order kinetics' model.

The results showed good correlation when v_0 values obtained via the different methods were validate against each other (Table 6.4).

Table 6.4: correlation equation and r^2 values obtained when v_0 values for a range of $P_{\lambda_{irr}}$ were plotted against each other for each irradiation wavelength

λ_{irr} /nm	255	276	300	330	360
$P_{\lambda_{irr}}$ (x 10^{-6})	0.4 - 1.28	0.13 – 0.94	0.14 – 0.53	0.32 – 1.05	0.53 - 1.86
$v_{0(mod.)}^{\lambda_{irr}/\lambda_{obs}}$ / $v_{0(cld.)}^{\lambda_{irr}}$	$v_{0(cld.)}^{\lambda_{irr}}$ = -7021.7 x $v_{0(mod.)}^{\lambda_{irr}/\lambda_{obs}}$ – 0.1727	$v_{0(cld.)}^{\lambda_{irr}}$ = -0.5213 x $v_{0(mod.)}^{\lambda_{irr}/\lambda_{obs}}$ – 7 x 10^{-6}	$v_{0(cld.)}^{\lambda_{irr}}$ = 0.6656 x $v_{0(mod.)}^{\lambda_{irr}/\lambda_{obs}}$ + 5 x 10^{-6}	$v_{0(cld.)}^{\lambda_{irr}}$ = 0.7481 x $v_{0(mod.)}^{\lambda_{irr}/\lambda_{obs}}$ – 3 x 10^{-6}	$v_{0(cld.)}^{\lambda_{irr}}$ = 0.7216 x $v_{0(mod.)}^{\lambda_{irr}/\lambda_{obs}}$ + 6 x 10^{-6}
r^2	0.89	0.99	0.98	0.99	0.97

Not only do these results show DBZ's potential as an actinometer in water solution, but it also validates the quantitative values determined via RK treatment of DBZ photokinetic data – further supporting the usefulness of RK to solve complex photokinetic data.

The excellent linear correlations (Fig. 6.13) obtained when measured experimental P_{irr} values were plotted against recalculated P values using the P equations (Annex A6.9) from the two methods.

In this study, DBZ has been successfully shown to be a potential drug actinometer for irradiation wavelengths above 300 nm in both water and ethanol (section 5.4).

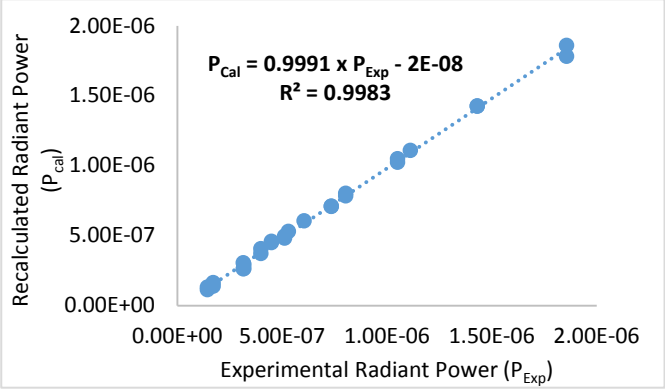

Fig. 6.13: Linear correlation obtained when experimental P_{Exp} values were plotted against calculated values (P_{cal})

More importantly, this study has shown viability of Φ-order kinetics' potential for the development of reliable actinometers without prior knowledge of any of the unknown reaction parameters – even for drugs' with a complex mechanism. This opens up the possibly for other drug actinometers.

6.9. THE EFFECT OF POLYCHROMATIC LIGHT

Solutions of DBZ, AXI and SUT were exposed for a period of time to ambient diffuse light (natural and artificial) at ambient room temperature in our laboratory (Fig. 6.14 and 6.15).

Photodegradation of DBZ and SUT recorded matches well that reported in the literature [17-23] and that observed under monochromatic irradiation in aqueous solution. While, AXI's was found to be predominantly thermal reaction, rather than photochemical.

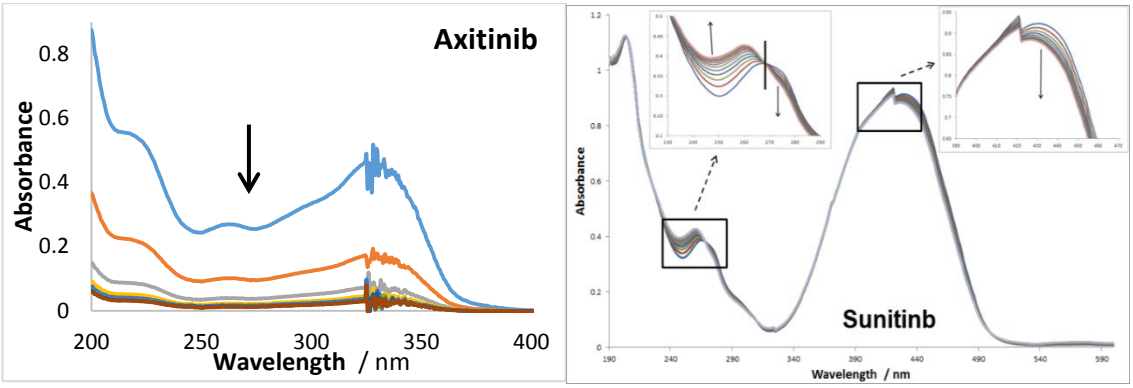

Fig 6.14: Evolution of the electronic absorption spectra of (Left) 1.02 x 10^{-5} M AXI in 2.5 % (v/v) ethanol/water solution and (right) 3.76 x 10^{-5} M SUT in water, when subjected to ambient polychromatic irradiation and ambient room temperature. (Annex A6.10 for DBZ)

The data for all three drugs were shown to obey AB(1Φ) or AB(2Φ) Φ-order kinetics (Fig. 6.15). This result has a dual importance. Firstly, it confirms that the DBZ's data could be modelled on a AB(1Φ) unimolecular reaction and AXI and SUT by an AB(2Φ) photoreversible reaction. Secondly, it represents the first example of modelling data obtained with polychromatic light. This also indicates that the kinetic data relative to the degradation of drugs using polychromatic irradiation is most likely to obey Φ-order kinetics. This may in fact help investigations of drugs' photodegradation as an alternative to first-order kinetic usually employed by the literature [7].

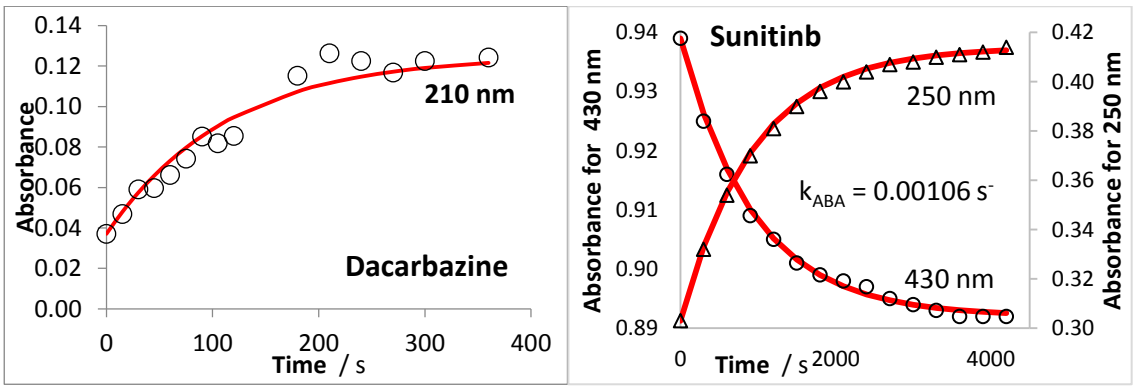

Fig 6.15: Kinetic traces obtained for (top left) DBZ in water, (right) 3.76 x 10^{-5} M SUT in water, when subjected to ambient polychromatic irradiation. Open shapes are experimental data and solid lines are fittings.

6.10. CONCLUSION

To the best of our knowledge, this study is the first to demonstrate the potential application of a new method to drug photokinetic data. It helped elucidate complex drug mechanisms (number of species and occurrence of thermal and photochemical steps). It enabled the determination of the quantum yields and absorption coefficients, not only of the mother compound but of all photoactive degradation products, in addition to showing the evolution of the species respective concentrations during reaction time - all with a better performance than separation techniques commonly employed.

The degradation of DBZ was found to involve at least four products – thermally stable: A_1, D_1 and E_1; and photochemically active: A_1, B_1 and C_1. In the literature, only the first step of DBZ's degradation was reported to be photochemically induced. Thus, the present study has proven for the first time that two of the products are both photochemically and thermally active.

For the first time, AXI and SUT have been shown to be thermally and photochemically active in aqueous solution. Both involving reversible reactions. While SUT's mechanism was determined to involve at least 4 species, AXI's degradation involves at least 7.

Analysis of AXI's photoreaction revealed that the thermal reaction has a greater role in AXI's degradation in aqueous solution. Although for SUT, the quantum yield of B_3 was found to be two times higher than A_3, its thermal reaction in aqueous solution may be problematic.

The relatively high quantum yield values of SUT and DBZ in the UVA-Visible region was shown to be problematic by their high sensitivity to ambient (natural and fluorescent) light. This presents a big problem in hospital applications.

For the first time, a method which enables complex drug photokinetic data to be resolved, based on photokinetic equations (not thermal), has been shown successfully. Not only will this allow the quantum yields of other photolabile pharmaceutics to be determined, but for them to be determined in a more reliable manner.

The Φ-order kinetics model applied here showed great potential as a new simple approach to developing actinometers with complex mechanisms. It was also shown to be applicable to data obtained by polychromatic irradiation. Further suggesting that that photodegradation of drugs are better described by Φ-order than the classic thermal reaction orders.

6.11. REFERENCES

1. Kovaleski J., Kraut B., Matiuz A., Giangiulio M., Brosbst G. and Cango W. (2007) Impurties in generic pharmaceutical development. *Adverse Drug Rev*, 59:56-63
2. Rao R.N. and Nagaraju V. (2003) A overview of the recent trends in the development of HPLC methods for determination of impurities in drugs, *Journal of Pharmaceutical and Biomedical Analysis*, 33:335-337
3. ICH Q1A (R2) (2003) Stability Testing of New Drug Substances and Products. International Conference on Harmonization, IFPMA, Geneva
4. ICH Q1B (R3) (2003) Photostability Testing of New Drug Substances and Products. International Conference on Harmonization, IFPMA, Geneva
5. de Azevedo Filho C.A., de Filgueiras Gomes D., de Mélo Guedes J.P., Batista R.M. and Santos B.S. (2011) Considerations on the quinine actinometry calibration method used in photostability testing of pharmaceuticals, *Journal of Pharmaceutical and Biomedical Analysis*, 54(4):886-888

6. Christensen K.L., Christensen J.O., Frokjaer S., Langballe P. and Hansen L.L. (2000) Influence of temperature and storage time after light exposure on the quinine monohydrochloride chemical actinometric system, *European Journal of Pharmaceutical Sciences*, 9(3):317-321

7. Piechocki J.T. and Thoma K. ed. (2010) Pharmaceutical photostability and stabilization technology, New York: Informa Healthcare

8. Tønnesen H.H. (1996) Photostability of Drugs and Drug Formulations, 2nd Edition, London: Tylor & Francis

9. El-Gindy A. and Hadad G.M. (2012) Chemometrics in Pharmaceutical Analysis: An Introduction, Review, and Future Perspectives, *Journal of AOAC International*, 95(3):609-623

10. Shamsipur M., Hemmateenejad B., Akhond M., Javidnia K. and Miri R. (2003) A study of the photo-degradation kinetics of nifedipine by multivariate curve resolution analysis, *Journal of Pharmaceutical and Biomedical Analysis*, 31(5):1013-1019

11. Borgen O.S. and Kowalski B.R. (1985) An extension of the multivariate component-resolution method to three components, Analytica Chimica Acta, 174:1–26

12. De Lucas M., Mas S., Ioele G., Oliverio F., Ragno G. and Tauler R. (2010) Kinetic studies of nitrofurazone photodegradation by multivariate curve resolution applied to UV-spectral data, International Journal of Pharmaceutics, 386(1–2):99-107

13. Shahjahan M. and Enever R.P. (1996) Photolability of nitrofurazone in aqueous solution II. Kinetic studies, International Journal of Pharmaceutics, 143:83-92

14. Javidnia K., Hemmateenejada B., Miri R. and Saeidi-Boroujeni M. (2008) Application of a self-modeling curve resolution method for studying the photodegradation kinetics of nitrendipine and felodipin, Journal of Pharmaceutical and Biomedical Analysis, 46: 597–602

15. De Luca M., Tauler R., Ioele G. and Ragno G. (2013) Study of photodegradation kinetics of melatonin by multivariate curve resolution (MCR) with estimation of feasible band boundaries, Drug Testing and Analysis, 5(2):96-102

16. Kubista M., Sjöback R. and Albinsson B. (1993) Determination of Equilibrium Constants by Chemometric Analyisis of Spectroscopic Data, *Analytical Chemistry*, 65:994-996

17. Bahrpeyma S., Hemmateenejad B. and Javidnia K. (2016) Photo-degradation study of dacarbazine by spectrophotometric-chemometrics and HPLC methods, *Journal of the Iranian Chemical Society*, 13(2):221-229

18. Saunders P.P. and Chao L.Y. (1976) Relevance of dimethylamine to mechanism studies of DIC (DTIC, NSC 45388), *Medical and Pediatric Oncology* 2(3):253-8.

19. Stevens M.F.G. and Peatey L. (1978) Photodegradation of Solutions of The Antitumour Drug DTIC, *Journal of Pharmacy and Pharmacology*, 30(S1):47.

20. Shetty B.V., Schowen R.L., Slavik M. and Riley C.M. (1992) Degradation of Dacarbazine in Aqueous Solution*, Journal of Pharmaceutical & Biomedical Analysis*, 10(9):675-683.

21. Horton J.K. and Stevens M.F.G. (1981) A New Light on the Photo-decomposition of the Antitumour Drug DTIC, *Journal of Pharmacy and Pharmacology*, 33(1):808-811

22. Horton J.K. and Stevens M.F.G. (1981) Triazines and Related Products. Part 23. New Photo-products from 5-Diazoimidazole-4-carboxamide (Diazo-IC), *Journal of the Chemical Society Perkin Transaction 1*, 1433-1436.

23. Saunders P.P. DeChang W. and Chao L.Y. (1986) Mechanisms of 5-(3,3-dimethyl-1-triazeno)imidazole-4-carboxamide (dacarbazine) cytotoxicity toward chinese hamster ovary cells in vitro are dictated by incubation conditions, Chem. Bio. Interaction, 58:319-331.

24. Albini A. and Fasani E. ed. (1998) Drugs: Photochemistry and Photostability, Cambridge: The Royal Society of Chemistry

25. Maafi M. and Brown R.G. (2005) General analytical solutions for the kinetics of AB (k,ϕ) and ABC(k,ϕ) systems, *International Journal of Chemical Kinetics*, 37:162-174

26. Maafi M. and Brown R.G. (2007) The kinetic model for AB(1ϕ) systems: A closed-form integration of the differential equation with a variable photokinetic factor, *Journal of Photochemistry and Photobiology A: Chemistry*, 187:319-324

27. Gilbert A. and Baggott J. (1991) Essentials of Molecular Photochemistry, Oxford: Blackwell Science Ltd

28. Brown W.H., Foote C.S., Iverson B.L. and Anslyn E. (2013) Organic Chemistry, USA: Wadsworth Cengage Learning

29. Mateo-Marti E. (2014) Planetary Atmosphere and Surfaces Chamber (PASC): A Platform to Address Various Challenges in Astrobiology, *Challenges*, 5:213-223

30. Rawat M.S.M., Mal S. and Singh P. (2015) Photochromism in Anils – A Review, *Open Chemistry Journal*, 2:7-19

31. Maafi M. and Maafi W. (2013) Modelling nifedipine photodegradation, photostability and actinometric properties, *International Journal of Pharmaceutics*, 456:153-164

32. Maafi M. and Maafi W. (2014) Φ-order kinetics of photoreversible-drug reactions, *International Journal of Pharmaceutics*, 471:536-543.

33. Maafi M. and Maafi W. (2014) Montelukast Photodegradation: Elucidation of Φ-Order Kinetics, Determination of Quantum Yields and Application to Actinometry, *International Journal of Pharmaceutics*, 471:544-552

34. Maafi M. and Lee L.Y. (2015) Actinometric and Φ-Order Photodegradation Properties of Anti-Cancer Sunitinib, *Journal of Pharmaceutical and Biomedical Analysis*, 110:34-41

35. Maafi M. and Lee L.Y. (2015) Determination of Dacarbazine Φ-Order Photokinetics, Quantum Yields, and Potential for Actinometry, *Journal of Pharmaceutical Sciences*, 104(10):3501-3509

36. Challis J.K., Hanson M.L., Friesen K.J. and Wong C.S. (2014) A critical assessment of the photodegradation of pharmaceuticals in aquatic environments: defining our current understanding and identifying knowledge gaps, *Environmental Science: Processes & Impacts*, 16:672-696

37. Kawahara M., Ishida T., Emoto C., Matsushita R., Ichimura F., Kataoka O., Mukai C., Hanaoka M., Ishizaki J., Asahi M. and Miyamoto K. (2001) Determination of a pain substance produced by the photodegradation of dacarbazine, *Japanese Journal of Clinical Pharmacology and Therapeutics*, 32(1): 15-22

CHAPTER SEVEN

NANOSPONGES/DRUG

FLUORIMETRIC CHARACTERIZATION

7.1. INTRODUCTION

Due to their unique property to form water-soluble inclusion complexes with a variety of molecules [1], the use of cyclodextrins (CDs) as pharmaceutical excipients has grown rapidly over the last two decades and has been the subject in a number of stability studies [2].

Recent advances in nanotechnology have increased attention paid to cyclodextrin polymers (CDP, chains of more than one α-, β- or γ-CD monomers) for applications in the field of nanomedicines. Nanosponges (3D cross-linked CDPs) have been successfully used to improve the water solubility of hydrophobic drugs. Compared to the monomers, nanosponges have the advantage of being much more soluble in water.

Besides increasing aqueous solubility of poorly water-soluble drugs, these systems are used for sustaining delivery of drugs and modifying pharmacokinetics, biodistribution and cellular trafficking of the active substances included within the nanostructure [3].

When preparing inclusion complexes, it is not enough to control these effects, it is important to know exactly what complex has been formed, by evaluating its stoichiometry, stability constant and unravel its structure. Knowledge of the complexation efficiency is useful in drug development.

The identification of the stoichiometry of the complex formed between on one hand a water soluble nanosponge, bearing "*p*" cyclodextrin units (CD_p), and on the other hand, "*n*" individual drug molecules (G_n), has represented a tedious task. The literature is well documented for monomer stiochiometry and methods to define it, but lacks any comprehensive reports in relation to polymer cyclodextrins. Spectroscopic characterisations and phase solubility studies employed thus far [4-8], provide good evidence for the

nanosponge:drug complexation but generally fall short in giving details on the stoichiometry of the complex.

As far as we are aware, the model equation of the isotherm for the general case, $G_n:(CD_p)_m$ has not been yet proposed in the literature.

Despite fluorimetry being one of the methods of choice for the characterization of drugs involved in cyclodextrin monomer complexes, it is not much employed for cyclodextrin polymers. Therefore, in this paper the fluoimetric monitoring of the nonosponge:drug interaction is quantified and analysed with the purpose to determining the stoichiometry of the complex. This will be achieved by proposing mathematical expressions linking the variable fluorescence intensity of the medium to the concentration of the nanosponge and presented using two fluorescent molecules, Axitinib (AXI) and 8-Anilino-1-naphthalenesulfonic acid ammonium salt (ANS), as models. Each of these molecules was been studied in the presence of either a β-cyclodextrin monomer (hydroxypropyl-β-cyclodextrin, HP-β-CD) or nanosponge (β-cyclodextrin polymer, β-CDP). AXI solutions were prepared in water/ethanol (v/v, 98/2).

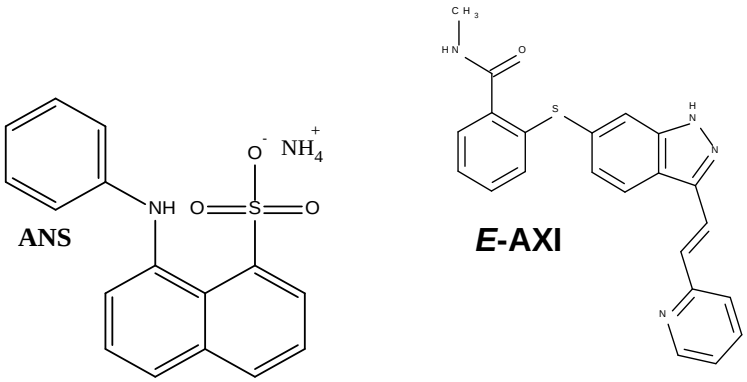

Scheme 7.1: Chemical structures of ANS and AXI.

7.2. MATHEMATICAL MODEL FOR A G_n:$(CD_p)_m$ COMPLEX

The association of "*n*" (one or more) guest species with a polymer "*m*" (one or more) cyclodextrin chain-molecules that may encompass each up to "*p*" cyclodextrin monomer–units, form a type of complex that will be labelled here as G_n:$\left(CD_p\right)_m$ (Scheme 7.1). Hence, for monomer cyclodextrins, *p* = 1. Such a complex is supposed to instantaneously occur in the solution medium with a unique stoichiometry for the guest/nanosponge complex (irrespective of the specific type of binding that may include an inclusion, non-inclusion, clustering or aggregation).

The overall association reaction is given by

$$n\,\mathbf{G} \quad + \quad m\,\mathbf{CD_p} \rightleftharpoons \mathbf{G_n}\text{:}(\mathbf{CD_p})_m$$

Scheme 7.2: Association reaction of n guest molecules with m cyclodextrin nanosponge units (CD_p).

A general equation for the variation of the medium total fluorescence intensity ($Fl_{tot,i,j}^{\lambda_{obs}}$) with nanosponge "*j*" concentration ($\left[CD_p\right]_{0,i,j}$) for a G_n:$\left(CD_p\right)_m$ complex can be describe by Eq. 1 (Details on the derivation of the equation are presented in Annex 7).

$$\frac{\left(Fl_{0,(G_n:(CD_p)_m)}^{\lambda_{obs}}-Fl_{tot,i,j}^{\lambda_{obs}}\right)^n}{Fl_{tot,i,j}^{\lambda_{obs}}-Fl_{0,G,i}^{\lambda_{obs}}}=\frac{\left(Fl_{0,(G_n:(CD_p)_m)}^{\lambda_{obs}}-Fl_{0,G,i}^{\lambda_{obs}}\right)^{n-1}}{n\times K_{G_n:(CD_p)_m}\times[G]_{0,i}^{n-1}}\times\frac{1}{[CD_p]_{0,i,j}^{m}} \qquad \text{Eq. 1}$$

Where $Fl_{0,(G_n:(CD_p)_m)}^{\lambda_{obs}}$ is the fluorescence intensity of the medium when every guest molecule is complexed, $Fl_{0,G,i}^{\lambda_{obs}}$ is the native fluorescence of the guest at "*i*" concentration ($[G]_{0,i}^{n-1}$) and $K_{G_n:(CD_p)_m}$ the association constant of the complex.

Transformation of Eq. 1 into a linear relationship (Eq. 2) allows the true stoichiometry of the complex to be determined in three steps.

$$Ln\left[\frac{Fl_{tot,i,j}^{\lambda_{obs}}-Fl_{0,G,i}^{\lambda_{obs}}}{Fl_{0,\left(G_n:(CD_p)_m\right)}^{\lambda_{obs}}-Fl_{0,G,i}^{\lambda_{obs}}}\times[G]_{0,i}\right]=n\times Ln\left[\frac{Fl_{0,\left(G_n:(CD_p)_m\right)}^{\lambda_{obs}}-Fl_{tot,i,j}^{\lambda_{obs}}}{Fl_{0,\left(G_n:(CD_p)_m\right)}^{\lambda_{obs}}-Fl_{0,G,i}^{\lambda_{obs}}}\times[G]_{0,i}\right]+Ln\left[n\times K_{G_n:(CD_p)_m}\times\left[CD_p\right]_{0,i,j}^{m}\right] \quad \text{Eq. 2}$$

where the gradient of this linear relationship, Eq. 2, is the parameter *n*. The latter parameter can readily be determined from Eq. 2 if the total fluorescence intensity of the medium $\left(Fl_{tot,i,j}^{\lambda_{obs}}\right)$, is measured for each of the individual "*i*" experiments at a unique CD concentration $\left(\left[CD_p\right]_{0,x}\right)$ value. Practically, this can amount to drawing a vertical line on the isotherms and reading the fluorescence intensity values corresponding to the point of intersection of the vertical line with each isotherm. It is worth noting that because of such a particular $\left[CD_p\right]_{0,x}$ value, the term representing the intercept $\left(Ln\left[n\times K_{G_n:(CD_p)_m}\times\left[CD_p\right]_{0,x}^{m}\right]\right)$ in Eq. 2, is a constant (only involving constant quantities).

Once the parameter *n* is known, the treatment of the data corresponding to one of the "*i*" isotherms (i.e. where $[G]_{0,i}$ is constant and $\left[CD_p\right]_{0,i,j}$ is variable), by the following equation that has been derived from Eq. 1,

$$Ln\left[\frac{\left(Fl_{0,\left(G_n:(CD_p)_m\right)}^{\lambda_{obs}}-Fl_{tot,i,j}^{\lambda_{obs}}\right)^{n}}{Fl_{tot,i,j}^{\lambda_{obs}}-Fl_{0,G,i}^{\lambda_{obs}}}\right]=-m\times Ln\left[CD_p\right]_{0,i,j}+Ln\left[\frac{\left(Fl_{0,\left(G_n:(CD_p)_m\right)}^{\lambda_{obs}}-Fl_{0,G,i}^{\lambda_{obs}}\right)^{n-1}}{n\times K_{G_n:(CD_p)_m}\times[G]_{0,i}^{n-1}}\right] \quad \text{Eq. 3}$$

will allow, in a second step, the determination of parameter *m* (from the gradient of Eq. 3).

Having determined the parameters *n* and *m*, the third and final step of the present method focuses on the determination of the association constant value from the intercept formula and numerical value of Eq. 3, as

$$K_{G_n:(CD_p)_m} = \frac{\left(Fl^{\lambda_{obs}}_{0,(G_n:(CD_p)_m)} - Fl^{\lambda_{obs}}_{0,G,i}\right)^{n-1}}{n \times e^{intercept} \times [G]^{n-1}_{0,i}} \quad \text{Eq. 4}$$

If the relative molar mass of the CD polymer ($RMM(CD_p)$) is not known with accuracy (which is indeed the case for a majority of nanosponges), then it is possible to employ a g/L unit for concentrations (instead of the molarity unit). An alternative "*pseudo–association*" constant, $K'_{G_n:(CD_p)_m}$ (Eq. 5), which will be expressed in $(g/L)^{1-m-n}$ or equivalent.

$$K'_{G_n:(CD_p)_m} = K_{G_n:(CD_p)_m} \times [RMM(G)]^{1-n}_{0,i} \times \left[RMM\left(CD_p\right)\right]^{-m}_{0,i} \quad \text{Eq. 5}$$

According to a great number of simulations performed on Eq. 1, the isotherms can have one of two general shapes. Either they are exponential-like (as for the usual isotherms observed for 1:1 complexes) when m = 1 and any n values, or S-shaped curves if *m* > 1 for any *n* (even for a 1:2 complex). Therefore, the shape of the isotherm can inform on whether m is equal to unity.

It is worth noting that the method presented here considers the treatment of the data collected for a series of isotherms corresponding to selected *"i"* concentrations of the guest molecule in the presence of increasing host concentrations *"j"* to overcome the distinguishability problems associated with a single isotherm involving a constant host concentration while that of the guest gradually increases. In this sense our approach is somewhat similar to Job's method of continuous variation as the data corresponding to the

variation of CD are also taken into account in the fluorescence intensity recorded at the plateau region [9].

Contrary to our approach, Job's method requires the total concentration of [CD] and [G] to be constant and the molar fraction of [G] to vary within the range 0-1 [9]. However, it has been found that while Job's method works well for NMR data, it is not practical for fluorescence data, due to the low guest concertation that must be used [10]. In addition, at high concentrations, analysis by fluorescence becomes difficult due to self-quenching.

This also means that Job's method is dependent on precise knowledge of the species' relative molar masses. This is problematic, if the RMM of one or both of the species is not available - as with a majority of nanosponges. Thus, our approach has the advantage of allowing the stoichiometry of the complex to be determined using g/L units for concentrations instead of molarity units.

Another advantage of our approach over Job's method is that it offers a reliable determination of the true stoichiometry without imposing preselected *n:m* complex stoichiometries (1:1, 1:2, 1:3, etc) on isotherm data treatment. Job's method makes assumptions on the composition and the number of complexes formed. But even so, higher-order stoichiometries (e.g. 2:1) are not considered [11]. Thus, if a sigmoidal curve is obtained, the higher-order stoichiometry must be determined by alternative approach [12].

Finally, our approach provides information on both stoichiometry and association constant of the complex – while Job's method does not provide any information on the binding constant.

7.3. FLUORESCENCE PROPERTIES OF THE SPECIES IN DIFFERENT MEDIA

Fluorescence excitation and emission spectra of ANS and AXI have been recorded in water and water/ethanol (v/v, 98/2) (respectively) in the presence and absence of HP-β-CD or β-CDP (Fig. 7.1).

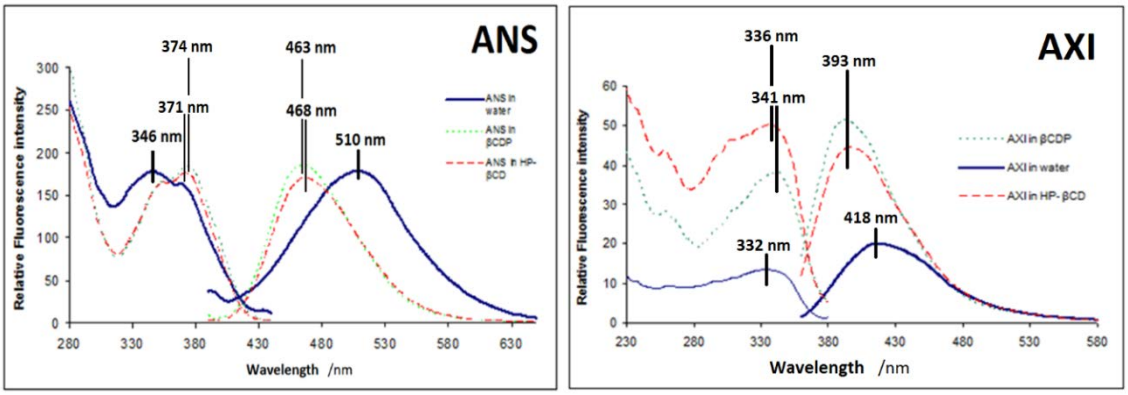

Fig 7.1: Excitation and Emission spectra of (left) 3.36 x 10^{-5} M ANS in water (plain lines), 5.41 x 10^{-6} M in 0.015 g/mL HP-β-CD (dashed lines), and 3.61 x 10^{-6} M in 0.002 mg/mL β-CDP (dotted lines) (Right) 1.53 x 10^{-5} M AXI in water/ethanol (v/v, 98/2) (plain lines), 1.02 x 10^{-5} M in 0.1 mg/mL HP-β-CD (dashed lines), and 9.6 x 10^{-7} M in 5 x 10^{-3} mg/mL β-CDP (dotted lines), at room temperature.

A red-shift (~10 nm) can be observed for the excitation spectra of ANS and AXI in the presence of cyclodextrin monomer and polymer compared to their homologues obtained in their absences. Whereas, the emission spectra undergo significant blue-shifts (30 nm for AXI and 50 nm for ANS) in the presence of the cyclodextrin molecules (Fig. 7.1 and Table 7.1).

As a consequence, the Stokes' shift considerably reduces from 86 nm to 52 nm for AXI and from 142 nm to 89 nm for ANS, in the absence and the presence of nanosponge, respectively.

A significant increase of the fluorescence intensity is also recorded, reaching over 90- and 670-folds (AXI and ANS, respectively) in the presence of the nanosponge compared to that measured in its absence (Fig. 7.2).

An increase in fluorescence intensity of polarity-sensitive molecules in the presence of CD monomers is well-documented [6,10]. Such an enhancement might be due to either lesser specific interactions of the polarity-sensitive guest with water or a reduction of fluorescence quenching by oxygen molecules when the guest species is shielded by the cyclodextrin from the bulk of the solution. Also, the sterical restriction of the guest intramolecular rotational freedom within the cavity might contribute to the observed increase of fluorescence quantum yield [6,10].

Table 7.1: Fluorescence features of AXI and ANS in the presence and absence of HP-β-CD and β-CDP in aqueous solution

	Fluorescence Excitation[a] (nm)	Fluorescence emission[a] (nm)	Stoke shift[b] (nm)	$\frac{Fl^{\lambda_{obs}}_{0,(G_n:(CD_p)_m)}}{Fl^{\lambda_{obs}}}$ [c]
AXI in Water/Ethanol (v/v, 98/2)	259 (325) <u>332</u>	418	86	1
AXI with HP-β-CD	258 (325) <u>336</u>	393	57	2.51
AXI with β-CDP	258.5 (331) <u>341</u>	393	52	93.1
ANS in Water	(329) <u>346</u> 368	510	142	1
ANS with HP-β-CD	(337) 355 <u>371</u>	468	97	2.14
ANS with β-CDP	(336) 355 <u>374</u>	463	89	671

[a] the spectral highest maximum is underlined and the shoulders are presented in brackets

[b] the stocks' shift was calculated as the difference between the emission maximum and the lowest energy excitation peak

[c] the fluorescence intensity in the numerator corresponds to that of the nanosponge/guest complex, whereas the denominator represents the fluorescence intensity in one of the media used ($Fl^{\lambda_{obs}}$ is equal to either $Fl^{\lambda_{obs}}_{0,G,i}$, $Fl^{\lambda_{obs}}_{0,(G_1:CD_1)}$ or $Fl^{\lambda_{obs}}_{0,(G_n:(CD_p)_m)}$).

The reduced polarity of the cyclodextrin interior has another effect relating to the shift of the emission maximum to shorter wavelengths, and as a result to a smaller Stokes' shifts, shown by guest molecules within cyclodextrin monomers compared to the free molecules. These effects can be attributed to a greater destabilization of the excited singlet–state (S_1) of the guest by the non-polar micro-environment offered by the cyclodextrin cavity, as in general, S_1 is more polar than the ground singlet-state (S_0) for many organic drug molecules [10, 13-15].

The above effects proven to take place for cyclodextrin monomer/guest complexes, would also be attributable to similar spectral changes caused by nanosponges. Accordingly, the data recorded for AXI and ANS (Table 7.1, Figs. 7.1 and 7.2) clearly indicate that both molecules form complexes with the nanosponge.

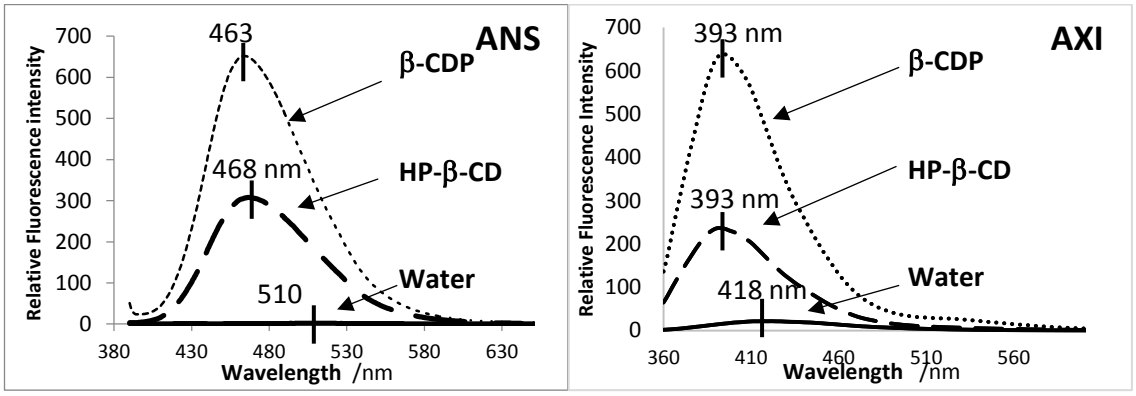

Fig 7.2: Comparative fluorescence emission spectra of (Left) 1.1 x 10^{-5} M ANS in water and (right) 1.02 x 10^{-5} M AXI in water/ethanol (v/v, 98/2) (plain line) in the presence of 0.02 g/mL of either HP-β-CD (dashed line) or β-CDP (dotted line)

When both AXI and ANS were in the presence of β-CDP, a greater fluorescence emission intensity enhancement was exhibited (313- and 37-fold, respectively), compared to their fluorescence intensities in the presence of HP-β-CD. Our findings for ANS agree with reported data which attributed an equatorial inclusion of the naphthalene moiety for the complex formed with various β-CD monomers [16]. So far, however, no literature data is available for

AXI. The difference in the induced fluorescence enhancement may indicate that there is a considerable sensitivity to polarity difference in the medium between the two molecules. This correlates with the fact that ANS is one of the most widely employed polarity-sensitive fluorescent probes [17-19].

When similar amounts of nanosponge (as HP-β-CD) are used, this enhancement in fluorescence intensity is further emphasized. A more significant increase of the fluorescence intensity were found for the complexes formed with both AXI and ANS molecules with nanosponges compared to the effects recorded when cyclodextrin monomers were used (Fig. 7.2). Such an increase further supports the hypothesis of a major role played by the sensitivity of the species to the medium polarity, which is probably more extended within the nanosponge structure [10].

7.4. EFFECT OF GUEST CONCENTRATION

A smooth increase of fluorescence intensity of the medium was observed with increasing concentration of both HP-β-CD monomer and β-CDP nanosponge. No other spectral features were observed on the spectra (Fig. 7.3).

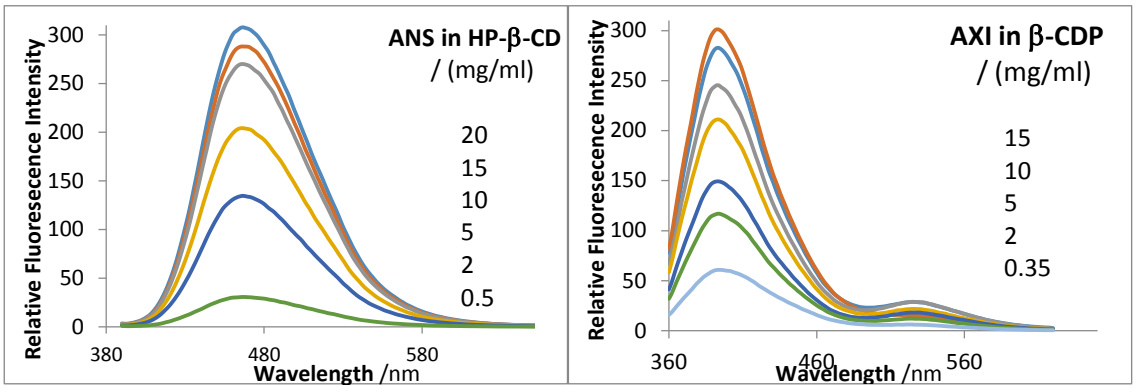

Fig 7.3: Evolution of the fluorescence emission spectrum of (left) 1.07 x 10^{-5} M ANS in water with increasing concentrations of HP-β-CD monomer at room temperature; (right) 5.15 x 10^{-6} M AXI in water/ethanol (v/v, 98/2) with increasing concentrations of β-CDP nanosponge at room temperature

The isotherms recorded, at the maximum fluorescence emission maxima, for both molecules with either HP-β-CD or β-CDP showed a steep increase in fluorescence intensity followed by a plateau (Fig. 7.4). However, the overall shape of the isotherms is found to be insensitive to the concentration of the guest. The latter observation together with the occurrence of a recurrent plateau region might suggest that the stoichiometry of the complexes is not concentration-dependent.

Also, the absence of S-shaped isotherms may qualitatively indicate that a single (monomer or polymer) cyclodextrin unit is involved in the complexation process, as has been discussed for the possible outcomes of Eq. 1 (Section 7.2). Therefore, the value of parameter "*m*" is expected to be close to unity for both complexes formed by ANS and AXI with either HP-β-CD monomer or β-CDP nanosponge.

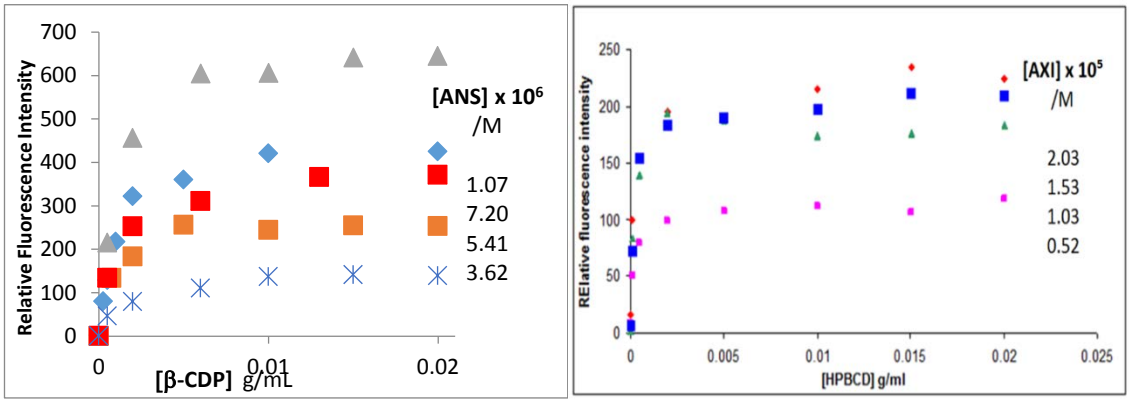

Fig 7.4: Isotherms of varying ANS and AXI concentrations (1.07 – 7.2 x 10^{-6} M and 5.15 x 10^{-6} – 2.03 x 10^{-5} M, respectively) in water or water/ethanol (v/v/, 98/2) with increasing concentrations of β-CDP or HP-β-CD at room temperature.

7.5. DETERMINATION OF THE STOICHIOMETRIES OF THE COMPLEXES

A set of isotherms corresponding to selected *"i"* concentrations of ANS and AXI in the presence of varying *"j"* concentrations of either HP-β-CD or β-CDP were treated using Eq.2. For each isotherm, the fluorescence data were collected in the absence of the host ($Fl_{0,G,i}^{\lambda_{obs}}$), at a specific

given concentration of either (monomer or polymer) host, $Fl_{tot,i,j}^{\lambda_{obs}}$ (e.g. at [HP-β-CD] = 20 mg/mL for AXI and [β-CDP] = 20 mg/mL for ANS) and at the plateau region, $Fl_{0,(G_n:(CD_p)_m)}^{\lambda_{obs}}$. The plots corresponding to Y_n against X_n (Eqs. 6), should yield straight lines.

$$Y_n = Ln\left[\left(Fl_{tot,i,j}^{\lambda_{obs}} - Fl_{0,G,i}^{\lambda_{obs}}\right) \times [G]_{0,i} \Big/ \left(Fl_{0,\left(G_n:(CD_p)_m\right)}^{\lambda_{obs}} - Fl_{0,G,i}^{\lambda_{obs}}\right)\right] \quad \text{Eq. 6a}$$

$$X_n = Ln\left[\left(Fl_{0,\left(G_n:(CD_p)_m\right)}^{\lambda_{obs}} - Fl_{tot,i,j}^{\lambda_{obs}}\right) \times [G]_{0,i} \Big/ \left(Fl_{0,\left(G_n:(CD_p)_m\right)}^{\lambda_{obs}} - Fl_{0,G,i}^{\lambda_{obs}}\right)\right] \quad \text{Eq. 6b}$$

The gradient of the linear relationship ($Y_n = f(X_n)$) corresponds to the number of guest molecules involved in the complex "*n*" (Eq. 2). Whereas, the number of the host molecules "*m*" can be worked out from the intercept of the line plotted as Y_m against X_m (Eqs. 7) as given in Eq. 3, using the data corresponding to any of the isotherm series.

$$Y_m = Ln\left[\left(Fl_{0,(G_n:(CD_p)_m)}^{\lambda_{obs}} - Fl_{tot,i,j}^{\lambda_{obs}}\right)^n \Big/ \left(Fl_{tot,i,j}^{\lambda_{obs}} - Fl_{0,G,i}^{\lambda_{obs}}\right)\right] \quad \text{Eq. 7a}$$

$$X_m = Ln[CD_p]_{0,i,j} \quad \text{Eq. 7b}$$

The association constant can then be determined, for each guest molecule, from the value and the formula of the intercept as given by Eq. 4.

For ANS, 1.06:1 stoichiometry was found when in the presence of HP-β-CD (Fig 7.5 and Table 7.2). This agrees well with the generally proposed 1:1 complexes for the widely studied ANS dyes [10,20]. The association constant ($K_{G_1:CD_1}^{ANS} = 456$ M^{-1}) determined here for ANS is also very close to those obtained through fluorimetric determination by other authors (*c.a.* 480 M^{-1}, [10]); However, it has been reported in the literature that the values of an association

constant for a given species and monomer cyclodextrin varied considerably with the analytical method used [21].

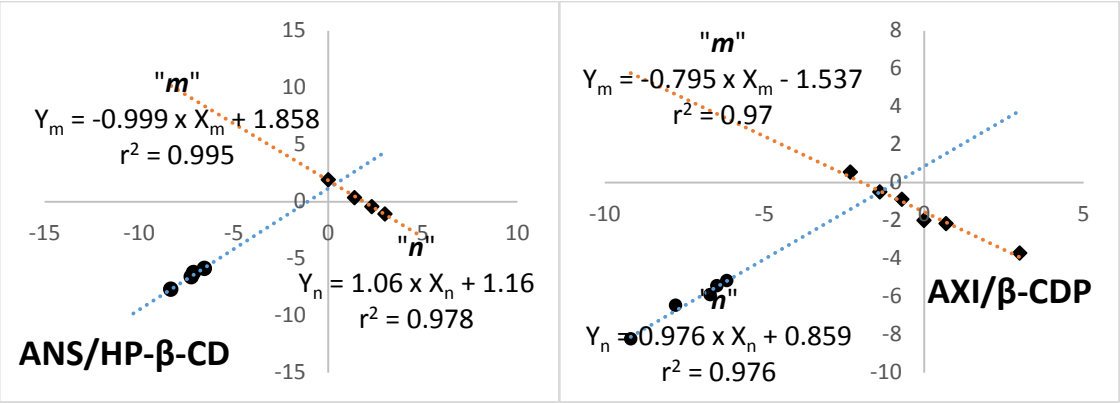

Fig 7.5: Determination of coefficients *n* and *m* for ANS/HP-β-CD (left) and AXI/β-CDP (right) complexes

Table 7.2: Correlation coefficients, stoichiometries and association constants determined obtained for AXI and ANS complexes with HP-β-CD and β-CDP.

	n [a]	int [b]	r [c]	m [d]	int	r	K' [e]	K
β-CDP								
ANS/β-CDP	1.32	3.22	0.96	1.09	1.75	0.98	6.44	- [f]
AXI/β-CDP	0.98	0.86	0.98	0.79	-1.54	0.97	3.33	-
HP-β-CD								
ANS/HP-β-CD	1.06	1.16	0.98	1.00	1.86	0.99	0.31	456
AXI/HP-β-CD	1.09	2.42	0.95	0.82	-0.89	0.99	6.84	2041

[a] n is the number of guest molecules
[b] int is the intercept of the linear relationship.
[c] *r* is the correlation coefficient of the linear relationship.
[d] m is the number of cyclodextrin molecules
[e] calculated using Eq. 5 for HP-β-CD
[f] not applicable

On the other hand, a 1.09:0.82 stoichiometry was found for AXI. Although, the fractional number found cannot be attributed with certainty, it might suggest the presence of partial inclusion and/or multiple binding site.

Due to β-CD's cavity diameter of 0.60 – 0.65 nm [1] and AXI's size, an inclusion of the benzene ring near the sulphur bond or the pyridine ring might be possible (Fig. 7.6 A1 and A2). Its association constant (K) is however almost 6-fold higher than that of ANS. The stronger binding of AXI to HP-β-CD might be due to the more suitable size of the pyridine ring to fit the cyclodextrin cavity compared the loose association of ANS which involves an equatorial inclusion (Fig 7.6 A3) of the much bigger naphthalenic structure [10]. The charge on ANS might also contribute to decreasing the value of $K_{G_1:CD_1}^{ANS}$, i.e. disfavouring ANS:HP-β-CD association, due to partition of the solute between hydrophobic inclusion in HP-β-CD and hydrophobic dissolution in the bulk aqueous solution.

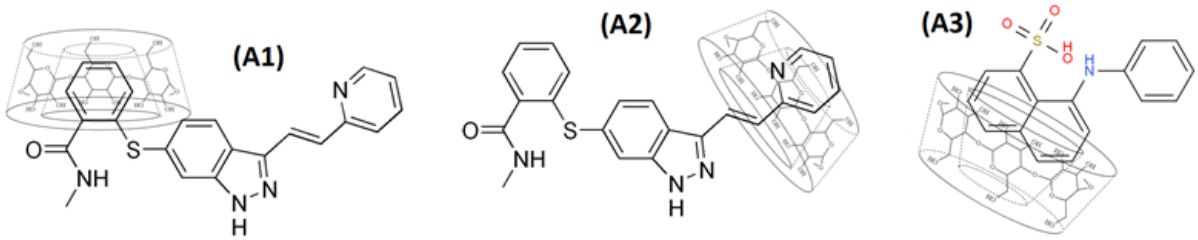

Fig 7.6: Possible complex formations between β-cyclodextrin unit and AXI (A1, A2) or ANS (A3).

A similar result to ours has been reported for complex formed between pentamidine isethionate and β-CD, where a stoichiometry ratio of 0.84 was found from a curve fitting using the non-linear adjustment based on Wiseman isotherm [22]. The latter value was attributed to the possible occurrence of different equilibria of the supramolecular system in solution, in agreement with other results previously reported in the literature [23,24].

The same set of equations employed for the monomers were applied to isotherms obtained with nanosponge, except Eq. 4 which is only applicable to monomers and polymers with known RMM. For the polymers whose RMM is not known with accuracy (as it is the case for the nanosponge used in this study), only the pseudo-association constant can be derived:

$$K'_{G_n:(CD_p)_m} = K_{G_n:(CD_p)_m} \times RMM(CD_P) = \frac{e^{intercept}}{n \times [CD_p]^m_{0,i,j}}$$ Eq. 8

with $[CD_p]^m_{0,i,j}$ expressed in mg/ml.

The results for the nanosponges indicate that AXI and ANS form a 0.98:0.79 and 1.32:1.09 complexes (respectively, Fig 7.5 and Table 7.2). These values further points to the possibility of multiple association sites and/or different types of binding offered by the nanosponges.

The K' determined for ANS in the presence of nanosponges is twice that of AXI. This might suggest a steric hindrance in the polymer, which led to the less efficient complexation in the nanosponge.

Nonetheless, the stoichiometries found for AXI and ANS strongly suggest simple associations between only very few guest molecules and the three-dimensional structure of the nanosponge. Overall, this finding is consistent with the considerable differences of concentrations between host and guest in solutions (i.e. w/w ratios of over 2000 at the plateau regions).

The hint of more than one complex structures in solution provided by our method is an advantage over Job's method, whereby further analysis by other techniques (such as isothermal calorimetric titration or electrospray mass spectrometry) is required [23]. In this respect, the stoichiometry obtained by Job's method can be viewed as an average rather than an absolute value in the case of cyclodextrin complexes.

7.6. CONCLUSION

In drug development, knowledge of the complexation efficiency is useful. However, even with increased interest in CDP due to advances in nanotechnology, only few studies have reported on the fluorimeteric characterisation of nanosponge-drug complexes.

The new mathematical framework proposed in this study for characterisation of such systems enabled a reliable determination of the true complex stoichiometry without imposing any preconception on the stoichiometry, as current methods do.

This flexibility in the system allows the method presented here to provide hints on the possible existence of multi-equilibria in solution.

In addition to not requiring the precise knowledge of the relative molar mass, the method gives information on both stoichiometry and association constant of the complex – while Job's method does not provide any information on the association constant.

Equations and method developed here for the purpose of fluorimetry can easily be adapted to other spectroscopic methods for the characterisation of other systems, not just cyclodextrin and nanosponge.

7.7. REFERENCES

1. Davis M.E. and Brewster M.E., 2004, Cyclodextrin-Based Pharmaceutics: Past, Present and Future, *Nature Reviews: Drug Discovery*, 3:1024-1035
2. Gidwani B. and Vyas A. (2015) A Comprehensive Review on Cyclodextrin-Based Carriers for Delivery of Chemotherapeutic Cytotoxic Anticancer Drugs, *BioMed Research International*, 2015:1-15
3. Irie T. and Uekama K. (1997) Pharmaceutical Applications Of Cyclodextrins. III. Toxicological Issues And Safety Evaluation, *Journal of Pharmaceutical Sciences*¸ 86(2):147-162
4. Shown I., Baek-Ko W. and Murthy C.N. (2012) Cyclodextrin-Based Low Molecular Weight Polymers As Encapsulates For Nonpolar Drug Molecules, *Polymer Bulletin*, 69(1):1-13

5. Castiglione F., Crupi V., Majolino D., Mele A. Panzeri W., Rossi B., Trotta F. and Venuti V. (2013) Vibrational Dynamics And Hydrogen Bond Properties Of β-CD Nanosponges: an FTIR-ATR, Raman And Solid-State NMR, *Journal of Inclusion Phenomena and Macrocyclic Chemistry*, 75(3):247-254

6. Bilensoy E. (Ed.) (2011) Cyclodextrins in Pharmaceutics, Cosmetics, and Biomedicine: Current and Future Industrial Applications, New Jersey: John Wiley & Sons Inc.

7. Tejashri G., Amrita B. and Darshana J. (2013) Cyclodextrin Based Nanosponges For Pharmaceutical Use: A Review, Acta Pharmactica, 63(3):335-358

8. Bolmal U.B., Manvi F.V., Rajkumar K., Palla S.S., Paladugu A. and Reddy K.R. (2013) Recent Advances in Nanosponges as Drug Delivery System, *International Journal of Pharmaceutical Sciences and Nanotechnology*, 6(1):1934-1944

9. Tablet C., Matei I. and Hillebrand M. (2012) The Determination of the Stoichiometry of Cyclodextrin Inclusion Complexes by Spectral Methods: Possibilities and Limitations, In: Stoichiometry and Research - The Importance of Quantity in Biomedicine, Innocenti A. (Ed.) INTECH Open Access Publisher [Online] Available at: http://cdn.intechopen.com/pdfs/30981.pdf [Accessed 13/03/2016]

10. Douhal A. (Ed.) (2006) Cyclodextrin Materials Photochemistry, Photophysics And Photobiology. Vol.1 in the series: Chemical, physical and biological aspects of confined systems. Oxford: Elsevier

11. Steed J.W. and Atwood J.L. (2009) Supramolecular Chemistry, West Sussex: John Wiley & Sons, Ltd.

12. Loukas Y.L. (1997) Multiple Complex Formation of Fluorescent Compounds with Cyclodextrins: Efficient Determination and Evaluation of the Binding Constant with Improved Fluorometric Studies, *Journal of Physical Chemistry B*, 101(24):4863–4866

13. Aaron J.J., Maafi M., Kersebet C., Párkányi C., Antonious M.S. and Motohashi N. (1996) A Solvatochromic Study Of New Benzo[a]phenothiazines For The Determination Of Dipole Moments And Specific Solute-Solvent Interactions In The First Excited Singlet-State, *Journal of Photochemistry and Photobiology A: Chemistry*, 101: 127-136

14. Aaron J.J., Maafi M., Párkányi C. and Boniface C. (1995) Quantitative Treatment Of The Solvent Effects On The Electronic Absorption And Fluorescence Spectra Of Acridines And Phenazines. The Ground And First Excited Singlet-State Dipole Moments. *Spectrochimica Acta Part A: Molecular and Biomolecular Spectroscopy*, 51(4):603-615

15. Párkányi C., Boniface C., Aaron J.J. and Maafi M. (1993) A Quantitative Study Of The Effect Of Solvent On The Electronic Absorption And Fluorescence Spectra Of Substituted Phenothiazines: Evaluation Of Their Ground And Excited Singlet-State Dipole Moments. *Spectrochimica Acta Part A: Molecular Spectroscopy*, 49(12):1715-1725

16. Wagner B.D. and MacDonald P.J. (1998) The fluorescence enhancement of 1-anilinonaphthalene-8-sulfonate (ANS) by modified β-cyclodextrins *Journal of Photochemistry and Photobiology A: Chemistry*, 114:151-157

17. Cramer F., Saenger W. and Spatz H.-Ch. (1967) Inclusion Compounds. XIX. The Formation Of Inclusion Compounds Of B-Cyclodextrin In Aqueous Solutions. Thermodynamics and kinetics. J. Amer. Chem. Soc. 89, 14-20

18. Schneider H.J., Blatter, T., Simova, S., 1991. NMR and Fluorescence Studies Of Cyclodextrin Complexes With Guest Molecules Containing Both Phenyl And Naphthyl Units, *Journal of the American Chemical Society*, 113(1):1996-2000

19. Tee O.S., Gadosy T.A. and Giorgi J.B. (1996) Dissociation Constants of Host-guest complexes of Alkyl-bearing Compounds with β-Cyclodextrin and Hydroxypropyl-β-cyclodextrin, *Canadian Journal of Chemistry*, 74(5):736-744

20. Sueishi Y., Fujita T., Nakatani S., Inazumi N. and Osawa Y. (2013) The Enhancement Of Fluorescence Quantum Yields Of Anilino Naphthalene Sulfonic Acids By Inclusion Of Various Cyclodextrins And Cucurbit[7]uril, *Spectrochimica Acta Part A: Molecular and Biomolecular Spectroscopy*, 114:344–349

21. Yañez C. and Günther G. (2014) Is The Determination Of The Association Constant Of Cyclodextrin Inclusion Complexes Dependent On The Technique, *Journal of the Chilean Chemical Society*, 59(2):2523-2525

22. Turnbull W.B. and Daranas A.H. (2003) On the value of c: can low affinity systems be studied by isothermal titration calorimetry?, *Journal of the American Chemical Society*¸ 125(48):14859-14866

23. Denadai A.M.L., Teixeira K.I., Santoro M.M., Pimenta A.M.C., Cortés M.E. and Sinisterra R.D., (2007). Supramolecular self-assembly of β-cyclodextrin: an effective carrier of the antimicrobial agent chlorhexidine, *Carbohydrate Research*, 342(15):2286-2296

24. De Sousa F.B., Denadai A.M., Lula I.S., Nascimento C.S. Jr., Fernandes Neto N.S., Lima A.C., De Almeida W.B. and Sinisterra R.D. (2008) Supramolecular self-assembly of cyclodextrin and higher water soluble guest: thermodynamics and topological studies, *Journal of the American Chemical Society*¸ 130(26):8426-8436

CHAPTER EIGHT

STABILITY OF THE DRUGS IN CYCLODEXTRINS

8.1. INTRODUCTION

As evident from this study, these drugs (DBZ, AXI and SUT) are very photochemically and thermally unstable in solution and require photoprotection.

Cyclodextrins (CDs) are cyclic oligomers of glucose known to form water-soluble inclusion complexes with a variety of molecules [1]. Due to their unique property, the use of cyclodextrins as pharmaceutical excipients has grown rapidly over the last two decades and has been the subject in a number of stability studies [2].

In the pharmaceutical industry, cyclodextrins are mainly used to aid the dissolution of poorly soluble drugs [3-9]. However, they have also been used to improve stability of drugs. When unstable molecules are entrapped within the cavity of cyclodextrins monomers, their thermal- and photostability could be enhanced [10-14], but no reports have ever been published on the effect of cyclodextrins on DBZ, AXI or SUT's stability or on CDP in general, in this respect. Here, a comprehensive study of the effect of both cyclodextrin monomers and polymers on these three drug samples when degraded thermally and photochemically is presented.

8.2. EFFECT OF CYCLODEXTRIN ON THE THERMALSTABILITY OF THE DRUGS

8.2.1 Absorption Spectrum Features of AXI and SUT with Cyclodextrins

AXI and SUT were shown to be thermally degradable in aqueous solution and DBZ was not (Chapter 6). Thus, solutions containing 2 mL of water or cyclodextrins were spiked with AXI or SUT. The effects of the addition of CD on the electromagnetic spectrum are shown in Fig 8.1.

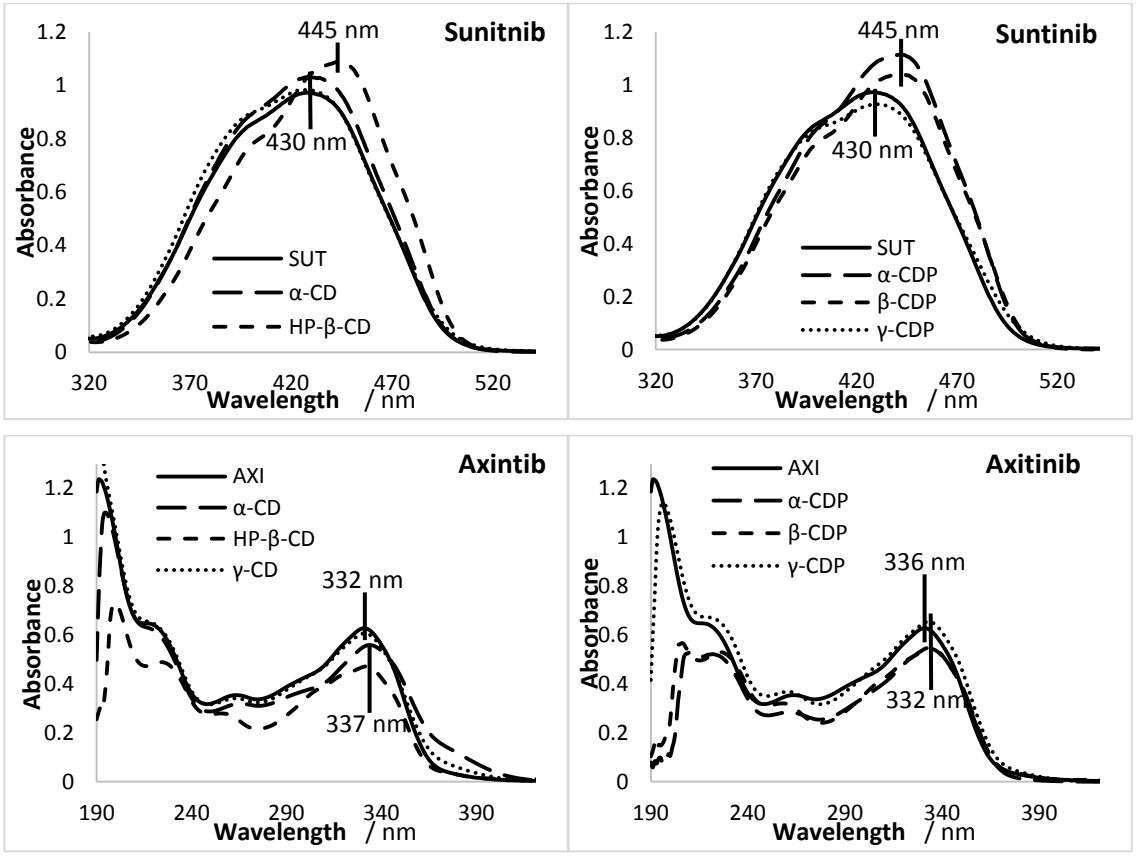

Fig 8.1: Electronic absorption spectra of SUT (0.020 mg/mL) and AXI (0.0095 mg/mL) in the presence and absence of α-, β- and γ-cyclodextrin monomers (24.94 mg/mL, 149.88 mg/mL and 0.23 mg/mL, respectively) and polymers (11.95 mg/mL, 20.55 mg/mL and 8 mg/mL, respectively). Bathochromic shift indicated by vertical lines.

The bathochromic shift of the maxima and change in absorbance values observed in all solutions containing cyclodextrins are good indicators of the inclusion within the cyclodextrins [15]. In α-CDP and β-CDP solutions, the change in absorbance of both drugs is greater than that seen for γ-CDP. This may be due better inclusion of the drug molecule within α-CDP and β-CDP.

While it is usual that changes in absorbance observed for free drugs and complexes are small and weak [15], as seen for AXI where a 6-8 nm redshift and 3-25 % hypochromic shift are recorded.

The more significant bathochromic and hyperchromic shift in SUT's spectrum in all CDs may reflect a greater interaction or effect of CD inclusion on SUT's polarity [15].

8.3. THERMALSTABILITY OF AXI AND SUT WITH CYCLODEXTRINS

Solutions of the two drugs in the presence and absence of α-, β- and γ-cyclodextrin monomers and polymers were thermally degraded at 22°C.

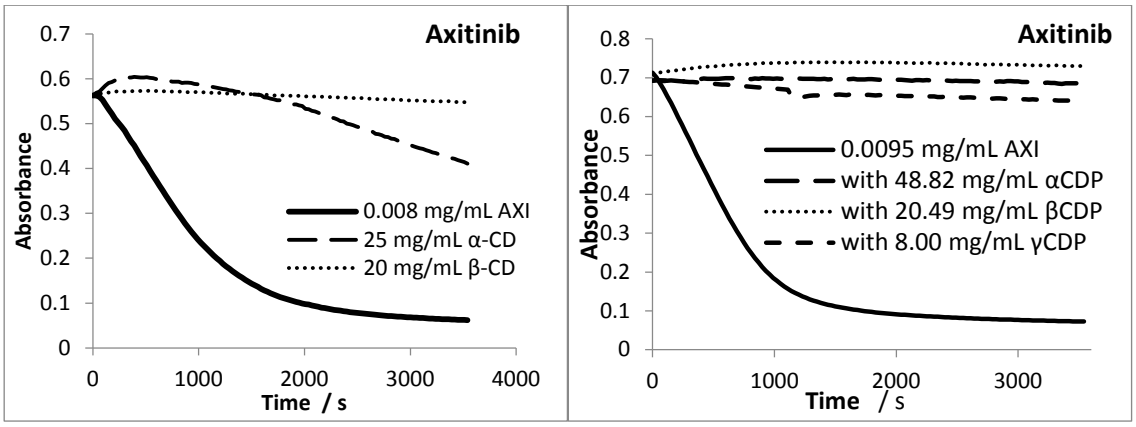

Fig 8.2: Effect of α- , β- and γ-cyclodextrin monomers and polymers on the thermal degradation of AXI observed at 332 nm, stirred and thermalstatically maintained at 22°C for an hour.

Addition of Cyclodextrin monomers and polymers were shown to reduce AXI's rate of degradation. In the absence of any cyclodextrins AXI degrades rapidly (Fig. 8.2, Table 8.1), completing its reaction within an hour. When cyclodextrins were added, AXI's stability was found to be enhanced greatly, if not completely, under the same conditions.

Of the CD monomers studied, 20 mg/mL β-CD provided more stability than 25 mg/mL α-CD (2.76 % and 27.04 % degradation, respectively). However, in their polymeric forms (where solubility is not an issue), 48.82 mg/mL α-CDP offered much better stability (2.03 % degradation) than the 20.49 mg/mL β- and 8 mg/mL γ-CDP (2.63 % and 7.72 %, respectively).

This may be due to the smaller cavity size of α-CDs, offering a better encapsulation than the two larger ones.

In the literature, CDPs have been reported to afford drugs better stabilizing effect than monomers, due to improved encapsulation [16-19].

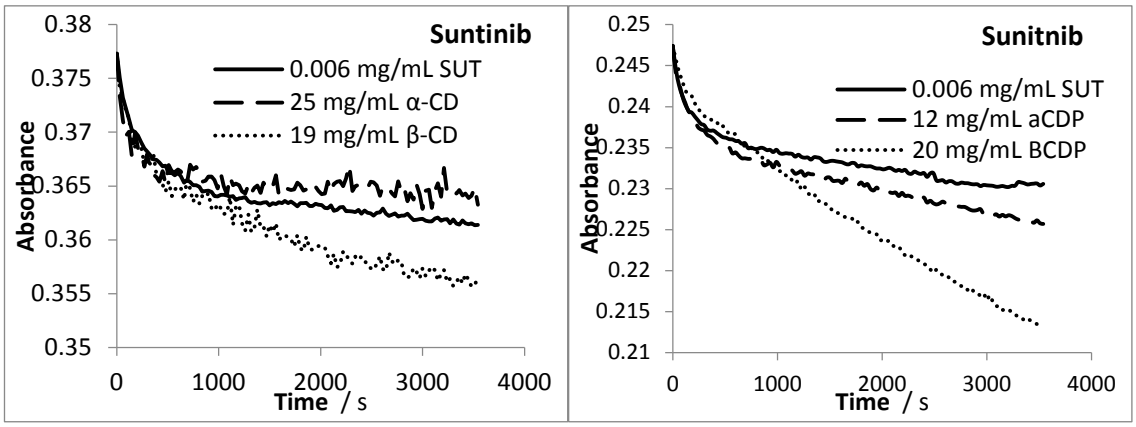

Fig 8.3: Effect of α- , β- and γ-cyclodextrin monomers and polymers on the thermal degradation of SUT observed at 430 nm, stirred and thermalstatically maintained at 22°C for an hour.

Table 8.1: Percentage of degradation recorded for AXI and SUT in the presence and absence of cyclodextrin monomer and polymers and their effects on the initial velocity of the thermal reaction.

	Water	α-CD	HP-β-CD	α-CDP	β-CDP	γ-CDP
AXI						
Concentration (mg/mL)	0.008	25	19	48.82	20.49	8.00
Initial Velocity (s^{-1}, x 10^{-4})	1.76	2.62	0.82	0.04	0.63	0.21
Percentage of Degradation (%)	88.95	27.04	2.76	2.03	2.63	7.72
SUT						
Concentration (mg/mL)	0.006	25	19	12	20	-[a]
Initial Velocity (s^{-1}, x 10^{-5})	6.01	7.17	6.44	7.80	6.45	-
Percentage of Degradation (%)	4.21	3.72	5.52	8.78	13.90	-

[a] Experiment were not carried out

On the other hand, presence of α-CDP and β-CDP were found to slightly increase the thermal degradation of SUT (Table 8.1, Fig. 8.3). As a result, it could be concluded that the addition of cyclodextrins (monomers or polymers) has no effect on SUT's stability – this is not an unknown phenomena [20]. As SUT has a number of potential inclusion sites, the drug might be included but the complex has no effect on its thermal reactions. If the *E/Z* reaction is accepted as postulated in Chapter 6 (scheme 6.2), then the inclusion does not involve the double bond. This might be explained by the large size of SUT.

8.4. EFFECT OF CYCLODEXTRIN ON THE PHOTOSTABILITY OF THE DRUGS

8.4.1. Photostability of AXI with Cyclodextrins

Samples of AXI in the presence and absence of α-, HPβ- and γ-cyclodextrin were exposed to ambient polychromatic light (laboratory light, Fig 8.4) and monochromatic irradiation (Fig 8.5).

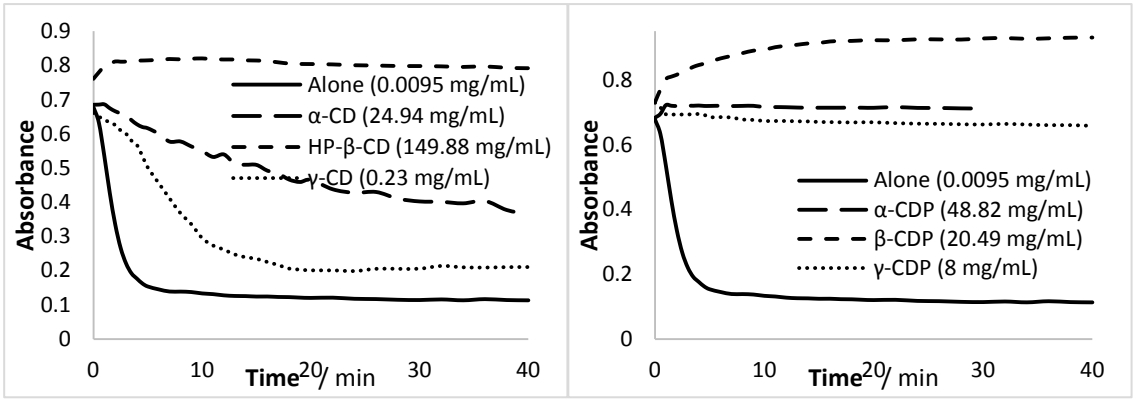

Fig. 8.4: Effect of cyclodextrin monomers (Left) and polymers (right) on 0.0095 mg/mL AXI's degradation under ambient room lighting and temperature conditions.

Under ambient lighting, both γ-CD and α-CD were found to reduce AXI's rate of degradation. Compared to 1.5 minutes in the absence of any cyclodextrins, AXI's half-life time was

significantly extended to 7 and 30 minutes when γ-CD and α-CD were added, respectively (Table 8.2).

However, when HP-β-CD was added, a rapid increase in absorbance was seen within the first 10 minutes, suggesting a different reaction is taking place or the product is included with a higher ε than that of AXI.

Table 8.2: Axitinib's half-life times in the presence and absence of cyclodextrins monomers

Sample	Half-Life Time ($t_{1/2}$, min)
AXI Alone	1.5
AXI with α-CD	30
AXI with HP-β-CD	N/A
AXI with γ-CD	7

Although an improved rate of degradation was achieved, the stabilizing effects of these cyclodextrins are limited by their solubility.

α- and γ-CDP were found to completely stabilise AXI under the given conditions (Fig. 8.4).

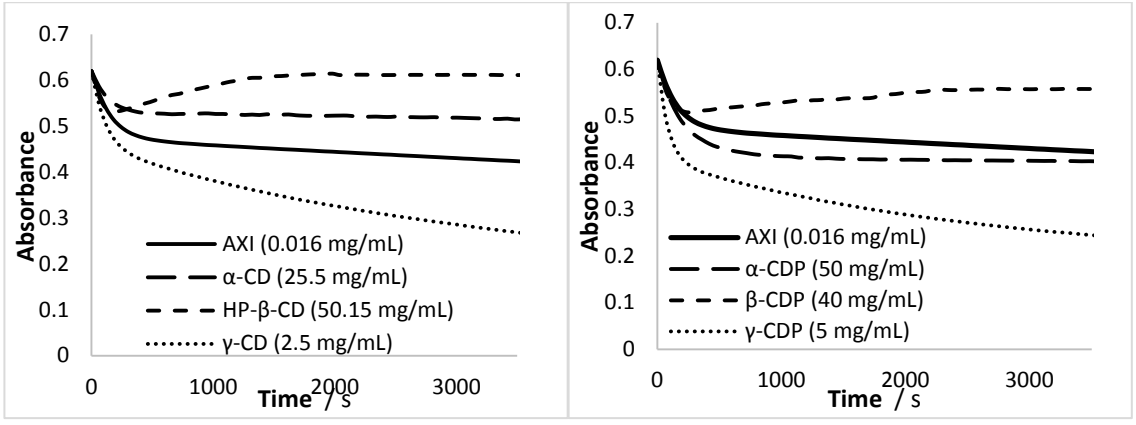

Fig. 8.5: Effect of α- , β- and γ-cyclodextrin monomers (Left) and polymers (Right) on the degradation of AXI (0.0095 mg/mL) observed at 332 nm, when monochromatically irradiated at 330 nm (3.07 x 10^{-6} einstein s^{-1} dm^{-3}, 22°C)

The presence of β-CDP appears to bring about the same reaction as that observed for HP-β-CD. However, in this case, the reaction is more defined and slower than that observed earlier - reaching maximum absorbance around 20 minutes rather than 10 minutes.

Contrary to the results observed under ambient conditions, monochromatic irradiation of γ-CD, γ-CDP and α-CDP was found to accelerate the photodegradation of AXI in aqueous media (Fig. 8.5). The fact that the concentrations in samples used were not significantly different, it suggests that under ambient conditions AXI mainly undergoes thermal degradation. So, the presence of α-CDP, γ-CD and γ-CDP appears to only thermally protect AXI under ambient conditions.

This idea seems evident in the trace obtained here for α-CD, where the photodegradation reaction of AXI ends with a plateau – as observed in organic media where no thermal reaction takes place; further confirming that α-CD, α-CDP, γ-CD and γ-CDP thermally protects AXI.

α-CD has a cavity diameter of just 0.47 – 0.53 nm [21], whereas the diameter of a benzene ring is ca. 0.6 nm [22] and so the inclusion of AXI is most likely to form around the amide group (Fig. 8.6 A1). In this formation, reaction of the amide group is hinder by the presence of α-CD and so preventing thermal degradation of AXI in aqueous media.

This corroborates our hypothesis postulated earlier for AXI's mechanism (Chapter 6, scheme 6.8).

γ-CD, on the hand, has a much larger cavity size of 0.75-0.83 nm [21], enabling much more of AXI to be included. Due to this and that γ-CD only thermally protect AXI, it can be supposed that it is most likely to be the amide end of AXI that is included within γ-CD (Fig. 8.6 A2) rather than the pyridine ring - which is of a similar size to benzenes [23] (Fig. 8.6 A3).

For both α-CD and γ-CD, the unlikely inclusion of the pyridine ring and double bond (Fig. 8.6 A3), agrees well with the lack of photoprotection provided – as isomerisation of the double bond occurs when AXI is irradiated. These findings suggest that the stability studies in the presence of various CDs gives valuable information on the structure of the complex.

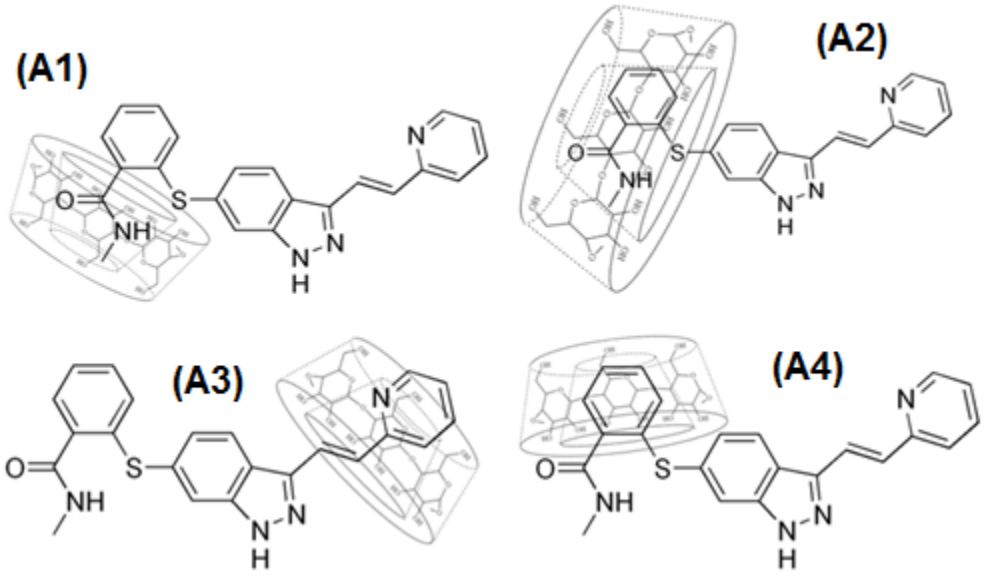

Fig 8.6: Possible complex formations between AXI and α-CD (A1), γ-CD (A2) and β-CD (A3 and A4).

Under monochromatic conditions, HP-β-CD and β-CDP was found to induce the same reaction observed under ambient conditions. It appears that neither thermal- nor photo-protection is provided. However, it is clear that there is some kind of interaction between AXI and the CD due to the presence of a different reaction.

β-CD has a cavity diameter of 0.60 – 0.65 nm [21], bigger than α-CD but smaller than γ-CD. Thus, it is possible for the amide group to be included like with α-CD. However, due to its slightly larger cavity, the fit is looser and so the inclusion of benzene or pyridine ring is much preferred (Fig. 8.6 A4 or A3). The fact that AXI's reaction in the presence of β-CD does not appear to be the *E-Z* isomerisation observed in the free AXI, it is plausible to propose that the complex involves the inclusion of the pyridine and double bond (Fig. 8.6 A3).

However, it could also be possible that benzene ring near the sulphur bond is included (Fig. 8.6 A4). Inclusion here, might hinder the reaction of amide group and so preventing the thermal degradation seen for free AXI in aqueous solution.

8.4.2. Photostability of DBZ and SUT with Cyclodextrin

The presence of cyclodextrins (HP-α-CD, α-CDP, HP-β-CD, β-CD Polymer, γ-CD and γ-CD polymer) were found to have little effect on the photodegradation of DBZ and SUT when monochromatically irradiated (Fig 8.7).

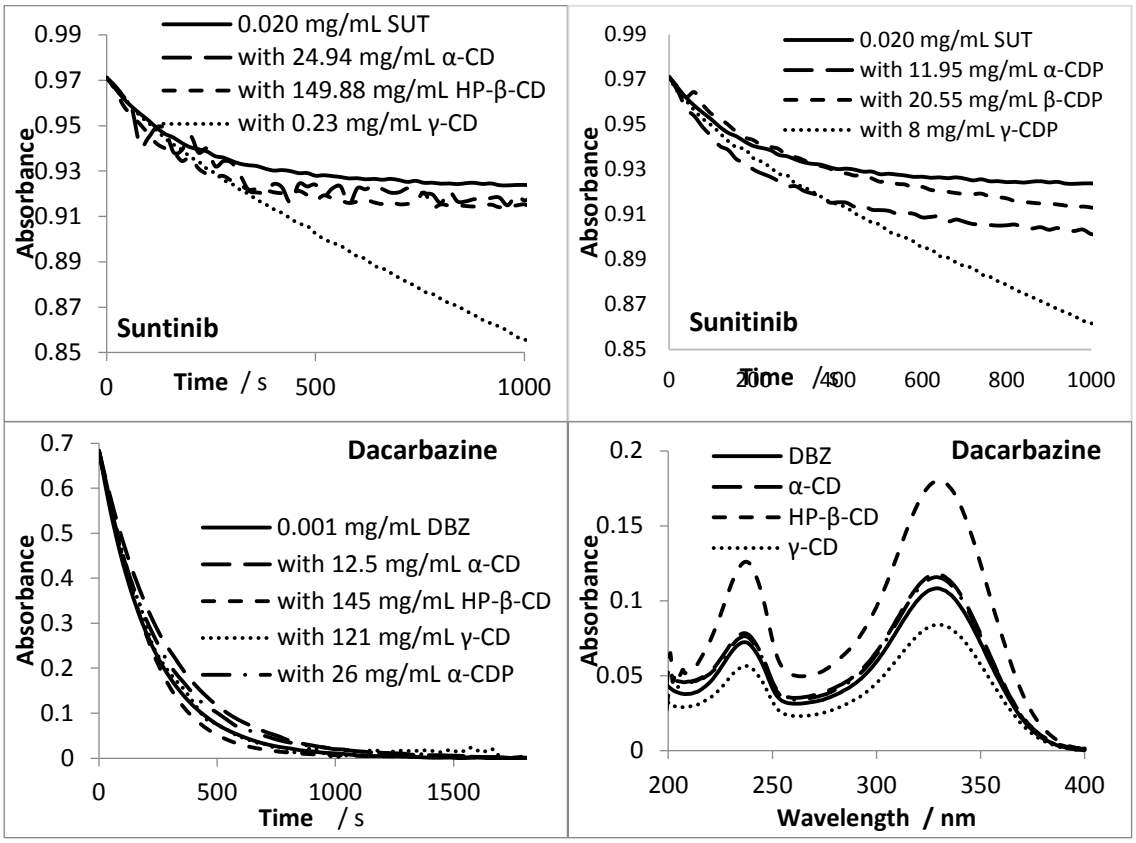

Fig 8.7: Effect of α- , β- and γ-cyclodextrin monomers and polymers on the degradation of 0.02 mg/mL SUT observed at 430 nm, when monochromatically irradiated at 430 nm (5.50 x 10^{-6} einstein s^{-1} dm^{-3}, 22°C, stirred) and 0.001 mg/mL DBZ observed at 330 nm, when irradiated monochromatically at 330nm (1.06 x 10^{-6} einstien^{-1} s^{-1} dm^{-3}, 22°C) (Bottom Left) Electronic absorption spectra of DBZ (0.001 mg/mL) in the presence and absence of α-, β- and γ-cyclodextrin monomers (12.5 mg/mL, 145 mg/mL and 121 mg/mL, respectively) and α-polymer (26 mg/mL).

The lack of improvement in photostability of DBZ may be due to the fact that the primary photochemical step in its photodegradation involves a scission of the N – N bond, which does not seem to be hindered by the cyclodextrin if we assume a total inclusion. Otherwise, these results (Fig. 8.7) may indicate that DBZ is only partially included within the cavity. Thus, inclusion within cyclodextrin did not provide photoprotection.

~5% degradation was observed for SUT in aqueous solution and similar percentage of degradation were observed when α-CD, HP-β-CD, α-CD-P and β-CD-P were present in solution. However, when γ-CD and γ-CDP were used, a greater degree of degradation was observed.

The initial velocity calculated for the reactions (Table 8.3) showed little/no change in rate, under both monochromatic and polychromatic conditions. As a result, it could be concluded that the addition of cyclodextrins (monomers or polymers) does not provide SUT with any protection from light.

Although the addition of cyclodextrins did not provide any stabilising effect on DBZ or SUT, this study is the first to carry out such investigation on the effect of both cyclodextrin monomers and polymers on the thermal- and photodegradation of DBZ and SUT, in both monochromatic and polychromatic light conditions. The acceleration of the guest compound's degradation by cyclodextrins seen here is not an unknown phenomenon [24-25].

Table 8.3: Percentage of Photodegradation for SUT in the presence and absence of cyclodextrins and their effects on the initial velocity of the reaction when exposed to monochromatic and polychromatic irradiation.

	SUT	α-CD	HP-β-CD	γ-CD	α-CDP	β-CDP	γ-CDP
Monochromatic irradiation at 430 nm[a]							
Concentration (mg/mL)	0.019	24.94	149.88	0.23	11.95	20.55	8
Initial Velocity (s^{-1}, x 10^{-4})	2.29	1.97	3.82	1.33	3.00	2.48	1.20
Percentage of Degradation (%)	5.54	4.76	7.62	20.75	9.87	8.43	23.53
Ambient laboratory light and temperature							
Concentration (mg/mL)	0.019	24.9	149.9	-[b]	11.9	20.5	-
Initial Velocity (min^{-1}, x 10^{-3})	2.18	2.75	4.39	-	3.78	2.82	-
Percentage of Degradation (%)	4.55	6.83	7.19	-	6.00	5.56	-

[a] 5.51 x 10^{-6} $einstien^{-1}$ s^{-1} dm^{-3}, 22°C, stirred

[b] experiment was not carried out

8.5. CONCLUSION

For the first time, a systematic study of the effects of cyclodextrin monomers and polymers on Dacarbazine, Axitinib and Sunitinib's thermal and photoactivities has been conducted in the present work.

Our results have proven that only minor effects on the stability of DBZ and SUT are expected to be observed from the involvement of such supramolecular systems. Therefore, DBZ and SUT's stability cannot be improved by this strategy.

Addition of Cyclodextrin monomers and polymers were shown to reduce AXI's rate of thermal degradation significantly. Of all the CDs, α-CDP offered the best thermal stability improvement.

Under monochromatic irradiation, a reduction in AXI's photosatbility was not seen. However, the photokinetic trace for AXI samples in the presence of α-CDP ends with a plateau – as observed in organic media where no thermal reaction takes place. Further confirming that complexation of AXI with α-CDP can provide thermal stability to the drug.

This was further proven by the complete stability observed when AXI was exposed to ambient light and temperature conditions. Under these conditions little/no photodegradation was observed, suggesting that thermal degradation is the main issue under ambient settings. Thus, here in this study, it has been shown that a thermally stable AXI could be made through inclusion complexation with α-CDP.

8.6. REFERENCES

1. Davis M.E. and Brewster M.E., 2004, Cyclodextrin-Based Pharmaceutics: Past, Present and Future, *Nature Reviews: Drug Discovery*, 3:1024-1035
2. Gidwani B. and Vyas A. (2015) A Comprehensive Review on Cyclodextrin-Based Carriers for Delivery of Chemotherapeutic Cytotoxic Anticancer Drugs, *BioMed Research International*, 2015:1-15
3. Qian L., Guan Y. and Xiao H. (2008) Preparation and characterisation of inlcuion complexes of a cationic-β-cyclodextrin polymer with butylparaben or triclosan, *International Journal of Pharmacy*, 357:244-251
4. Zhang N., Li J., Jiang W., Ren C., Li J., Xin J. and Li K. (2010) Effective protection and controlled release of insulin by cationic β-cyclodextrin polymers from alginatechitosan nanoparticles, *International Journal of Pharmaceutics,* 393:212-218
5. Li J., Xiao H., Li J. and Zhong Y. (2004) Drug carrier systems based on water-soluble cationic β-cyclodextrin polymers, *International Journal of Pharmaceutics*, 278:329-342
6. Ammar H.O., Salama H.A., Ghorab M. and Mahmoud A.A. (2006) Implication of inclusion complexation of glimepiride in cyclodextrin-polymer systems on its dissolution, stability and therapeutic efficacy, *International Journal of Pharmaceutics*, 320:53-57
7. Ammar H.O., Salama H.A., Ghorab M. and Mahmoud A.A. (2006) Formulation and biological evaluation of glimepiride-cyclodextrin-polymer systems, *International Journal of Pharmaceutics,* 309:129-138
8. Szeman J., Ueda H., Szejtli J., Fenyvesi E., Machida Y. and Nagai T. (1987) Complexation of several drugs with water-soluble cyclodextrin polymer, *Chemical and Pharmaceutical bulletin*, 35:282-288

9. Uekama K., Otagiri M., Irie T., Seo H. and Tsuruoka M. (1985) Improvement of dissolution and absorption characteristics of phenyton by a water-soluble β-cyclodextrin-epichlorohydrin polymer, *International Journal of Pharmaceutics*, 23:35-42

10. Lutka A. and Koziara T. (2000) Interaction of trimeprazine with cyclodextrins in aqueous solution*, Acta Poloniae Pharmaceutica,* 57:369-374

11. Lutka A. (2002) Investigation of interaction of promethazine with cyclodextrin in aqueous solution, *Acta Poloniae Pharmaceutica,* 59:45-51

12. Sortino S., Giuffrida S., De Guldi G., Chillemi R., Petralia S., Marconi G., Condorelli G. and Sciuto S. (2001) The photochemistry of flutamide and its inclusion complex with beta-cyclodextrin. Dramatic effect of the microenvironment on the nature and on the efficiency of the photodegradation pathways, *Photochemistry and Photobiology*, 73(1):6-13.

13. Peng M., Liu Y., Zhang H., Cui Y., Zhai G. and Chen C. (2010) Photostability Study of Doxorubicin Aqueous Solution Enhanced by Inclusion Interaction between Doxorubicin and Hydroxypropyl-β-cyclodextrin, *Chinese Journal of Chemistry*, 28:1291-1295.

14. Scalia S., Villani S. and Casolari A. (1999) Inclusion complexation of the sunscreen agent 2-ethylhexyl-p-dimethylaminobenzoate with hydroxypropyl-beta-cyclodextrin: effect on photostability, *Journal of Pharmacy and Pharmacology*, 51(12):1367-74.

15. Dodziuk H. (*ed.*) (2006) Cyclodextrins and Their Complexes: Chemistry, Analytical Methods, Applications, Darmstadt:WILEY-VCH Verlag GmbH & Co.

16. Dordunoo S.K. and Burt H.M. (1996) Solubility and Stability of Taxol: Effects of Buffers and Cyclodextrins, *International Journal of Pharmaceutics*, 133:191-201

17. Mognetti B., Barberis A., Marino S., Berta G., De Francia S., Trotta F. and Cavalli R. (2012) In vitro enhancement of anticancer activity of paclitaxel by a Cremophor free cyclodextrin-based nanosponge formulation, *Journal of Inclusion Phenomena and Macrocyclic Chemistry*, 74:201 - 210

18. Swaminathan S., Pastero L., Serpe L., Trotta F., Vavia P., Aquilano D., Trotta M., Zara G. and Cavalli R. (2010) Cyclodextrin-based nanosponges encapsulating camptothecin: Physicochemical characterization, stability and cytotoxicity, *European Journal of Pharmaceutics and Biopharmaceutics*, 74:193–201

19. Kang J., Kumar V., Yang D., Chowdhury P.R. and Hohl R.J. (2000) Cyclodextrin complexation: influence on the solubility, stability, and cytotoxicity of camptothecin, an antineoplastic agent., *European Journal of Pharmaceutical Sciences*, 15(2):163-70.

20. Boonleang J. and Tanthana C. (2010) Effect of hydroxypropyl-β-cyclodextrin on the stability of cisapride in oral suspensions, *Songklanakarin Journal of Science and Technology*, 32(6):605-611

21. Martin Del Valle E.M. (2004) Cyclodextrins and their uses: a review, *Process Biochemistry*, 39(9):1033-1046

22. Terzyk A.P., Gauden P.A., Furmaniak S., Wesołowski R.P. and Harris P.J. (2010) Molecular dynamics simulation insight into the mechanism of phenol adsorption at low coverages from aqueous solutions on microporous carbons, *Physical Chemistry Chemical Physics: PCCP*, 12(4):812-817

23. Vakalov I.A. and Shakhparonov M.I. (1966) Dielectric properties and molecular structure of pyridine-benzene solutions, *Journal of Structural Chemistry*, 7(4):479-483

24. Horspool W.M. and Lenci F. ed. (2004) CRC Handbook of Organic Photochemistry and Photobiology, 2nd Edition, USA: CRC Press

25. Loftsson T. and Brewster M.E. (1996) Pharmaceutical Applications of Cyclodextrins. 1. Drug Solubilization and Stabilization, *Journal of Pharmaceutical Sciences*, 85(10):1017-1025

CHAPTER NINE

IMPROVING DRUGS' PHOTOSTABILITY BY SELECTED PHARMACEUTICAL EXCIPIENTS

9.1. INTRODUCTION

The addition of inactive substances (pharmaceutical excipients) with similar absorption spectra to the drug formulation, film coating and capsule shell is a well-established method of photoprotection [1-14]. For this the excipient must have an absorption spectrum that overlays the absorption spectrum of the drug requiring protection [1-7]. The idea is that the excipient will compete with the drug for the energies from the light source and as a result, reducing the amount of damage done to the drug by reducing the amount of light absorbed [1-7]. Obviously, not only does the excipient requires the appropriate absorption spectrum for overlay, but it must also be pharmaceutically inactive, non-toxic and be photostable itself. Hence, the potentially useful materials is limited [5].

This application was shown very effective when applied to many drugs [6-14]: nifedipine [6,7], sorivudine [7], molsidomine [8], Axitinib [9], furosemide [6], daunorubicin [6], nitrofurazone [6], dihydroergotamine [6] and haloperidol [6]; and in solution for colchicine [10], tetracycline [11], reserpine [12], doxorubicin [13] and dacarbazine [14].

Yet, in the literature there is a lack of method to quantify this effect. Most commonly HPLC [6-9] and spectrophotometers [10-14] are employed for analysis. The percentage of decomposition [6-9] or rate-constants are calculated using thermal kinetic plots [10-14] as measures of photostabilization.

Even though the method was found to be effective in photostabilizing DBZ solutions [14] and AXI tablets [9], glutathione is not employed in commercial formulations because inhibits DBZ-induced cell apoptosis [15] and AXI is still only available in solid dosage form. No studies on the application of this method have been reported for SUT yet and thus, a suitable photoprotective excipient for liquid formulation is still yet to be discovered for these drugs.

Excipients selected for this study are four pharmaceutical excipients (Sunset Yellow, Tartrazine, Vanillin and β-Carotene) and an anti-emetic drug often co-administered with DBZ (Ondansetron) [16]. They are mainly selected based on their absorption spectra, safety for human consumption and compatibility with DBZ, AXI and SUT (scheme 9.1).

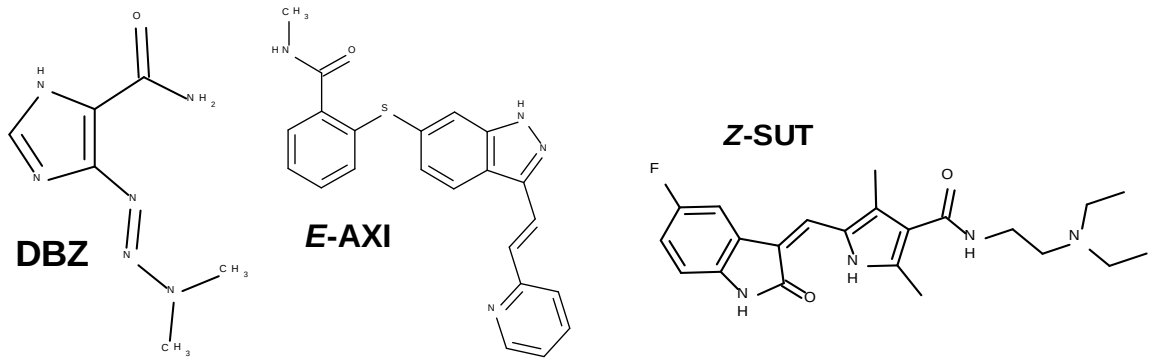

Scheme 9.1: Molecular structures of Dacarbazine (DBZ), Axitinib (E-AXI) and Sunitinb (Z-SUT)

9.2. EFFECT OF AZO DYES: SUNSET YELLOW AND TARTRAZINE

Sunset Yellow (E110, SSY) and Tartrazine (E102, TRZ) are two of the most widely used artificial colouring agent present in many in confectionery, soft drinks, drugs and cosmetics.

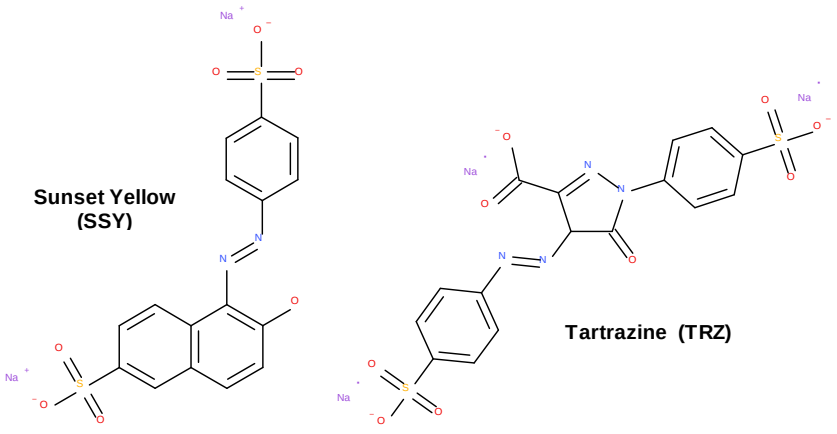

Scheme 9.2: Molecular structures of Sunset Yellow and Tartrazine

They can be found in various pharmaceutical products such as Beechams [17], a drug for the treatment of common flu; HIV drug, Kaletra [18] and throat lozenge, Strepsils [19]; the

antimicrobial drug Metronidazole [20]; the cough syrup, Buttercup [21]; Lemsip's Cold and Flu Relief Capsules [22]; cough medicine, Acetaminophen and Codeine Phosphate Oral Solution [23] and the antibiotic drug Oxytetracycline tablets [24].

SSY and TRZ absorbs within the range 200 nm – 550 nm, which fully cover the absorption spectrum of DBZ, AXI and SUT (Fig. 9.1). Thus, absorbing light of the same wavelength and could potentially act as competitive light absorbers for all three drugs.

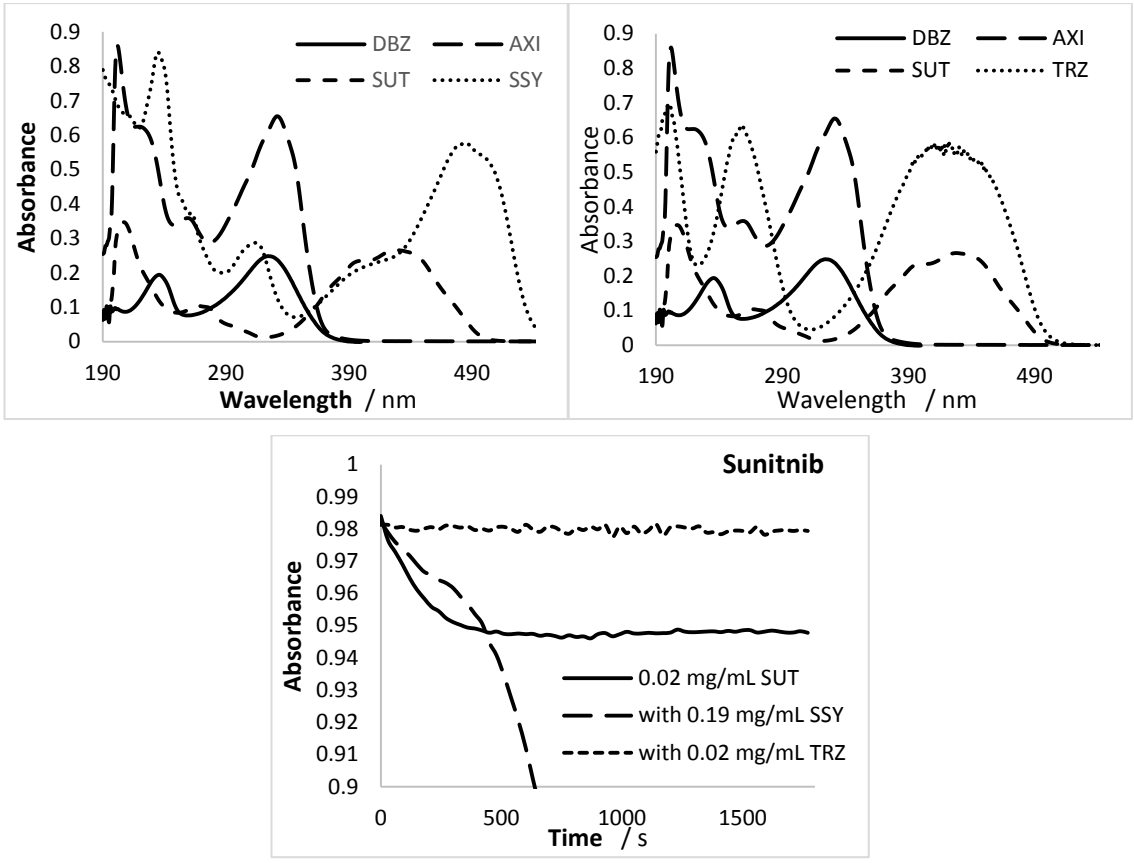

Fig 9.1: Absorption spectra of Dacarbazine (DBZ), Axitinib (AXI), Sunitinib (SUT), Sunset Yellow (SSY, Left) and Tartrazine (TRZ, Right) in water or 2.5% v/v ethanol/water for AXI.

Irradiation of the drugs in the presence of SSY and TRZ were found to reduce the rate of degradation (Fig. 9.1 and 9.2). For DBZ and AXI, SSY appears to be more effective than TRZ due to TRZ's low absorptivity at the two drugs' main absorption band.

On the other hand, TRZ was shown to almost completely stabilise SUT, while SSY induced a reaction which produced orange precipitates to form in solution. This may be an interaction between the SSY and fluoro end of SUT, as SSY has been reported to form non-covalent aggregates with fluorophenols and form liquid crystals at high concentrations [25].

This may present a huge problem for patients on SUT treatment, as mentioned, SSY can be found in a large number of confectionery, soft drinks, drugs and cosmetics.

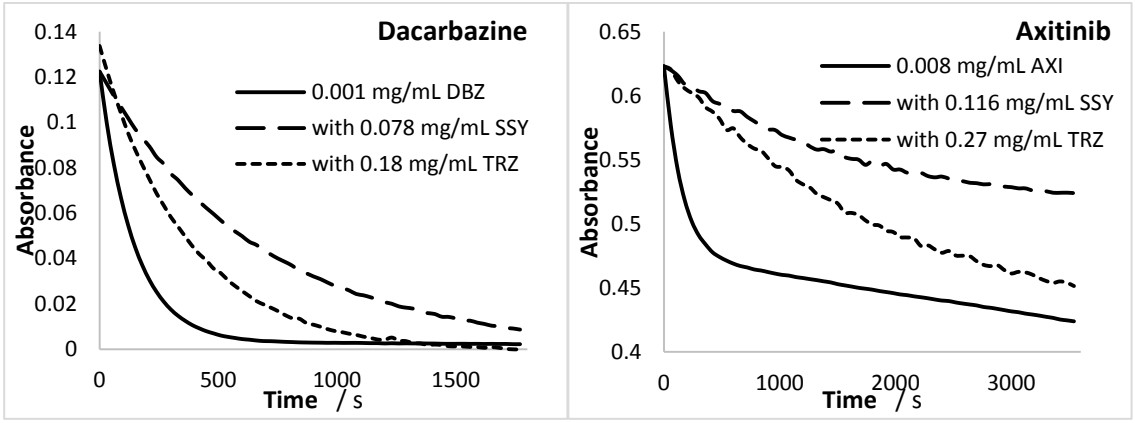

Fig 9.2: Effect of tartrazine (TRZ) and sunset yellow (SSY) on the photodegradation of 0.001 mg/mL DBZ observed at 330 nm, when irradiated monochromatically at 330nm (1.96 x 10^{-6} einstien^{-1} s^{-1} dm^{-3}, 22°C) and 0.008 mg/mL AXI in 2.5% (v/v) ethanol/water solution observed at 430 nm, when monochromatically irradiated at 330 nm (3.05 x 10^{-6} einstein s^{-1} dm^{-3}, 22°C, stirred)

To quantify the effects, the initial velocity ($v_{0(mod.)}^{\lambda_{irr}/\lambda_{obs}}$) was determined by differential equation of the model equation describing Φ-order kinetics at t=0 (eq. 12, Annex A5.3), AB(1Φ) for DBZ and AB(2Φ) for AXI and SUT.

The presence of TRZ, both AXI and SUT showed a significant increase of 10 and 18.1-fold in stability in aqueous solution (respectively, Table 9.1). Their $v_{0(mod.)}^{\lambda_{irr}/\lambda_{obs}}$ were reduced from 7.23 x 10^{-4} s^{-1} and 2.40 x 10^{-4} s^{-1} (AXI and SUT, respectively) to 7.26 x 10^{-5} s^{-1} and 1.33 x 10^{-5} s^{-1}. While only 2.3-fold increase was found for DBZ.

Due to SSY's higher absorption around DBZ and AXI's peak maxima (320 nm and 330 nm, respectively) than TRZ, an even greater increase in stability were observed (4.5 and 13-fold, respectively).

The low photostability effect of SSY and TRZ on DBZ, in comparison to that on AXI and SUT, may be due to the dyes low absorptivity at the irradiation wavelength – even at increased concentrations.

Table 9.1: Initial velocities of DBZ, AXI and SUT degradation in water, tartrazine (TRZ) and sunset yellow (SSY) and the percentage of degradation observed

Dye Added	$P_{\lambda_{irr}}$ x 10^{-6} einstien^{-1} s^{-1} dm^{-3}	$v_{0(mod.)}^{\lambda_{irr}/\lambda_{obs}}$ / s^{-1}	Ratio[a]	Percentage of Degradation (%)
1.05 x 10^{-3} mg/mL Dacarbazine (λ_{irr} = 330 nm)				
None	1.96	6.55 x 10^{-4}	1	100.00
0.18 mg/mL TRZ	2.03	2.90 x 10^{-4}	2.3	100.00
0.078 mg/mL SSY	2.03	1.45 x 10^{-4}	4.5	92.88
0.008 mg/mL Axitinb (λ_{irr} = 360 nm)				
None	3.05	7.23 x 10^{-4}	1	34.18
0.27 mg/mL TRZ	3.06	7.26 x 10^{-5}	10	27.54
0.116 mg/mL SSY	3.06	5.55 x 10^{-5}	13	22.50
0.01 mg/mL Sunitinib (λ_{irr} = 430 nm)				
None	5.67	2.40 x 10^{-4}	1	3.68
0.02 mg/mL TRZ	5.67	1.33 x 10^{-5}	18.1	0.88
0.19 mg/mL SSY	5.85	-[b]	-	100.00

[a] Ratio = ratios of the initial velocities to that of the drug's photodegradation in water alone

[b] solution precipitated

In the literature the percentage degradation is often used as a measure of photostabilization [6-9]. However, the percentage of degradation alone is not sufficient enough to express the effect of the excipient – as shown here in the case of DBZ with SSY and TRZ (Table 9.1). While the percentage of degradation indicates little difference between the effect of SSY and TRZ to DBZ's photodegradation, calculation of $\nu_{0(mod.)}^{\lambda_{irr}/\lambda_{obs}}$ demonstrates that SSY is in fact almost two times more effective at half the concentration.

Increasing concentrations of SSY (0 mg/mL to 0.025 mg/mL) in DBZ solution were investigated to see if increasing SSY concentration had an effect; as well as whether it will be possible to quantify such an effect using RK treatment.

A good fit between the experimental and RK data was found. The fact that the RK data was obtained on basis of Scheme 6.5 reinforces the validity of the proposed reaction mechanism. It was found to gradually reduce the drug's photodegradation reaction (Fig 9.3). Suggesting that at higher SSY concentrations, it may be possible to reduce DBZ's photodegradation even more.

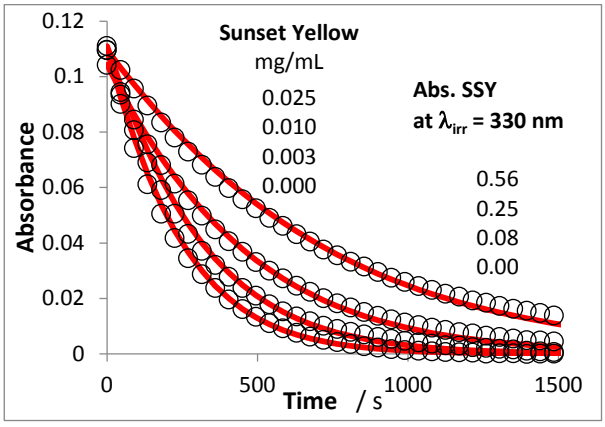

Fig 9.3: Changes in 1.05 x 10^{-3} DBZ photodegradation rate observed at 330 nm when increasing amount of SSY was added, when monochromatically irradiated at 330 nm (1.10 x 10^{-6} einstien^{-1} s^{-1} dm^{-3}, 22°C). Open circles are experimental data points and lines are RK fitting on the basis of Scheme 6.5.

9.3. EFFECT OF VANILLIN

Vanillin (4-hydroxy-3-methoxybenzaldehyde, VAN) is a flavouring additive obtained from vanilla beans used to produce natural vanilla and from by-products from the production of the paper for artificial vanilla. Because of its characteristic taste and odour of natural vanilla, it is widely used in pharmaceuticals, foods, beverages and as an aromatic ingredient in candles, air fresheners, perfumes and incense [26].

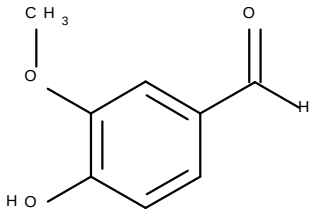

Vanillin (VAN)

Scheme 9.3: Molecular structure of Vanillin

As a pharmaceutical excipient, vanillin is used in tablets, solutions (0.01-0.02 % w/v), syrups and powder to mask the unpleasant taste and odour of various formulations [27]. Vanillin has also been investigated as a photostabilizer in furosemide 1 % (w/v) injection, haloperidol 0.5 % (w/v) injection and thiothixene 0.2 % (w/v) injections [26]. Therefore, it would be interesting to investigate the effect of vanillin on the photostability of DBZ and AXI as their spectra overlaps (Fig. 9.3).

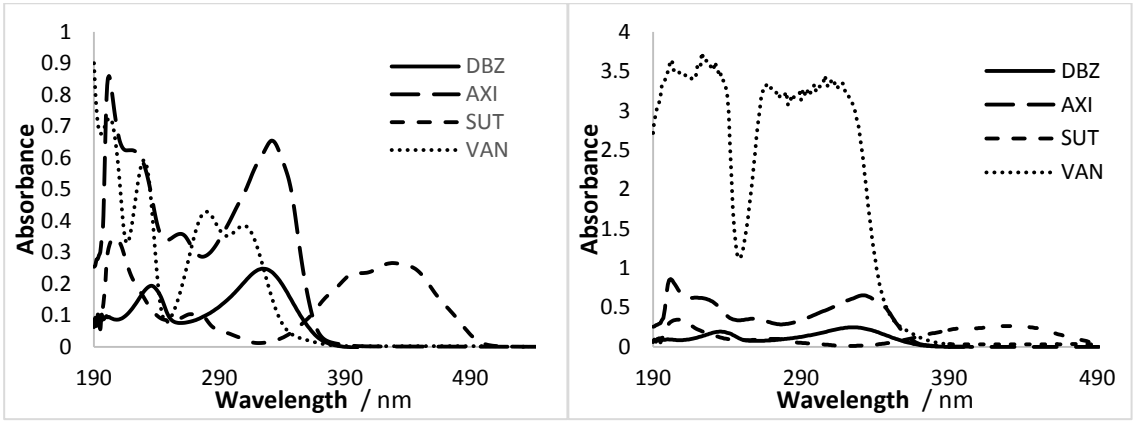

Fig 9.4: Absorption spectra of Dacarbazine (DBZ), Axitinib (AXI), Sunitinib (SUT) and 0.012 mg/mL Vanillin (VAN, Left) and the higher concentration used (0.1 mg/mL, Right)

Irradiation of DBZ (Fig. 9.5) and AXI in the presence of VAN showed significant improvement in the photostability of both drugs, DBZ in particular.

In the presence of VAN, the initial velocity of DBZ's photodegradation in water was reduced from 6.55 x 10^{-4} s^{-1} to 1.29 x 10^{-5} s^{-1}. That gives an impressive 50.7-fold increase in photostability (Table 9.2).

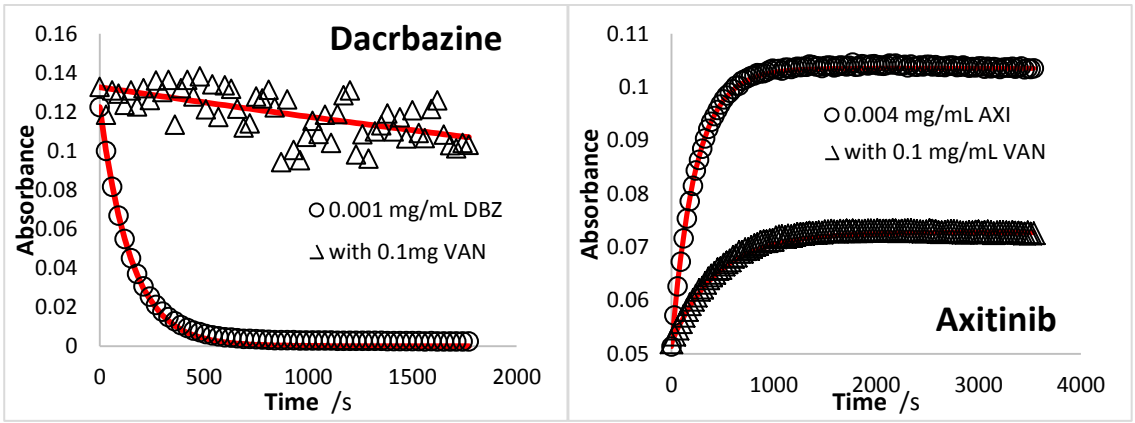

Fig 9.5: Change in absorbance observed at 330 nm when 0.001 mg/mL DBZ was irradiated monochromatically at 330 nm (1.97 x 10^{-6} einstien^{-1} s^{-1} dm^{-3}, 22°C) with 0.1 mg/mL Vanillin and when 0.004 mg/mL AXI was monochromatically irradiated at 430 nm (1.18 x 10^{-6} einstien^{-1} s^{-1} dm^{-3}, 22°C). Open shapes represents experimental data and solid lines represents fitting with eq. 12, Annex A5.3.

However, VAN had less of a stabilizing effect on AXI, with just 6.9-fold increase in photostability. This is due to the fact that VAN's absorption at 360 nm is not much more than AXI's. Therefore, is less efficient as a competitive light absorber for AXI than SSY.

Table 9.2: Initial velocities of DBZ and AXI degradation in water in the presence and absence of vanillin and the percentage of degradation observed

Vanillin Added mg/mL	$P_{\lambda_{irr}}$ x 10^{-6} einstien^{-1} s^{-1} dm^{-3}	$v_{0(mod.)}^{\lambda_{irr}/\lambda_{obs}}$ / s^{-1}	**Ratio[a]**	**Percentage of Degradation (%)**
1.05 x 10^{-3} mg/mL Dacarbazine (λ_{irr} = 330 nm)				
None	1.87	6.55 x 10^{-4}	1	100.00
0.1	1.97	1.29 x 10^{-5}	50.7	18.83
3.96 x 10^{-3} mg/mL Axitinb (λ_{irr} = 360 nm)				
None	1.18	1.14 x 10^{-5}	1	100.00
0.1	1.18	1.66 x 10^{-6}	6.9	39.34

[a] Ratio = ratios of the initial velocities to that of the drug's photodegradation in water alone

9.4. EFFECT OF ODANSETRON HYDROCHLORIDE

Ondansetron Hydrochloride (OHCl) is used to prevent nausea and vomiting caused by cancer chemotherapy, radiation therapy and surgery. It works by blocking the action of serotonin (5-HT3), a natural substance that may cause nausea and vomiting [28].

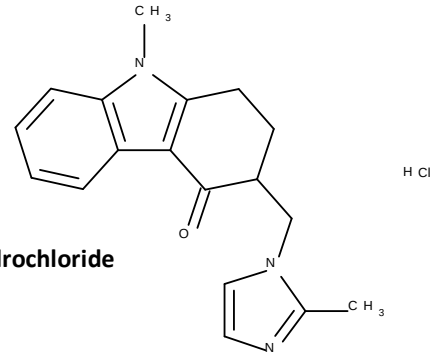

Ondansetron Hydrochloride (OHCl)

Scheme 9.4: Molecular structure of Ondansetron Hydrochloride

Stewart et al. [29] investigated the photostability of solutions containing 0.3 mg/L OHCl and 1 mg/L DBZ and reported that when stored in polyvinyl chloride (PVC) bags under ambient room temperature and fluorescence light intensity, DBZ injections were slightly more stable by a modest (5.7 %) when combined with OHCl than when alone in solution.

However, as stated by the authors, the instability of DBZ found in their study (48 hours) was inconsistent with that found by Benvenuto *et al.* [30] and that stated by the manufacturer (24 and 8 hours, respectively).

Thus, in this study the photostabilizing effect of ondansetron on DBZ was investigated as OHCl can act as a competitor for light absorption as its absorption spectrum overlays that of DBZ (Fig 9.6). It is also interesting to see whether a higher photoprotection rate than that previously obtained (5.7 %) can be achieved.

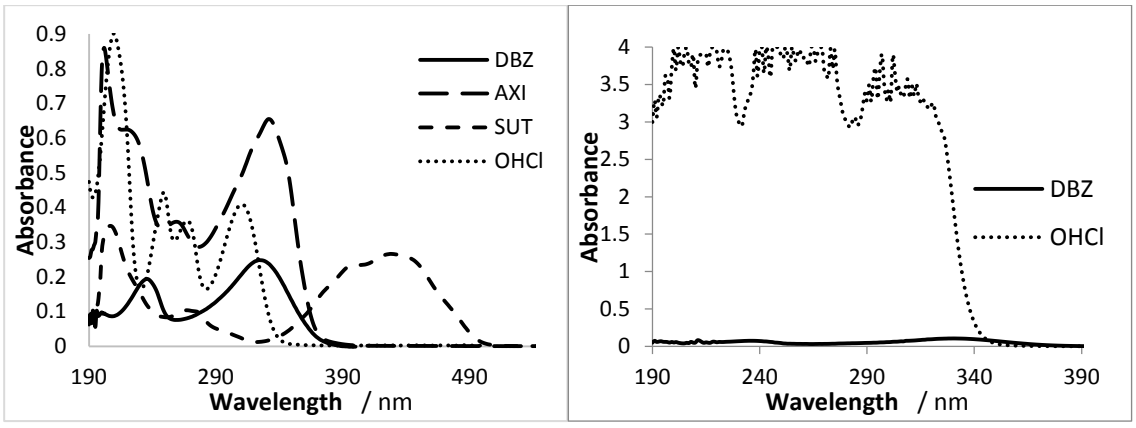

Fig 9.6: Absorption spectra of Dacarbazine (DBZ), Axitinib (AXI), Sunitinib (SUT) and 0.014 mg/mL Ondansetron Hydrochloride (OHCl, Left) and the higher concentration used (0.17 mg/mL, Right)

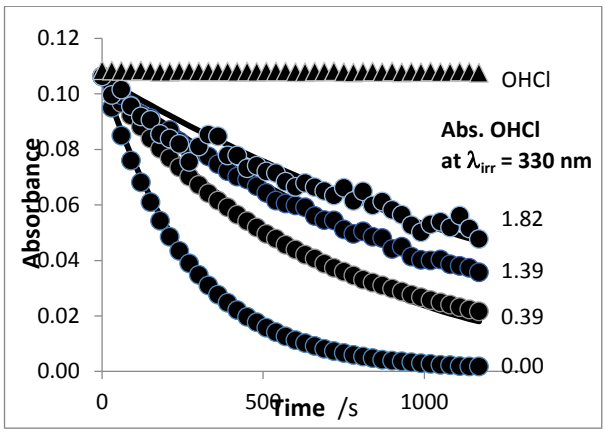

Fig 9.7: Changes in 0.001 mg/mL DBZ photodegradation rate observed when increasing amount of Odansetron was added, when monochromatically irradiated at 330 nm (1.05×10^{-6} einstien^{-1} s^{-1} dm^{-3}, 22°C). Data points are experimental data and lines are RK fitting on the basis of Scheme 6.5.

OHCl is photostable in the irradiation conditions used for DBZ photodegradation (Fig. 9.7). With increasing amount of OHCl, the photostability of DBZ increased.

RK treatment of the experimental data gave a good fit (Fig. 9.7). The fact that the RK data was obtained on basis of Scheme 6.5 further reinforces the validity of the proposed reaction mechanism. It can be clearly seen, that with increasing concentrations of OHCl, the rate (k_A) of DBZ is reduced, hence extending its life-time.

The recommended daily dose of OHCl is 32 mg or 2 mg/mL solutions for injection [31]. In this study, the highest amount of OHCl used to photostabilize 0.00098 mg/mL DBZ was 0.18 mg/mL. This means that for 1 mg/mL of DBZ, 181 mg/mL of ondansetron is required. This is much higher than the recommended dose.

However, it has been reported that individual intravenous doses as large as 150 mg and total daily intravenous doses as large as 252 mg have been inadvertently administered without significant or lasting adverse events [31].

In any case, the limitation due to the maximum recommended intake amount makes it clear that OHCl cannot represent a practical solution to improving DBZ photostability.

9.5. EFFECT OF β-CAROTENE

Carotenoids such as β-carotene (provitamin A) and lycopene that are found in many yellow and red vegetables are powerful antioxidants that protect cells from free radicals that can damage DNA and lead to cancer. Nutrients like vitamin A and β-carotene are found to be anti-carcinogenic and are often used in chemoprevention and treatment [32].

In 1994, Prasad *et al.* [33] investigated the effect of a mixture of vitamins (vitamin C, β-Carotene, d-alpha-tocopheryl succinate and 13-cis-retinoic acid) in modifying the efficacy of commonly used drugs in the treatment of human melanoma. It was found that the mixture of vitamins can enhance the growth-inhibitory effect of currently used chemotherapeutic agents on human melanoma cells, one of which was DBZ.

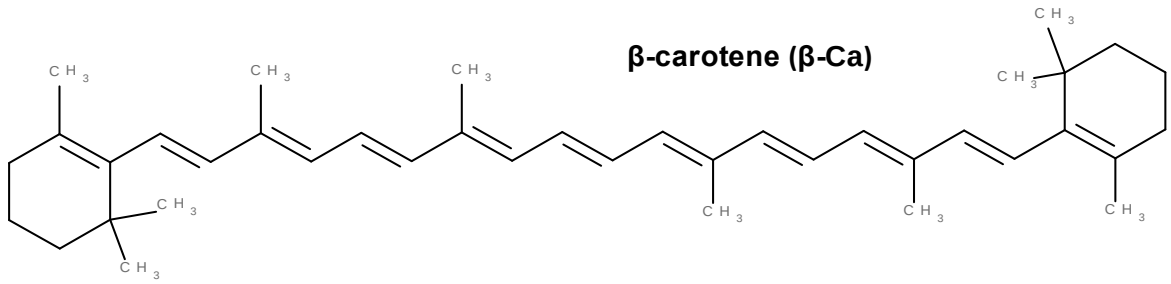

Scheme 9.5: Molecular structure of β-carotene

A later study [34] showed that mice with metastasis melanoma, fed a diet supplemented with beta-carotene, had 71% fewer tumours than mice not fed β-carotene.

Photochemically, β-Carotene was found to enhance the photostability of nisoldipine (a calcium-channel blocker) [35]. Therefore, it was considered interesting to investigate the effect of β-Carotene, as a competitor for light absorption, on the photostability of DBZ.

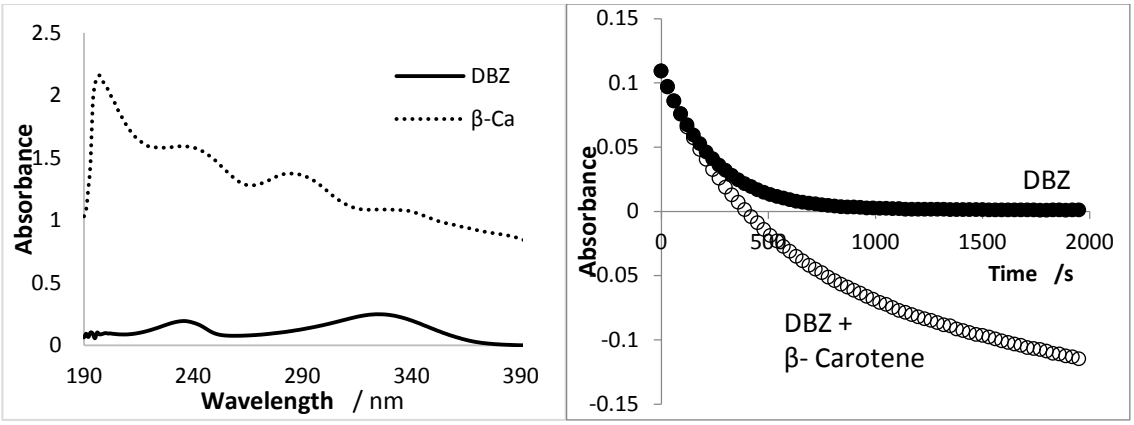

Fig 9.8: (Left) Absorption spectra of Dacarbazine (DBZ) and β-Carotene (β-Ca). (Right) Photokinetic trace of 0.001 mg/mL DBZ, irradiated monochromatically at 330nm (9.96 x 10^{-7} eintsien^{-1} s^{-1} dm^{-3}, 22°C, stirred) compared with that in the presence of 0.088 mg/mL β-carotene.

Although β-Carotene itself was found to be slightly photoactive in the irradiation conditions used for DBZ, the idea of spectral overlay and competition for light was used. That is by using a higher concentration of β-Carotene (0.88 mg/mL) than DBZ (0.01 mg/mL), less light would be absorbed by DBZ and so reducing its photodegradation rate.

Unfortunately, photostabilization of DBZ was not observed. Instead, a major drop in absorbance at wavelength 330 nm was seen, as shown in Fig. 9.8.

In order to understand this observation better, the effect of DBZ on β-Carotene was studied.

Thus, a constant concentration of β-Carotene (0.88 mg/mL) was added to increasing concentrations of DBZ (0, 0.010, 0.027 and 0.044 mg/mL) and the initial velocity ($v_{0(mod.)}^{\lambda_{irr}/\lambda_{obs}}$)

determined by differential equation of the model equation describing AB(2Φ) Φ-order kinetics at t=0 (eq. 12, Annex A5.3).

It was found that as the concentration of DBZ increased, the rate at which β-Carotene degraded increased as well (Fig. 9.9, Table 9.3). Thus, it can be concluded that β-Carotene is photosensitised by DBZ and therefore the usage of β-Carotene (with DBZ) must be considered with care.

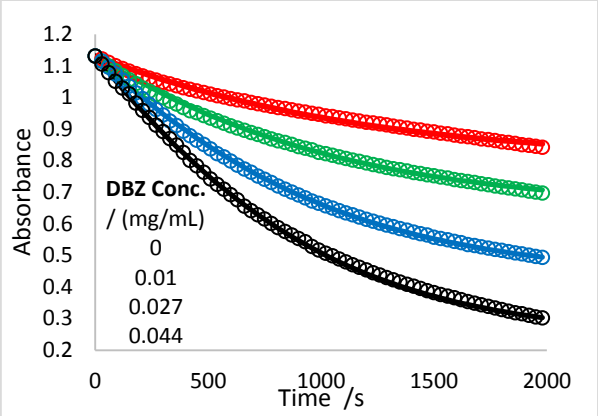

Fig. 9.9: Effect of increasing DBZ concentrations of (0 - 0.044 mg/mL) on the photostability of β-Carotene (0.88 mg/mL). λ_{irr} = 330 nm (9.96 x 10^{-7} eintsien^{-1} s^{-1} dm^{-3}, 22°C, stirred) and λ_{obs} = 330 nm.

Table 9.3: Initial velocities of β-Carotene (0.88 mg/mL) in water in the presence and absence of DBZ and the percentage of degradation observed.

λ_{irr} = 330 nm (9.96 x 10^{-7} eintsien^{-1} s^{-1} dm^{-3}, 22°C, stirred) and λ_{obs} = 330 nm.			
DBZ Added mg/mL	$\nu_{0(mod.)}^{\lambda_{irr}/\lambda_{obs}}$ / s^{-1}	**Ratio**	**% Degradation**
0	1.70 x 10^{-4}	1	25.6
0.01	2.32 x 10^{-4}	1.37	38.4
0.027	2.92 x 10^{-4}	1.72	56.5
0.044	3.42 x 10^{-4}	2.01	73.4

9.6. CONCLUSION

For the first time, two new ways of modelling and quantifying the effect of excipients on drugs' photodegradation has been reported. Application of Φ-order kinetics and RK treatment has been found very useful and successful.

The methods used here are shown to be much more appropriate and effective in quantifying the effect of excipients on drug photodegradation than those used in the literature - providing a clear indication of an excipient's effectiveness.

The effect of excipients on the reduction of the rate of DBZ, AXI and SUT degradation has been found to depend markedly on the absorbance of the excipient at the irradiation wavelength. While VAN and TRZ have been found to completely photostablize DBZ and SUT (respectively) in water solution, SSY has been shown to increase AXI's photostability by 13-fold.

These results has shown the importance and requirement of a systematic study on the effects of excipients on pharmaceutics' degradation since different excipients have different effects on photostability and some might show unexpected behaviour (SSY and β-Carotene). While some are limited by their recommended daily intake (SSY, TRZ and OHCl).

Nonetheless, the use of pharmaceutical excipients in drug photostabilization has been shown to be very useful. This opens up the possibilities of liquid formulations AXI and SUT (both of which are currently only available as solid dosage forms) for alternative routes of administration.

Alternatively, a solution containing a combination of various excipients may have an increased photostabilizing effect of the drugs than they do on their own (see Chapter 10).

9.7. REFERENCES

1. Tønnesen H.H. (ed.) (2004) Photostability of Drugs and Drug Formulations, 2nd Edition, USA:CRC Press LLC
2. Piechocki J.T. and Thoma K. ed. (2010) Pharmaceutical photostability and stabilization technology, New York: Informa Healthcare
3. Albini A. and Fasani E. (1998) Drugs Photochemistry and Photostability, Cambridge: The Royal Society of Chemistry
4. Rowe R.C., Sheskey P.J. and Weller P.J. (2003) Handbook of Pharmaceutical Excipients, Pharmaceutical Press and American Pharmaceutical Association
5. Crowley P.J. (1999) Excipients as Stabilizer, *Pharmaceutical Science & Technology Today*, 2(6):237-243

6. Thoma K. and Klimek R. (1991) Photostabilization of drugs in dosage forms without protection from packaging materials, *International Journal of Pharmaceutics*, 67(2):169–175

7. Desai D.S., Abdelnasser M.A., Rubitski B.A. and Varia S.A. (1994) Photostabilization of uncoated tablets of sorivudine and nifedipine by incorporation of synthetic iron oxides, *International Journal of Pharmaceutics*, 103(1):69–76

8. Aman W. and Thoma K. (2003) How to Photostabilize Molsidomine Tablets, *Journal of Pharmaceutical Sciences*, 93(7):1860-6

9. Gierer D.S., Morgado J.E., Murphy B.J. and Simmons D.M., Pfizer Inc. (2013) Pharmaceutical compositions of n-methyl-2-[3-((e)-2-pyridin-2-yl-vinyl)-1h-indazol-6-ylsulfanyl]-benzamide, U.S., Pat. WO 2013046133 A1

10. Habib M.J. and Asker A.F. (1989) Influence of certain additives on the photo-stability of colchicine solutions, *Drug Development and Industrial Pharmacy*, 15(5):845-849

11. Asker A.F and Habib M.J. (1991) Effect of certain additives on photodegradation of tetracycline hydrochloride solutions, *Journal of Pharmaceutical Science and Technology*, 45(2):113-115

12. Habib M.J. and Asker A.F. (1989) Photostabilization of doxorubicin hydrochloride with radioprotective and photoprotective agents: Potential mechanism for enhancing chemotherapy during radiotherapy, *Journal of Pharmaceutical Science and Technology*, 43(6): 259-261

13. Asker A.F., Helal M.A. and Motawi M.M. (1970) Light stability of some parenteral solutions of reserpine, *Die Pharmazie*, 26(2):90-2

14. Islam M.S. and Asker A.F. (1994) Photostabilization of Dacarabzine with Reduced Glutathione, *Parenteral Drug Association Journal of Pharmaceutical Science and Technology*, 48:38-40.

15. MedSafe (2012) Dacarbazine Datasheet [Online] Available from: http://www.medsafe.govt.nz/profs/datasheet/d/Dacarbazineinj.pdf [Accessed 20/10/2012]

16. Stewart J.T., Warren F.W., King D.T., Venkateshwaran T.G., Ponder G.W. and Fox J.L. (1997) Stability of ondansetron hydrochloride, doxorubicin hydrochloride, and dacarbazine or vincristine sulfate in elastomeric portable infusion devices and polyvinyl chloride bags, *American Society Health-System Pharmacists*, 54(8):915-20

17. electronic Medicines Compendium (2016) BEECHAMS ALL-IN-ONE [Online] Available at: http://www.medicines.org.uk/emc/medicine/16036/SPC/Beechams+All-in-One/#tableOfContents [Accessed 28/02/2016]

18. European Medicines Agency , SUMMARY OF PRODUCT CHARACTERISTICS [Online] Available at: http://www.ema.europa.eu/docs/en_GB/document_library/EPAR_-_Product_Information/human/000368/WC500039043.pdf [Accessed 20/10/2012]

19. Medicine and Healthcare Regulatory Agency (2010) Prescription Information [Online] Available at: http://www.mhra.gov.uk/home/groups/spcpil/documents/spcpil/con1349674252658.pdf [Accessed 20/10/02012]

20. Crescent Pharma Limited (2011) Patient's Information Leaflet [Online] Available at: http://www.crescentpharma.com/wp-content/uploads/2011/06/P0117T-Metronidazole-PIL-200mg-400mg-Clean-Version.pdf [Accessed 20/10/2012]

21. electronic Medicines Compendium (2016) Patient Information [Online] Available at: https://www.medicines.org.uk/emc/PIL.29777.latest.pdf [Accessed 29/02/2016]

22. The Medicines and Healthcare Products Regulatory Agency (2006) Public Assessment Report of Lemsip Max Day and Night Cold and Flu Relief Capsules [Online] Available at: http://www.mhra.gov.uk/home/groups/par/documents/websiteresources/con2025173.pdf [Accessed 30/04/2015]

23. Acetaminophen and Codeine Phosphate Oral Solution (2010) Patient Information [Online] Available at: http://www.accessdata.fda.gov/spl/data/e9dc3ce6-9c97-4881-b89e-eb1a5e552373/e9dc3ce6-9c97-4881-b89e-eb1a5e552373.xml [Accessed 09/02/2016]

24. Intrapharm Laboratories Limited (2014) Patient Information [Online] Available at: http://www.medicines.org.uk/emc/PIL.26648.latest.pdf [Accessed 30/04/2015]

25. Rowe R.C., Sheskey P.J. and Quinn M.E. ed. (2009) Handbook of Pharmaceutical Excipients (Sixth Edition) London: Pharmaceutical Press [e-book] Available through: http://www.scribd.com/doc/77286620/Handbook-of-Pharmaceutical-Excipients-6th-Edition [Accessed 21/09/2012]

26. Katz J.R., Day L.J. and Day I.J. (2013) NMR Investigations of the Interaction Between the Azo-Dye Sunset Yellow and Fluorophenol, Journal of Physical Chemistry B, 117(39):11793-11800

27. Gjorgjeska, B. (1991) Determination of polythiazide in the presence of vanillin in Renese tablets by second odred derivate UV spectroscopy, *Acta Pharmaceutica Jugoslavica*, 41:2:117-122

28. GlaxoSmithKline (2012) Zofran Prescribing Information [Online] Available at: http://us.gsk.com/products/assets/us_zofran.pdf [Accessed 20/10/2012]

29. Stewart J.T., Warren F.W., King D.T. and Fox J.L. (1996) Stability of Ondansetron Hydrochloride and Five Antineoplastic Medications, *American Society Health-System Pharmacists*, 53:1297-300.

30. Benvenuto J.A., Anderson R.W., Kerkof K., Smith R.G. and Loo T.L. (1981) Stability and Compatibility of Antitumour Agents in Glass and Plastic Containers, American Journal of Hospital Pharmacy, 38(12):1914-1918.

31. GlaxoSmithKline (2012) Zofran Prescribing Information [Online] Available at: http://us.gsk.com/products/assets/us_zofran.pdf [Accessed 20/10/2012]

32. Lupulescu A. (1994) The role of vitamins A, beta-carotene, E and C in cancer cell biology. *International Journal of Vitamin and Nutrition Research*, 64(1):03-14

33. Prasad K.N., Hernandez C., Edwards-Prasad J., Nelson J., Borus T. and Robinson W.A. (1994) Modification of the effect of tamoxifen, cis-platin, DTIC, and interferon-alpha 2b on human melanoma cells in culture by a mixture of vitamin, *Nutrition and Cancer*, 22(3):233-245

34. Pradeep C.R. and Kuttan G. (2003) Effect of beta carotene on the inhibition of lung metastasis in mice. *Phytomedicine* 10:159-164.

35. Mielcarek J., Grobelny P., Szamburska P. (2005) The effect of beta-carotene on the photostability of nisoldipine, *Methods & Findings in Experimental & Clinical Pharmacology*, 27(3):167

CHAPTER TEN

FORMULATION

10.1. INTRODUCTION

The lack of commercially available oral liquid dosage forms is an on-going problem in the pharmaceutical industry [1] – limiting their availability to paediatric patients, adults unable to swallow tablets or capsules and patients receiving medicines via nasogastric or gastrostomy tubes [1]. However, a range of problems are encountered when developing drugs into a stable liquid formulations, from the drug's solubility, photo- and thermal-stability to the stability of the excipients and packaging [2,3].

As most drug substances and excipients absorb in the UV and visible range, exposure to light could potentially lead to photochemical reactions. These reactions may cause the drug substance or components of the formulation to degrade and reduce the efficacy of the formulation or give rise to a toxic formulation [4]. Therefore, initial solutions would be to package the drug in a protective material. However, this is not the only solution and it is known that some types of protective packaging is not sufficient enough in preventing photodegradation – as in the case of DBZ [5].

AXI and SUT are commercially only available as solid dosage forms and when required, liquid dosage forms are prepared extemporaneously [1,6,7]. However, extemporaneously prepared oral suspensions are susceptible to caking, making the suspension excessively thick and un-pourable [8]. In addition, there is a lack of stability data available [9,10].

Thus, this chapter presents and explores for the first time, new stable liquid formulations for DBZ, AXI and SUT based on nanosponges.

There are two main goals of pharmaceutical formulation development [11,12]. First, to produce a drug that is stable to ensure that efficacy and safety characteristics of the active

substance are maintained. Second, to make drug administration easier and convenient to the patient who will use it, whilst keeping the use of excipients at a safe and minimal level [13].

10.2. CYCLODEXTRIN-BASED AXI FORMULATION

10.2.1. Water solubility

Solubility of the active drug in aqueous solution is critical in the design of formulation [14-16]. Many poorly soluble drugs can be made more water soluble by modifying their chemistry, such as introducing a hydrophilic group on the molecule [15]. Salts and derivatives of poorly soluble drugs are very common, but great care is required with modifications like these because different salts and forms may not have the same chemical stability and the biologic activity may be modified [15].

Furthermore, the very low water solubility limit of many anticancer drugs is the greatest challenge in the pharmaceutical industry, drug delivery in particular – limiting their use in clinical practice [17]. Nanosponges, such as cyclodextrin polymers, have been shown to improve solubility of some cancer drugs by incorporating drugs within their structure via complexation [17-19]. Yet, no such studies have been reported for DBZ, AXI or SUT.

As shown in previous chapters, of the three drugs studied, cyclodextrins (CD) complexes well with AXI. Since its use in pharmaceutical products, cyclodextrins have shown to be very effective in solubilising hydrophobic drugs – allowing solution-based dosage forms such as intravenous parenteral or oral solutions [27-29]. With increasing interest in nanoparticles and the benefits CDs bring, CDs are used to improve drug delivery systems.

Table 10.1: Examples of the maximum increase in solubility observed for various CD and drugs.

CD	Drugs	Increase in Solubility	Reference
α-CD	Cyclosporine A	10	20
β-CD	Carvedilol	110	21
γ-CD	Nystatin	103	22
HP-β-CD	Delta9-tetrahydrocannabinol Estradiol	1,000 248,600	23 24
DM-β-CD	Estradiol	214,900	24
HE-β-CD	Estradiol	92,250	24
SBE-β-CD	Curcumin	183.5	25
β-CDP	Dexamethasone Erlotinib	4 4	18 26

It is common practice to use the phase solubility diagram described to determine the solubility of drug and CDP complexes [27,30]. The method is based on the assumption of monomolecular inclusions (1:1, 1:2, 1:3, etc) and is perform with excess drug in solution. Not only can this process be costly, it does not give the solubility limit of the complex, the minimum water and CD required to solubilize the drug at its required dosage. Thus, an alternative method have been employed here for determining the solubility of the AXI/CDP complex.

Table 10.2: Solubility limits of AXI in water before and after complexation with α- and β-cyclodextrin polymers

Formulation	AXI / mg	CD / mg	Solubility[a] mg/mL	Increase in solubility
AXI	5	0	2×10^{-4}	0
AXI/α-CDP	5	300	10	50,000
AXI/β-CDP	5	770	5	25,000

[a] amount of AXI (mg) that can be dissolved by 1 mL of water

AXI has very poor solubility in water, 2 x 10^{-4} mg/mL [31]. One dose of Inlyta® contains 5 mg AXI [32]. Therefore, to dissolve and administer this drug as a liquid formulation, 25000 mL (25 L) of water would be required. For any patient, this is completely impractical.

Yet, with the addition of α-CDP and β-CDP, a single 5 mg dose of AXI can be solubilized with just 0.5 – 1 mL of water (Table 10.2). The original solubility of AXI in water (2 x 10^{-4} mg/mL) has now significantly improved to 5 mg/mL through complexation with cyclodextrin polymers. That is, an impressive 25,000 times increase with β-CDP and 50,000 times increase with α-CDP.

Because only 1 mL or less is required, great potential for other routes of administration to be considered (such as a parenteral to be injected intravenously and oral liquid formulation) and so making the drug available to paediatrics, elderly and patients who have difficulty swallowing tablets.

Current commercially available AXI (Inlyta®) tablets, containing the anhydrous form of AXI, has a bioavailability of only 58% - partly due to low solubility [33]. This means that only 2.9 mg of the 5 mg enters the bloodstream. Studies have shown that complexation with cyclodextrins improves a drug's bioavailability through the improvement of its solubility [27-29]. Therefore, the AXI/α-CDP and AXI/β-CDP formulations has the potential to demonstrate higher bioavailability than the current Inlyta formulation marketed by Pfizer. If the bioavailability is improved through complexation with CDPs, then the current 5 mg dose administered may be reduced without comprising the drug's efficacy.

10.2.2. Thermal stability

In the absence of any CDPs, AXI completely thermally degrades within an hour (See Chapter 6). Complexation with β-CDP showed complete stabilization for at least 5 hours. The changes in

absorbance observed at 330 nm remained within ± 1 standard deviation of the average absorbance reading (Fig. 10.1). Complexation with α-CDP also showed substantial improvement to AXI's thermal stability. Thermal degradation of AXI/α-CDP was found to have slowed down significantly from completion within 1 hour to requiring over 9 hours to complete.

The difference in the stabilizing effect of the two CDPs may be due to the fact that the amount of β-CDP (770 mg) present in the AXI/β-CDP formulation is more than twice that of α-CDP (300 mg) in the AXI/α-CDP formulation. It should be noted that the amount used in this study is the minimum required to completely solubilise 5 mg AXI.

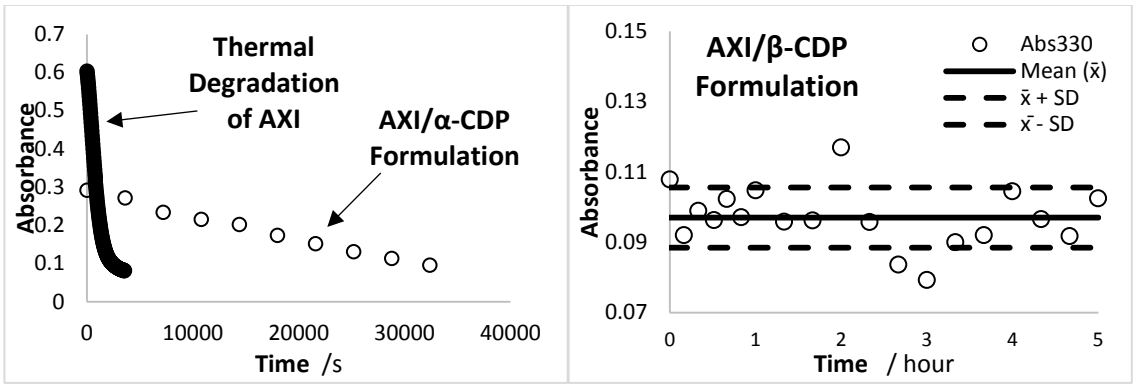

Fig 10.1: Thermaldegradation kinetic trace of (left) 2.16 x 10^{-5} M Axitinib (AXI) in 2.5 % (v/v) ethanol/water solution, as AXI/α-CDP formulation and (right) as AXI/β-CDP formulation, where circles represent experimental data and the mean values (0.097 ± 8.85 x 10^{-3}) represented as a line, with only four data points out of the range. Kept 22°c, stirred, observed at 330 nm

10.2.3. Photostability

10.2.3.1. Monochromatic Irradiation

As seen in previous chapters, irradiation of AXI in aqueous solution forms a new peak at 380 nm, which belongs solely to the photoproduct since an increase in absorption at 380 nm is not seen during the thermal degradation of AXI.

The evolution spectra and kinetic trace obtained (Fig. 10.2) for both formulations is proof that the thermal reaction has been completely stopped through the inclusion of CDPs and a plateau has been reached - indicating the end of a reaction.

Therefore, the Φ-Order kinetic model equation (as seen in Chapter 5) can be used to calculate the rate constant (k) of the reaction. The rate constant of AXI/α-CDP and AXI/β-CDP formulations were determined to be 2.4 min^{-1} and 12 min^{-1} (144 s^{-1} and 720 s^{-1}, respectively) - AXI/α-CDP being 5 times slower than β-CDP. In water, AXI's k was determined to be 0.004 s^{-1} (0.24 min^{-1}) at low concentration. Thus, neither formulations photostabilized AXI in UV light.

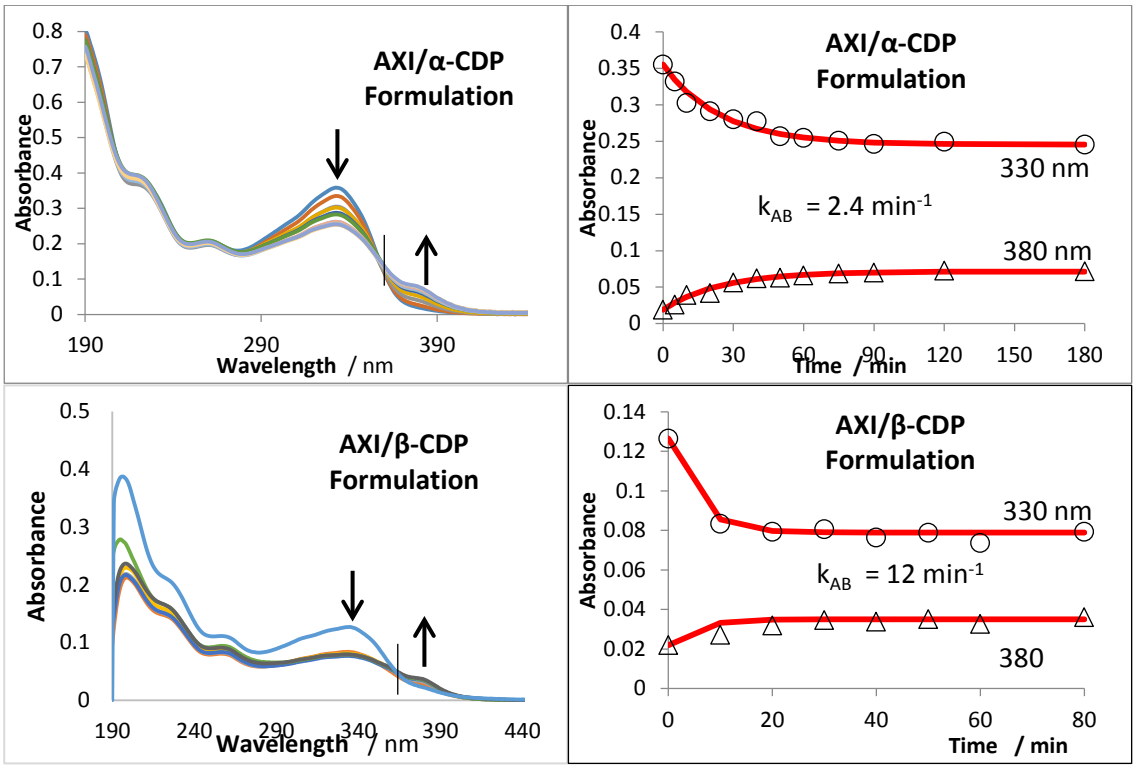

Fig. 10.2: Evolution of the electronic absorption spectra of AXI/α-CDP and AXI/β-CDP formulations in water and the photokinetic traces obtained at 330 nm (circles) and 380 nm (triangles), where open shapes represent experimental data and the solid lines are the fitting of the traces to the Φ-order kinetic model (k_{AB} = 2.4 min^{-1} and k_{AB} = 12 min^{-1}, respectively), when irradiated continuously with a monochromatic beam at 360 nm (1.47 x 10^{-6} einstein s^{-1} dm^{-3}, 22°C).

10.2.3.1. Polychromatic Irradiation

Photokinetic traces obtained for AXI/β-CDP at 330 nm and 380 nm (Fig 10.3) showed that a majority of the absorbance values remained within ± 1 standard deviation of the mean absorbance value for both throughout the experiment, i.e. there is very little change in absorbance throughout testing and the photoreaction is very stable for at least 7 hours. The formulation has extended the shelf life of AXI by an additional 6 hours because as shown before in Fig 10.1 thermal degradation alone caused AXI to be completely degraded within 1 hour.

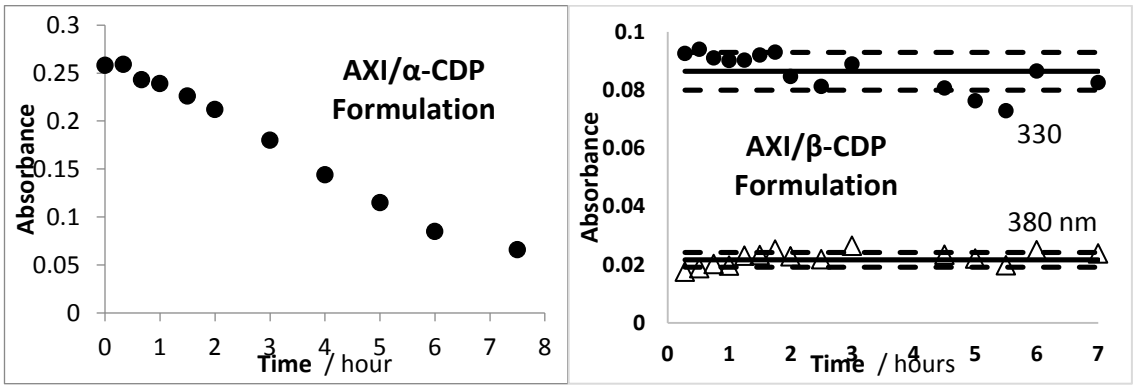

Fig 10.3: Kinetic traces of AXI/α-CDP (left) and AXI/β-CDP (right) formulations in water solution when exposed to polychromatic irradiation and ambient room temperature, stirred, obtained at 330 nm (circles) and 380 nm (triangles). Traces obtained for AXI/β-CDP, the mean values are represented as a line (0.0865 ± 6.49 x 10^{-3} for 330 nm and 0.0217 ± 2.55 x 10^{-3} for 380 nm), with only three data points out of range (dotted lines = mean ± SD).

AXI/α-CDP on the other hand, demonstrated that over 8 hours will be required to completely degrade AXI under ambient conditions. An increase in absorption at 380 nm was not seen. The reaction observed here was comparable to that recorded earlier for thermal degradation (section 10.2.2). Consequently, it can be inferred that the reaction recorded here was predominantly the thermal degradation of the formulation.

Although, looking at the formulation under polychromatic conditions whilst being continuously stirred is useful as it gives an indication of a situation where it is being agitated. It would be interesting to see if the formulation was made up a period of time before administration (without agitation). Therefore, tests have been conducted on the complex under polychromatic conditions unstirred (Fig 10.4).

In comparison to the complex tested in polychromatic stirred conditions, the absorbance readings in the unstirred conditions are shown to be just as stable over a period of 4 hours (Fig 10.4). Readings for the absorbance values observed at 330 nm and 380 nm are within ±1 standard deviation meaning that there is no change in absorbance for 4 hours.

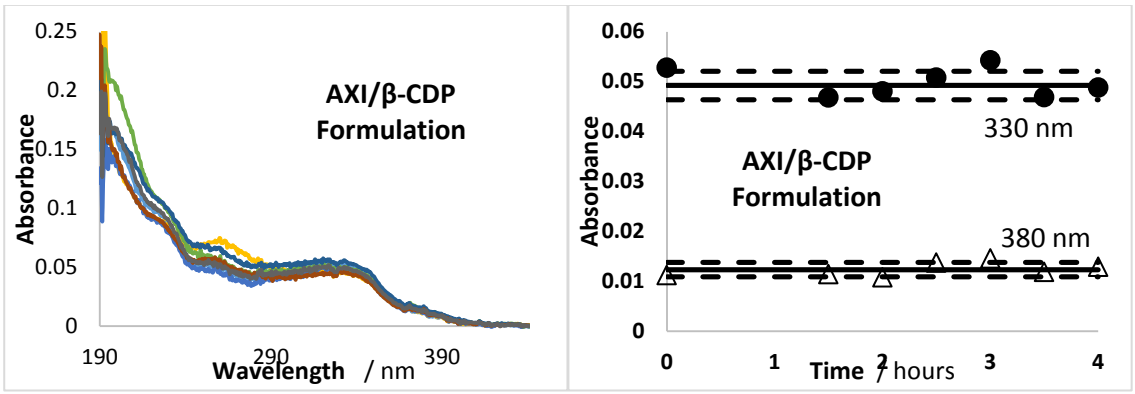

Fig 10.4: (Left) Evolution of the electronic absorption spectra of AXI/β-CDP formulation in water solution when exposed to polychromatic irradiation and ambient room temperature, not stirred. (Right) Photokinetic traces obtained at 330 nm (circles) and 380 nm (triangles), circles represent experimental data and the mean values (0.0493 ± 2.85 x 10^{-3} and 0.0123 ± 1.44 x 10^{-3}, respectively) represented as a line, with only data points out of the range (dotted lines = mean ± SD).

During dosage form design, many pharmaceutical characteristics must be addressed depending on the drug and delivering system. Liquid formulations must be palatable (if taken orally), soluble and stable, whilst ensuring efficacy and safety [2,3,11-13]. Improving a drug's solubility and stability presents the biggest challenge to formulators [1-3,15]. Not only do the

AXI/α-CDP and AXI/β-CDP formulations meets these criteria, they are simple in comparison to the current Inlyta® tablet formulations [32].

Manufacturing liquid formulations is generally less complex than a tablet. However, it must be noted that any form of heat and light needs to be avoided during the manufacturing process of the complexes, due to AXI's high degradation lability. Thus, the sensitivity of the drug to degradation by these routes needs to be held with the utmost importance. The risk of developing impurities in the formulation must be avoided.

Another issue to consider is the palatability as patients may be concerned with the palatability of the formulation. If the formulation is not pleasant tasting then this could be an issue with patient compliance. However, α-CDP and β-CDP come from a family of cyclodextrins which are made up of sugar molecules that are bound in a ring together. Therefore, the CDPs in AXI/α-CDP and AXI/β-CDP complexes are also playing the role of taste-masking agents. The use of cyclodextrins in this manner is not unknown. For example, Zinc acetate dihydrate used in lozenge formulations carries a bitter taste; it is masked by the use of anethol-β-cyclodextrin complex [34]. The high quantity of CDPs in the formulation allows the bitter taste of AXI to be masked.

It is recommended that AXI tablets are swallowed whole with a glass of water [31]. However, pharmacist and nurses frequently encounter patients with nasogastric tube or those unable to swallow oral medications for other reasons [6]. Even though it is advised against, current practice is to crush the tablet and administering it as a suspension [6]. This method can impact on the drug's stability, especially when exposed to light, and the safety of pharmacists and nurses who would require protection from inadvertent exposure.

An alternative preparation method which does not involve the crushing of the tablet, outlined by Pfizer for healthcare professionals, is to prepare a suspension by placing the tablet in an amber oral syringe with 15 mL of United States Pharmacopeia (USP) graded water and waiting 10 minutes for the tablet to disintegrate [6]. This then must be keep away from light and administered via nasogastric tube within 15 minutes of preparation. As shown in this study, AXI degrades rapidly in water even in the absence of light. The method described here has at least a 25 minutes gap between placing AXI in water and absorption. Thus, by that time, half of AXI would have already thermally degraded, as shown by our findings.

In this aspect, the new AXI powder formulation is especially useful and convenient as it is thermally stable and easily reconstituted. As well as, providing flexibility when other routes of administration, such as parenteral preparations, are required.

Furthermore, it is known for renal cell carcinoma metastases to develop in the neck. 15% of renal cell carcinoma cases report metastases to the head and neck regions [35] and for patients to develop painful swellings in the neck and head [36]. In these circumstances, it is advantageous that AXI the drug used to treat this condition can be administered as a solution instead of being administered as a tablet such as Inlyta, which is more likely to cause discomfort towards the patient [37].

10.2.4. AXI/α-CDP and AXI/β-CDP Formulation As Parenteral Injections

For a drug be administered parenterally, the drug must be non-toxic and readily dissolved [38]. Bioavailability is defined as the proportion of drug or substance that has entered the circulation in order to have an active effect in the body [39]. Here, a single dose of AXI (5 mg) was readily dissolved in 0.5 mL and 1 mL of double distilled water as a formulation with α-CDP

and β-CDP, respectively. Also, intravenously administering AXI/α-CDP and AXI/β-CDP formulation avoids first pass metabolism as opposed to the oral route of administration [40].

α-CDP and β-CDP has been approved by the FDA as being safe to be use in pharmaceutical formulations [41]. It is also known that orally administered cyclodextrins are not toxic; this is due to the fact that they are not absorbed well in the gastrointestinal tract. But it is also important to assure that the use of CDP in parenteral is safe and suitable.

Nanosponges like CDP have been shown to be safe, biodegradable materials with negligible toxicity on cell cultures that were well-tolerated after injection with no apparent side effects [20,29]. In Swiss albino mice, nanosponges were found to be safe up to 5000 mg/kg without showing any signs of toxicity or adverse reactions [42].

Accordingly, the newly developed AXI/α-CDP and AXI/β-CDP formulations can potentially be used parenterally. Currently, AXI cannot be administered intravenously and there are no studies reporting to have attempted. Thus, the two new formulations presented here could possibly provide healthcare professionals and patients an alternative route of administration which may be more ideal for some patients.

A final point to consider when looking at the formulation as a parenteral to be injected is that it is possible to deliver the effective dose of drug; in the event of an emergency where a patient becomes unconscious, providing the drug instantly via the parenteral route would become inevitable.

10.2.5. Characterisation of the Formulations

The variation of the IR spectrum can provide information of the occurrence of inclusion between the drug and CD [43-45]. Fig 10.5 shows the IR spectra of AXI, α-CDP, AXI/α-CDP

formulation, AXI/α-CDP physical mixture, β-CDP, AXI/β-CDP formulation and AXI/β-CDP physical mixture.

For both α- and β-CDP, a wide band at 3000-3610 cm^{-1} is seen due to OH bonds stretching. Due to C-O- bonds stretching, a strong absorption band at 900-1170 cm^{-1} is also observed.

Whilst the former band remains relatively unchanged after complexation, a decrease in intensity of the latter band in both AXI/α-CDP and AXI/β-CDP formulation is seen. This indicates inclusion of AXI within the CDPs. The lack of change in band intensity seen in the physical mixtures strongly suggests this conclusion.

The greater decrease in band intensity observed for AXI/α-CDP is indicative of a strong guest-host interaction and a better inclusion complex formed between AXI and α-CDP than β-CDP [43-45]. This collaborates well with the enhanced water solubility and stabilising effect found for AXI/α-CDP.

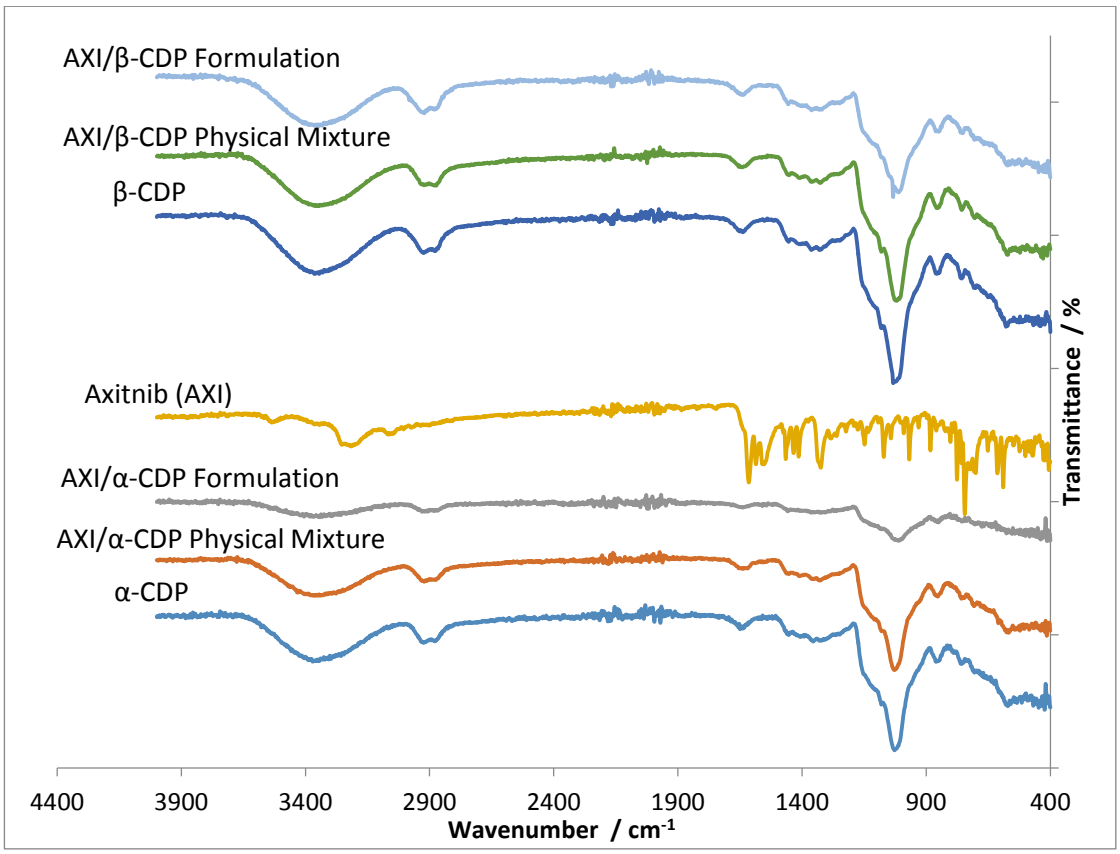

Fig. 10.5: The IR spectra of AXI, α-CDP, AXI/α-CDP formulation, AXI/α-CDP physical mixture, β-CDP, AXI/ β-CDP formulation and AXI/β-CDP physical mixture

Evaluation of surface morphology the powder of AXI/α-CDP and AXI/β-CDP formulations using Scanning Electron Microscope (SEM) showed the change in the crystallinity of AXI in the inclusion complex compared to the other. AXI powder consists of irregular rod-like crystals (Fig 10.6). Microphotographs of α-CDP and β-CDP shows large sheet-like structures.

In the powder of AXI/α-CDP and AXI/β-CDP formulations the morphology of the original AXI and CDPs disappeared and it was not possible to differentiate the two. The change in surface morphology is indicative of a new solid-state (most likely amorphous), which may be due to the encapsulation of AXI within α-CDP and β-CDP [46,47]. Whereas, the physical mixture clearly displays the structure of both AXI and the CDPs.

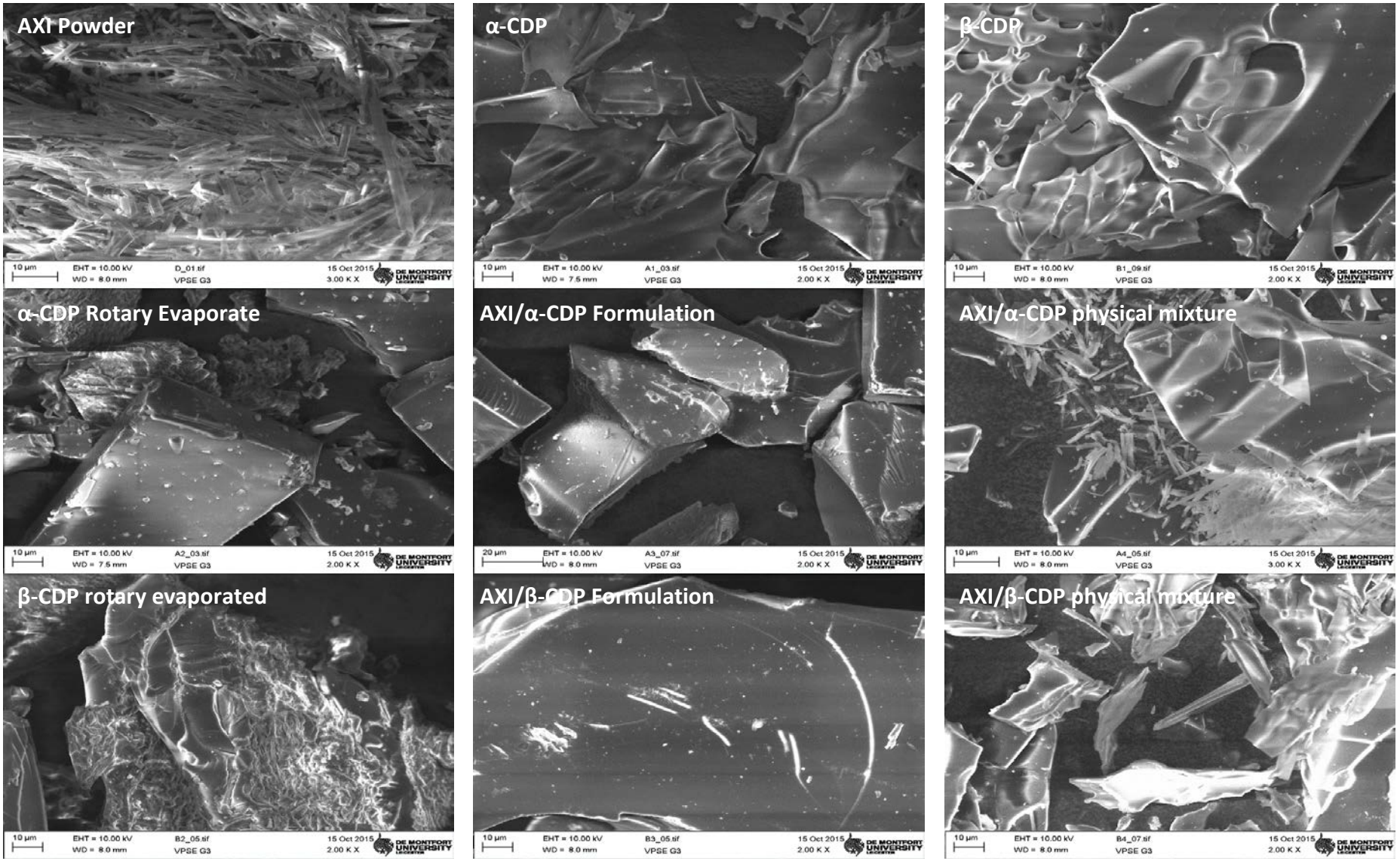

Fig 10.6: Scanning electron microphotographs

10.3. FORMULATIONS FOR DBZ AND SUT

The usefulness and requirement of liquid formulations of drugs cannot be denied. Yet, no liquid formulation of sunitinib malate is commercially available and no stable liquid formulation of DBZ exist.

DBZ is administered by intravenous bolus injection or by short term intravenous infusion due to poor oral bioavailability [48]. The use of an opaque infusion set suggested by Shükla & Koriech [49,50] and Baird & Willoughby [51] shows to be effective but are simply inconvenient due to the inability to see and follow the infusion. On the other hand, the light filtering administration set developed by Kirk [52] enables the user to see and follow the infusion clearly and protect DBZ from photodegradation; thus preventing the formation of the vascular pain causing agent.

To the best of our knowledge, only Islam and Asker [53] attempted to photoprotect DBZ solutions with the use of excipients. Even though the method was found to be effective, it is not commercially employed due to the fact that glutathione inhibits DBZ-induced cell apoptosis [54]. Thus, a suitable photoprotective excipient is still yet to be discovered.

In this study, a photostable liquid formulation for DBZ has been found (Fig 10.7). Besides 1 mg/mL DBZ, the formulation contains Sunset Yellow (0.02 mg/mL, SSY) and Tartrazine (100 mg/mL, TRZ) and Odansetron (2 mg/mL, OHCl). SSY and TRZ are azo-dye commonly used in food and pharmaceuticals which are both deemed safe for injections by European Food Safety Authority [55,56], while OHCl is a drug co-administered with DBZ to prevent nausea and vomiting. This formulation was shown to provide a 10 times increase in photostability (Table 10.3), making the solution practically photostable when irradiated monochromatically for more than an hour at its maximum peak (330 nm).

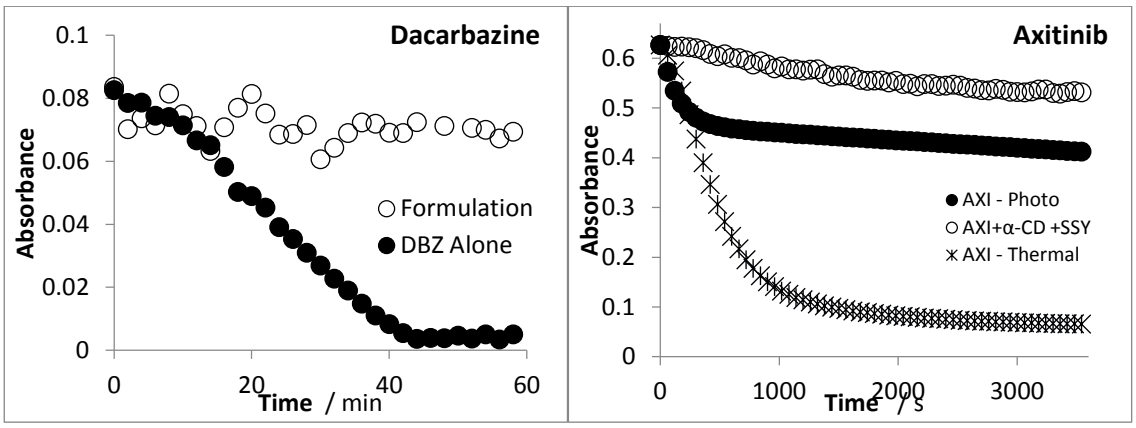

Fig 10.7: (Left) Changes in absorbance observed for 1 mg/mL DBZ alone and in liquid formulation containing Sunset Yellow (0.02 mg/mL) and Tartrazine (100 mg/mL) and Odansetron (2 mg/mL), when monochromatically irradiated at 330 nm (4.69 x 10^{-6} einstein s^{-1} dm^{-3}) (Right) Effect of a combination of α-Cyclodextrin monomer (25 mg/mL), Sunset Yellow (0.16 mg/mL) on the degradation of AXI (0.008 mg/mL) observed at 332 nm, when kept in the dark at 22°C and monochromatically irradiated at 360 nm (3.08 x 10^{-6} einstein s^{-1} dm^{-3})

This DBZ formulation will enable standard infusion sets to be used without the need to photoprotect the content. It should be noted that this is the first time DBZ is shown to be completely photostabilized through the use of pharmaceutical excipients.

As shown in the previous chapter, TRZ is serves as a good competitive light absorber for SUT. In liquid form TRZ's Maximum Permit Level (MPL) is 100 mg/mL [56]. The amount of TRZ permitted for 1.88 x 10^{-4} M SUT (0.1 mg/mL) was then calculated based on the person taking a single dose of 50 mg. This was determined to be 0.2 mg/mL.

This was then subjected to polychromatic irradiation and monitored by HPLC. The results found showed at high drug concentrations a decrease in photodegradation rate is observed, as with the other drugs. Addition of TRZ to solutions of SUT hindered the formation of its photoproduct, this is shown by the lack of peak found for the photoproduct.

Table 10.3: Initial velocities of DBZ, AXI and SUT degradation in different media

Sample	$P_{\lambda_{irr}}$ x 10^{-6} einstien^{-1} s^{-1} dm^{-3}	Condition	Initial Velocity s^{-1} , x 10^{-4}
Dacarbazine (λ_{irr} = 330 nm, 22°C)			
DBZ (0.001 mg/mL)	1.96	Light	6.55
DBZ + SSY (0.078 mg/mL)	2.03	Light	1.45
DBZ + TRZ (0.18 mg/mL)	2.03	Light	2.90
DBZ + OHCl (0.18 mg/mL)	1.05	Light	1.29
DBZ (1 mg/mL)	4.69	Light	10.03
DBZ (1 mg/mL) + SSY (0.02 mg/mL) + TRZ (100 mg/mL) + OHCl (2 mg/mL)	4.69	Light	1.04
Axitinb (λ_{irr} = 360 nm, 22°C)			
AXI (0.008 mg/mL)	0.00	Dark	1.76
AXI (0.008 mg/mL)	3.05	Light	7.23
AXI + SSY (0.16 mg/mL)	3.06	Light	5.55
AXI + α-CD (25.5 mg/mL)	3.07	Light	5.20
AXI + α-CD (27.4 mg/mL)+SSY (0.16 mg/mL)	3.04	Light	0.26
Sunitnib (λ_{irr} = 430 nm, 22°C)			
SUT (0.01 mg/mL)	0.00	Dark	3.00
SUT (0.01 mg/mL)	5.67	Light	2.40
SUT + TRZ (0.02 mg/mL)	5.67	Light	0.13
SUT (0.1 mg/mL)	-[a]	Light	2.0
SUT + TRZ (0.2 mg/mL)	-	Light	1.0

[a] Polychromatic ambient light was used

Current practice for patients requiring liquid doses of SUT is to use a mortar and pestle to mix the contents of SUT capsules with a 1:1 mixture of ORA-PLUS®:ORA-SWEET® and store in an amber plastic bottle [57].

This new SUT oral liquid formulation containing TRZ offers a quicker and simpler preparation method for busy clinical environments. Since, both TRZ and SUT come as powders, the formulation can simply be reconstituted by the addition of water when required. However, the solution must be administered immediately or be kept refrigerated.

10.4. COSTS

The current Inlyta formulation is very costly to purchase at approximately £62.80 a tablet (containing 5 mg AXI) [59]. While the money used to develop this formulation throughout the project approximates the cost of one dose to be less than £30 (Table 10.4). Table 10.4 shows the approximate price of one dose of 5 mg based on the pricing of each component used in the formulation.

To produce one 5 mg dose of the AXI/α-CDP and AXI/β-CDP formulation it costs only ~£11.14 and ~£27.17, respectively. The vast difference in price of the new AXI formulation using α-CDP and β-CDP will make AXI more readily available as costs are lower for the manufacturer, NHS and patient.

As for SUT, the price for a pack of 50 mg capsules (30 capsules per pack) is £3363.00 (excluding VAT) [58]. That is £112.10 per capsule. Whereas, 50 mg of SUT costs £79 from SelleckChem and 100 mg tartrazine costs £0.02, brings the single dose of SUT down to just £79.02.

Table 10.4: Cost of materials used to develop AXI/α-CDP and AXI/β-CDP formulation

Material	Supplier	Cost[a] (£)	Quantity Purchased (mg)	Units	Cost /unit (£)	Quantity Required /dose	Units	Quantity Cost per dose (£)
AXI	Selleckchem	83.00	50	mg	1.66	5	mg	8.30
α-CDP	CycloLab	94.6	10000	mg	0.01	300	mg	2.84
β-CDP	Sigma Aldrich	122.50	5000	mg	0.02	770	mg	18.87
Ethanol	Sigma Aldrich	38.90	500	mL	0.08	-[b]	-	-
Purified Water	Amount not specified. During complex formation, the purified water and ethanol are evaporated.							
Total cost per dose (£)			**AXI-β-CDP**		27.17			
			AXI/α-CDP		11.14			

[a] Includes cost of compound and shipping

[b] not applicable

10.5. CONCLUSION

The prime objective of this study was to develop aqueous formulation for our three drugs (DBZ, AXI and SUT) that present improved thermal and/or photochemical stabilities compared to their solution ones (i.e. in ethanol, water or ethanol/water as discussed in chapters 5 and 6).

For the case of AXI, there was an extra challenge to achieve a liquid formulation as this molecule is naturally very poorly soluble in water.

The results obtained in chapter 8 demonstrates that AXI was complexed with CD monomers and polymers at low concentration (2×10^{-5} M). The test of such complexation at high AXI concentration in this chapter proved its solubility in water could be improved by 2500-times in the presence of β-CDP and 5000-times with α-CDP. It meant that now the concentration of AXI could get to 5 mg/mL in 10 mg/mL in water; which represents the dosage of the drug in Inlyta®

tablets. Such high concentration cannot be achieved by the CD monomers due to their own relatively low solubility limits in water, compared to the polymers.

One of the primary consequence of AXI/CDP complex, in addition to increasing AXI's solubility in water, was the total disappearance of the significant thermal degradation of this molecule, observed earlier in ethanol/water (v/v, 2.5/97.5) solutions, as been proven for low AXI concentration in chapter 6. This might suggest that the results obtained at low drug concentration could well be representative of what occurs at high drug concentration. This point is true for AXI, but this needs to be supported by more experimental evidence as the literature lacks a discussion about this issue. Its importance comes from the fact that the studies performed at low concentration of the drug are less time consuming and cheaper than those leading to the optimization/definition of the solubility limit of AXI/CDP complex.

The improvement of SUT thermal stability in water was suggested here to be obtained by leaving SUT solution in the fridge at ~4-6°C. DBZ is naturally thermally stable at room temperature in water. The photostability of their formulation was proven to considerably improve by using the same strategy that involves light absorption competitors represented by selected excipients (chapter 9).

1.6. REFERENCES

1. Haywood A. and Glass B.D. (2013) Liquid Dosage Forms Extemporaneously Prepared from Commercially Available Products – Considering New Evidence on Stability, *Journal of Pharmacy and Pharmaceutical Sciences*, 16(3):441-455
2. Allen L.V. Jr., Popovich N.G. and Ansel H.C. (2014) Dosage Form Design: Pharmaceutic and Formulation Considerations, In: Ansel's pharmaceutical dosage forms and drug delivery systems, USA: Wolters Kluwer Health/Lippincott Williams & Wilkins
3. Allen L.V. Jr. (2008) Dosage form design and development, Clinical Theurapeutics, 30(11):2102-2111
4. Bhalekar M.R., Harinarayana D., Madgulkar A., Pandya S.J. and Jain D.K. (2008) Improvement of Photostability in Formulation: A Review, Asian Journal of Chemistry, 20(7):5095-5108

5. Aatmani M.E., Poujol S., Astre C., Malosse F. and Pinguet F. (2002) Stability of Dacarbazine in Amber Glass Vials and Polyvinyl Chloride Bags, *American Society of Health-System Pharmacists*, 59:1351-1356.

6. Borst D.L., Arruda L.S., MacLean E., Pithavala Y.K. and Morgado J.E. (2014) Common questions regarding clinical use of axitinib in advanced renal cell carcinoma, American Journal of Health-System Pharmacy, 71:1092-1096

7. Navid F., Christensen R., Minkin P., Stewart C.F., Furman W.L., Baker S. (2008) Stability of sunitinib in oral suspension, *The Annals of Pharmacotherapy*, 2(7):962-6

8. Patel V.P., Desai T.R., Chavda B.G. and Katira R.M. (2011) Extemporaneous Dosage Form for Oral Liqiuds, *Pharmacophere*, 2(2):86-103

9. Lowey A. and Jackson M. (2008) How to ensure the quality and safety of unlicensed oral medicines. The Pharmaceutical Journal 281:240.

10. Donovan G., Parkin L. and Wilkes S. (2015) Special unlicensed medicines: what we do and do not know about them, *British Journal of General Practice*, 65(641):e861-e863

11. Sousa e Silva J.P. (2013) Pharmaceutical Formulation, *Pharmaceutica Analytica Acta*, 4(1):145

12. World Health Organisation (2001) Guidelines for the formulation, implementation, monitoring and evaluation of national drug policies [Online] Available at: http://apps.who.int/medicinedocs/en/m/abstract/Js16220e/ [Acessed 30/01/2016]

13. Pavliv L. and Cahill J.F. (2007) Formulation and Manufacturing, In: Drug and Biological Development: From Molecule to Product and Beyond, Evens R. (*ed.*), New York: Springer Science + Business Media, LLC

14. Gad S.C. (2008) Pharmaceutical Manufacturing Handbook: Production and Processes, New Jersey: John Wiley & Sons, Inc.

15. Niazi S.K. (2009) Handbook of Pharmaceutical Manufacturing Formulations: Liquid Products, Vol. 3, 2nd Edition, New York: Informa Healthcare, Inc.

16. Rasool Hassan B.A. (2012) Overview on Pharmaceutical Formulation and Drug Design, *Pharmaceutica Analytica Acta*, 3:10

17. Trotta F., Dianzani C., Caldera F., Mognetti B. and Cavalli R. (2014) The application of nanosponges to cancer drug delivery, *Expert Opinion*, 11(6):931-941

18. Rita L., Amit T. and Chandrashekhar G. (2011) Current Trends in β-Cyclodextrin Based Drug Delivery Systems, *International Journal of Research in Ayurveda and Pharmacy*, 295):1520-1526

19. Malaekeh-Nikouei B., Nassirli H., Davies N.M. (2007) Enhancement of cyclosporine aqueous solubility using alpha- and hydroxypropyl beta-cyclodextrin mixtures, *Journal of Inclusion Phenomena and Macrocyclic Chemistry*, 59(3)245-250.

20. Swaminathan S., Pastero L., Serpe L., Trotta F., Vavia P., Aquilano D., Trotta M., Zara G. and Cavalli R. (2010) Cyclodextrin-based nanosponges encapsulating camptothecin: Physicochemical characterization, stability and cytotoxicity, *European Journal of Pharmaceutics and Biopharmaceutics*, 74:193–201

21. Pokharkar V., Khanna A., Venkatpurwar V., Dhar S. and Mandpe L. (2009) Ternary complexation of carvedilol, β-cyclodextrin and citric acid for mouth-dissolving tablet formulation, *Acta Pharmaceutica,* 59(2):121–132.

22. Wang J., Zhengyu Jin Z. and Xu X. (2014) Gamma-cyclodextrin on enhancement of water solubility and store stability of nystatin*, Journal of Inclusion Phenomena and Macrocyclic Chemistry*, 78(1):145-150.

23. Jarho P., Pate D.W., Brenneisen R. and Järvinen T. (1998) Hydroxypropyl-beta-cyclodextrin and its combination with hydroxypropyl-methylcellulose increases aqueous solubility of delta9-tetrahydrocannabinol, *Life Sciences*, 63(26):381-384.

24. Brewster M.E., Estes K.S., Loftsson T., Perchalski R., Derendorf H., Mullersman G. and Bodor N. (1988) Improved delivery through biological membranes. XXXL: Solubilization and stabilization of an estradiol chemical delivery system by modified beta-cyclodextrins, *Journal of Pharmaceutical Sciences*, 77(11):981-985.

25. Cutrignelli A., Lopedota A., Denora N., Iacobazzi R.M., Fanizza E., Laquintana V., Perrone M., Maggi V. and Franco M. (2014) A New Complex of Curcumin with Sulfobutylether-β-Cyclodextrin: Characterization Studies and In Vitro Evaluation of Cytotoxic and Antioxidant Activity on HepG-2 Cells, *Journal of Pharmaceutical Sciences*, 103(12):3932–3940

26. Dora C.P., Trotta F., Kushwah V., Devasari N., Singh C., Suresh S. and Jain S. (2016) Potential of Erlotinib Cyclodextrin Nanosponge Complex to Enhance Solubility, Dissolution Rate, *In Vitro* Cytotoxicity and Oral Bioavailability, Carbohydrate Polymers, 137:339-349

27. Tejashri G., Amrita B. and Darshana J. (2013) Cyclodextrin based nanosponges for pharmaceutical use: a review, Acta Pharmactica, 63(3):335-358

28. Gidwani B. and Vyas A. (2015) A Comprehensive Review on Cyclodextrin-Based Carriers for Delivery of Chemotherapeutic Cytotoxic Anticancer Drugs, *BioMed Research International*, 2015:1-15

29. Trotta F., Zanetti M. and Cavalli R. (2012) Cyclodextrin-based nanosponges as drug carriers, *Beilstein Journal of Organic Chemistry*,8:2091-2099

30. Bolmal U.B., Manvi F.V., Rajkumar K., Palla S.S., Paladugu A. and Reddy K.R. (2013) Recent Advances in Nanosponges as Drug Delivery System, *International Journal of Pharmaceutical Sciences and Nanotechnology*, 6(1):1934-1944

31. Chen Y., Tortorici M.A., Garrett M., Hee B., Klamerus K.J. and Pithavala Y.K. (2013) Clinical Pharmacology of Axitinib, *Clinical Pharmacokinetics*, 52:713-725

32. Food and Drug Administration (2012) Inlyta: Patient Information Leaflet [Online] Available at: http://www.accessdata.fda.gov/drugsatfda_docs/label/2012/202324lbl.pdf [Accessed 08/03/2016]

33. European Medicines Agency (2012) "Committee for Medicinal Products for Human Use Assessment report EMA/CHMP/453325/2012 Inlyta." [Online] Available at: http://www.ema.europa.eu/docs/en_GB/document_library/EPAR_-_Public_assessment_report/human/002406/WC500132190.pdf [Accessed 04/03/2016]

34. Sohi, H., Sultana, Y. and Khar, R. (2004). Taste Masking Technologies in Oral Pharmaceuticals: Recent Developments and Approaches. *Drug Development and Industrial Pharmacy*, 30(5):429-448.

35. Pritchyk, K., Schiff, B., Newkirk, K., Krowiak, E. and Deeb, Z. (2002). Metastatic Renal Cell Carcinoma to the Head and Neck. *The Laryngoscope*, 112(9):1598-1601.

36. Jayasooriya, P., Gunarathna, I., Attygalla, A. and Tilakaratne, W. (2004). Metastatic renal cell carcinoma presenting as a clear cell tumour in the head and neck region. *Oral Oncology Extra*, 40(3):50-53.

37. Katdare, A. and Chaubal, M. (2006). Excipient development for pharmaceutical, biotechnology, and drug delivery systems. New York: Informa Healthcare, pp.155-159.

38. Griffin J. and O'Grady J. (2009) The textbook of pharmaceutical medicine. 6th ed. Oxford: Blackwell Publishing Ltd.

39. Semple K., Doick K., Jones K., Burauel P., Craven A. and Harms H. (2004) Peer Reviewed: Defining Bioavailability and Bioaccessibility of Contaminated Soil and Sediment is Complicated. Environmental Science & Technology, [online] 38(12):228A-231A. Available at: http://pubs.acs.org/doi/pdf/10.1021/es040548w [Accessed 20/03/2015]

40. Howland R., Mycek M., Harvey R. and Champe P. (2006). *Pharmacology*. Philadelphia: Lippincott Williams & Wilkins

41. FDA (2004) GRAS Notice 000155: alpha -Cyclodextrin. 1st ed. [ebook] FDA, pp.1-24. Available at: http://www.fda.gov/ucm/groups/fdagov-public/@fdagov-foods-gen/documents/document/ucm268159.pdf [Accessed 13/03/2015]

42. Van der Manakker F., Vermonden T., Van Nostrum C.F. and Hernik W.E. (2009) Cyclodextrin-Based Polymeric Materials: Synthesis, Properties, and Pharmaceutical/Biomedical Applications, *Biomacromolecules*, 10(12):3157–3175

43. Bilensoy E. (ed.) (2011) Cyclodextrins in Pharmaceutics, Cosmetics, and Biomedicine: Current and Future Industrial Applications, New Jersey: John Wiley & Sons

44. Dora P.C., Trotta F., Kushwah V., Devasari N., Singh C., Suresh S. and Jain S. (2016) Potential of erlotinib cyclodextrin nanosponge complex to enhance solubility, dissolution rate, in vitro cytotoxicity and oral bioavailability, *Carbohydrate Polyme*rs, 137:339–349

45. Ansari K.A., Vavia P.R., Trotta F. and Cavalli R. (2011) Cyclodextrin-based nanosponges for delivery of resveratrol: in vitro characterisation, stability, cytotoxicity and permeation study, *AAPS PharmSciTech*, 12(1):279-286

46. Sinha V.R., Anitha R., Ghosh S., Nanda A. and Kumria R. (2005) Complexation of celecoxib with β-cyclodextrin: Characterization of the interaction in solution and in solid state, *Journal of Pharmaceutical Sciences*, 94(3):676-687

47. Yadav V.R., Suresh S., Devi K. and Yadav S. (2009) Effect of Cyclodextrin Complexation of Curcumin on its Solubility and Antiangiogenic and Anti-inflammatory Activity in Rat Colitis Model, *AAPS PharmSciTech*, 10(3):752-762

48. Oncologic Emergencies

49. Shükla V.S. (1980) A Device to Prevent Photodegradation of Dacarbazine (DTIC), *Clinical Radiology*, 31:239-240.

50. Shükla V.S. and Koriech O.M. (1981) Dacarbazine (DTIC) in Malignant Melanoma: Reduced Toxicity with Protection From Light, *Clinical Radiology*, 32:53-55

51. Baird G.M. and Willoughby M.L.N. (1978) Photodegradation of Dacarbazine, *The Lancet*, 2:681.

52. Kirk B. (1987) The Evaluation of a Light-Protective Giving Set: The Photosensitivity of Intravenous Dacarbazine Solutions, *Intensive Therapy and Clinical Monitoring*, 8:78-86.

53. Islam M.S. and Asker A.F. (1994) Photostabilization of Dacarabzine with Reduced Glutathione, *Parenteral Drug Association Journal of Pharmaceutical Science and Technology*, 48:38-40.

54. Abdalla M.Y. (2011) Glutathione as Potential Target for Cancer Therapy; More or Less is Good?, *Jordan Journal of Biological Sciences*, 4(3):119-124

55. European Food Safety Authority (2009) Scientific Opinion on the re-evaluation of Sunset Yellow FCF (E 110) as a food additive, EFSA Journal, 7(11):1330

56. European Food Safety Authority (2009) Scientific Opinion on the re-evaluation Tartrazine (E102), EFSA Journal, 7(11):1331

57. Navid F., Christensen R., Minkin P., Stewart C.F., Furman W.L., Baker S. (2008) Stability of sunitinib in oral suspension, *The Annals of Pharmacotherapy*, 2(7):962-6

58. NICE (2009) Sunitinib for the first-line treatment of advanced and/or metastatic renal cell carcinoma [online] Available at: https://www.nice.org.uk/guidance/ta169/chapter/3-the-technology [Accessed 30/07/2015]

59. Light D. and Kantarjian H. (2013) Market spiral pricing of cancer drugs, *Cancer*, 119(22):3900-3902.

CHAPTER ELEVEN

CONCLUSION

11.1. CONCLUSION

Photodecomposition of unstable drug formulations could lead to undesirable side effects. A loss of potency of the drug and the development of adverse effects may be due to the formation of photoproducts during storage or administration. Therefore, photostability testing of drug substances is important for the evaluation of the overall photosensitivity of the material for development. Hence, the photostability of drug substances has developed into an important area of research, especially as increasing number of drugs are considered photolabile.

The ICH made provision of photostability data for all new drug licence applications compulsory. A guideline was established to regulate photostability test conclusions from different laboratory but it lacked protocols for the treatment and analysis of kinetic data of drug photodegradation. Often photokinetic data of drugs are treated using thermal zero-, first- and/or second-order thermal kinetic models. They were used irrespective of the photochemical mechanism governing the drug and its photoproducts, and the fact that the equations were originally developed for pure thermal reactions. So, in many cases, only part of the kinetic data of the photodegradation trace was used. In addition, poor fittings and data equally well fitting more than one reaction-order model were achieved.

The photokinetic traces of DBZ, AXI and SUT were all well described by the newly proposed Φ-order model for unimolecular and photoreversible reactions obeying an AB mechanism, even when subjected to non-isosbestic irradiation. These and previous results presented by our team strongly suggests that photodegradation of drugs are better described by Φ-order than the classic thermal reaction orders.

The application of Φ-order here to determine the quantum yields (the only physical parameter capable of indicating the photoreactivity of a drug) and develop drug-actinometers are not only straightforward to implement, but they also allow the generation of reliable and quantitative data on the photodegradation reaction.

Drug actinometers developed using Φ-order kinetic equations here can be used without prior knowledge of the reaction attributes, such as quantum yields. The proposed procedure and actinometers should work well for monochromatic irradiations. But, it is not advised to be used for polychromatic light as quantum yield values are shown in this study to be wavelength dependant and so are their $\beta_{\lambda_{irr}}$ factors. Therefore, the average quantum yield values obtained using polychromatic irradiations, as reported on by many studies in the pharmaceutical literature, must be considered with caution. However, Φ-order was also shown to be applicable to data obtained by polychromatic irradiation – even those of complex drug mechanism.

Analysis of complex degradation mechanisms can be circumvented by the use of mathematical software procedures. However, current methods do not provide a unique answer and require chromatographic data to determine the component spectral profiles and concentrations. More importantly, these models are based on the thermal differential equations - which are completely different to that of photokinetic.

Thus, the successful application of the new Runge-Kutta numerical treatment proposed here for analysis of spectrokinetic data of complex drug photoreaction is the first of its kind. It helped elucidate complex drug mechanisms (number of species and occurrence of thermal and photochemical steps). It enabled the determination of the quantum yields and absorption coefficients, not only of the mother compound but of all photoactive degradation products, in addition to showing the evolution of the species respective concentrations during reaction

time. Such a performance cannot be expected from chromatography techniques, especially when thermally unstable products are concerned.

Until now, stable liquid dosage forms of DBZ, AXI and SUT do not exist in water. For the case of AXI, there was an extra challenge to achieve a liquid formulation as this molecule is naturally very poorly soluble in water.

Our results demonstrate that formation of AXI/CDP complexes significantly increased its solubility in water by up to 5000-times. It meant that now the concentration of AXI could get up to 5-10 mg/mL in water, which represents the dosage of the drug in Inlyta® tablets. Such high concentrations cannot be achieved by the CD monomers due to their own relatively low solubility limits in water, compared to the polymers.

In addition to increasing AXI's solubility in water, formulation of AXI with CDP yield a total disappearance of the significant thermal degradation of this molecule observed earlier in ethanol/water (v/v, 2.5/97.5) solutions.

The improvement of SUT thermal stability in water was suggested here to be obtained by leaving SUT solution in the fridge at ~4-6°C. DBZ is naturally thermally stable at room temperature in water. The photostability of their formulations were proven to considerably improve by using the same strategy that involves light absorption competitors represented by selected excipients (chapter 8).

In drug development, knowledge of the complexation efficiency is useful. However, even with increased interest in CDP due to advances in nanotechnology, only few studies have reported on the fluorimeteric characterisation of nanosponge-drug complexes.

The new mathematical framework proposed in this study for characterisation of such complexes enabled a reliable determination of the true complex stoichiometry without imposing preselected values (i.e. 1:1, 1:2, etc) – as with current methods.

In addition to not requiring the precise knowledge of the relative molar mass, the method gives information on both stoichiometry and association constant of the complex.

Some of the problems often encountered in photostability testing and liquid formulation development had been addressed here in this study. The successful application of the methods proposed to the model anti-cancer drugs has set out new approaches that might be found useful for future treatments of photodegradation data, development of drug-actinometers and liquid formulations of drugs.

APPENDIX 5

A5.1. Φ-Order Kinetic Model for non-isosbestic irradiations

The model equation describing Φ-order kinetics for the photoreversible degradation of initial compound (A) to photoproduct (B) species is:

$$A_{tot}^{\lambda_{irr}/\lambda_{obs}}(t) = A_{tot}^{\lambda_{irr}/\lambda_{obs}}(\infty) + \frac{A_{tot}^{\lambda_{irr}/\lambda_{obs}}(0) - A_{tot}^{\lambda_{irr}/\lambda_{obs}}(\infty)}{A_{tot}^{\lambda_{irr}/\lambda_{irr}}(0) - A_{tot}^{\lambda_{irr}/\lambda_{irr}}(\infty)} \times \frac{l_{\lambda_{obs}}}{l_{\lambda_{irr}}} \times Log\left[1 + \left(10^{\left[\left(A_{tot}^{\lambda_{irr}/\lambda_{irr}}(0) - A_{tot}^{\lambda_{irr}/\lambda_{irr}}(\infty)\right) \times \frac{l_{\lambda_{irr}}}{l_{\lambda_{obs}}}\right]} - 1\right) \times e^{-k_{A \leftrightharpoons B}^{\lambda_{irr}} \times t}\right] \quad \text{Eq.1}$$

where $A_{tot}^{\lambda_{irr}/\lambda_{obs}}(t)$, $A_{tot}^{\lambda_{irr}/\lambda_{obs}}(0)$, $A_{tot}^{\lambda_{irr}/\lambda_{obs}}(\infty)$, $A_{tot}^{\lambda_{irr}/\lambda_{irr}}(0)$ and $A_{tot}^{\lambda_{irr}/\lambda_{irr}}(\infty)$ are the total absorbance of the reaction medium at reaction time (t), at the start of the reaction (t = 0) and at infinity (∞), when irradiated at a certain wavelength and observed at the same wavelength ($\lambda_{irr}/\lambda_{irr}$) or irradiated and observed at different wavelengths ($\lambda_{irr}/\lambda_{obs}$).

The rate constant $k_{A \leftrightharpoons B}^{\lambda_{irr}}$ of the photoreaction is given by:

$$k_{A \leftrightharpoons B}^{\lambda_{irr}} = \left(\Phi_{A \to B}^{\lambda_{irr}} \times \varepsilon_A^{\lambda_{irr}} + \Phi_{B \to A}^{\lambda_{irr}} \times \varepsilon_B^{\lambda_{irr}}\right) \times l_{\lambda_{irr}} \times P_{\lambda_{irr}} \times F_{\lambda_{irr}}(\infty) = \beta_{\lambda_{irr}} \times P_{\lambda_{irr}} \quad \text{Eq.2}$$

where $\Phi_{A \to B}^{\lambda_{irr}}$ and $\Phi_{B \to A}^{\lambda_{irr}}$ are the forward and reverse quantum yields at the irradiation wavelength (λ_{irr}), $\varepsilon_A^{\lambda_{irr}}$ and $\varepsilon_B^{\lambda_{irr}}$ the extinction coefficients of A and B, $P_{\lambda_{irr}}$ the light intensity received, $l_{\lambda_{irr}}$ the path length of the irradiation light and $F_{\lambda_{irr}}(\infty)$ the photokinetic factor expressed as:

$$F_{\lambda_{irr}}(\infty) = \frac{1 - 10^{-\left(A_{tot}^{\lambda_{irr}/\lambda_{irr}}(\infty) \times \frac{l_{\lambda_{irr}}}{l_{\lambda_{obs}}}\right)}}{A_{tot}^{\lambda_{irr}/\lambda_{irr}}(\infty) \times \frac{l_{\lambda_{irr}}}{l_{\lambda_{obs}}}} \quad \text{Eq.3}$$

It is possible to use Eq.1 to describe the kinetic behaviour of any AB photoreaction at any observation/irradiation conditions. Thus, for an AB(2Φ) system where both species absorb at the irradiation wavelength , the absorbance at infinity will be represented by the photostationary state (pss). As a result, $A_{tot}^{\lambda_{irr}/\lambda_{obs}}(\infty)$ and $F_{\lambda_{irr}}(\infty)$ becomes $A_{tot}^{\lambda_{irr}/\lambda_{obs}}(pss)$ and $F_{\lambda_{irr}}(pss)$. For an unimolecular AB(1Φ) system where only the A absorbs at the irradiation wavelength, $A_{tot}^{\lambda_{irr}/\lambda_{obs}}(\infty)$, $\Phi_{B\to A}^{\lambda_{irr}}$ and $\varepsilon_B^{\lambda_{irr}}$ = 0 and $F_{\lambda_{irr}}(\infty)$ = ln(10) = 2.3. This returns Eq.1 to the model equations obtained through closed-form integration for this AB(1Φ) system [1].

The $\beta_{\lambda_{irr}}$ in Eq.2 is a proportionality factor between the overall rate-constant and the radiant power.

A5.2. Equations for isosbestic irradiations

The equation expressing the time-based variation of the total absorbance observed for monochromatic irradiation at an isosbestic point ($\lambda_{irr} = \lambda_{isos}$) can be obtained by closed-form integration [1] as

$$A_{tot}^{\lambda_{isos}/\lambda_{obs}}(t) = A_{tot}^{\lambda_{isos}/\lambda_{obs}}(pss) + \left(A_{tot}^{\lambda_{isos}/\lambda_{obs}}(0) - A_{tot}^{\lambda_{isos}/\lambda_{obs}}(pss)\right) e^{-k_{A\leftrightharpoons B}^{\lambda_{isos}}\times t} \qquad \text{Eq.4}$$

where $k_{A\leftrightharpoons B}^{\lambda_{isos}}$ can be worked out from Eq. 2 with the time-dependent photokinetic factor as $F_{\lambda_{isos}}$ instead of $F_{\lambda_{irr}}(pss)$ and $F_{\lambda_{isos}}$ calculated using Eq. 3 with the absorbance measured at λ_{isos} , so replacing $A_{tot}^{\lambda_{irr}/\lambda_{irr}}(pss)$ with $A_{tot}^{\lambda_{isos}/\lambda_{isos}}$.

A5.3. Photokinetic Elucidation Method

By fitting experimental data with the Φ-order kinetic equations for non-isosbestic and isosbestic irradiation above, the rate-constant of the reaction can be determined.

For an AB(1Φ) system, a simple rearrangement of eq.2 (into eq. 5) enables $\Phi_{A\to B}^{\lambda_{irr}}$ to be calculated:

$$\Phi_{A\to B}^{\lambda_{irr}} = \frac{k_{A\to B}^{\lambda_{irr}}}{\varepsilon_A^{\lambda_{irr}} \times l_{\lambda_{irr}} \times P_{\lambda_{irr}} \times F_{\lambda_{irr}}(\infty)} \qquad \text{Eq.5}$$

For an AB(2Φ) reaction, determination of the rate-constant of the reaction alone is not sufficient to work out the unknown parameters of the reactions, i.e. the forward quantum yield ($\Phi_{A\to B}^{\lambda_{irr}}$), the reverse quantum yield ($\Phi_{B\to A}^{\lambda_{irr}}$) and the absorption coefficient of the photoproduct ($\varepsilon_B^{\lambda_{irr}}$) at the irradiation wavelength.

For an AB(2Φ) reaction, the original compound (A) and its product (B) reach equilibrium, and so the final absorption spectrum recorded is in fact that of both A and B. Thus, determination of $\varepsilon_B^{\lambda_{irr}}$ is not possible with just spectrographic data. Without knowing the concentration of species B at pss, $\Phi_{A\to B}^{\lambda_{irr}}$ and $\Phi_{B\to A}^{\lambda_{irr}}$ cannot be calculated. As a result, further information is required to determine the values of these three unknown parameters.

This problem can be solved in three steps: (i) determine the reaction quantum yields at isosbestic irradiation; (ii) reconstruct the whole spectrum of the photoproduct (PP); and (iii) determine the reaction quantum yields for any non-isosbestic irradiation.

Firstly, the photodegradation reaction is subject to a monochromatic irradiation at the isosbestic point where $\varepsilon_A^{\lambda_{isos}} = \varepsilon_B^{\lambda_{isos}}$. Hence, reducing the number of unknowns to two ($\Phi_{A\to B}^{\lambda_{isos}}$ and $\Phi_{B\to A}^{\lambda_{isos}}$). Thus, allowing the quantum yields to be determined using Eq. 6 and Eq.7:

$$\Phi_{A\to B}^{\lambda_{isos}} = \frac{k_{A\to B}^{\lambda_{isos}}}{\varepsilon_A^{\lambda_{isos}} \times l_{\lambda_{isos}} \times P_{\lambda_{isos}} \times F_{\lambda_{isos}}} \times \frac{(C_A(0) - C_A(pss))}{C_A(0)} \quad \text{Eq.6}$$

$$\Phi_{B\to A}^{\lambda_{irr}} = \left(\frac{k_{A\leftrightharpoons B}^{\lambda_{irr}}}{l_{\lambda_{irr}} \times P_{\lambda_{irr}} \times F_{\lambda_{irr}}(pss)} \right) - \Phi_{A\to B}^{\lambda_{irr}} \quad \text{Eq.7}$$

Where $k_{A\leftrightharpoons B}^{\lambda_{isos}}$ can be determined by fitting the concentration profiles (obtained using the HPLC) with Eq.4.

The equilibrium constant ($K_{A\leftrightharpoons B}^{\lambda_{isos}}$, Eq.8) - which expresses the species' concentrations at pss for the isosbestic irradiation as a ratio - can be calculated.

$$K_{A\leftrightharpoons B}^{\lambda_{isos}} = \frac{C_B(pss)}{C_A(pss)} = \frac{\Phi_{A\to B}^{\lambda_{isos}}}{\Phi_{B\to A}^{\lambda_{isos}}} \quad \text{Eq.8}$$

The ratio of the concentrations of species A and B at equilibrium, independent of the wavelength, corresponds with the ratio of the quantum yields at the isosbestic wavelength. It is also important to note that $K_{A\leftrightharpoons B}^{\lambda_{isos}}$ is independent of the concentration of the initial species. This is important as the concentration used for HPLC experiment is often too high for quantitative spectrophotometric measurement of the reaction. Hence, a lower concentration of the initial species can be used for the second elucidation step – reconstruction of the full spectrum of the photoproduct.

Using the value of $K_{A\leftrightarrows B}^{\lambda_{isos}}$, the total absorption spectra of the initial species and that of the reactive medium at pss (from an isosbestic irradiation experiment), the whole spectrum of the photoproduct could therefore be reconstructed:

$$\varepsilon_B^{\lambda_x} = \frac{\left(K_{A\leftrightarrows B}^{\lambda_{isos}}+1\right) \times A_{tot}^{\lambda_{irr}/\lambda_{obs}}(pss) - \varepsilon_A^{\lambda_x} \times C_A(0) \times l_{\lambda_{obs}}}{K_{A\leftrightarrows B}^{\lambda_{isos}} \times C_A(0) \times l_{\lambda_{obs}}} \quad \text{Eq.9}$$

Once the absorption coefficients of the photoproducts are known for all wavelengths, the photochemical quantum yields at any irradiation wavelength can readily be determined, by using eq. 10 and 11.

$$\Phi_{A\to B}^{\lambda_{irr}} = \frac{v_{0(mod.)}^{\lambda_{irr}/\lambda_{obs}}}{\left(\varepsilon_B^{\lambda_{obs}} - \varepsilon_A^{\lambda_{obs}}\right) \times l_{\lambda_{obs}} \times \varepsilon_A^{\lambda_{irr}} \times l_{\lambda_{irr}} \times P_{\lambda_{irr}} \times F_{\lambda_{irr}}(0) \times C_0} \quad \text{Eq.10}$$

$$\Phi_{B\to A}^{\lambda_{irr}} = \left(\frac{k_{A\leftrightarrows B}^{\lambda_{irr}}}{l_{\lambda_{irr}} \times P_{\lambda_{irr}} \times F_{\lambda_{irr}}(pss)}\right) - \Phi_{A\to B}^{\lambda_{irr}} \times \frac{\varepsilon_B^{\lambda_{irr}}}{\varepsilon_A^{\lambda_{irr}}} \quad \text{Eq.11}$$

Where the numerical value of the reaction's initial velocity ($v_{0(mod.)}^{\lambda_{irr}/\lambda_{obs}}$) can be obtained using Eq. 12:

$$v_{0(mod.)}^{\lambda_{irr}/\lambda_{obs}} = \frac{A_{tot}^{\lambda_{irr}/\lambda_{obs}}(0) - A_{tot}^{\lambda_{irr}/\lambda_{obs}}(pss)}{A_{tot}^{\lambda_{irr}/\lambda_{irr}}(0) - A_{tot}^{\lambda_{irr}/\lambda_{irr}}(pss)} \times \frac{k_{A\leftrightarrows B}^{\lambda_{irr}}}{l_{\lambda_{irr}}/l_{\lambda_{obs}} \times \ln(10)} \times \left(10^{\left(A_{tot}^{\lambda_{irr}/\lambda_{irr}}(pss) - A_{tot}^{\lambda_{irr}/\lambda_{irr}}(0)\right) \times \left(l_{\lambda_{irr}}/l_{\lambda_{obs}}\right)} - 1\right) \quad \text{Eq.12}$$

A5.4. Determination of the Reaction Quantum Yields for an Isosbestic Irradiation

Table A5.1: Changes in DBZ, AXI, SUT and their photoproduct's peak area and concentration over the irradiation period determined by HPLC

Time /mins	Concentration / M		Time /mins	Concentration / M		Time /mins	Concentration / M	
	DBZ	**PP**		**t-AXI**	**c-AXI**		***Z*-SUT**	***E*-SUT**
0	1.32×10^{-4}	0	0	8.13×10^{-5}	0	0	7.51×10^{-5}	0
10	8.60×10^{-5}	4.59×10^{-5}	2	6.21×10^{-5}	1.92×10^{-5}	5	6.51×10^{-5}	1.01×10^{-5}
24	5.35×10^{-5}	7.84×10^{-5}	5	5.14×10^{-5}	2.99×10^{-5}	10	6.07×10^{-5}	1.44×10^{-5}
36	1.48×10^{-5}	1.17×10^{-4}	10	3.16×10^{-5}	4.97×10^{-5}	20	5.91×10^{-5}	1.60×10^{-5}
49	0	1.32×10^{-4}	15	2.00×10^{-5}	6.13×10^{-5}	30	5.78×10^{-5}	1.73×10^{-5}
63	0	1.32×10^{-4}	20	1.82×10^{-5}	6.31×10^{-5}	40	5.68×10^{-5}	1.83×10^{-5}
92	0	1.32×10^{-4}	30	1.79×10^{-5}	6.34×10^{-5}	50	5.22×10^{-5}	2.29×10^{-5}
104	0	1.32×10^{-4}	40	1.57×10^{-5}	6.56×10^{-5}	60	5.73×10^{-5}	1.78×10^{-5}
120	0	1.32×10^{-4}	60	1.82×10^{-5}	6.31×10^{-5}	-	-	-

Table A5.2: First-order equations for the three drugs and their products and the rate-constant determined for isosbestic irradiation

	Change in Concentration of A	**Change in Concentration of B**	$k_{A \leftrightarrows B}^{\lambda_{isos}}$ / s^{-1}	**P** / einstein s^{-1} dm^{-3}
DBZ	$C_{DBZ}(t) = \frac{l_{obs}}{l_{irr}} \times \frac{C_{DBZ}(0)}{A_{tot}^{\lambda_{irr}/\lambda_{irr}}(0)} \times \log\left[1 + \left(10^{A_{tot}^{\lambda_{irr}/\lambda_{irr}}(0) \times \frac{l_{irr}}{l_{obs}}} - 1\right)\right] e^{-kt}$	$C_B(t) = C_{DBZ}(t) - C_{DBZ}(0)$	4.72×10^{-3}	1.02×10^{-6}
AXI	$C_{t-AXI}(t) = C_{t-AXI}(\infty) + \left(C_{t-AXI}(0) - C_{t-AXI}(\infty)\right)e^{-kt}$	$C_{C-AXI}(t) = C_{C-AXI}(\infty) + \left(C_{C-AXI}(\infty)\right)e^{-kt}$	2.78×10^{-3}	3.12×10^{-6}
SUT	$C_{Z-SUT}(t) = C_{Z-SUT}(\infty) + \left(C_{Z-SUT}(0) - C_{Z-SUT}(\infty)\right)e^{-kt}$	$C_{E-SUT}(t) = C_{E-SUT}(\infty) + \left(C_{E-SUT}(\infty)\right)e^{-kt}$	2.83×10^{-3}	2.19×10^{-6}

A5.5. REFERENCES

1. Maafi M and Brown R.G. (2007) The kinetic model for AB(1Φ) systems: A closed-form integration for the differential equations with a variable photokinetic factor, *Journal of Photochemistry and Photobiology A: Chemistry*, 187:319-324

APPENDIX 6

A6.1. SUNITINIB'S ABSORPTION SPECTRUM IN WATER

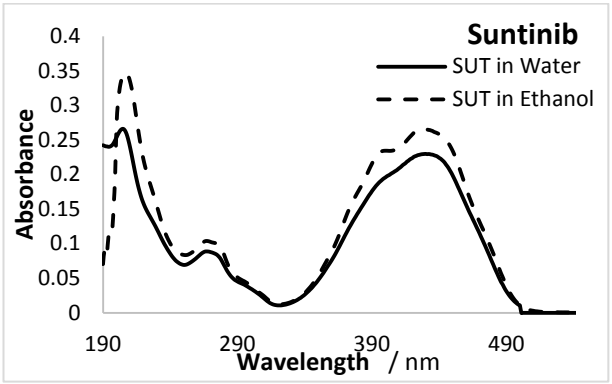

Fig. 6.1: Native absorption spectra of sunitinib in water and ethanol (SUT, 8.97 x 10^{-6} M and 8.94 x 10^{-6} M respectively).

A6.2. DIFFERENTIAL EQUATIONS OF AXI AND SUT

According to Scheme 6.1, the differential equations for AXI's system are:

$$\frac{dC_{A_2}}{dt}(t) = -k^{\Delta}_{A_2 \to C_2} \times C_{A_2} \quad \text{Eq.1}$$

$$\frac{dC_{C_2}}{dt}(t) = -k^{\Delta}_{C_2 \to D_2} \times C_{C_2} + k^{\Delta}_{A_2 \to C_2} \times C_{A_2} \quad \text{Eq.2}$$

$$\frac{dC_{D_2}}{dt}(t) = +k^{\Delta}_{C_2 \to D_2} \times C_{C_2} \quad \text{Eq.3}$$

And the differential equations for SUT are:

$$\frac{dC_{A_3}}{dt}(t) = -k^{\Delta}_{A_3 \to B_3} \times C_{A_3} + k^{\Delta}_{B_3 \to A_3} \times C_{B_3} - k^{\Delta}_{A_3 \to C_3} \times C_{A_3} \quad \text{Eq.4}$$

$$\frac{dC_{C_3}}{dt}(t) = +k^{\Delta}_{A_3 \to C_3} \times C_{A_3} \quad \text{Eq.5}$$

A6.3. SUNITINIB'S PHOTOSTABILITY IN AQUEOUS SOLUTION

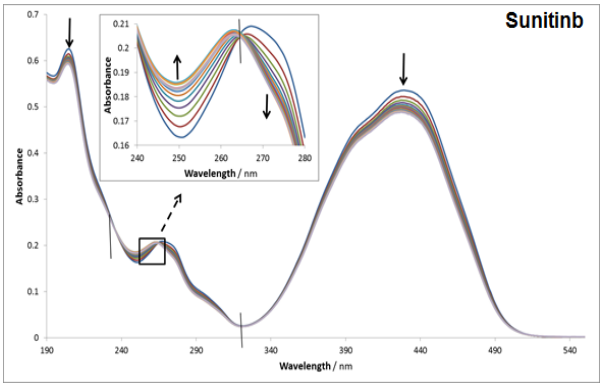

Fig 6.4: Evolution of the electronic absorption spectra of 1.92 x 10^{-5} M SUT in water, when irradiated continuously with a monochromatic beam at 430 nm (4.90 x 10^{-6} einstein s^{-1} dm^{-3}, 22°C)

A6.4. RATE LAWS OF THE SYSTEMS

AXI's were written in accordance to scheme 6.8:

$$\frac{dC_{A_2}}{dt}(t) = -k^{\Delta}_{A_2\to C_2} \times C_{A_2} - k^{\lambda_{irr}}_{A_2\to B_2} \times F_{\lambda_{Irr}}(t) \times C_{A_2} + k^{\lambda_{irr}}_{B_2\to A_2} \times F_{\lambda_{\mathrm{irr}}}(t) \times C_{B_2} + k^{\lambda_{irr}}_{C_2\to A_2} \times F_{\lambda_{\mathrm{irr}}}(t) \times C_{C_2} \quad \text{Eq.13}$$

$$\frac{dC_{B_2}}{dt}(t) = -k^{\Delta}_{B_2\to F_2} \times C_{B_2} + k^{\lambda_{irr}}_{A_2\to B_2} \times F_{\lambda_{Irr}}(t) \times C_{A_2} - k^{\lambda_{irr}}_{B_2\to A_2} \times F_{\lambda_{\mathrm{irr}}}(t) \times C_{B_2} + k^{\lambda_{irr}}_{F_2\to B_2} \times F_{\lambda_{\mathrm{irr}}}(t) \times C_{F_2} - k^{\lambda_{irr}}_{B_2\to E_2} \times F_{\lambda_{\mathrm{irr}}}(t) \times C_{B_2} \quad \text{Eq.14}$$

$$\frac{dC_{C_2}}{dt}(t) = k^{\Delta}_{A_2\to C_2} \times C_{A_2} - k^{\Delta}_{C_2\to D_2} \times C_{C_2} - k^{\lambda_{irr}}_{C_2\to A_2} \times F_{\lambda_{\mathrm{irr}}}(t) \times C_{C_2} - k^{\lambda_{irr}}_{C_2\to F_2} \times F_{\lambda_{\mathrm{irr}}}(t) \times C_{C_2} + k^{\lambda_{irr}}_{F_2\to C_2} \times F_{\lambda_{\mathrm{irr}}}(t) \times C_{F_2} + k^{\lambda_{irr}}_{D_2\to C_2} \times F_{\lambda_{\mathrm{irr}}}(t) \times C_{D_2} \quad \text{Eq.15}$$

$$\frac{dC_{D_2}}{dt}(t) = k^{\Delta}_{C_2\to D_2} \times C_{C_2} - k^{\lambda_{irr}}_{D_2\to C_2} \times F_{\lambda_{\mathrm{irr}}}(t) \times C_{D_2} \quad \text{Eq.16}$$

$$\frac{dC_{E_2}}{dt}(t) = k^{\lambda_{irr}}_{B_2\to E_2} \times F_{\lambda_{\mathrm{irr}}}(t) \times C_{B_2} \quad \text{Eq.17}$$

$$\frac{dC_{F_2}}{dt}(t) = k^{\Delta}_{B_2\to F_2} \times C_{B_2} - k^{\Delta}_{F_2\to G_2} \times C_{F_2} - k^{\lambda_{irr}}_{F_2\to B_2} \times F_{\lambda_{\mathrm{irr}}}(t) \times C_{F_2} - k^{\lambda_{irr}}_{F_2\to C_2} \times F_{\lambda_{\mathrm{irr}}}(t) \times C_{F_2} + k^{\lambda_{irr}}_{C_2\to F_2} \times F_{\lambda_{\mathrm{irr}}}(t) \times C_{C_2} + k^{\lambda_{irr}}_{G_2\to F_2} \times F_{\lambda_{\mathrm{irr}}}(t) \times C_{G_2} \quad \text{Eq.18}$$

$$\frac{dC_{G_2}}{dt}(t) = k^{\Delta}_{F_2 \rightarrow G_2} \times C_{F_2} - k^{\lambda_{irr}}_{G_2 \rightarrow F_2} \times F_{\lambda_{\mathrm{irr}}}(t) \times C_{G_2} \quad \text{Eq.19}$$

SUT's were written to scheme 6.2:

$$\frac{dC_{A_3}}{dt}(t) = -k^{\lambda_{irr}}_{A_3 \rightarrow B_3} \times C_{A_3} \times F_{\lambda_{Irr}}(t) + k^{\lambda_{irr}}_{B_3 \rightarrow A_3} \times C_{B_3} \times F_{\lambda_{Irr}}(t) - k^{\Delta}_{A_3 \rightarrow B_3} \times C_{A_3} + k^{\Delta}_{B_3 \rightarrow A_3} \times C_{B_3} - k^{\Delta}_{A_3 \rightarrow C_3} \times C_{A_3} \quad \text{Eq.20}$$

$$\frac{dC_{B_3}}{dt}(t) = k^{\lambda_{irr}}_{A_3 \rightarrow B_3} \times C_{A_3} \times F_{\lambda_{Irr}}(t) - k^{\lambda_{irr}}_{B_3 \rightarrow A_3} \times C_{B_3} \times F_{\lambda_{Irr}}(t) + k^{\Delta}_{A_3 \rightarrow B_3} \times C_{A_3} - k^{\Delta}_{B_3 \rightarrow A_3} \times C_{B_3} - k^{\Delta}_{B_3 \rightarrow D_3} \times C_{B_3} \quad \text{Eq.21}$$

$$\frac{dC_{C_3}}{dt}(t) = k^{\Delta}_{A_3 \rightarrow C_3} \times C_{A_3} \quad \text{Eq.22}$$

$$\frac{dC_{D_3}}{dt}(t) = k^{\Delta}_{B_3 \rightarrow D_3} \times C_{B_3} \quad \text{Eq.23}$$

A6.5. RUNGE-KUTTA ANALYSIS OF THE PHOTODEGRADATION REACTION

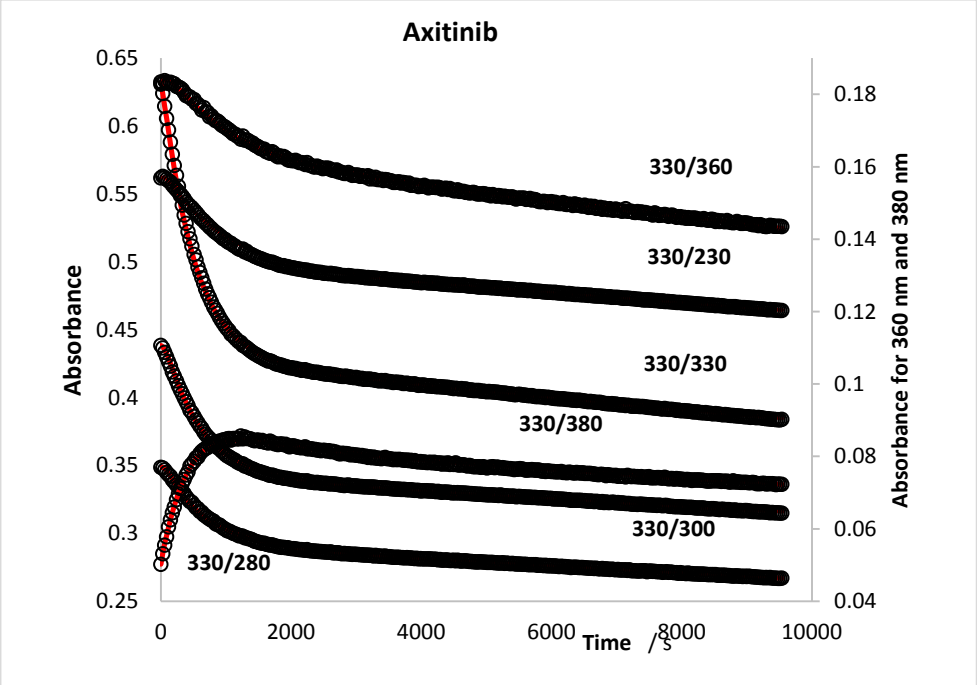

Fig 6.9: Fitting of 2.03 x 10^{-5} M AXI in 2.5 % (v/v) ethanol/water solution when monochromatically irradiated at 330 nm (6.99 x 10^{-7} einstein s^{-1} dm^{-3}, 22°C) and observed at 230nm, 280 nm, 300 nm, 330 nm, 360 nm and 380 nm. Experimental kinetics traces (open circles) and RK data (lines)

A6.6. DETERMINATION OF AXITINIB'S DEGRADATION REACTION IN AQUEOUS MEDIA

In ethanoic solution, both AXI was shown to be thermally stable. However, this was not the case in water. AXI's absorption spectrum decreased simultaneously at every wavelength (Fig A6.1).

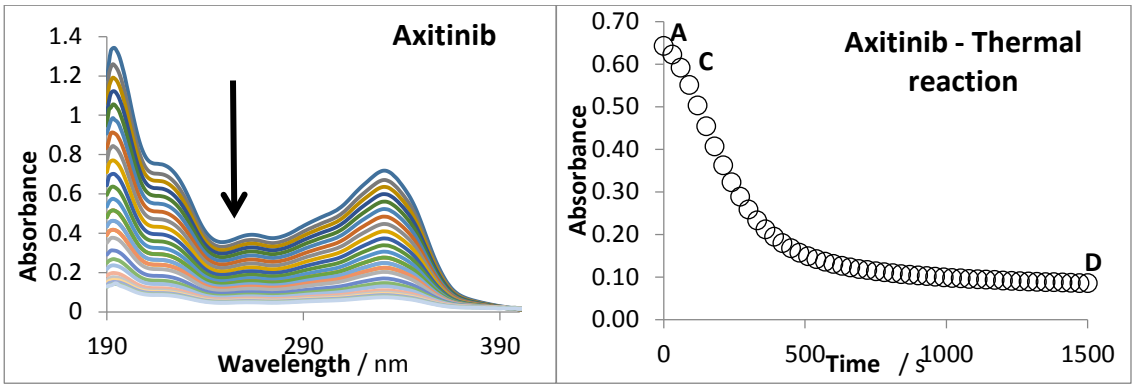

Fig A6.1: Changes in the spectrum of (left) 1.97 x10^{-4} M AXI 2.5% v/v ethanol/water solution, stirred and thermalstatically maintained at 22°C. (Right) Kinetic trace obtained when observed at 430 nm

Looking at Fig A6.1, the decrease in absorbance under thermal conditions within the first 60 seconds is relatively quick in comparison to the rest. It is clear that the reaction is not unimolecular, but maybe an A to B to C reaction involving three species.

The small change in absorbance can be seen in the first reaction suggesting that the first thermal product (C) has an epsilon that's very similar to AXI (A) and very possibly a similar chemical structure as well. On the other hand, the epsilon of the final thermal product (D) is significantly lower and hugely different to A and C. A consecutive reaction mechanism involving three species is proposed (scheme A6.1):

$$A \xrightarrow{\Delta} C \xrightarrow{\Delta} D$$

Scheme A6.1: proposed consecutive reaction mechanism for the thermal degradation of AXI

The thermal reaction seems to deplete A in less 500 s while the photochemical reaction in the same conditions looks like it does not allow A to react thermally, this supported by the variation of the spectra since in the latter case we observe a similar behaviour to that obtained in ethanol and not the decrease of the whole spectrum as observed during the thermal reaction (Fig. A6.1). This further suggests the formation of different products.

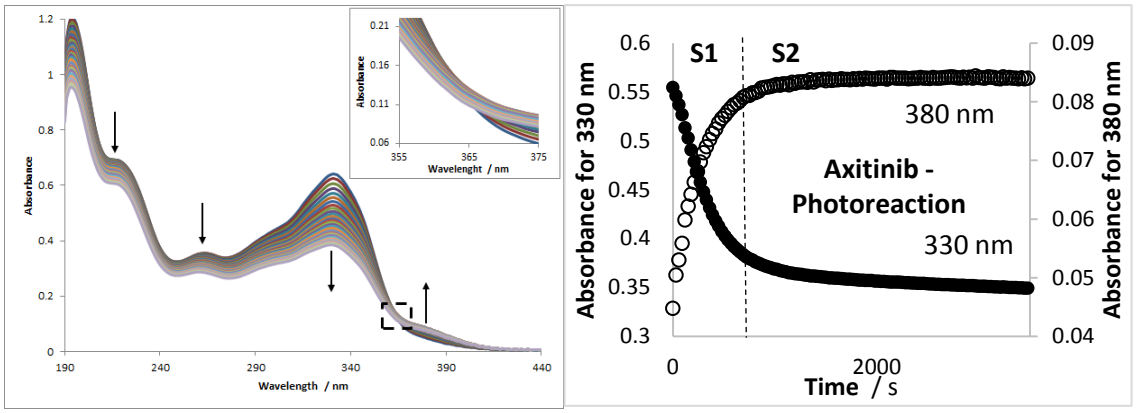

Fig. A6.2: Irradiation of 2.03 x 10^{-5} M AXI in 2.5 % (v/v) ethanol/water solution continuously with a monochromatic beam at 360 nm (1.15 x 10^{-6} einstein s^{-1} dm^{-3}, 22°C); (left) spectral evolution; (right) kinetic traces obtained when observed at 330 nm and 380 nm.

As seen in Fig. A6.2 (right), the photodegradation of AXI is very fast in the first 800 s (broken line) of the reaction (S1) and then slows down (S2). The absorbance at 330 nm in S1 changes by 0.2 AU in just 800 s, whereas in S2 only 0.03 AU change in absorbance is observed over 3000 s. The change in absorbance in the latter section is of the same magnitude of that in thermal reaction (0.03 AU) from 800 s onwards. Coinciding with the fact that thermal reaction continues to occur, even when the solution is exposed to light, the slower reaction in S2 at 330 nm and 380 nm is then highly possibly the thermal reaction.

The difference in the spectral evolution and increase in absorbance observed at 380 nm (peak established in ethanol as belonging to the photoproduct, *Z*-AXI) points to the occurrence of photoreaction.

The significant difference in the evolution of the thermal and photo-degradation strongly suggests that the products produced are different. A comparison of AXI's spectra and the spectra obtained at the end of the photo- and thermal reaction further supports the idea that these reaction produce different end products (Fig. A6.3).

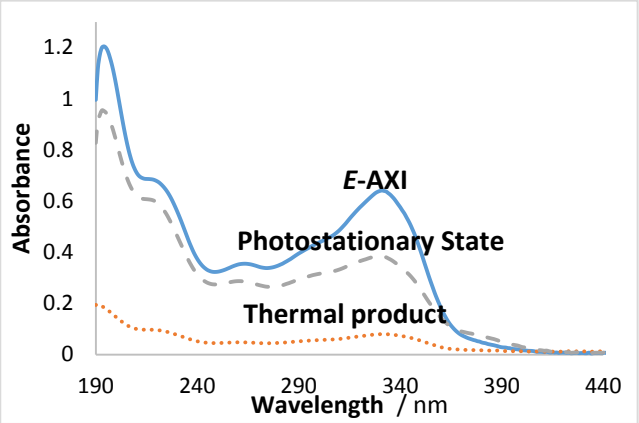

Fig. A6.3: The spectra of *E*-AXI, the last spectra of the photoreaction (λ_{irr} = 330 nm, 6.99 x 10^{-7} einstein^{-1} s^{-1} dm^{-3}, 22°C, stirred) and the last spectra of the thermal reaction (22°C, stirred).

Therefore, AXI's reaction in water can deemed to involve at least 4 species:

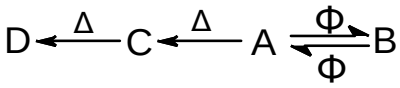

Scheme A6.2: proposed reaction mechanism for the degradation of AXI in water involving 4 species

Comparison of the thermal and photokinetic traces (Fig. A6.4) suggests that during photoreaction, the formation of Species C is hampered as the change in absorbance recorded is significantly different. This may be because less C is formed than B and so the absorbance at the beginning is lower in the photokinetic trace. However, this does not explain why the

photo- and thermal kinetic traces do not finish at the same point. If the formation of species C is constant, A and B will require to re-equilibrate to compensate for the loss of A to C. Therefore, species C must photochemically reverse to A.

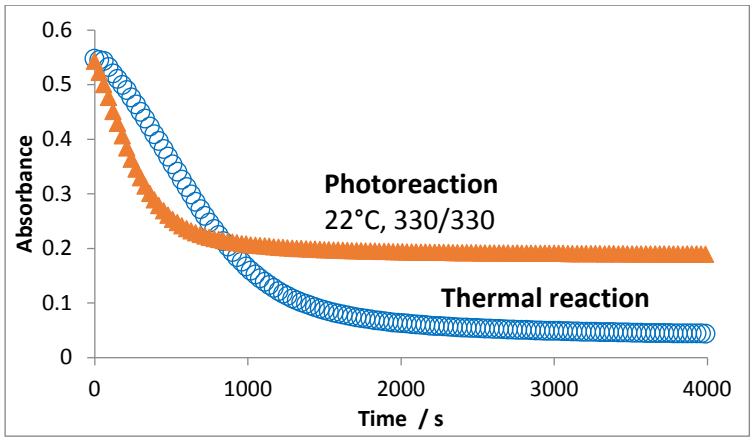

Fig. A6.4: Thermal and photokinetic traces of *E*-AXI in water.

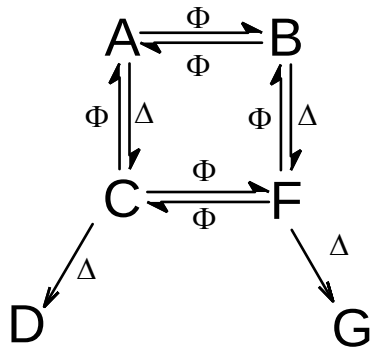

Scheme A6.3: proposed reaction mechanism for the degradation of AXI in water involving 6 species

This also indicates that during the thermal degradation the double bond at which photoisomerisation occurs is not broken. Accordingly, it is highly probable that species C is also photochemically active, transforming into its isomer equivalent (Species F). Because A and B are similarly structured and thermal degradation does not occur at the double bond, it can be deemed that B thermally degrades into F and then G to F as well (scheme A6.3).

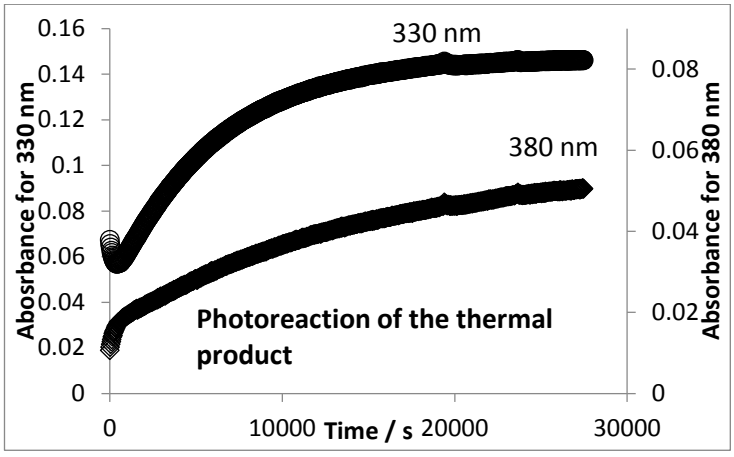

Fig. A6.5: Irradiation of the solution at the end of the thermal reaction at 330 nm for 7.5 hours.

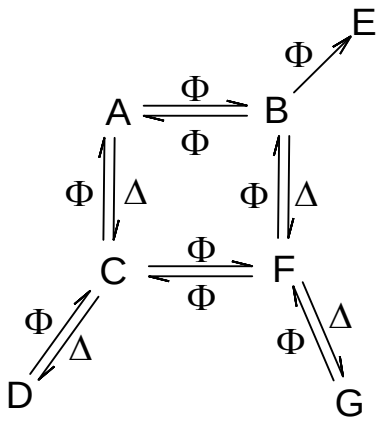

Scheme A6.4: proposed reaction mechanism for the degradation of AXI in water involving 7 species

Irradiation of the solution at the end of the thermal reaction induced a very slow increase of absorbance (Fig. A6.5) at all wavelength, indicating a slow reverse photoreaction of species D to C - and so G to F.

Closer inspection of the photokinetic trace at 380 nm revealed that a plateau is not reached and a small change in absorbance can be observed pointing to the presence of a very slow reaction which is not reversible.

Finally from these data, AXI's degradation mechanism in aqueous medium is proposed (Scheme A6.4).

A6.7. SPECIES' CONCENTRATIONS

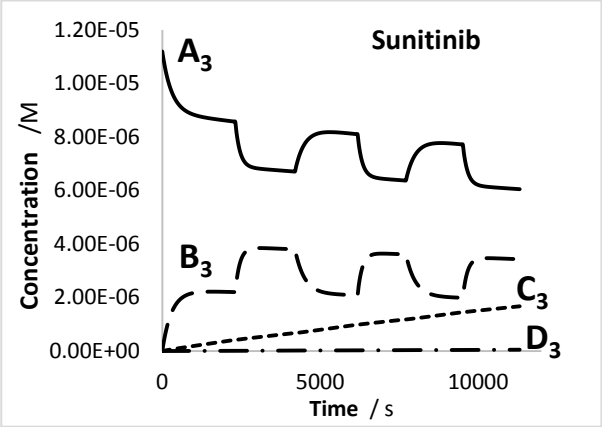

Fig. 6.10: Concentration profiles obtained for 1.12 x 10^{-5} M *Z*-SUT and its products when monochromatic irradiation at 460 nm was repeatedly interrupted (2.66 x 10^{-6} einstein s^{-1} dm^{-3}, 22°C).

A6.8. ELECTRONIC ABSORPTION SPECTRA OF SUNITINIB AND ITS PRODUCTS

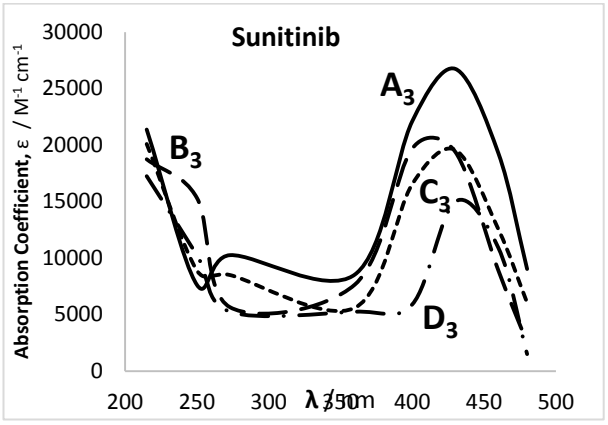

Fig 6.11: Estimated electronic absorption spectra of SUT and its products

A6.9. PHOTOCHEMICAL QUANTUM YIELD VALUES OF AXITINIB

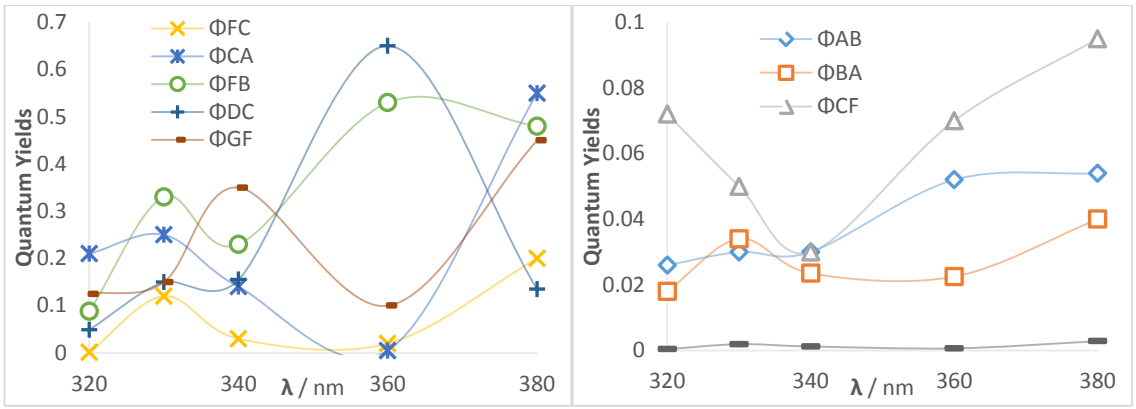

Fig 6.14: Photochemical quantum yield values of Axitinib and its products determined at different irradiation wavelengths.

A6.10. POTENITAL DEVELOPMENT OF ACTINOMETERS

Table 6.5: Equations for the recalculation of radiant power (P) for three irradiation wavelengths obtained using the theoretical (theo) and Φ-order kinetics model (fit) equations

λ_{irr} /nm	300	330	360
P_{theo}	$P_{300} = 880.17 \times P_{theo} - 2x10^{-5}$	$P_{330} = -302.21 \times P_{theo} + 1x10^{-6}$	$P_{360} = 199.67 \times P_{theo} - 3x10^{-7}$
r^2	1	1	1
P_{fit}	$P_{300} = -208.33 \times P_{fit} - 2x10^{-5}$	$P_{330} = -397.8 \times P_{fit} - 2x10^{-6}$	$P_{360} = -269.41 \times P_{fit} - 2x10^{-5}$
r^2	0.99	0.98	0.97

A6.11. THE EFFECT OF POLYCHROMATIC LIGHT

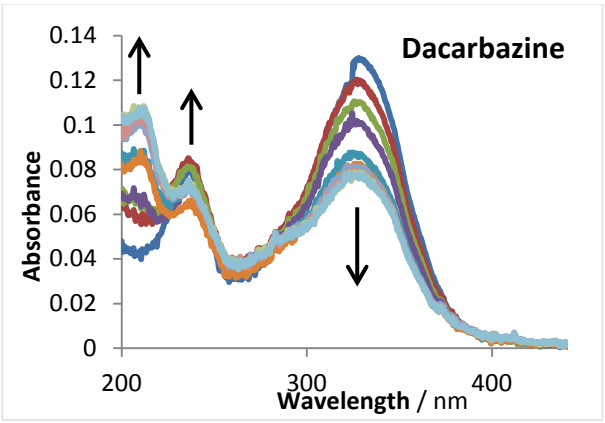

Fig 6.16: Evolution of the electronic absorption spectra of 5.38 x 10^{-6} M DBZ in water

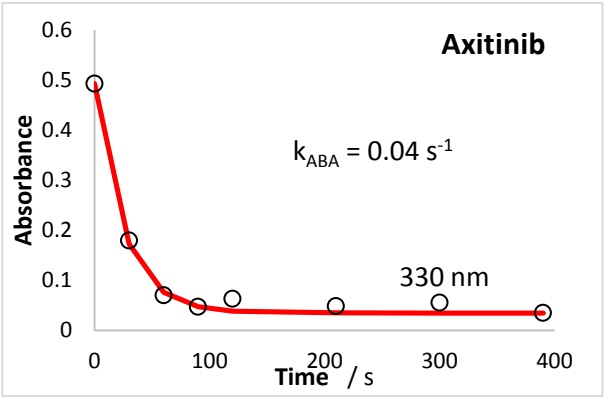

Fig 6.16: Kinetic traces obtained for AXI in water when subjected to ambient polychromatic irradiation. Open shapes are experimental data and solid lines are fittings

APPENDIX 7

A7.1. THE MATHEMATICAL BACKGROUND FOR A G_n:$(CD_p)_m$ COMPLEX

The association of "*n*" (one or more) guest species with a polymer "*m*" (one or more) cyclodextrin chain-molecules that may encompass each up to "*p*" cyclodextrin monomer–units, form a type of complex that will be labelled here as G_n:$\left(CD_p\right)_m$ (Scheme 7.1). Hence, for monomer cyclodextrins, *p* = 1. Such a complex is supposed to instantaneously occur in the solution medium with a unique stoichiometry for the guest/nanosponge complex (irrespective of the specific type of binding that may include an inclusion, non-inclusion, clustering or aggregation).

The overall association reaction is given by

$$n\,\mathbf{G} \quad + \quad m\,\mathbf{CD_p} \rightleftharpoons \mathbf{G_n}\text{:}(\mathbf{CD_p})_m$$

Scheme 7.1: Association reaction of *n* guest molecules with *m* cyclodextrin nanosponge units (CD_p).

The thermodynamic association (or binding) constant of the complex at equilibrium for a given temperature, is

$$K_{G_n:(CD_p)_m} = \frac{\left[G_n:(CD_p)_m\right]_{i,j}}{[G]_{0,i}^{n} \times [CD_p]_{0,i,j}^{m}} \qquad \text{Eq. 1}$$

Here, we consider the most general case where the experiment "*i*" is performed by keeping constant the guest (drug) molecule concentration throughout, $[G]_{0,i}$, and gradually increasing the concentrations of the host-nanosponge, $\left[CD_p\right]_{0,i,j}$, in a set of "*j*" separate solutions.

For each solution, the mass balance for CD is given by

$$\left[CD_p\right]_{0,i,j} = \left[CD_p\right]_{i,j} + m \times \left[G_n:\left(CD_p\right)_m\right]_{i,j} \qquad \text{Eq. 2}$$

where $\left[CD_p\right]_{0,i,j}$ is the actual initial concentration of CD_p in the j^{th} solution for experiment "*i*"; $\left[CD_p\right]_{i,j}$ and $\left[G_n{:}\left(CD_p\right)_m\right]_{i,j}$ are respectively the concentrations of free and complexed nanosponge molecules in the medium at equilibrium for a given temperature.

If we assume that the concentration of the guest molecule is very small compared to that of CD then Eq. 2 becomes

$$\left[CD_p\right]_{0,i,j} \cong \left[CD_p\right]_{i,j} \qquad \text{Eq. 3}$$

We also consider the mass balance relative to the guest species, as

$$[G]_{0,i} = [G]_{i,j} + n \times \left[G_n{:}\left(CD_p\right)_m\right]_{i,j} \qquad \text{Eq. 4}$$

where $[G]_{0,i}$ is the constant initial concentration of the guest for the i^{th} experiment (used for the "*j*" solutions). $[G]_{i,j}$ and $\left[G_n{:}\left(CD_p\right)_m\right]_{i,j}$ are respectively the concentrations relative to free and complexed guest molecules in the medium at equilibrium for the j^{th} solution of experiment "*i*".

Each of the *j* solutions of an experiment *i,* is individually analysed by fluorimetry.

The total fluorescence intensity ($Fl_{tot,i,j}^{\lambda_{obs}}$) recorded for the medium, for each individual solution "*j*" at a given observation wavelength (λ_{obs}, e.g. at the maximum of the emission spectrum of the complex), is given as

$$Fl_{tot,i,j}^{\lambda_{obs}} = Fl_{G,i,j}^{\lambda_{obs}} + Fl_{G_n:\left(CD_p\right)_m,i,j}^{\lambda_{obs}} \qquad \text{Eq. 5}$$

The measured fluorescence intensities of free guest $\left(Fl_{G,i,j}^{\lambda_{obs}} = \sigma_G \times [G]_{i,j}\right)$ and complex $\left(Fl_{G_n:(CD_p)_m,i,j}^{\lambda_{obs}} = \sigma_{G_n:(CD_p)_m} \times \left[G_n:(CD_p)_m\right]_{i,j}\right)$ are proportional to the respective species concentrations ($[G]_{i,j}$ and $\left[G_n:(CD_p)_m\right]_{i,j}$, respectively), according to the Beer-Lambert law, where the proportionality factors are the fluorescence molar coefficients (σ_G and $\sigma_{G_n:(CD_p)_m}$, respectively [1]).

Therefore, $Fl_{tot,i,j}^{\lambda_{obs}}$ can be re-written as

$$Fl_{tot,i,j}^{\lambda_{obs}} = \sigma_G \times [G]_{i,j} + \sigma_{G_n:(CD_p)_m} \times \left[G_n:(CD_p)_m\right]_{i,j} \quad \text{Eq. 6}$$

Rearranging Eq. 4 for $[G]_{i,j}$ and introducing its expression in Eq. 6, yields

$$Fl_{tot,i,j}^{\lambda_{obs}} = \sigma_G \times [G]_{0,i} + \left(\sigma_{G_n:(CD_p)_m} - n \times \sigma_G\right) \times \left[G_n:(CD_p)_m\right]_{i,j} \quad \text{Eq. 7}$$

Since the native fluorescence of the guess (i.e. measured in the absence of the host) is expressed as $Fl_{0,G,i}^{\lambda_{obs}} = \sigma_G \times [G]_{0,i}$, then Eq. 7 can be rearranged as

$$\left[G_n:(CD_p)_m\right]_{i,j} = \frac{Fl_{tot,i,j}^{\lambda_{obs}} - Fl_{0,G,i}^{\lambda_{obs}}}{\left(\sigma_{G_n:(CD_p)_m} - n \times \sigma_G\right)} \quad \text{Eq. 8}$$

Introducing the resulting rearranged equation from combining Eqs. 8 and 4, in the resulting equation from introducing Eq. 8 in Eq. 1 gives a new expression for the association constant $K_{G_n:(CD_p)_m}$ (Eq. 9) which is exclusively dependent on experimentally accessible quantities.

$$K_{G_n:(CD_p)_m} = \frac{\frac{Fl^{\lambda_{obs}}_{tot,i,j} - Fl^{\lambda_{obs}}_{0,G,i}}{\left(\sigma_{G_n:(CD_p)_m} - n \times \sigma_G\right)}}{\left([G]_{0,i} - n \times \frac{Fl^{\lambda_{obs}}_{tot,i,j} - Fl^{\lambda_{obs}}_{0,G,i}}{\left(\sigma_{G_n:(CD_p)_m} - n \times \sigma_G\right)}\right)^n \times [CD_p]^m_{0,i,j}} \quad \text{Eq. 9}$$

Assuming that at high CD_p concentrations ($\left[CD_p\right]_{0,i,j} \cong \infty$), every molecule of the guest is complexed $\left([G]_{0,i} = n \times \left[G_n{:}\left(CD_p\right)_m\right]^{\infty}_{i,j}\right)$, therefore the fluorescence intensity of the medium is

$$Fl^{\lambda_{obs}}_{0,(G_n:(CD_p)_m)} = \left[G_n{:}\left(CD_p\right)_m\right]^{\infty}_{i,j} \times \sigma_{G_n:(CD_p)_m} = \frac{1}{n} \times [G]_{0,i} \times \sigma_{G_n:(CD_p)_m} \quad \text{Eq. 10}$$

Hence, combining the latter Eqs. 9 and 10, leads to a general equation for the variation of the medium total fluorescence intensity ($Fl^{\lambda_{obs}}_{tot,i,j}$) with nanosponge concentration ($\left[CD_p\right]_{0,i,j}$) for a $G_n{:}\left(CD_p\right)_m$ complex, as

$$\frac{\left(Fl^{\lambda_{obs}}_{0,(G_n:(CD_p)_m)} - Fl^{\lambda_{obs}}_{tot,i,j}\right)^n}{Fl^{\lambda_{obs}}_{tot,i,j} - Fl^{\lambda_{obs}}_{0,G,i}} = \frac{\left(Fl^{\lambda_{obs}}_{0,(G_n:(CD_p)_m)} - Fl^{\lambda_{obs}}_{0,G,i}\right)^{n-1}}{n \times K_{G_n:(CD_p)_m} \times [G]^{n-1}_{0,i}} \times \frac{1}{[CD_p]^m_{0,i,j}} \quad \text{Eq. 11}$$

If the relative molar mass of the CD polymer ($RMM(CD_p)$) is not known with accuracy (which is indeed the case for a majority of nanosponges), then it would be useful, from an experimental point of view, to employ a g/L unit for concentrations (instead of the molarity unit involved in Eq. 11), as

$$\frac{\left(Fl^{\lambda_{obs}}_{0,(G_n:(CD_p)_m)} - Fl^{\lambda_{obs}}_{tot,i,j}\right)^n}{Fl^{\lambda_{obs}}_{tot,i,j} - Fl^{\lambda_{obs}}_{0,G,i}} = \frac{\left(Fl^{\lambda_{obs}}_{0,(G_n:(CD_p)_m)} - Fl^{\lambda_{obs}}_{0,G,i}\right)^{n-1}}{n \times K_{G_n:(CD_p)_m} \times [RMM(G)]^{1-n}_{0,i} \times \left[RMM(CD_p)\right]^{-m}_{0,i}} \times \frac{1}{[G]^{n-1}_{0,i} \times \left[CD_p\right]^m_{0,i,j}} \quad \text{Eq. 12}$$

where, RMM(G) and RMM(CD_p) are the relative molar masses of guest (G) and nanosponge (CD_p), respectively (expressed in g/mol); and in Eq. 12, the species concentrations ($[G]_{0,i}$ and $\left[CD_p\right]_{0,i,j}$) are expressed in g/L, mg/mL or equivalent.

The unit of the association constant, $K_{G_n:(CD_p)_m}$, that can be worked out from either Eq. 11 or 12, is expressed either in molarity or g/L units as M^{1-m-n} or $(g/L)^{1-m-n}$, respectively. In the cases were the relative molar mass of the nanosponge is not known with precision, it is possible to work with an alternative "*pseudo–association*" constant, $K'_{G_n:(CD_p)_m}$ (Eq. 13), which will be expressed in $\left(g^2/(mol \times L)\right)^{1-m-n}$ or equivalent.

$$K'_{G_n:(CD_p)_m} = K_{G_n:(CD_p)_m} \times [RMM(G)]_{0,i}^{1-n} \times \left[RMM\left(CD_p\right)\right]_{0,i}^{-m} \quad \text{Eq. 13}$$

It is clear that Eq.11 is non-linear relative to the variation of the medium fluorescence intensity, $Fl_{tot,i,j}^{\lambda_{obs}}$, with increasing nanosponge concentration, $\left[CD_p\right]_{0,i,j}$, in the solution. This mean that is impossible to derive a classical formulation for the isotherm, i.e. where the fluorescence intensity is directly expressed as a function of CD concentration, $Fl_{tot,i,j}^{\lambda_{obs}} = f\left(\left[CD_p\right]_{0,i,j}\right)$, for the general case where *n* has any given values higher than 1.

However, it is possible to derive from Eq.11 a general expression for the isotherm corresponding to complexes involving a single guest molecule (*n* = 1) associated to *m* nanosponge host-molecules ($G_1:\left(CD_p\right)_m$), as:

$$Fl_{tot,i,j}^{\lambda_{obs}} = \frac{Fl_{0,G,i}^{\lambda_{obs}} + Fl_{0,(G_1:(CD_p)_m)}^{\lambda_{obs}} \times K_{G_1:(CD_p)_m} \times [CD_p]_{0,i,j}^{m}}{1 + K_{G_1:(CD_p)_m} \times [CD_p]_{0,i,j}^{m}}$$ Eq.14

Eq.14 reduces down to the equations that have been previously proposed in the literature for complexes involving CD monomers [2,3].

The limit value of the first term of Eq.11 tends to 0 (i.e. $Fl_{tot,i,j}^{\lambda_{obs}} \cong Fl_{0,(G_n:(CD_p)_m)}^{\lambda_{obs}}$) when the CD concentration tends to infinity. This means that in all cases, irrespective of *n* and *m* values, the isotherm ends with a plateau that indicates the occurrence of a saturation (where the majority of guest molecules are involved in a complex). It is then evident that any variation to the final part of the curve (by an increase or a decrease of the medium total fluorescence intensity after the plateau region) for given experimental data would strongly suggest the occurrence of another phenomenon.

According to a great number of simulations we performed on Eq.11, the isotherms can have one of two general shapes (Fig. A7.1); they are either exponential-like (as for the usual isotherms observed for 1:1 complexes) when *m* = 1 and any *n* values, or an S-shaped curves if *m* > 1 for any n (even for a 1:2 complex). Therefore, the shape of the isotherm can inform on whether *m* is equal to unity.

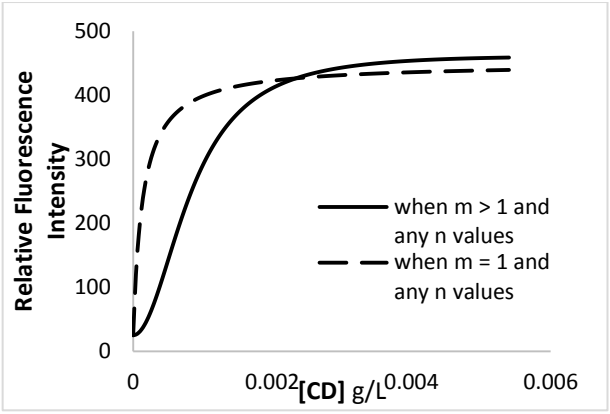

Fig. A7.1: Possible isotherm shapes obtained by simulation for different complex stoichiometries.

Theoretically, plotting the first term $\left[\frac{\left(Fl^{\lambda_{obs}}_{0,(G_n:(CD_p)_m)}-Fl^{\lambda_{obs}}_{tot,i,j}\right)^n}{Fl^{\lambda_{obs}}_{tot,i,j}-Fl^{\lambda_{obs}}_{0,G,i}}\right]$ of Eq.11 against $\frac{1}{[CD_p]^m_{0,i,j}}$ will always yield a straight line. However, in practice this means that the stoichiometry of the complex (i.e. parameters *n* and *m*) must be known or pre-selected.

This relationship may nevertheless be used either for confirmation of the results of the parameters found by another method, or for successive iterations on preconceived stoichiometries of the complex (iterations run with imposed values for *n* and *m*, until a good linear fit is obtained).

The latter strategy is generally adopted in the literature for monomers (*p* = 1) where a linear treatment is sought, by assuming that a single parameter (e.g. $K_{G_n:(CD_p)_m}$) is unknown; an approach that can be applied for Eq.11, where several options might be proposed until a good fit is found. Generally, one starts with *n* = *m* = 1, defines the equations to which the data will be fitted to, for instance, the Benesi-Hildebrand equation for 1:1 complexes [4,5]. If a poor fitting is found then n and/or *m* is incremented by one unit at a time to define the appropriate equations and proceed to the fitting. This procedure is repeated until a good fitting is found, hence defining the couple *n* and *m*. This strategy would be tedious if the stoichiometry of the complex involves a high number of species.

A7.2. REFERENCES

1. Liu Y., Han B.H. and Zhang H.Y. (2004) Spectroscopic studies on molecular recognition of modified cyclodextrins, *Current Organic Chemistry*, 8(1):35-36
2. Connors K.A. (1987) binding constants: the measurement of molecular complex stability, New York: John Wiley & Sons, Ltd.
3. Maafi M., Aaron J.J. and Mahedero M.C. (1997) Spectrofluorimetric properties of a 2-hydroxypropyl-β-cyclodextrin: 9-methylnenzo[a]phenothiazine inclusion complex in aqueous medium. Analytical usefulness, *Talanta,* 44:2193-2199

4. Szejtli J. (1982) Cyclodextrins and their Inclusion Compounds (Akademiai Kiado, Budapest.
5. Maafi M., Aaron J.J., Mahedero M.C. and Salinas F. (1998) Evidence for the formation of a benzo[a]phenothiazine/2-hydroxypropyl-β-cyclodextrin inclusion complex using a fluorescence method, *Applied Spectroscopy*, 52(1):91-95.